CASE FILE COPY

ANALYTICAL STUDY AND EXPERIMENTAL INVESTIGATION OF TECHNIQUES FOR IMPROVING ELECTRON TUBES FOR SPACE APPLICATION

By E.C. Conway and M.J. Kelley

December 1968

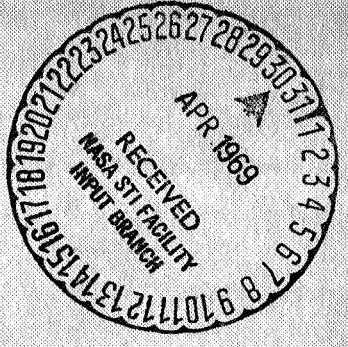

Distribution of this report is provided in the interest of information exchange and should not be construed as endorsement by NASA of the material presented. Responsibility for the contents resides with the organization that prepared it.

Prepared under Contract No. NAS 12-565 by

General Electric Company
Missile and Space Division
Valley Forge, Penna.

Electronics Research Center

NATIONAL AERONAUTICS AND SPACE ADMINISTRATION

Robert W. Wilmarth
Technical Monitor
NAS 12-565
Electronics Research Center
575 Technology Square
Cambridge, Massachusetts 02139

Requests for copies of this report should be referred to:

NASA Scientific and Technical Information Facility
P.O. Box 33, College Park, Maryland 20740

ANALYTICAL STUDY AND EXPERIMENTAL INVESTIGATION OF TECHNIQUES FOR IMPROVING ELECTRON TUBES FOR SPACE APPLICATION

By E.C. Conway and M.J. Kelley

December 1968

Prepared under Contract No. NAS 12-565 by

General Electric Company
Missile and Space Division
Valley Forge, Penna.

Electronics Research Center

NATIONAL AERONAUTICS AND SPACE ADMINISTRATION

FOREWORD

This final report, covering a 1-year analytical and experimental investigation of the thermal problems associated with spaceborne electron tubes, was conducted under Contract NAS 12-565 from the National Aeronautics and Space Administration, Electronic Research Center. The study was conducted by E. C. Conway and M. J. Kelley of the General Electric Company, Space Systems Organization, under the direction of R. H. Swartley, Program Manager. Principal contributors, in addition to Messrs. Conway and Kelley, include J. E. Beggs of the General Electric Research and Development Center and, within Space Systems, F. J. Witt, A. W. Schnacke, and R. B. Hand of Nuclear Systems Programs and R. P. Eisenberg, A. J. Geia, M. J. Carpitella, J. M. Darrohn, and W. J. Taunton of Research and Engineering.

TABLE OF CONTENTS

TABLE OF CONTENTS (Cont'd)

LIST OF ILLUSTRATIONS

LIST OF ILLUSTRATIONS (Cont'd)

LIST OF TABLES

ANALYTICAL STUDY AND EXPERIMENTAL INVESTIGATION OF TECHNIQUES FOR IMPROVING ELECTRON TUBES FOR SPACE APPLICATION

By E. C. Conway and M. J. Kelley
General Electric Company
Valley Forge, Penna.

SECTION 1
SUMMARY

An analytical and experimental study was conducted to determine means of improving electron tubes for space applications. The two major areas of improvement examined were:

a. Elimination of Electric Cathode Heaters. A triode was designed and constructed with a heat pipe integrated into its cathode structure to allow the use of an external heater. The tube was operated using a promethium-147 isotope heat source to heat the cathode. Problems encountered in utilizing the source made available by the AEC show that a higher power density source, such as curium-244, is much better suited to cathode heating. Using curium-244, the isotope is small enough to be inserted into the cathode support, thus eliminating the need for a heat pipe.

b. Heat Pipe Cooling of High Power Microwave Tubes. An investigation of high power tubes indicates that most existing tubes are not suited to heat pipe cooling, since passages designed for liquid cooling are inadequate for use as evaporators. Integration of heat pipe evaporators into these tubes can be accomplished, however, with either modifications in existing designs or a completely integrated approach to the overall tube design. To demonstrate heat pipe cooling, a travelling wave tube was operated using heat pipe cooling. With 930 watts dissipated at the collector, the operating temperature of 200°C was not exceeded.

SECTION 2
INTRODUCTION

This report presents the results of the work performed on National Aeronautics and Space Administration Contract Number NAS 12-565. The purpose of the contract was to analytically and experimentally develop methods of improving spaceborne electron tubes. The work was directed toward two specific areas: elimination of electrical heaters and cooling of high power dissipation elements.

The power required by the heater of an electron tube emitter can significantly reduce the overall efficiency of low power tubes. Elimination of this power drain can result in a significant reduction in total power requirement of a vehicle. A radioisotope dissipates heat which can be supplied directly to the emitting surface of a tube, thus eliminating the electrical heater. With the proper isotope and an efficient thermal design, a saving in weight and cost can be realized.

High-power spacecraft proposed for operation during the next decade add several problems to spacecraft thermal design. One of the most vital will be to provide adequate cooling for transmitter output devices dissipating power at levels which are orders of magnitude above anything yet used in a space vehicle. When these power levels exceed the capacity of passive fins, some type of liquid cooling system, where a fluid is circulated through a closed loop to transfer heat from a source to a radiator, is required. A mechanically pumped loop is life-limited by moving parts and requires electrical power for operation. A heat pipe or a capillary pumped heat transfer loop can in many cases replace the mechanically pumped loop, thereby increasing thermal system performance while reducing weight and eliminating the need for electrical power to circulate the coolant.

Application of the heat pipe to cool the dissipating elements of a high power electron tube probides a system capable of highly reliable operation over very long periods

of time. Since many high power tubes do not have suitable interfaces for cooling by heat pipes, designs of both tube and heat pipe evaporator must be integrated.

Sections 4 and 5 of this report describe the work performed which applies directly to electron tubes, while supporting analyses and additional data are contained in the appendixes. Appendixes A and B describe heat pipe design and its application to space radiators. Appendix C discusses various means of temperature control which, while not used in the program, would be required for spacecraft applications. All data from the TWT cooling tests which is not included in the body of the report is given in Appendix D. Appendix E contains a copy of the report which accompanied the application to the Atomic Energy Commission for a license to use the isotope in the cathode heating tests. Additional data on the circuitry and characteristics of the TWT are given in Appendix F.

SECTION 3

NOMENCLATURE

NOMENCLATURE

ρ	-	density
γ	-	surface tension
σ	-	Stefan Boltzmann constant
λ	-	latent heat of vaporization
η	-	viscosity or fin effectiveness
V	-	velocity
d	-	reflux wick interlayer spacing
P	-	pressure
R	-	thermal resistance
K	-	thermal conductivity
A	-	area
T	-	temperature
r	-	radius
q	-	heat dissipation or rejection
$\dot{q}$	-	volumetric heat generation rate
x, y	-	length
L	-	total length
ϵ	-	emissivity

SUBSCRIPTS

ℓ	-	property of liquid phase
v	-	property of the vapor phase
i	-	inside dimension or surface
o	-	outside dimension or surface or initial condition
s	-	sink
t	-	thermal power
e	-	electrical power

SECTION 4

NON-ELECTRIC CATHODE HEATING

The use of a radioisotope heat source to heat a vacuum tube cathode eliminates a portion of the electrical power required and thus increases the overall efficiency. Two basic approaches can be taken to the application of heat from the isotope. First, and much preferred, where the volumetric heat generation of the isotope is high enough, the total volume required by the source is such that it can be placed directly against the cathode. Second, if the volume of the isotope required is too large to be placed at the cathode, heat must be carried from the isotope to the cathode. While a high thermal conductivity material can be used to carry the heat, the extremely high conductance of a heat pipe makes an ideal device for this approach.

A list of isotopes suitable for use as heat sources is given in Table I. From the standpoint of power density and half-life, curium-244, plutonium-238, and promethium-147, in the order given, are good possibilities. Curium is exceptionally good, since its power density is high enough that it could be placed in direct contact with the cathode.

The radioisotope heat source used in this program was supplied by the Atomic Energy Commission as GFE, since the cost of a source designed specifically for the program was prohibitive. The source, shown in Figure 1, is described in detail in Appendix E. This Appendix is the document submitted to AEC for the license required to obtain the radioisotope source. The capsule was originally used by the Air Force in the Advanced Manned Strategic Aircraft program. To ensure the integrity of the source during this program, the capsule was designed to contain the isotope after impact at terminal velocity.

Thus, the capsule walls are thick and the ends are rounded, making the configuration far from optimum for cathode heating. The wall thickness results in increased surface area, thus making it more difficult to insulate. The rounding of the ends leaves

Table I. Characteristics of Radioisotopic Heat Sources

	^{60}Co	^{90}Sr	^{106}Ru	^{137}Cs	^{144}Ce	^{147}Pm	^{170}Tm	^{210}Po	^{238}Pu	^{242}Cm	^{244}Cm
1. Watts/Gram (100% Basis)	17.4	0.96	33.1	0.42	25.6	0.33	13.6	141	0.56	120	2.65
2. Half Life, Years	5.24	28	1.0	30	0.78	2.6	0.35	0.38	87.4	0.45	18.1
3. Estimated Isotopic Purity, %	10[a]	55[b]	3.3[b]	35	4.5[b]	95[b]	10[a]	95	80	90	95
4. Compound Form	Metal	$SrTiO_3$	Metal	CsCl	Ce_2O_3	Pm_2O_3[c]	Tm_2O_3	Metal	PuO_2	Cm_2O_3	Cm_2O_3
5. Melting Point of Compound, °C	1480	1910	2310	646	2190	2130	2375	255	2250	1950	1950
6. Active Isotope in Compound, %	10	23	3.3	28	3.8	82	8.8	95	70	82	86
7. Watts/Gram Compound	1.74	0.22	1.1	0.12	1.0	0.27	1.2	134	0.39	98	2.27
8. Density of Compound, g/cm^3, actual or 90% TD	8.8	4.6	12.4	3.2	6.2	6.6	8.0	9.3	10	9	9
9. Power Density, W/cm^3 Compound	15.8	1.01	13.7	0.38	6.2	1.8[c]	9.6	1210[d]	3.9[d]	882[d]	20.4[d]
10. Dimension of capsule for 50 W_t, cm[e]	2.2	4.4	2.3	6.1	2.8	3.9	2.5	2.0	3.8	2.0	2.4
11. Availability	Avail.	Avail.	Poten. Avail.	Avail.	Avail.	Avail.	Avail.	Avail.	Avail.[f]	Poten. Avail.	Avail.[f]
12. Type of Radiation (Major)*	$\gamma\beta$	$\beta\chi$	$\gamma\beta\chi$	$\beta\gamma\chi$	$\beta\gamma\chi$	β	β	α	α	αn	αn
13. Shielding Required[g] [MeV of significant β or γ]	Heavy (9.5) [1.33γ]	Heavy (6) [2.26β]	Heavy (9) [3.35β]	Heavy (4.6) [1.17β 0.67γ]	Heavy (10.2) [2.98β 2.18γ]	Minor (1) [0.23β]	Moderate (2.5) [0.97β]	Minor (1) [0.8γ]	Minor (0.1) [0.04γ]	Minor (0.4) [0.04γ]	Moderate (2) [0.04γ]
14. Biological Hazard Ci/m^3	3×10^{-9}	10^{-10}	2×10^{-9}	5×10^{-9}	2×10^{-9}	2×10^{-8}	10^{-8}	7×10^{-11}	7×10^{-13}	4×10^{-11}	3×10^{-12}
MPC, AIR, W/m^3	4.6×10^{-11}	6.8×10^{-13}	2×10^{-11}	2.4×10^{-11}	1.6×10^{-11}	7.2×10^{-12}	2.3×10^{-11}	2.2×10^{-12}	2.3×10^{-14}	1.4×10^{-12}	10^{-13}
Continuous Exposure g/m^3	2.7×10^{-12}	7×10^{-13}	5.9×10^{-13}	5.8×10^{-11}	6.3×10^{-13}	2.2×10^{-11}	1.7×10^{-12}	1.6×10^{-14}	4.1×10^{-14}	1.2×10^{-14}	3.7×10^{-14}
15. Estimated Future Price $/g (Pure) [Present price]	280 [452]	20[h] [29]	120[h]	6.5[h] [10.9]	50[h] [477]	75[h] [186]	136	2800[i]	300[i]	2000[i]	170[h]
16. Estimated Future Price, $/W	16	21	5	15.5	2	220	10	20	540	17	64
17. Curies/Gram (100% Basis)	1130	142	3394	87	3180	928	6048	4500	17	3320	81
18. Curies/Watt	65	148	102	207	124	2788	445	32	30	28	29
19. Total kWht/initial gram for (yr) mission	575 (5)	74 (10)	210 (1)	33 (10)	150 (1)	6 (3)	33 (0.4)	350 (0.4)	47 (10)	310 (0.4)	190 (10)
20. Minim Cost, $/$kWh_e$[k] for (yr) mission	15 (5)	6 (10)	23 (1)	4 (10)	11 (1)	350 (3)	125 (0.4)	235 (0.4)	138 (10)	180 (0.4)	22 (10)
21. Spontaneous Fission Half-Life, Yr	---	---	---	---	---	---	---	---	4.9×10^{10}	7.2×10^{6}	1.4×10^{7}
22. Estimated Recovery from Power Reactor Fuels: g/metric ton at 25,000 MWd/ton	---	360	53	835	89	60 (aged)	---	---	(345 Np)	---	9(200 Pu Recycle)
23. Production in Power Reactors Kg/1000 MWY_e	---	16	2.3	36	3.8	2.6 (aged)	---	---	(15 Np)	---	0.4 (9 Pu Recycle)
24. Availability in 1980, KW_t[l]	MWs	1200	11,000	1200	8400	53	MWs	MWs	250[l]	---	93 156[m]

DEFINITIONS:

(a) Could be produced at higher concentrations, at least double this value, with higher neutron flux and longer exposures.

(b) From U.S. power reactor fuels, 1 year after discharge (one half-life for Pm).

(c) Metal may be preferred: m.p. = 1080°C (F. Weigel, Angew. Chem. 75 451 (1963); expected power density = 2.3 W/cm^3.

(d) Does not include the usual 1:1 void volume allowance for helium pressurization with this and all other encapsulated alpha emitters.

(e) Capsule is a right cylinder with diameter = height; ^{210}Po and ^{242}Cm assumed to be diluted to 50 W/cm^3. Capsule wall thickness is 0.3 cm.

(f) From spent fuels from civilian power reactors (150,000 MW_e in 1980), except for ^{60}Co, ^{170}Tm, ^{210}Po which could be produced in megawatt quantities via neutron irradiation of targets.

(g) Except for shielding against neutrons, Number in parentheses indicates approximate inches of lead shielding required for 1 KW source for 10 mR/hr at 1 m. (See *ORNL-3576 except for promethium.*)

(h) From large, civilian, power reactor, spent fuel processing and isotope recovery facility, after 1970 (see BNWL-25).

* α Alpha
β Beta
γ Gamma
η Neutron
χ Penetrating bremsstrahlung

Source: Battelle Memorial Institute

(i) Upward revision of minimum costs shown in "Holsted-Albaugh Hanford Diversification Report," 1/15/64, p. 13.

(j) Anticipated price with large scale reactor fueling with plutonium (Pu at $10/g), and ^{241}Am recycle.

(k) At terminal or lowest specific power, (Wg); at 5% thermal-to-electrical conversion efficiency. For comparison, power from chemical batteries (specifically flashlight batteries) is calculated to cost $100/$kWh_e$.

(l) From accumulated ^{237}Np from spent fuels from civilian power reactors (550 kg neptunium recoverable in the year 1980).

(m) With recycle of plutonium and americium.

(n) This chart is an extension of Table VI, page 52, HW-76323, Rev 1, "Radioisotopic Heat Sources," 10/15/63. C.A. Rohrmann, Batelle-Northwest, Richland, Washington. Re-issues are made about twice a year to include the most current data. Users of previous issues will note the omission of ^{171}Tm, ^{204}Tl, ^{228}Th, ^{232}U and ^{241}Am which are not expected to be available in kW or Kg quantities because of large investments required for R&D and production.

160,000 CURIES

≈ 50 WATTS (SUMMER '68)

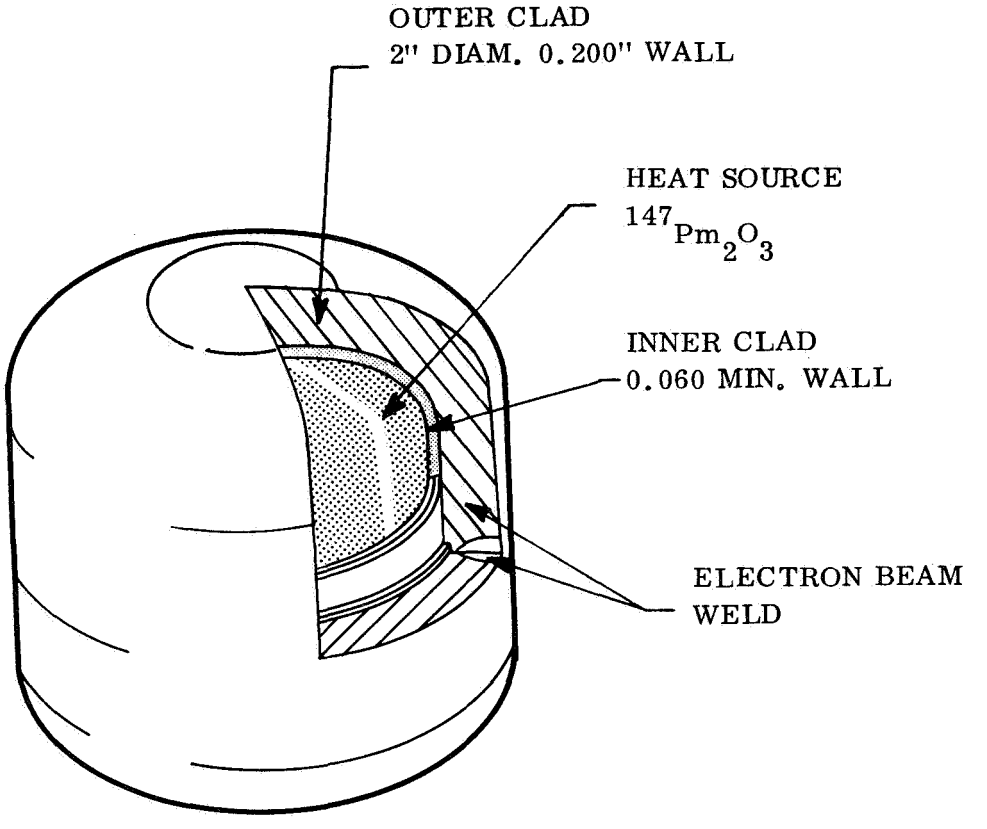

Figure 1. AMSA Thermal Power Capsule

very little flat surface to use for heat transfer from the capsule. The curved surfaces do not make good interfaces because of the exact tolerance on the radius of the mating part. Furthermore, the large difference in the part temperatures between the time the capsule is loaded and when it is operating at cathode temperature requires a very close match in thermal expansion.

4.1 TUBE DESIGN

To demonstrate the feasibility of non-electric cathode heating, a General Electric L-65 planar triode vacuum tube was chosen. This tube was chosen due to its readily accessible cathode, small physical size, relatively low cost, and rapid availability with the required modifications.

The General Electric Company's Research and Development Center undertook the modifications necessary to incorporate a heat pipe within the L-65 cathode structure.

4.1.1 STANDARD CONSTRUCTION

The construction of the anode, grid, and insulator sections of the tube was performed according to standard procedures. Note should be made of the fact that the method used on the L-65 to accomplish the ceramic-to-metal seals possesses several unique advantages (Ref. 1). Sealing metal and ceramic parts by forming reactive alloys, with titanium in this case, produces seals that are capable of operation at high temperatures. The seals are strong and durable and can withstand repeated cycles between 600^{o}C and room temperature; they have been shown to be unaffected by exposure to nuclear radiation for periods in excess of 1000 hours.

4.1.2 L-65 MODIFICATIONS

In the final design, shown in Figure 2, a 599 nickel disk is brazed to the end of the heat pipe protruding into the vacuum tube. This disk is coated with barium strontium oxide to form the cathode. The grid-to-cathode dimension (0.051 millimeter) is maintained by the spacer (grid to cathode) shown in Figure 2. The heat pipe/platinum seal interface is held against this spacer by atmospheric pressure. In a vacuum environment a light spring pressure would be used to hold the platinum seal on the spacer and thus preserve the cathode-to-grid dimension. Outside the tube envelope, a portion of the heat pipe is threaded to provide a means of attachment to a heat source. Above the threads, the pipe is machined to a hexagonal cross section so that a wrench can be used to avoid placing a torque on the thin platinum (0.127 millimeter) seal shown in the figure.

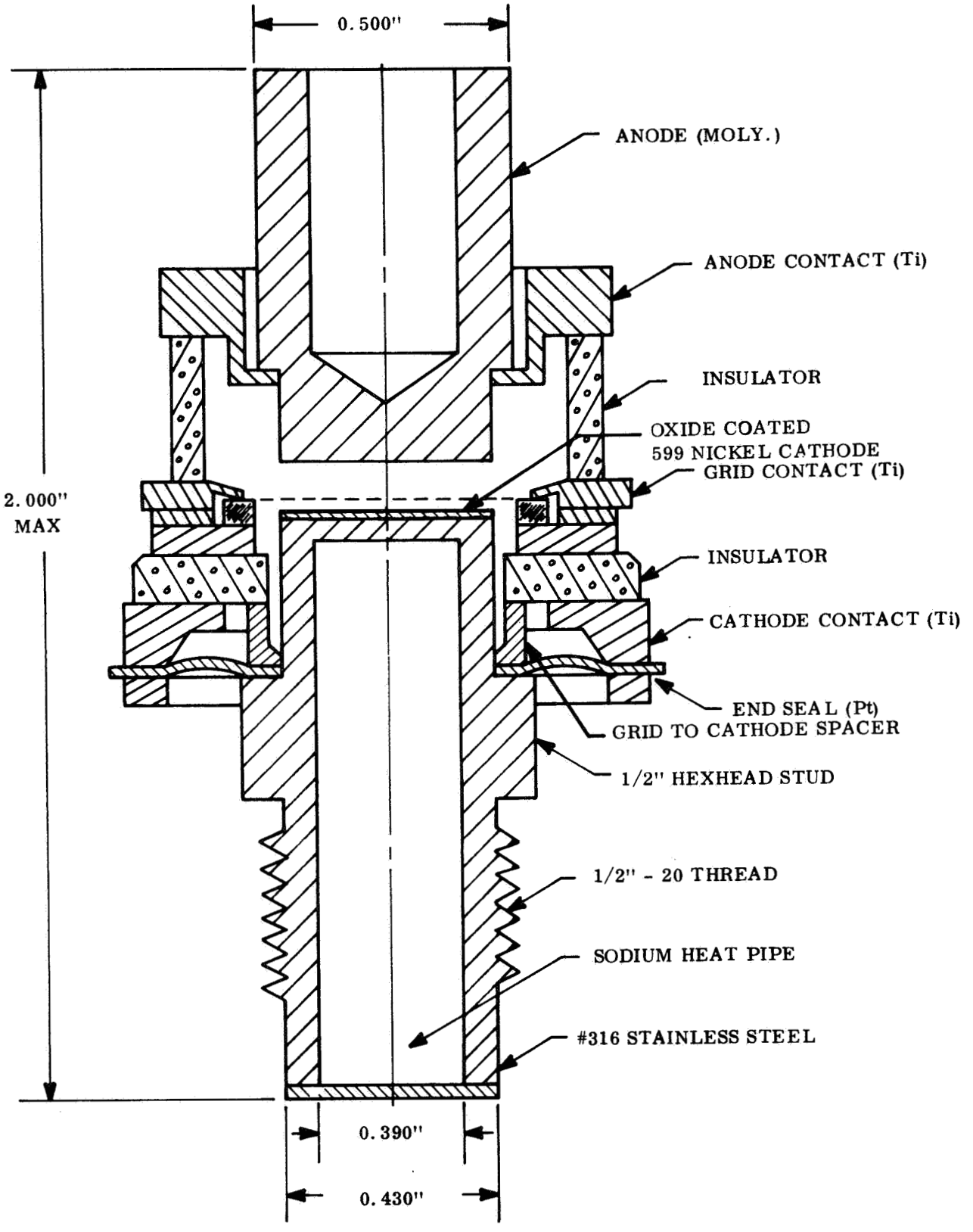

Figure 2. GE Triode with Heat Pipe Cathode

Heat transfer is through the threads and wall to the working fluid where vapor flow carries it to the cathode end. The condensing vapor transfers the heat to this surface where it is conducted through to the oxide layer which forms the cathode. If the heat source is at a high enough temperature, sufficient cathode emission is provided to obtain the proper characteristics.

In the manufacture of the modified L-65, designated L-65RIH, the primary problems encountered were due to a requirement that the tube be capable of operating in air. For a standard vacuum tube, this presents no problem, since the cathode is completely internal. Thus, corrosion due to high temperatures can be prevented by thermally isolating the hot cathode from surfaces of the tubes which are in contact with air. The heat pipe, however, being an isothermal device, operates at cathode temperature over its entire surface. Since this includes surfaces outside the tube vacuum envelope, corrosion must be considered in the choice of a heat pipe material. Type 316 stainless steel was chosen due to its resistance to corrosion both by air and sodium and its acceptable mechanical properties at temperatures up to 750^{o}C. This choice of material, however, introduces two additional problems, differential expansion and the high-temperature braze between the stainless steel and the end seal. The differential expansion between the heat pipe and other parts of the tube was taken care of by making the end seal from very thin material with a slight convolution to provide stress relief. The end seal itself was made from platinum due to its corrosion resistance. The braze between the stainless steel and platinum was made using copper at 1080^{o}C. Prior attempts using gold failed due to severe embrittlement of the platinum in the vicinity of the braze.

Three L-65 RIH tubes were constructed. End caps were brazed over the open ends of the heat pipes during tube bake-out to guard against contamination. Figure 3 shows the three tubes with the end caps in place.

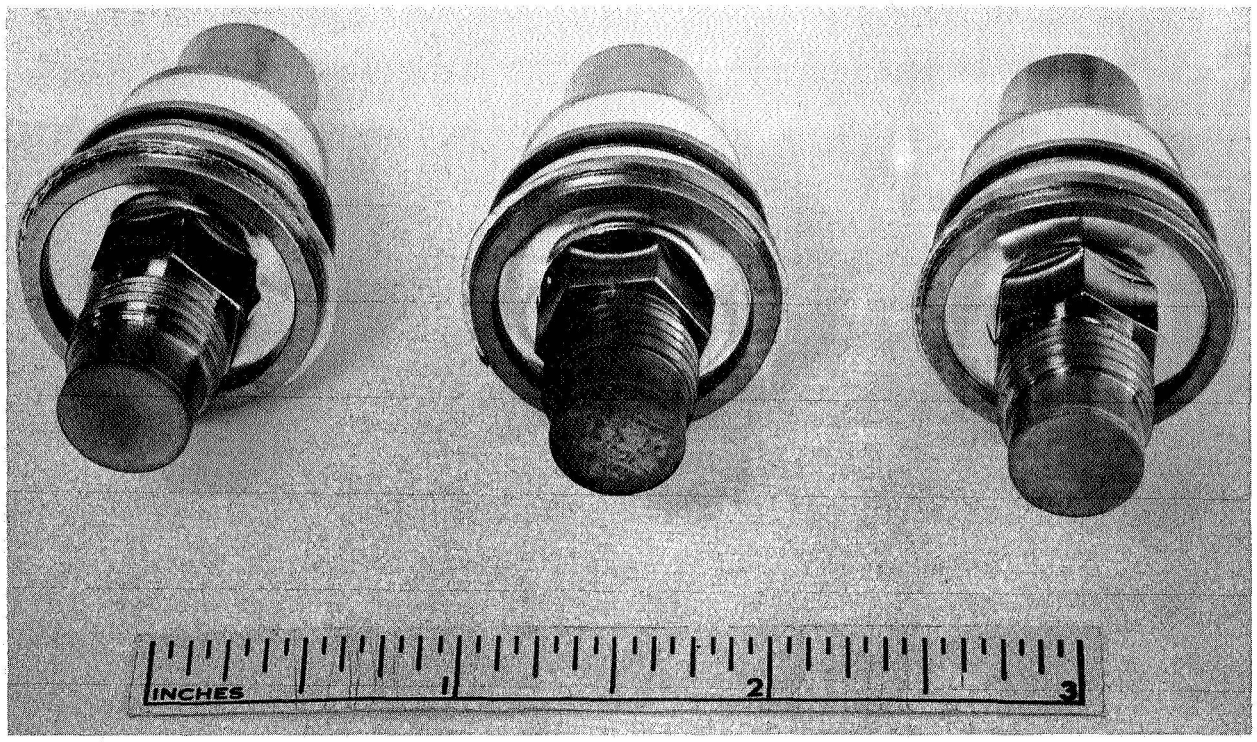

Figure 3. Triodes Prior to Filling

4.2 HEAT PIPE DESIGN

4.2.1 WORKING FLUID SELECTION

Criteria for selection of the heat pipe working fluid include the following: (1) liquid transport parameter $\frac{\rho_\ell \gamma \lambda}{\eta_\ell}$, a means of evaluating the performance of the various fluids in a capillary transport system; (2) vapor phase velocity parameter $\lambda \rho_v$; and (3) limiting level of evaporation heat flux. For each of these parameters the material with the highest value is the most favorable selection. The emission temperature of the cathode suggests sodium, potassium, and cesium as possible working fluids. Parameters (1) and (2) above are plotted versus temperature in Figures 4 and 5 for the three candidate working fluids. Vapor velocity in the heat pipe is plotted versus temperature for Na, K, and Cs working fluid in Figure 6. In order to better evaluate the effect of vapor velocity on heat pipe performance, a calculation was made of the condensate flow Weber

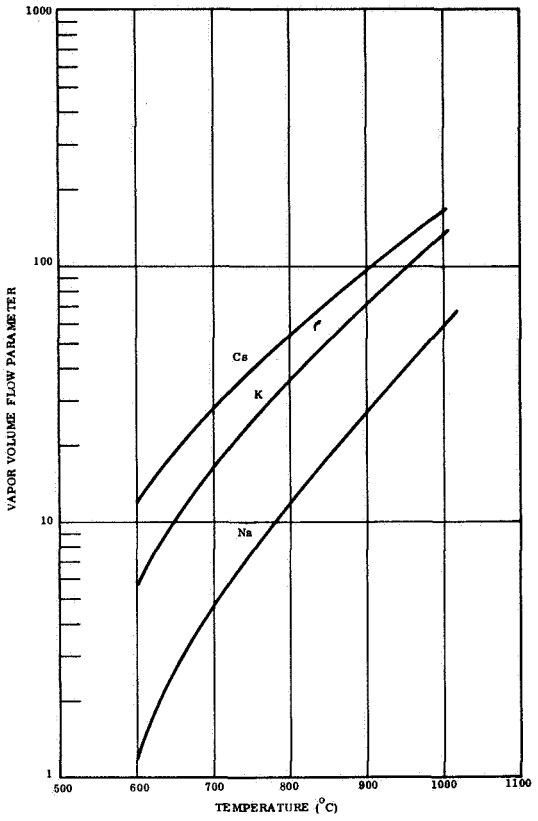

Figure 4. Vapor Volume Flow Versus Temperature

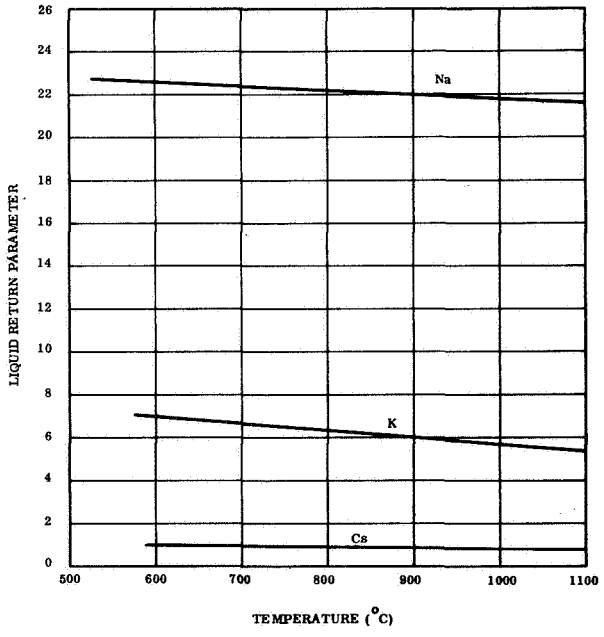

Figure 5. Vapor Velocity Parameter Versus Temperature

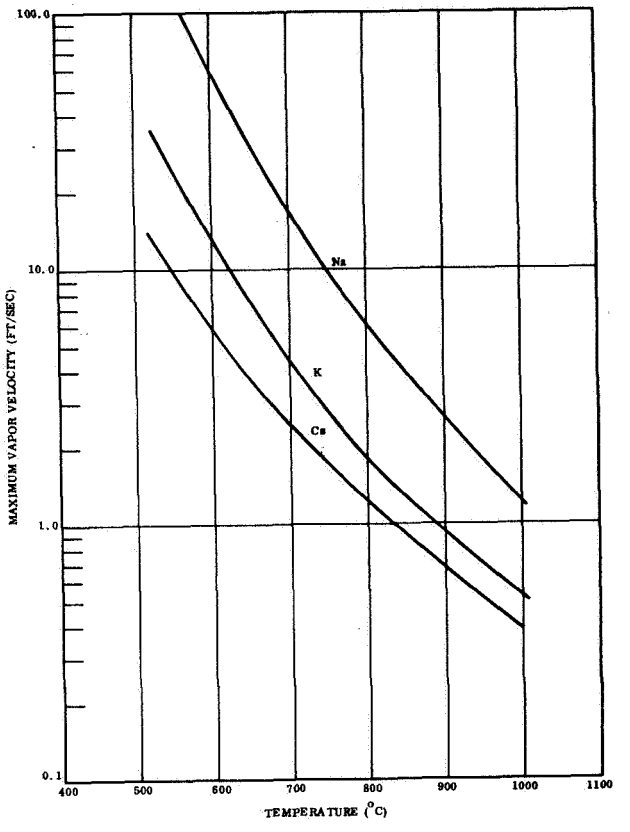

Figure 6. Maximum Vapor Velocity Versus Temperature

number defined as $\frac{\rho_v V_v^2 d}{\gamma}$. This Weber number parameter is a measure of the ratio between dynamic vapor flow entrainment forces (those forces which tend to dislodge liquid from the wick) on the return liquid stream and the surface tension forces. Its value should be well below 1. For the 600°C operating condition, which is the most severe condition considered, the Weber numbers for Na, K, and Cs are, respectively, 0.008, 0.0067, and 0.062 (for wick spacing of 0.025 centimeter), all of which are low enough that fluid entrainment in the vapor stream should be no problem. It is interesting to note that although Cs has the lowest vapor velocity, it has the highest Weber number parameter. This is due to high vapor density and low surface tension. Sodium, with the highest vapor velocity, because of its low vapor density and high surface tension, has a Weber number parameter value close to that of potassium.

In order to better evaluate the comparison between condensate flow parameters, the wick friction head $\frac{\Delta P}{P_\ell}$ was calculated for the three fluids. This parameter is insensitive to temperature and has the values 0.027 centimeter, 0.0495 centimeter, and 0.0576 centimeter for sodium, potassium, and cesium respectively. All of these values are quite low, and may be compared against demonstrated wick pumping heads of approximately 15.3 centimeter for sodium, 7.62 centimeter for potassium, and 2.28 centimeter for cesium.

The conclusion which can be reached is that all three fluids--sodium, potassium, and cesium--are satisfactory as heat pipe working fluids. Sodium is the preferred choice because of its superior liquid transport and heat transfer characteristics.

4.2.2 WICK FABRICATION

This phase of tube fabrication was performed at General Electric's Space Power and Propulsion Facility at Evendale, Ohio, since the tube development laboratory at Schenectady was not equipped for heat pipe work. Where larger numbers of tubes are to be fabricated, tube and heat pipe fabrication processes, being similar in nature, could be combined.

A special aluminum fixture was fabricated, into which the triodes could be screwed. After screwing each one in, the caps were removed on a lathe, the motor and cutting tool of which had been reversed so that the torque on the triode tended to tighten rather than loosen the triode in the fixture. No torque was placed on the platinum diaphragm during this operation. The wicks were formed from 59 x 59 mesh per centimeter (150 x 150 mesh per inch), plain weave, type 316 stainless steel screen made of 0.0762 millimeter (0.003 inch) diameter wire. The aluminum mandrel shown in Figure 7 was used to form the precut screen; and the outer tube, also shown in Figure 7, was used to hold the screen during spot welding. Each wick consisted of three full layers of screen made by overlapping a single continuous strip. The wicks had an outside diameter of 0.99 centimeter (0.390 inch), an inside diameter of 0.88 centimeter (0.347 inch), and a length of 2.108

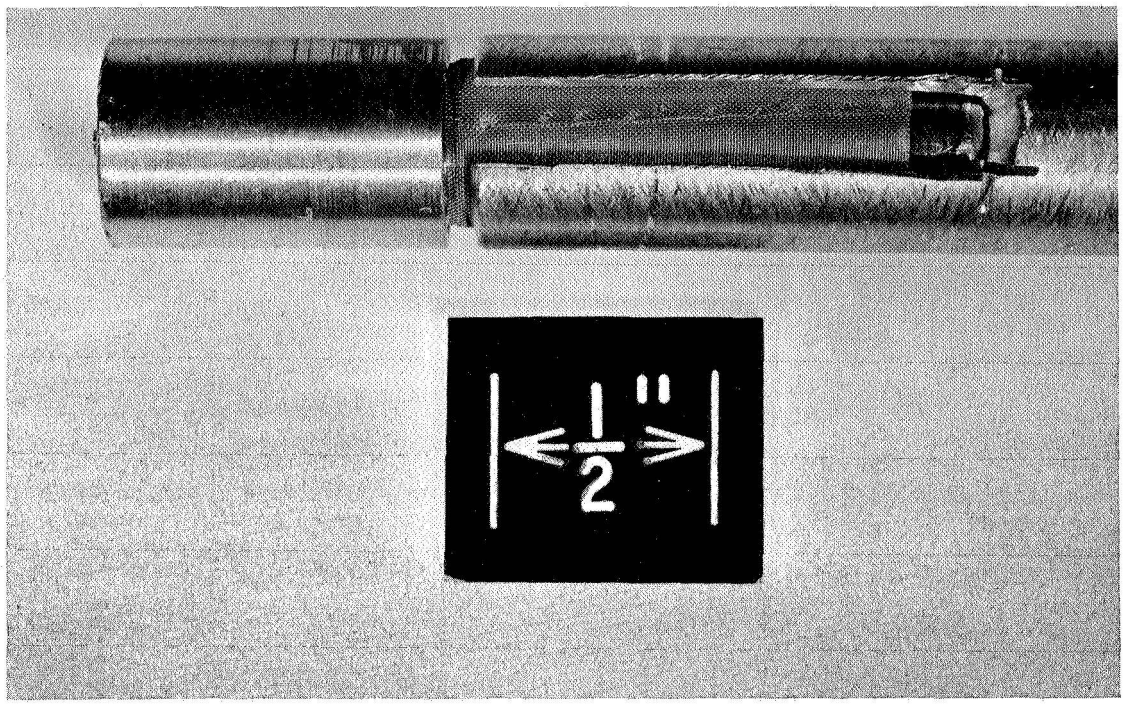

Figure 7. Wick Forming Mandrel

centimeter (0.83 inch). In order to provide an uninterrupted path for the liquid sodium to return to the boiling area under the threads from the condensing area under the cathode, the end of the wick was notched and bent over the end of the mandrel as shown in Figure 8.

After fabrication, the wicks were cleaned ultrasonically in acetone and alcohol, and then in an alkaline cleaner at 77°C. They were then washed in distilled water, and finally they were pickled.

The cathode cavity was polished with emery cloth around the top, inside and outside, to remove any brazing alloy that might have remained after removal of the caps. The inside of the cathode cavity was then cleaned and pickled.

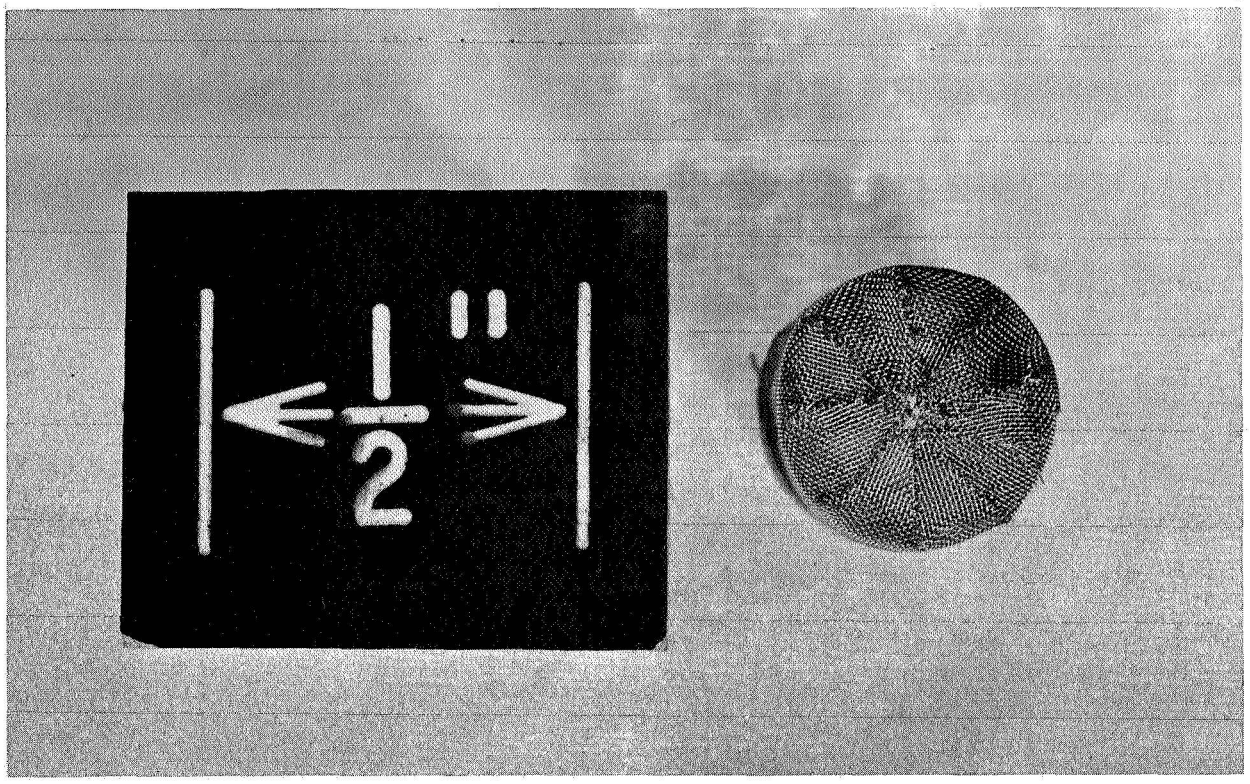

Figure 8. Cathode End of Wick

Finally, the wick, shown in Figure 9, was pushed into the cathode cavities. The bottom of each wick was tack-welded to the bottom of the cathode cavity. During insertion of the wicks the triode was held in the same fixture that was used during the removal of the caps so that no stress was applied to any other part of the triode. Figure 10 shows the cathode end of a triode after insertion of the wick.

4.2.3 SODIUM FILLING PROCEDURE

New caps were made for the cathode cavities from type 316 stainless steel and placed in the electron beam welding chamber along with the triodes and the extruder containing the sodium. The triodes were screwed into specially built copper chill blocks and the welding chamber seated. The chamber was then pumped down overnight to a pressure of 5×10^{-5} torr and then back-filled to one atmosphere with argon. The glove ports were then opened.

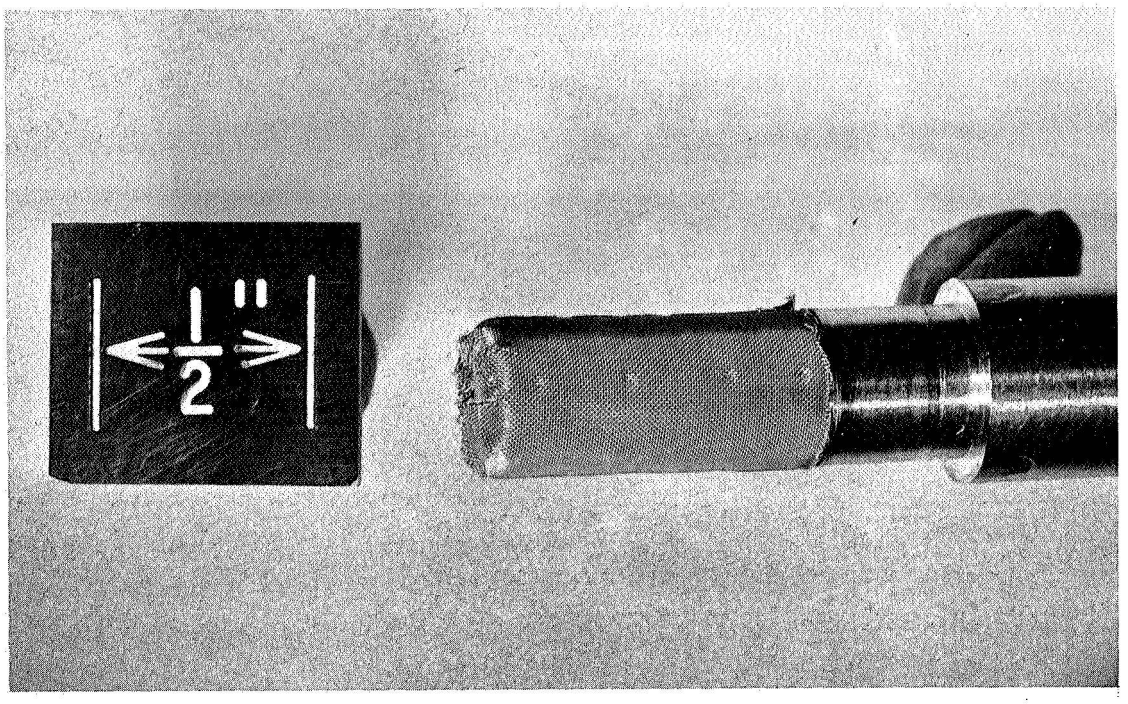

Figure 9. Completed Wick

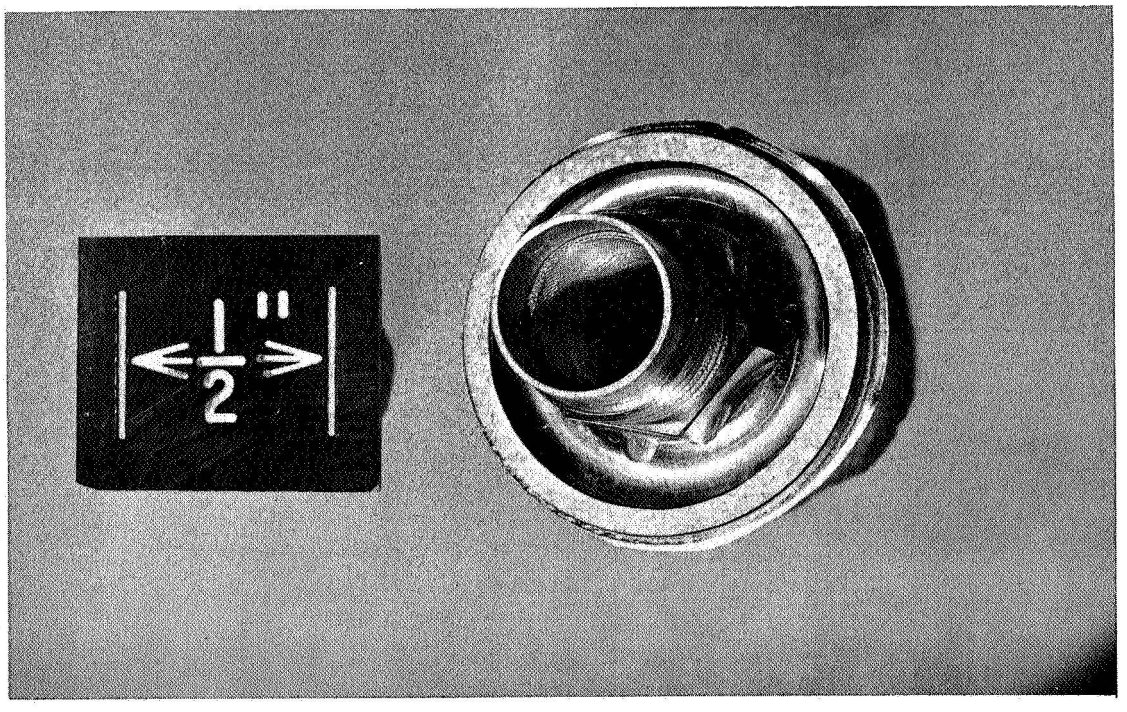

Figure 10. Completed Heat Pipe

The Swagelok fitting on the extruder was removed, and a waste piece of sodium was extruded and cut off. The sodium was extruded through a 0.635 centimeter (0.25 inch) ID stainless steel tube. A piece 1.397 centimeter (0.55 inch) long was extruded and cut off with a stainless steel spatula for each triode. This represents a volume of 0.44 cubic centimeter of sodium. The sodium sticks to the spatula, but can be detached from it and dropped into the cathode cavity quite easily.

After inserting the sodium, the caps were placed over the cathode cavities and the welding chamber was evacuated to less than 5×10^{-5} torr. The fixture holding the triodes was then traversed to the opposite end of the welding chamber and the caps electron beam welded in place.

The entire filling procedure was performed on an incomplete triode containing a wick prior to filling the completed triodes in order to qualify the techniques used.

During the filling and welding procedures two problems were anticipated. The first was that the cylinder of sodium would stick to the wick and be prevented from dropping to the bottom of the cathode cavity. This did not occur. The second was that during the welding operation, the sodium would melt and creep up the wick and wall and contaminate the weld. The coppor chill blocks were able to prevent this.

4.2.4 SODIUM PURITY

The sodium used to fill the triodes was reactor grade sodium which had been hot trapped with zirconium in a titanium lined, stainless steel hot trap for at least 20 hours at 704°C (1300°F). Prior to filling the triodes, samples of the sodium which was used were extruded and analyzed. The results of these analyses, reported as parts per million in sodium, are shown in Table II.

Although the increase in oxygen content caused by exposure to water vapor and oxygen in the welding chamber is unknown, previous experience indicates that the oxygen

Table II. Analysis of Sodium Used in Cathode Heat Pipe

Element	PPM in Sodium
Oxygen	6-9
Carbon	25
Silver	< 2.5
Aluminum	< 2.5
Boron	< 37
Barium	< 13
Beryllium	< 2.5
Calcium	< 2.5
Columbium	< 13
Cobalt	< 2.5
Chromium	< 2.5
Copper	< 2.5
Iron	< 2.5
Magnesium	< 2.5
Manganese	< 2.5
Molybdenum	< 2.5
Nickel	< 2.5
Lead	< 13
Silicon	< 2.5
Tin	< 13
Strontium	< 2.5
Titanium	< 13
Vanadium	< 2.5
Zirconium	< 13

content of the sodium after final closure was less than 50 parts per million. This conclusion was drawn because samples of liquid sodium and potassium taken in the evacuated welding chamber during capsule filling have shown increases in oxygen content of no greater than 10 parts per million. In this case, the liquid metals enter the capsules as a fine stream or as small drops. Furthermore, no discoloration of the sodium used to fill the triodes was noted during the filling operation.

4.2.5 L-65 RIH OPERATIONAL TEST

In order to verify the operation of the L-65 RIH, a series of test was run using an electric heater block to attain emission temperatures. This block was fabricated from a dowel of hot pressed boron nitride. It had a nichrome wire heater wound about it and included a tapped hole to accept the threaded end of the L-65 RIH heat pipe. A thermocouple was installed in the boron nitride block to monitor temperature.

The tubes were placed in the 150-megahertz Colpitts oscillator circuit described in Figure 11. Satisfactory performance was achieved at cathode heat pipe temperatures of 720^{o}C to 800^{o}C.

Figure 12 is a representative display of the characteristic curves of the L-65 RIH. An identical tube in which the heat pipe was not filled with sodium barely began to emit with the heater at slightly over 800^{o}C, showing that the heat pipe was indeed operating. Since the temperature drop from evaporator to condenser has been shown to be very nearly the same for far greater lengths, nearly identical operation can be expected where the heat pipe is much longer. Two of the three tubes showed excellent emission characteristics at temperatures between 700^{o} and 800^{o}C, while the third tube appeared to need additional cathode aging.

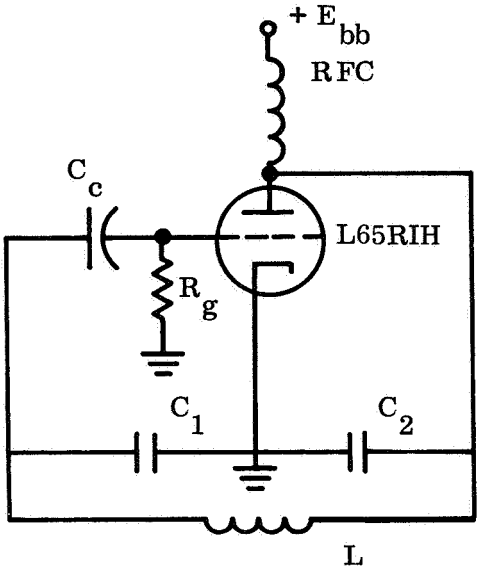

RFC	OHMITE Z 144
C_c	470 PF
C_1	0.8 TO 18 PF PISTON TRIMMER
C_2	8 PF
L	0.15 μH

Figure 11. 150-Megahertz Colpitts Oscillator Circuit

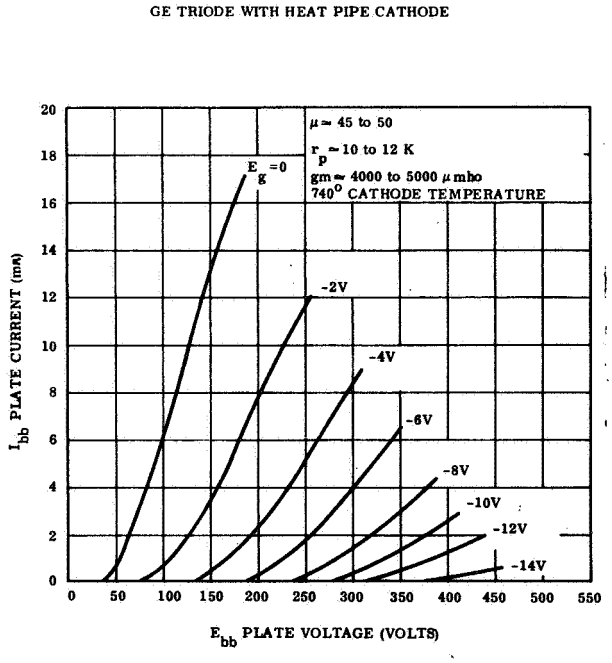

Figure 12. Triode Characteristics

4.3 RADIOISOTOPE SOURCE ENCLOSURE

4.3.1 INITIAL DESIGN

Initial calculations for an effective thermal conductivity of the source insulation and mounting supports must not exceed 3×10^{-4} w/cm^2 ^oC. This was based on the assumption that the source would have 48 watts of thermal output at the time of test, the source and device attaching it to the L65RIH would have a surface area no greater than 232 cm^2 (0.25 ft^2), and the cathode heat pipe interface temperature would be 700^oC.

The initial attempt at mating the isotope with the L-65 RIH is illustrated in Figure 13. As shown, the isotope simulator was clamped between two contoured copper blocks forming a cylinder 8.64 centimeters long and 7.62 centimeters in diameter. One of the blocks contained a tapped boss to accept the cathode heat pipe; beneath the boss an 8-inch diameter disk was attached by high temperature brazing. This disk formed the lid of a container that housed the copper blocks with the enclosed isotope simulator. The inside diameter of the container was 12.7 centimeters (5 inches) and its depth was 15.24 centimeters (6 inches).

With the lid in place, the copper blocks were suspended in the can. The space between the blocks and the container wall was filled with 20 layers of 1 mil stainless steel foil insulation separated by 5 mil nickel wire. With this method the insulated isotope was contained in a vacuum environment while the vacuum tube was exposed to the atmosphere.

Ports were installed in the container for attaching a vacuum pump. Electrical and instrumentation penetrations entered the container through the lid.

The system was constructed of 316 stainless steel, and the seal between the lid and the container was made with a silicone rubber O-ring.

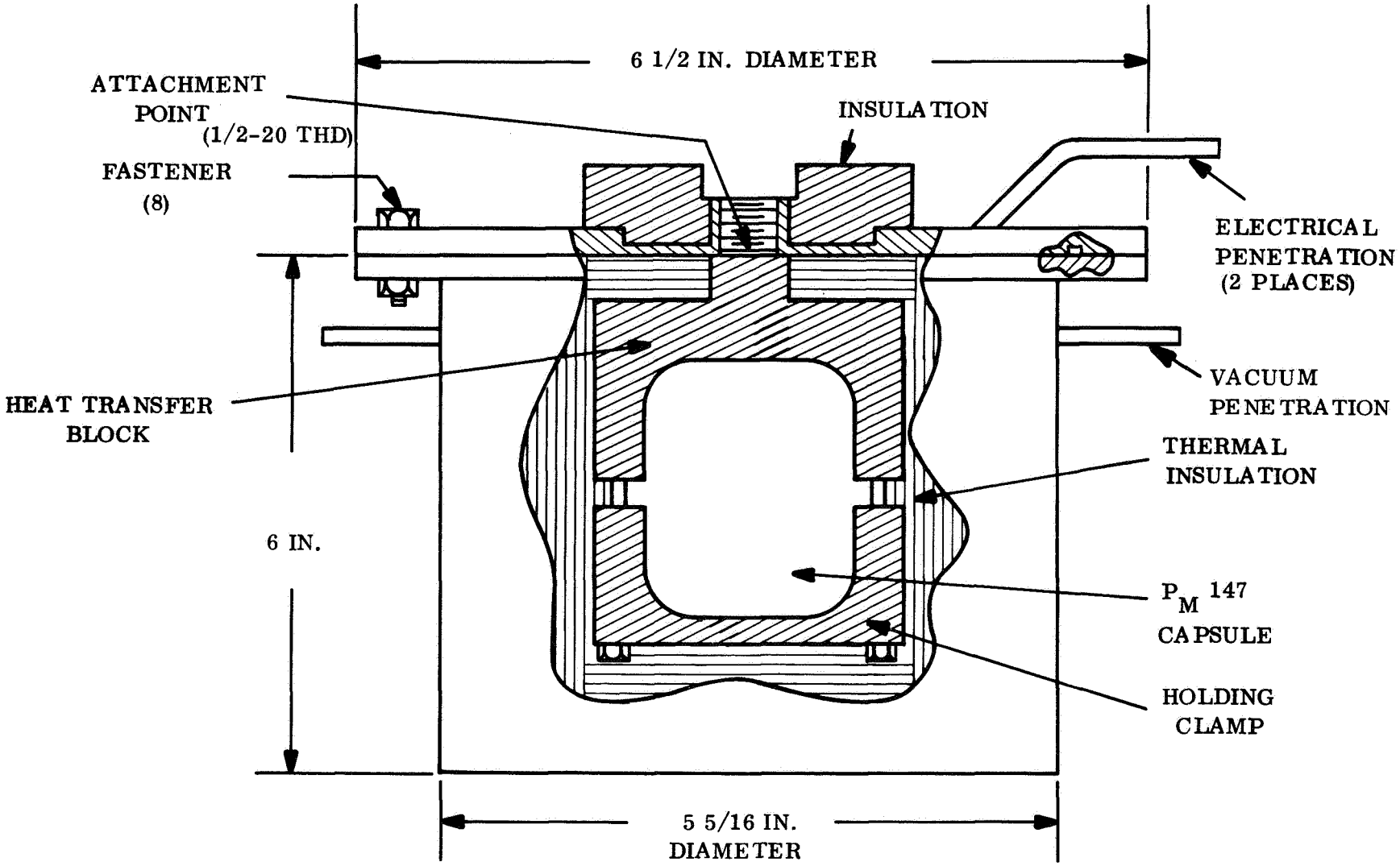

Figure 13. Isotope Heater Insulation

The insulation effectiveness was predicted upon reaching a vacuum of 1×10^{-5} torr. During trial runs with the electrically heated isotope simulator, however, it was found that the silicone O-ringseal reached a temperature of 300^{o}C. The temperature rating of the seal compound for continuous duty was 232^{o}C.

Degradation of the seal effectiveness, compounded by warpage of the lid of the container, caused leakage around the lid that prevented the vacuum from going below 300×10^{-3} torr. At this pressure 48 watts of isotope simulator power was not sufficient to attain emission temperature at the cathode heat pipe.

4.3.2 FINAL DESIGN

Although the leakage problem could have been solved by increasing the number of bolts used to hold the lid to the canister and replacing the silicone O-ring with a metal O-ring, the acquisition of a metal seal of this particular size would have affected the scheduling of the preliminary cathode heating tests. To eliminate this problem a method was devised to insert both the isotope and the electron tube into a vacuum chamber. Another set of copper blocks was machined. This set did not have a lid attached and allowed the L-65 RIH to be positioned closer to the isotope. Provisions were made to suspend the copper blocks enclosing the isotope from a ring stand by means of 0.381 millimeter (0.015-inch) nickel wires. This assembly would then be insulated as before with stainless steel foil and installed in a bell jar vacuum system.

Early test runs to check out the mating of the isotope simulator with the copper blocks suggested that auxiliary heaters be added to the copper blocks to reduce the time constant of the system so that the system could be activated and tests run within the span of an 8-hour workday. Figure 14 is a sketch of the final design of the capsule heat transfer block.

While these blocks were being fabricated, the original set of blocks was modified to accept a heater cartridge. Chromel-alumel thermocouples were mounted on the copper blocks to monitor temperature.

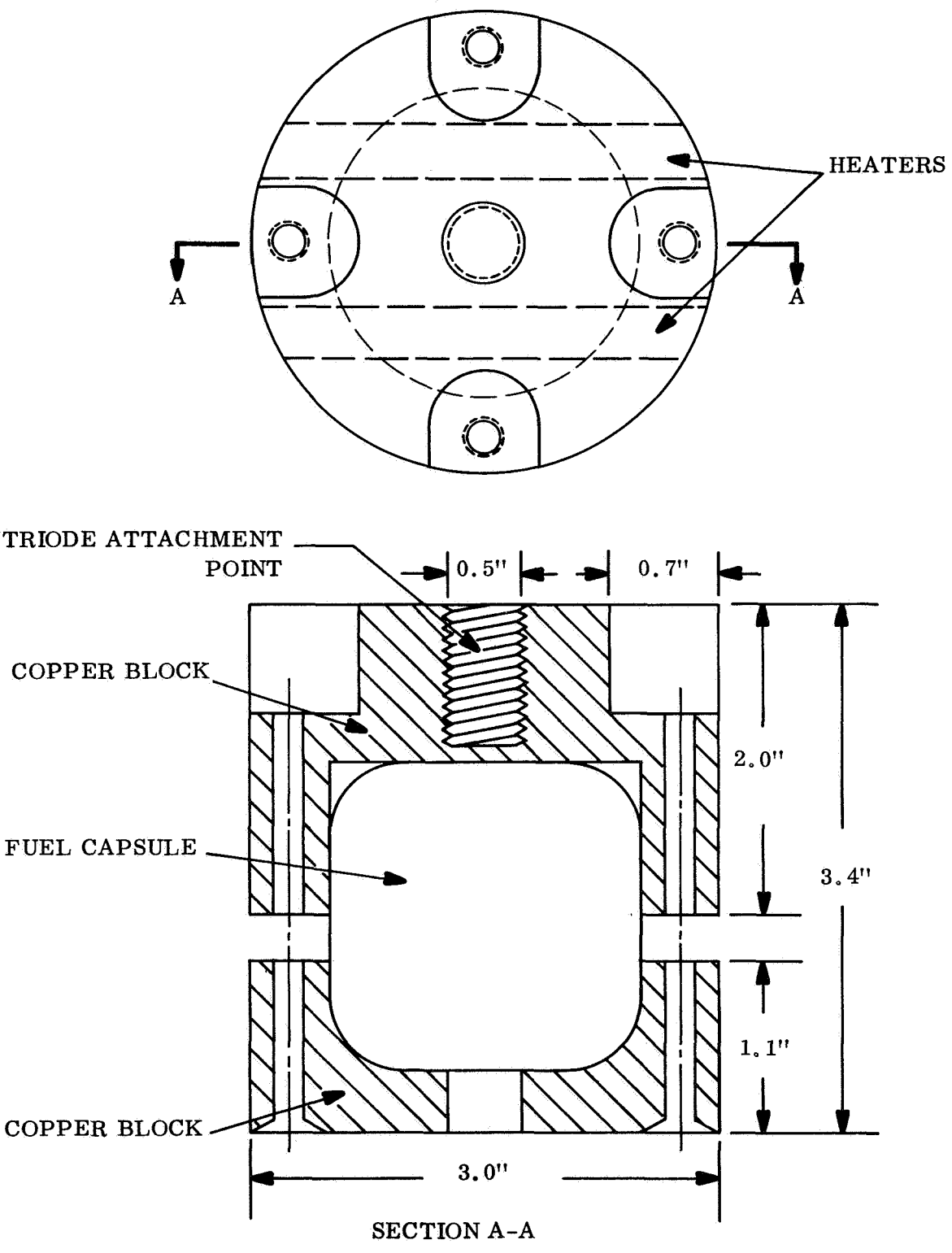

Figure 14. Heat Transfer Block

4.4 TESTING

Testing of the isotope heating concept was accomplished in two steps. The first series of tests was conducted using an electrical simulator to power the tube to determine system performance. The second and final step was the test to be run with the actual radioisotope. Because of the fact that special safety procedures were required with the radioisotope for runs, their number was kept to a minimum.

4.4.1 TESTING USING THE ELECTRICAL ISOTOPE SIMULATOR

The electrical and thermal performance of the L-65 RIH was checked periodically during the testing sequence to determine if its characteristics had been changed in any way due to handling. This check was performed by attaining emission temperature with the boron nitride heater and observing and noting the tube characteristic curves. The type of multilayer foil insulation described in Section 4.3.1 was used throughout the test series.

After the copper blocks with isotope simulator and L-65 RIH installed were suspended in the vacuum chamber and insulated with the foil, the assembly was covered with two layers of aluminum foil separated by refrasil felt to cover any remaining heat leaks. The chamber was evacuated and the assembly allowed to come to thermal equilibrium.

A temperature of 600^{o}C (1112^{o}F) was attained at the cathode heat pipe-copper block interface after 10 hours with an isotope simulator power of 48 watts. A small amount of cathode emission was noted on a vacuum tube curve tracer oscilloscope. The vacuum attained in the chamber was 1×10^{-4} torr, too high to provide the desired thermal performance from the insulation. The test was terminated and an attempt was made to improve the vacuum chamber performance.

4.4.1.1 Heat Pipe Failure

In the interim, while the L-65 RIH was undergoing a routine operational check with the boron nitride heater, a heat pipe failure occurred. A hole appeared immediately

above the threaded portion of the cathode heat pipe. Testing was halted as a study was made to investigate the mechanism of the failure. A survey of the test history of this particular tube showed that the heat pipe had several excursions above 800°C (1472°F) during testing.

According to the electrochemical theory of stress corrosion cracking proposed by Dix (Ref. 2) in 1940, it is believed that chromium carbides precipitated in the grain boundaries by this heating robbed the adjacent areas of chromium. These chromium-depleted areas were then active paths for corrosion (Ref. 3). A probable contributing cause was the fact that as thermal stresses increased with temperature, these areas became stressed in tension and thus were more susceptible to attack by liquid metal.

4.4.1.2 Boron Nitride Heater Arcing

The second L-65 RIH was installed in the vacuum system using the same techniques demonstrated with the first tube. The tube emission was similar to the first tube. As an operational check was being made of the second tube while installed in the boron nitride heater (see Figure 15), a short occurred in the nichrome heater windings and the resultant arc punctured the thin platinum end seal above the cathode heat pipe hex nut.

4.4.2 TESTING WITH THE PROMETHIUM-147 RADIOISOTOPE

The temperature at which the cathode was operated was determined by the configuration and power of the capsule used in the test. While analysis had shown that a temperature below 700°C would be attained, the isotope demonstration was performed since the characteristic of the cathode, shown in Figure 16, indicated that emission temperature would be achieved.

Handling procedures for the isotope capsule were developed during several practice runs made using the isotope simulator. During these runs the techniques used to move the capsule from its shipping container to the copper isotope capsule heat transfer blocks were checked to ensure that the capsule would not be dropped and that personnel would not be subjected to significant exposure to the radioactive material.

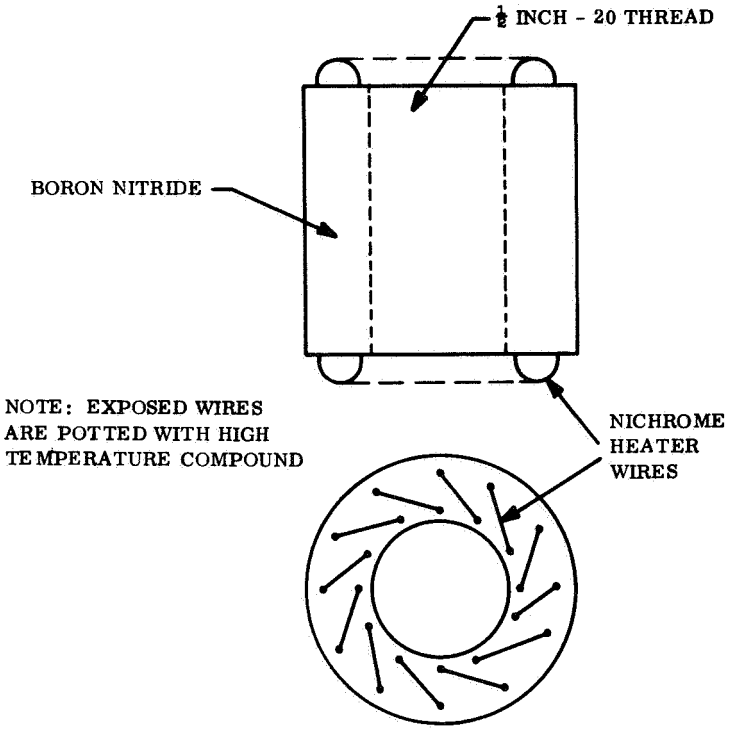

Figure 15. Electrical Heater

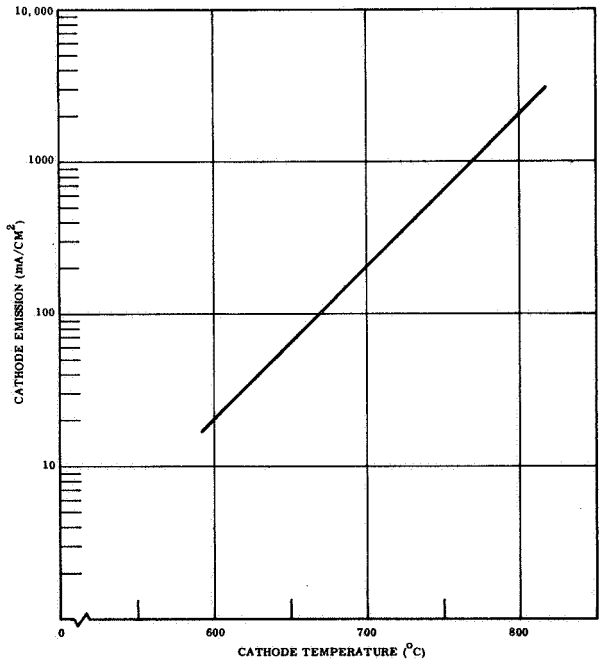

Figure 16. Typical Cathode Characteristics of L-65 Oxide Cathode

4.4.2.1 First Test With Isotope

The isotope was loaded into the copper blocks, the L-65 RIH was inserted into the threaded section of the block, and the assembly was insulated and suspended from a ring stand just as was done during the electrically powered simulator tests. Figures 17, and 18 show that test setup in various stages of preparation. In Figure 18, the system is ready for test.

The vacuum system was evacuated and the auxiliary heaters were powered to bring the system to equilibrium. The heaters failed after 4 hours of operation. The cathode heat pipe temperature was 482°C (900°F). At this point the vacuum system developed a leak in an instrumentation penetration, and some backstreaming of silicone diffusion pump fluid occurred. This further reduced the effectiveness of the insulation; and although the isotope was allowed to remain in the system for 4 more hours, 588°C (1090°F) was the highest temperature reached at the cathode heat pipe. Although emission had been noted on the other L-65 RIH tubes at this temperature, this particular tube would not show emission on a vacuum tube curve tracer oscilloscope.

4.4.2.2 Second Test With Isotope

The isotope was removed from the system and the insulation cleaned and replaced. The vacuum system leak was repaired. The isotope was then placed in the system and the testing started again.

A temperature of 628°C (1163°F) was observed at the cathode heat pipe after 6 hours of operation. At this time a small amount of cathode emission was noted on a vacuum tube curve tracer oscilloscope.

4.5 DISCUSSION

The results of the test described in the preceding part of this section show clearly that a vacuum tube cathode can be heated with a non-electric heat source. The tube developed for this demonstration was tested at various times using three distinct heat

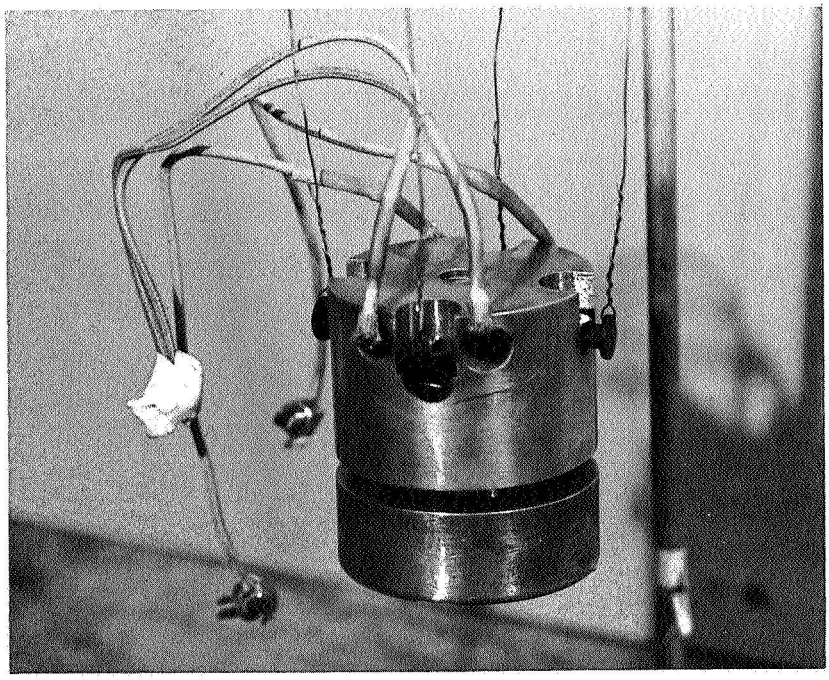

Figure 17. Heat Transfer Block

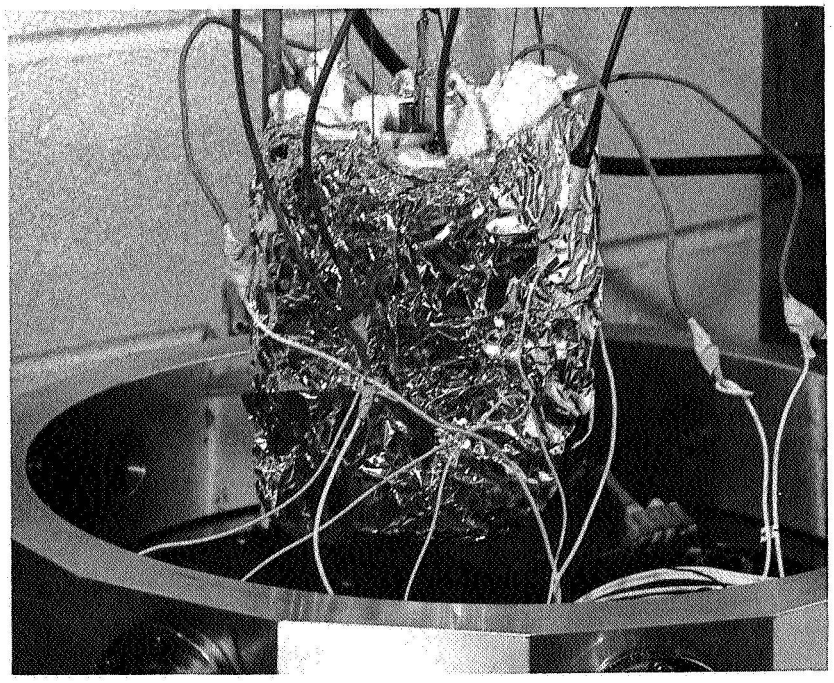

Figure 18. Insulated Assembly

sources. Immediately after the L-65 RIH was fabricated, a propane torch was used to heat the cathode in order to verify performance. Later, an electrical heater, previously described, was used during long duration testing. Finally, the promethium-147 thermal power capsule successfully heated the L-65 RIH cathode to emission temperature. While only a small amount of emission was actually attained, it is clear that only the configuration and level of power generated by the capsule limited cathode temperature and thus emission. Figure 19 shows the relationship between radioisotopic heat generation and cathode temperature for the configuration tested. By reducing the emissivity of the insulation layers, a significant improvement can be realized, as shown in Figure 19, since almost all of the heat is lost through the insulation. Gold plate on the layers of insulation would seem to be advantageous due to the low emissivity of gold, but at cathode temperatures intermetallic diffusion causes the gold to disappear in a matter of seconds, leaving the relatively high emissivity surface of the stainless steel.

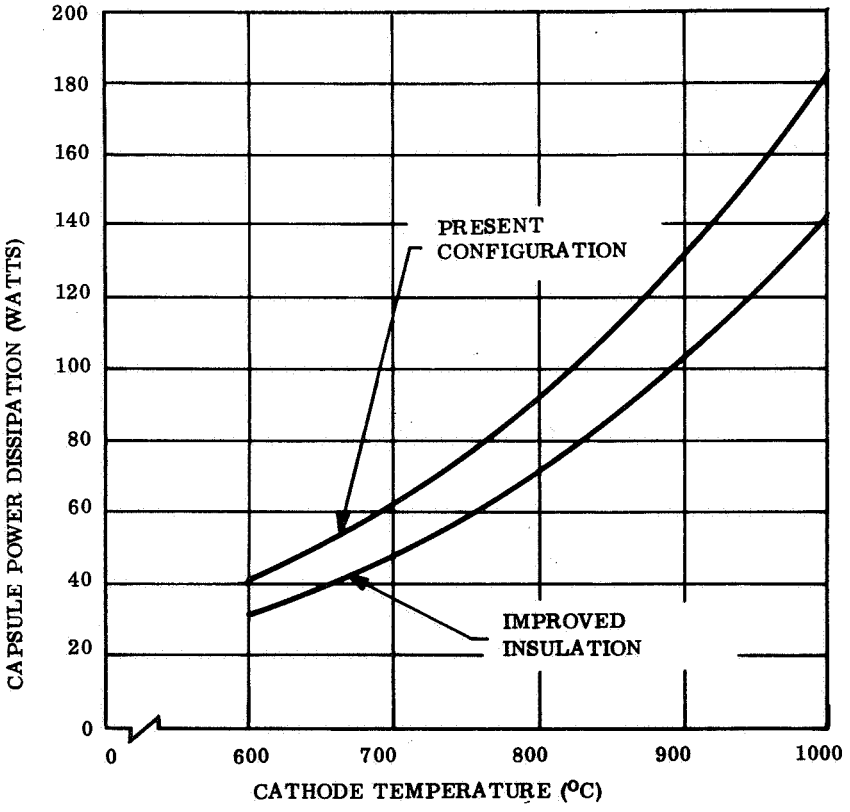

Figure 19. Cathode Power Requirements

As was mentioned at the beginning of this section, the direct application of heat from a high power density source is the most efficient, since exposed surface area at cathode temperature is minimized. The L-65 requires approximately 15 watts of electrical heater power in its standard configuration. If the isotope were small enough to fit inside the tube itself, little additional power above that required by the electrical heater would be needed.

Using the L-65 RIH as an example, the heat pipe can be merely left open for insertion of a curium-244 capsule. Using a 0.2 centimeter thick cylindrical container allows the cylinder of fuel to be 0.6 centimeter in diameter, since the heat pipe has a 1 centimeter internal diameter. Thus, the capsule generates 10.2 watts for each centimeter of length, excluding the end caps of the capsule. The heat leak from the exposed area of the isotope container can easily be kept below 10 watts. Thus the total power requirement is 25 watts. A typical arrangement is shown in Figure 20. Note the void shown in the capsule. This volume is required since alpha emitters give off helium, which in the current state of the art must be contained. Future designs may incorporate barriers which are permeable to helium but not to the radioactive materials, thus eliminating the need for the void.

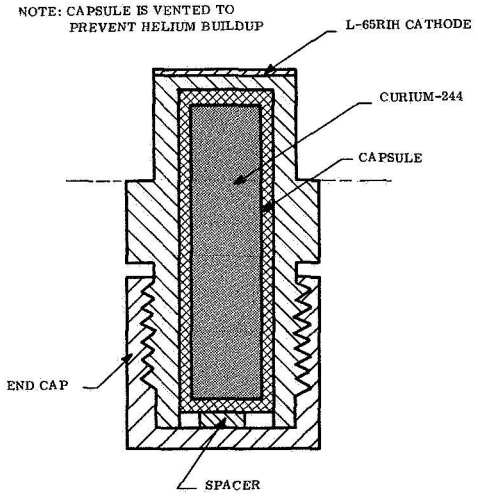

Figure 20. L-65 RIH Cathode with Directly Inserted Cathode

The direct application of isotope heat to a cathode has an advantage over any other spaceborne power supply in both cost and weight, excluding development costs. Table III shows the requirements for three power supplies. To provide a proper basis for the comparison, the electrical power requirement is taken at 15 watts, while the isotope is assumed to require an additional 10 watts to account for the added heat leak. As the figures show, direct heating has the advantage over both RTG and solar power. Development cost might tend to diminish the advantage of direct heating, however, since the spacecraft would be powered by either an RTG or a solar array and development costs are not a linear function of power.

Table III. Power Source Comparison

	Cathode Heating Method		
	Direct Isotope Heating (25 watt capsule)	Electrical Heater (15 watts)	
		RTG	Solar Power
Estimated Cost ($)	$3,600	$45,000	$10,500
Estimated Weight (kg)	0.068	4.8	6.7

Notes:
1. Isotope costs from Table I.
2. Isotope encapsulation and safety testing costs assumed to be $2000 for each of 10 capsules (cost for a single capsule would be considerably higher).
3. RTG weight taken to be 0.32 kg/electrical watt and cost at $3000 per electrical watt.
4. Solar power includes batteries and is assumed to weigh 0.45 kg/watt and cost $700 per watt.

SECTION 5

HIGH POWER MICROWAVE TUBE COOLING

Ground cooling of high-power microwave tubes is normally accomplished by forcing a cooling fluid through the heat-producing elements of the device and then cooling or disposing of the fluid. In a space vehicle, pumps and control valves introduce life-limited parts which severely limit the reliability of the thermal control system and thus the entire transmitter. This section investigates, first analytically and then experimentally, the feasibility of integrating a heat pipe with a microwave tube to provide an efficient heat transfer system capable of high reliability over time periods of several years as required with high-power spaceborne transmitters.

5.1 INVESTIGATION OF HIGH-POWER MICROWAVE TUBE COOLING

The application of heat pipe cooling to gridded tubes, crossed field amplifiers, klystrons and travelling wave tubes is investigated in this section. In each case, the design is developed for the evaporator-tube interface. The penetration of the vacuum tube envelope by the heat pipe is typical in each case and can be changed to meet specific configurational requirements. The cross-sectional area of the penetration must meet the requirements outlined in Appendix A. Heat pipe condenser configurations are not shown, since they are strongly influenced by vehicle configuration.

5.1.1 GRIDDED TUBES

The cooling of high-power gridded tubes is concerned with holding certain elements and vacuum seals below a maximum temperature and minimizing temperature gradients in the insulators to avoid fracture. While a great variety of gridded tubes is available, discussion is restricted to a metal-ceramic planar triode designated L-64S, which is under development by the General Electric Company's Research and Development Center. The thermal considerations for this tube should be representative of those of a great many gridded tubes and more severe than most others. The thermal requirements for the L-64S, shown on Figure 21, are:

a. Cathode. This element is electrically heated. The power to the heater is adjusted to maintain the cathode at a constant temperature.

b. Grid. A high conductance heat flow path is provided internally from the grid to the grid contact, which in turn is heat sunk to the cavity.

c. Anode. The L-64S dissipates heat at the anode; the heat must be conducted from the inner anode surface to the heat rejection system while not allowing the anode surface to exceed 500°C. This temperature limit is actually imposed by the grid. The anode itself can operate at 1000°C, but above 500°C the heat radiated from the anode to the grid becomes excessive and can result in grid failure. Future versions of the L-64 may increase the anode temperature limit to 1000°C. In this tube, the thin molybdenum foil used as the anode will be extended to provide adequate thermal isolation from the circuit.

d. Seals. The metal-ceramic seals cannot exceed 600°C without risking damage to the tube. A more severe limit, however, is imposed by the grid contact being used to remove heat from the grid. This contact must be kept relatively close to room temperature to keep the grid cool. If the other contacts are allowed to go much above 150°C, excessive gradients in the ceramic portions of the tube may cause cracking.

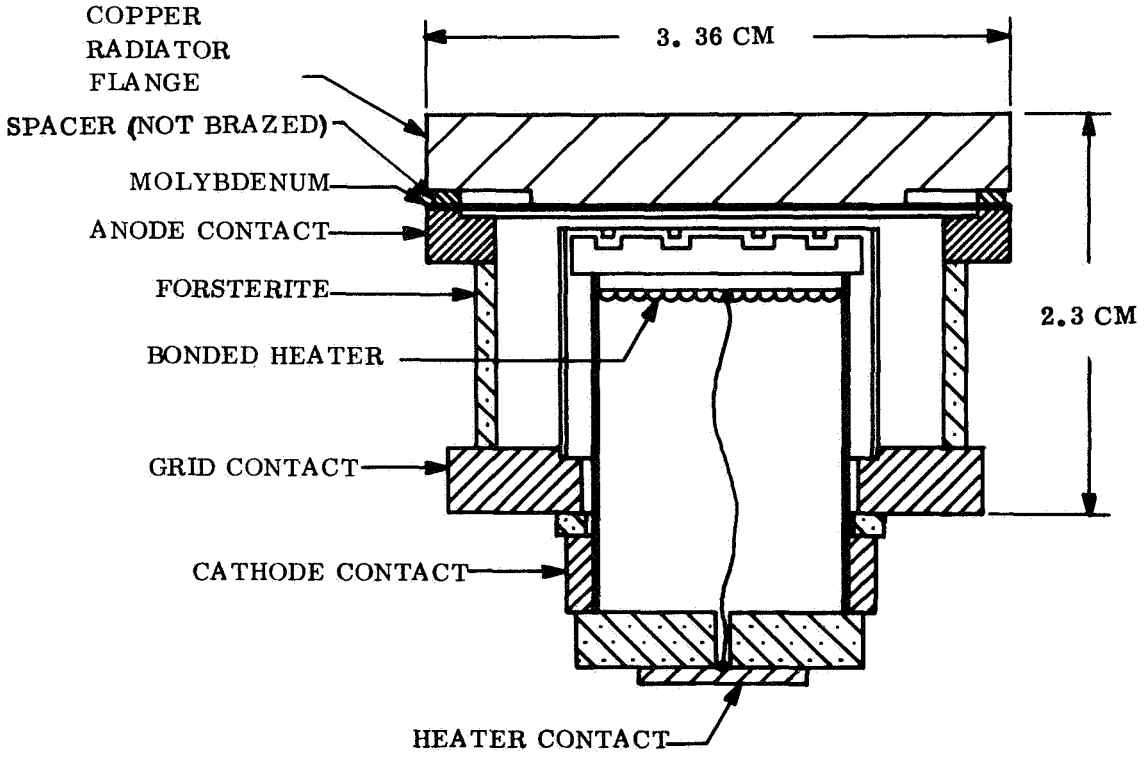

Figure 21. L-64S Triode Cross Section

The potential between cathode and anode is approximately 3000 volts, with either element at ground potential, depending on the circuitry.

The grid and cathode contacts of the L-64S are cooled by attaching them to the cavity with sufficient pressure at the interface to transfer the heat without an excessive interface temperature drop. The quantity of heat thus removed is small enough that it can be radiated from the surfaces of the cavity or conducted to the vehicle structure. The anode, however, presents a very severe cooling problem and must be considered separately.

The design power dissipation for the L-64 cooling system is 2.5 kilowatts (8530 Btu/hr). Thus, using the criterion for evaporation area given in Appendix A, the evaporator must have an area of at least 54 square centimeters. Since this would require a disk 8.3 centimeters in diameter, which cannot be accommodated by the mechanical configuration, the cylindrical surfaces of the pipe must be used as the evaporator. To provide a path for the heat to flow from the anode to the sides of the heat pipe, the collar shown in Figure 22 is used. The heat fluxes shown on the figure, however, far exceed the restrictions described in Appendix A. The excessive heat load at the base of the evaporator would force that section into the film boiling region, reducing its capacity. This would overload the adjacent portion of the cylindrical area, and it too would be forced into the film boiling region. This reaction would continue until the entire evaporator surface overheated enough to cause tube failure. To correct this condition, the heat flow path must be adjusted to maintain a constant heat flux throughout the evaporator. An extremely heavy cross section of copper might relieve the condition, but would be very heavy and could cause clearance problems with parts of the cavity. An alternate means of solving the problem is to size the collar for mechanical clearance and adjust the conductance to the heat pipe as a function of distance from the L-64S anode. The resistance network shown in Figure 23 represents the heat flow paths along the collar and from the collar to the inside surface of the heat pipe which serves as the evaporator. If the conductances between points C1 and C2,

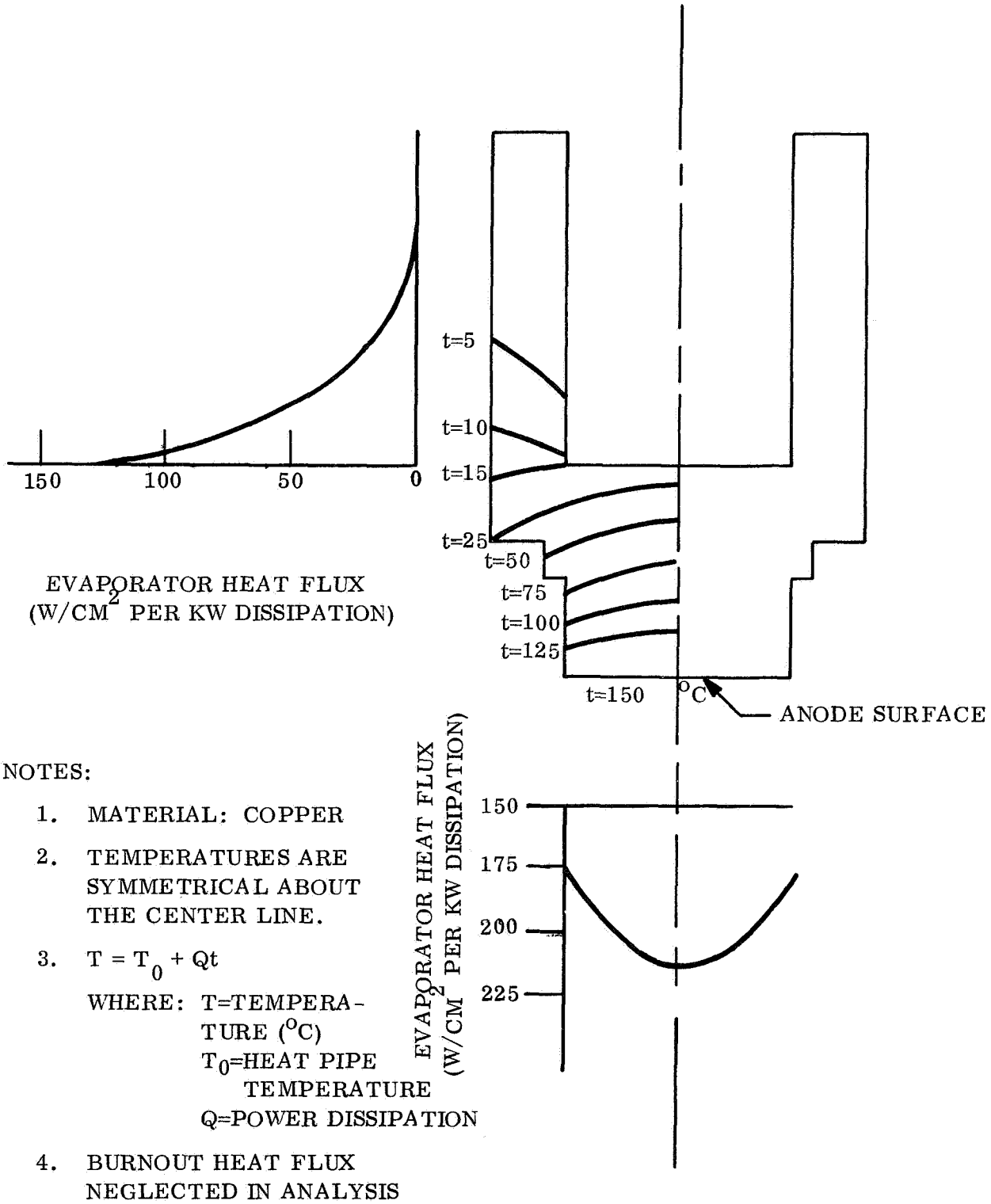

NOTES:

1. MATERIAL: COPPER
2. TEMPERATURES ARE SYMMETRICAL ABOUT THE CENTER LINE.
3. $T = T_0 + Qt$

   WHERE: T=TEMPERATURE (^{o}C)
   T_0=HEAT PIPE TEMPERATURE
   Q=POWER DISSIPATION
4. BURNOUT HEAT FLUX NEGLECTED IN ANALYSIS

Figure 22. Collar Temperature Distribution Neglecting Burnout Heat Flux

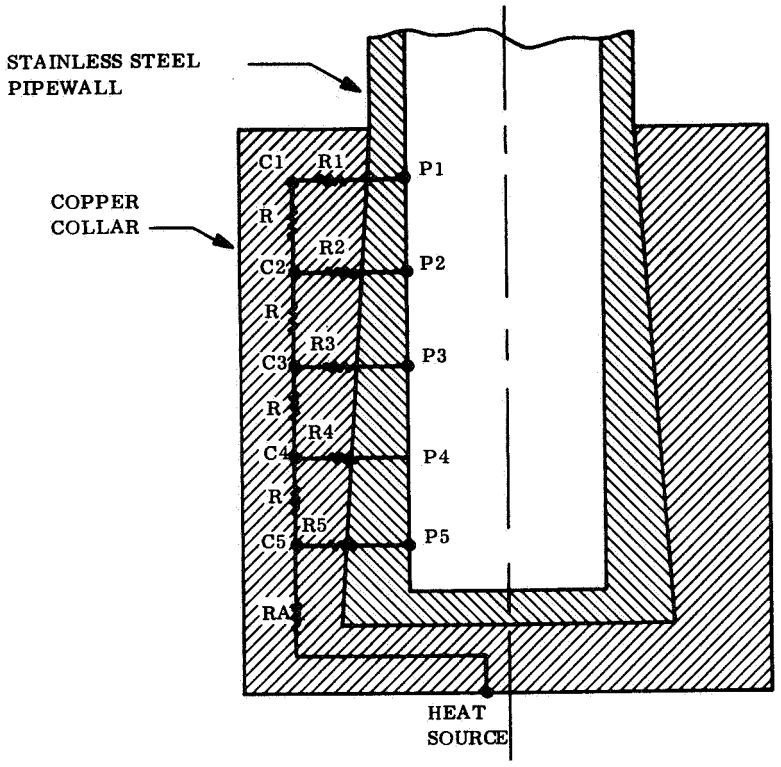

Figure 23. Heat Pipe Evaporator with Constant Heat Flux

C2 and C3, C3 and C4, and C4 and C5 are equal to R and each point labeled "P" represents an equal evaporator area, then one unit of heat flows through each resistance R1, R2, R3, R4, and R5. Thus, one unit of heat flows from C4 to C5, two units from C3 to C4, three units from C2 to C3, four units from C1 to C2 and five units through RA. To yield this division of heat flow, the following relationship must hold:

$$R_i = R_1 + \sum_{N=1}^{i} (N - 1)R \qquad (5\text{-}1)$$

This distribution of thermal resistance can be attained by adjusting contact area, varying thickness of two materials of different thermal conductivity or a combination of the two. Since the conductivities of copper (the collar material) and stainless steel (the pipe material) differ by a factor of 20, a tapered OD on the pipe fitting into a

corresponding taper in the collar can provide a close approximation to the required resistance-position relationship. As shown on Figure 23, the thickest portion of the low-conductivity stainless steel pipe provides the high thermal resistance path to the evaporator surface, while at the end of the taper farthest from the anode most of the radial path is through high-conductivity copper.

The temperature distribution in a collar designed according to Equation 5-1 is shown in Figure 24. Comparison with Figure 22 shows that an additional drop of 135°C results from the additional resistance used to even out the evaporator heat flux and the increased heat flow along the collar. (The end of the heat pipe in Figure 24 is not used as part of the evaporator.) Where clearance is not a problem, a solid copper block can be used to expand the area from the anode to a size which will maintain the evaporator heat flux below the maximum.

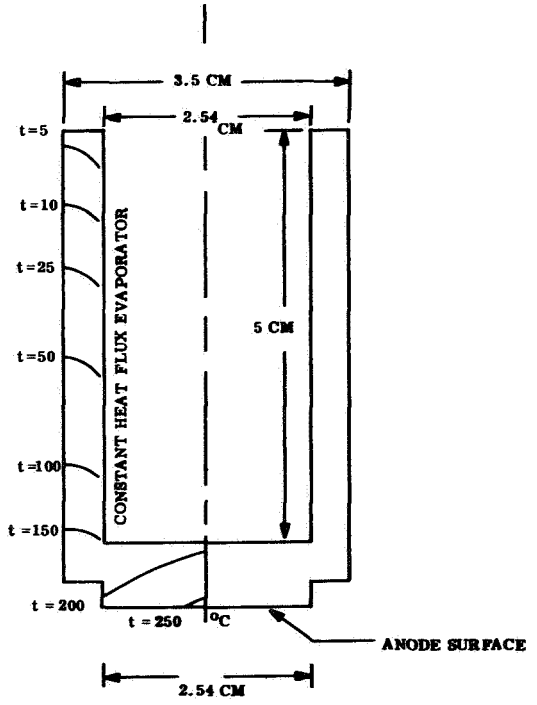

NOTE:
1) TEMPERATURES ARE SYMMETRICAL ABOUT CENTER LINE
2) MATERIAL - COPPER
3) $T = T_o + Qt$

WHERE: T = TEMPERATURE (°C)
T_o = HEAT PIPE TEMPERATURE
Q^o = POWER DISSIPATION (KW)

Figure 24. Constant Heat Flux Evaporator Temperature Distribution

A heat pipe interface for the L-64S has actually been designed and successfully tested as a part of an independent program by the General Electric Company's Space Systems Organization. To provide redundancy, the collar incorporates three heat pipes as shown in Figure 25. The total cross section of copper along the collar was increased to reduce the temperature drop. Test results showed good agreement with analysis.

5.1.2 CROSSED FIELD AMPLIFIER

A crossed field amplifier (CFA) has several elements which require thermal control: sole, delay line, collector, and magnets. The magnets generate no heat and therefore can be kept well below their Curie temperature (platinum-colbalt magnets) by insulating them from the tube while providing a good thermal interface with the magnetic yoke. This is feasible with both linear and circular format CFA shown in Figures 26 and 27. As these figures show, the magnets contact the yoke, but do not directly contact the tube itself. Thus, by allowing the yoke to conduct or radiate to the inside of the vehicle or to space, the temperature of the magnets can be kept below their upper limit.

The internal elements of the CFA, namely, the sole, the delay line, and the collector vary widely in design. In addition, the electrical potential on any of these elements varies from tube to tube, thus precluding any completely general considerations. In any CFA, however, some of the elements must be at a high potential relative to the other elements and thus require some form of electrical isolation. For thermal as well as mechanical considerations, this electrical isolation is best provided by a high-thermal-conductivity ceramic such as beryllia. The element itself is brazed to the beryllia insulator, and the insulator in turn is brazed to the heat sink which also provides structural support. For ease of fabrication and to avoid excessively long metal-ceramic brazes, each element of the sole or delay line is brazed to separate insulating blocks. This type of construction also provides additional distance between elements along the surface of the ceramic which provides a higher breakdown path where needed.

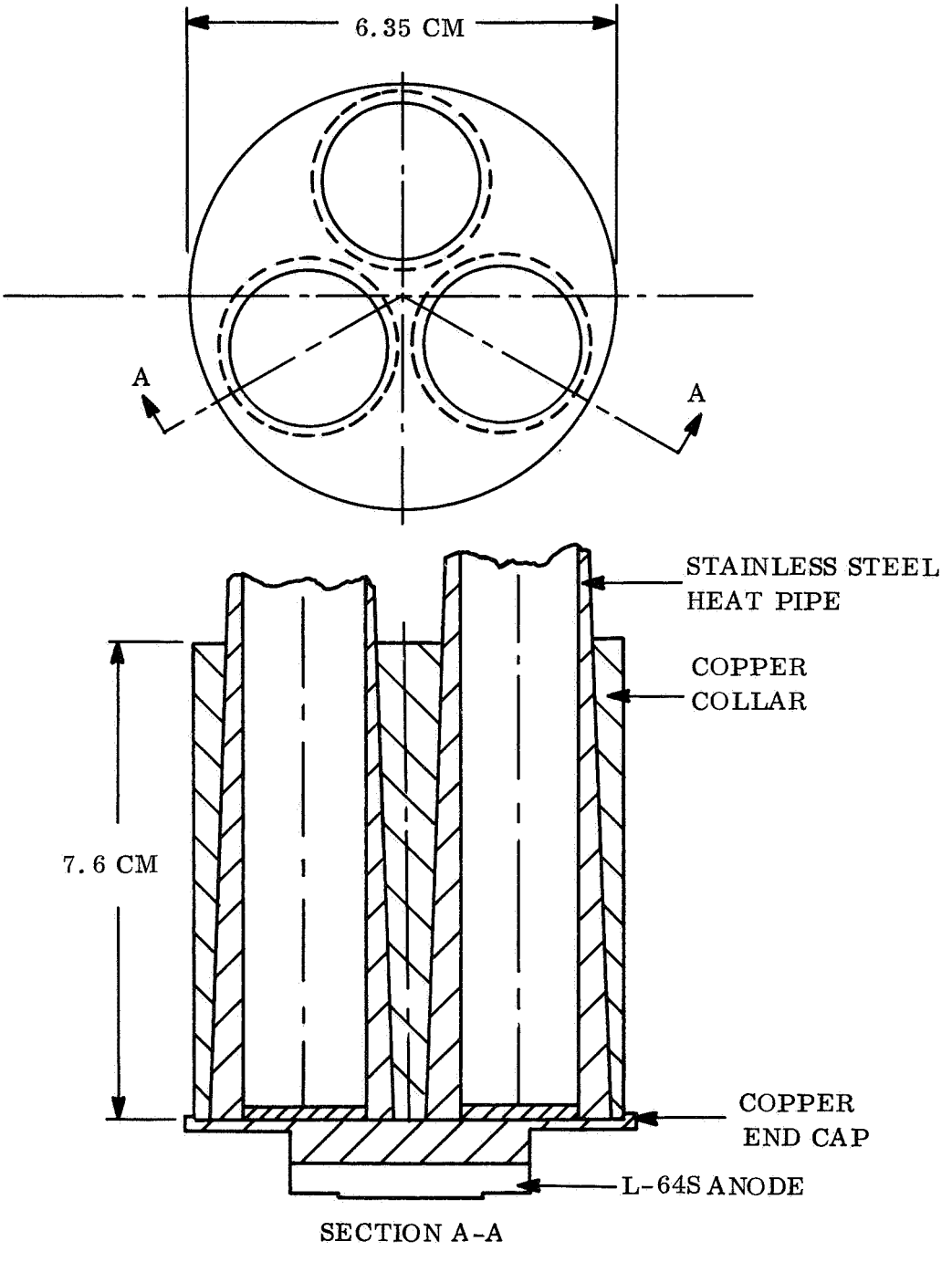

Figure 25. L-64S Anode Cooling Interface

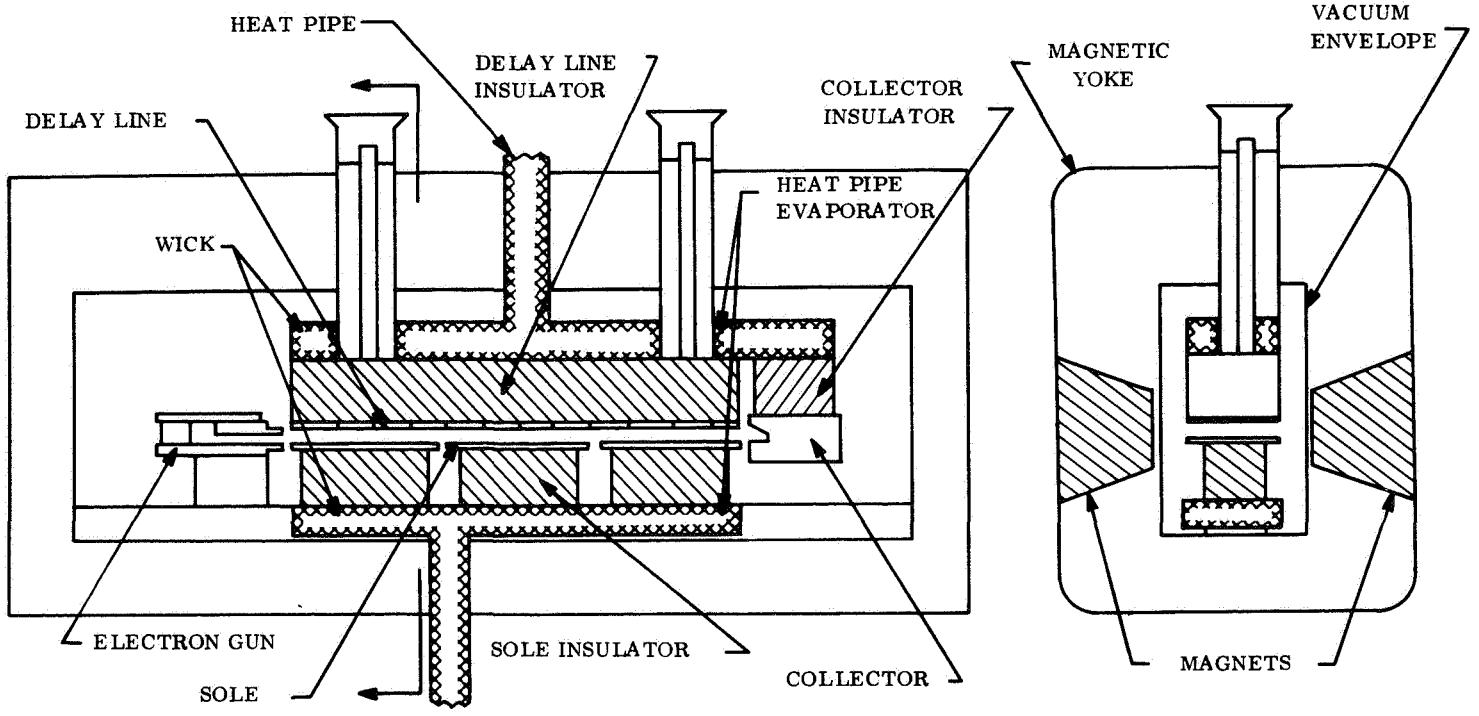

Figure 26. Linear Format Crossed Field Amplifier

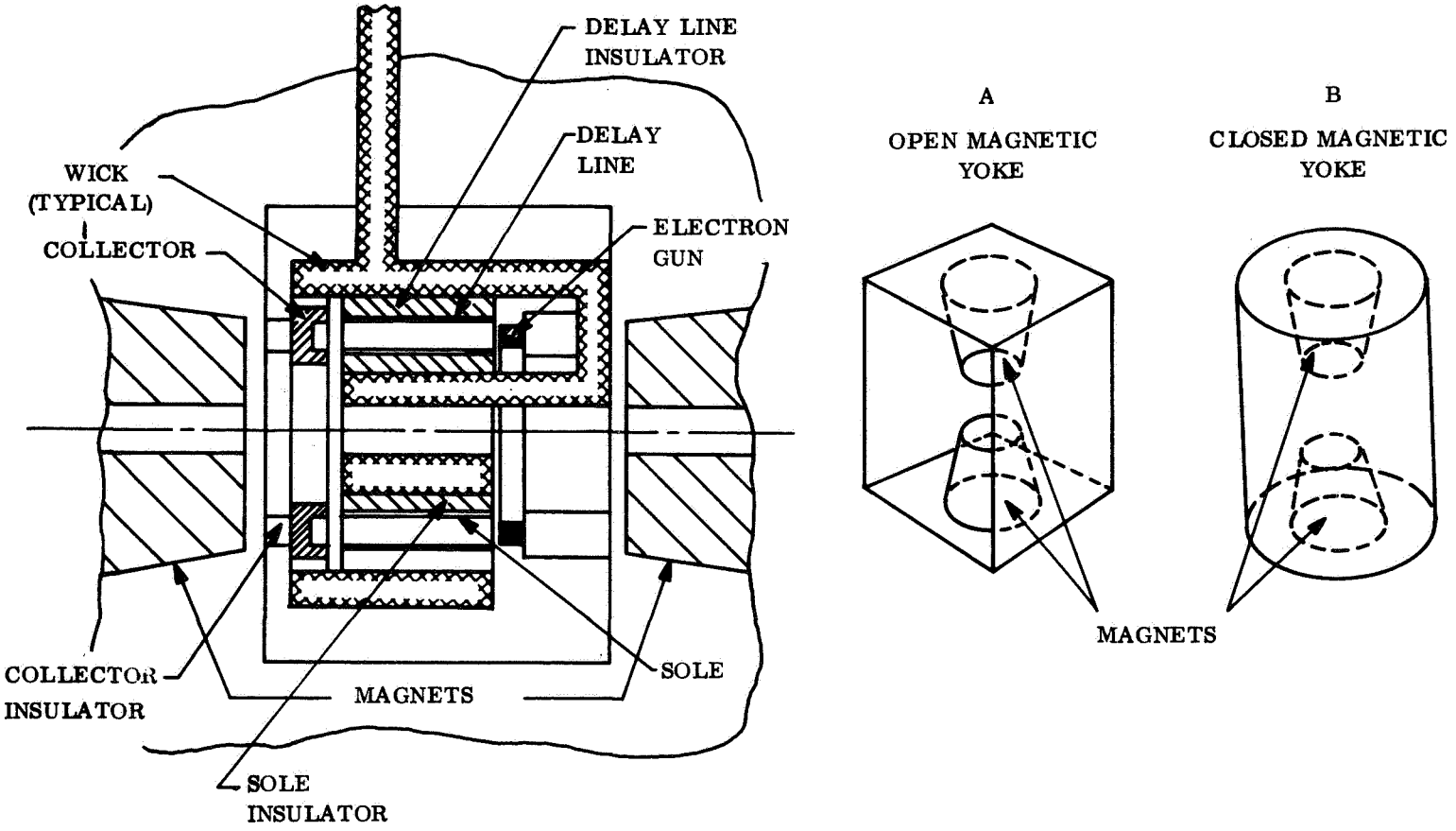

Figure 27. Circular Format Crossed Field Amplifier

The heat pipe interface with a CFA can be arranged in any of several configurations, depending on the configuration of CFA being considered and the internal arrangement. While the intent is to minimize the temperature drop from the heat-producing surface to the heat pipe evaporator, it must be kept in mind that the evaporator limit as described in Appendix A cannot be exceeded.

Cooling of the linear format CFA can be accomplished by replacing the water cooling lines currently used with heat pipes. The evaporator surfaces are built integral with the internal structure along the entire length of the delay line and at the collector. The sole can be cooled in the same manner as the delay line, but in a tube with a beam power of about 1 kilowatt or less, this heat can probably be conducted to the heat pipe evaporator at the delay line without excessive temperature drop. Figure 26 shows a typical heat pipe evaporator integrated into a linear format CFA. While an evaporator surface is shown for the sole, as previously noted, it is not necessarily required.

Integration of a heat pipe into a circular format CFA presents somewhat more difficulty. Cooling of the delay line can be accomplished in the same manner as with the delay line of the linear format CFA. The evaporator for the heat generated at the collector must be carefully designed to avoid excessive thickness in the axial dimension, since this gap increases the requirements on the magnets. Cooling of the sole can be accomplished by conduction and radiation to other elements if the dissipation is low enough. Where required, a heat pipe evaporator can be integrated into the sole as with the linear format CFA. Figure 27 shows a typical arrangement of a circular format CFA using heat pipes to cool critical parts. As with the linear format CFA, the evaporator shown at the sole may not be required in many designs.

Thus far, only integration of the heat pipe evaporators has been discussed. The vapor produced in removing heat from these surfaces and the liquid produced in the condenser must be provided with a passage through both the tube envelope and the magnetic yoke. The penetrations through the tube wall are not critical as long as they do not

impair mechanical integrity or electrical isolation. The penetration through the magnetic yoke presents a problem only where the yoke is completely continuous. Where it is two-dimensional, as shown in Figure 27a, the heat pipe can be easily brought out through either of the open sides. The magnetic yokes shown in Figures 26 and 27b, however, must be penetrated by the heat pipe in one or more locations. This penetration locally interrupts the magnetic path and may require compensation in the form of an increase in the thickness around the penetrations. The minimum disturbance occurs at the point on the surface of the yoke farthest from the magnets.

5.1.3 KLYSTRON

High-power klystrons are generally designed to be cooled by liquid flow. Passages are integrated into the device to carry a coolant, normally water, past the heat producing elements. The fluid is then cooled and recirculated or disposed of, depending on the type of cooling system being used. While these conventional methods are completely compatible with a liquid loop cooling system suitable for use in spacecraft, the flow passages are too small to be adapted for use with a heat pipe. Therefore, the standard klystron design must be altered to integrate the heat pipe evaporator into the structure of the tube itself, and passages must be provided for liquid and vapor flow.

The thermal control of a klystron is concerned with maintaining the temperature of several parts within limits imposed by the design. The maximum temperature is set by considerations such as copper vapor pressure, seal limits and the rise in electrical resistance of conductors with temperature. The peak temperature occurs at the tunnel tip and is limited in this discussion to $300^{o}C$. In addition to the maximum temperature, the klystron average temperature must be controlled within a given range because thermal expansion of the tube body in the axial direction causes detuning of the cavities. Thus, the temperature control range is determined by the physical dimensions and material of the klystron body and the excess band width of the tube with respect to the bandwidth required for the mission. In practical spaceborne klystron designs with 20 percent excess bandwidth, this range can be as small as $\pm 10^{o}C$, depending on frequency and power level.

Power is dissipated at several locations within the klystron. In current state-of-the-art designs, approximately 2.5 percent of the total beam power is intercepted along the drift tube, 2.5 percent at the output cavity, and 50 percent at the collector. Analysis of future designs using depressed collectors shows that these losses can be reduced to 1 percent of the beam power intercepted by the drift tube and output cavity and 15 to 20 percent at the collector.

If the magnetic field required for beam focusing is produced by a solenoid, this additional heat source must also be considered in the thermal design.

The physical size of the klystron is dependent on power and frequency. The body length can range from a few feet for a several hundred megahertz klystron to a few inches at 10 gigahertz. Clearly, then, a single thermal design cannot be developed to cover all klystrons. Problem areas can be investigated generally, however, by considering each part of the klystron separately.

5.1.3.1 Electron Gun

The electron gun is common to all klystrons and does not vary to any extent from tube to tube. The cross section shown in Figure 28 is typical. The primary goal is to minimize the power required for the heater without adversely influencing the emitter characteristics. While optimization of the heater power should not be overlooked, it is not critical, since it is almost negligible compared with the total power input to the klystron.

5.1.3.2 Magnets

A magnetic field is used to focus the electron beam in the klystrons considered in this report. The field is produced by permanent magnets (where their weight is not prohibitive) or a solenoid. Figure 29 shows a general layout for a klystron using permanent magnets. As the figure shows, the body of the klystron is exposed on two sides, allowing ready access. The solenoid configuration shown in Figure 30 completely

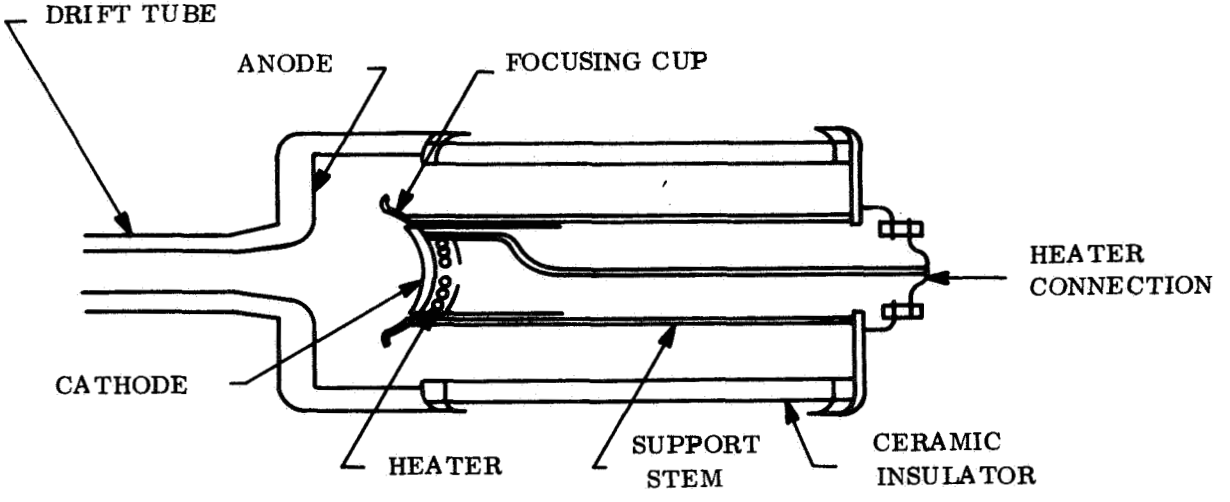

Figure 28. Klystron Electron Gun

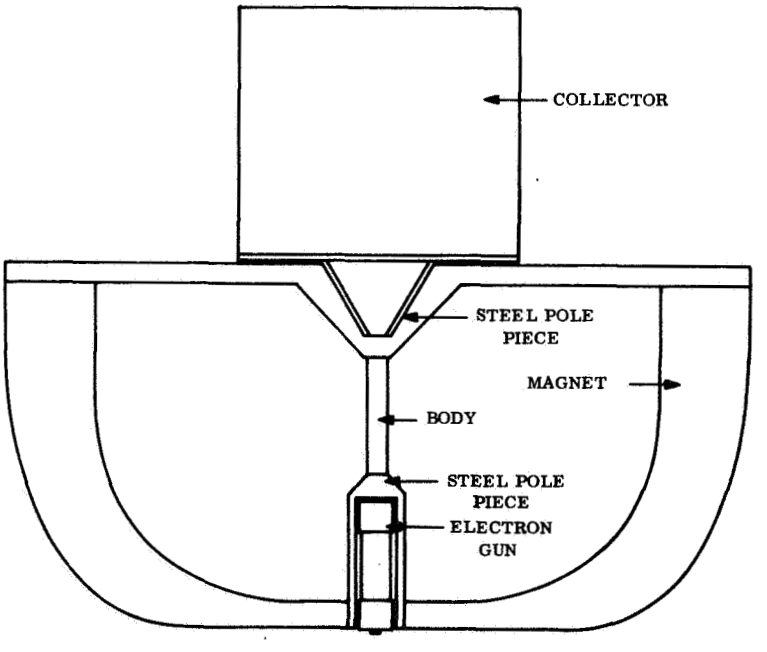

Figure 29. Klystron Using Permanent Magnets for Beam Focusing

surrounds the body and thus must be penetrated to remove heat generated along the drift tube and in the output cavity. In order to avoid disturbing the electron beam, this is best accomplished at the end of the solenoid nearest the output cavity, although small penetrations of the solenoid can be tolerated all along its length.

The temperature distribution within the solenoid can be determined by heat balance on the differential element shown in Figure 31. The sum of the heat flowing into the element and heat generated within the element must flow out. Expressed mathematically:

$$-K A_r \left.\frac{dT}{dr}\right|_r + \dot{q}\, \ell_2\, \pi\, r\, dr = -K A_{r+dr} \left.\frac{dT}{dr}\right|_{r+dr} \qquad (5\text{-}2)$$

Equation 5-2 can be integrated to yield

$$\frac{\dot{q} r^2}{2} = -Kr \frac{dT}{dr} + C_1 \qquad (5\text{-}3)$$

and

$$\frac{\dot{q}}{4K} r^2 = T + C_1 \ln r + C_2 \qquad (5\text{-}4)$$

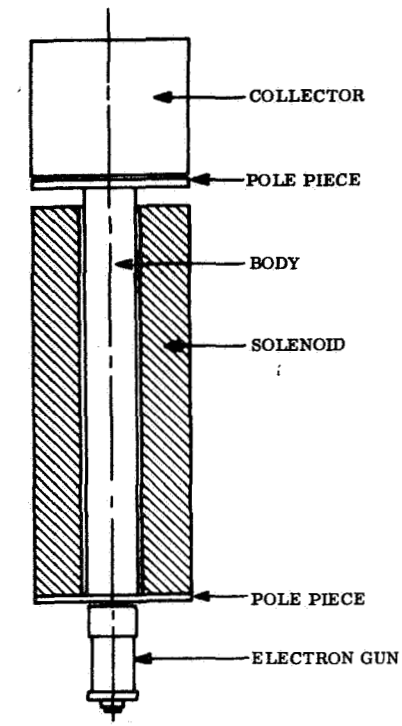

Figure 30. Klystron Using a Solenoid for Beam Focusing

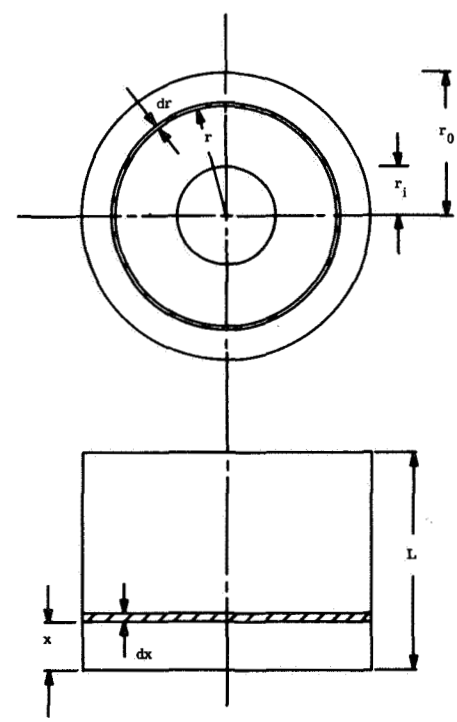

Figure 31. Solenoid Thermal Analysis

By applying appropriate boundary conditions to Equations 5-3 and 5-4 to solve for the constants of integration C_1 and C_2, the temperature distribution within the solenoid can be determined for cooling from the inside surface, cooling from the outside surface, or a combination of the two. The ends of the solenoid can also be used for cooling. In this case the heat balance is written as follows (see Figure 31):

$$-KA \left.\frac{dT}{dx}\right|_x + \dot{q}\, A dx = -KA \left.\frac{dT}{dx}\right|_{x+dx} \tag{5-5}$$

Integration of Equation 5-5 yields:

$$\frac{dT}{dx} = -\frac{\dot{q}}{K} x + C_1 \tag{5-6}$$

and

$$T = -\frac{\dot{q}}{2K} x^2 + C_1 x + C_2 \tag{5-7}$$

Applying boundary conditions appropriate to cooling at one or both ends yields the temperature distributions. A tabulation of the results of Equations 5-3, 5-4, 5-6, and 5-7 for various boundary conditions is given in Table IV, Also indicated is the radius at which the temperature is maximum. Thus, knowing the maximum operating temperature of the solenoid (typically 150°C), the required sink temperature can be calculated for each cooling configuration.

Solenoid cooling can be accomplished in any of several ways, depending on the particular configuration. Where the solenoid is physically very large, direct radiation from the surface may be feasible. If a small amount of additional radiating surface is required, fins can be attached as shown in Figure 32a. Heat pipes can be added as

Table IV. Solenoid Temperature Distribution

Surface Temperature	Internal Temperature Distribution T =	$T = T_{max}$ @ r =
Outside Surface @ T_o	$T_o + \frac{\dot{q}}{4K}\left[r_o^2 - r^2 + 2r_i^2 \ln \frac{r}{r_o}\right]$	r_i
Inside Surface @ T_i	$T_i + \frac{\dot{q}}{4K}\left[r_i^2 - r^2 + 2r_o^2 \ln \frac{r}{r_i}\right]$	r_o
Inside Surface and Outside Surface @ T_o	$T_o + \frac{\dot{q}}{4K}(r_o^2 - r^2) + \left[\frac{(T_o - T_i) + \frac{\dot{q}}{4K}(r_o^2 - r_i^2)}{\ln (r_o/r_i)} \ln \frac{r}{r_o}\right]$	$\sqrt{\frac{(T_o - T_i) + \frac{\dot{q}}{4K}(r_o^2 - r_i^2)}{\frac{\dot{q}}{2K} \ln (r_o/r_i)}}$
One End @ T_e	$\frac{\dot{q}}{2K}(2Lx - x^2)$	L
Both Ends @ T_e	$\frac{\dot{q}}{2K}(Lx - x^2)$	$\frac{1}{2}$ L

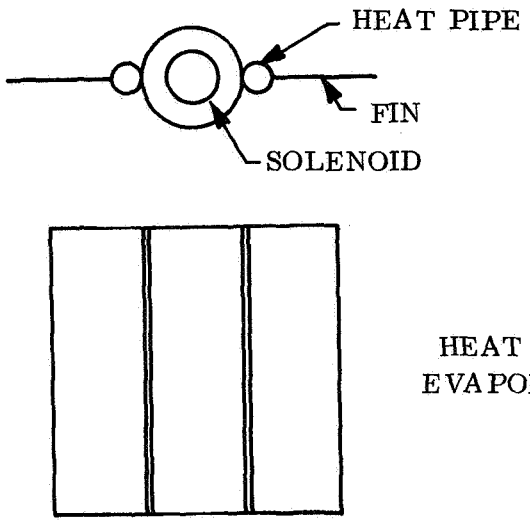

(A) SOLENOID DIRECT RADIATION

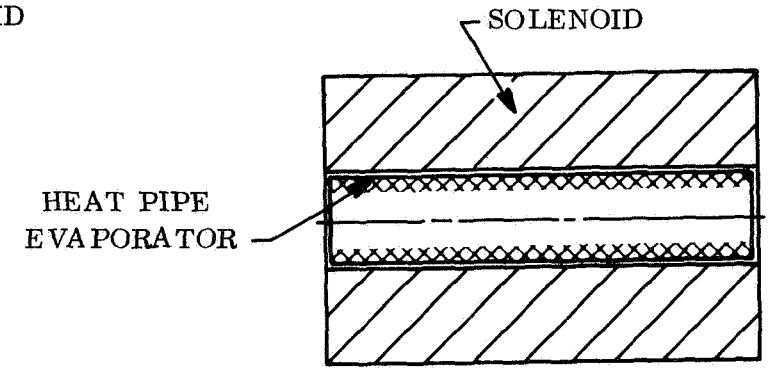

(B) SOLENOID WOUND DIRECTLY ON HEAT PIPE

NOTE: METHOD (B) MUST BE USED WITH BODY COOLING METHOD (A) ON FIGURE 34

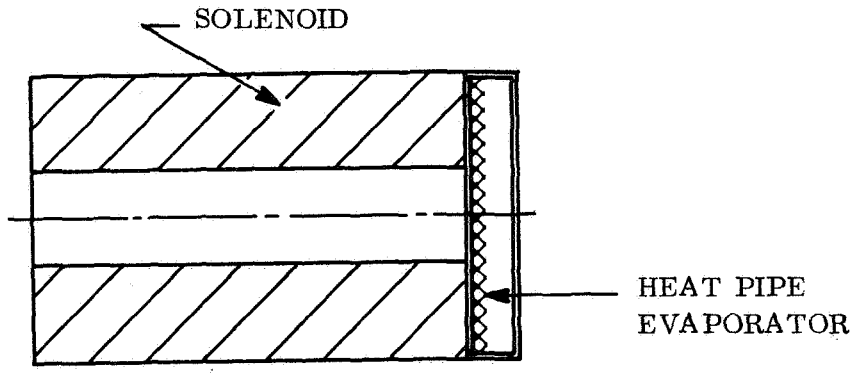

(C) END COOLING OF SOLENOID

Figure 32. Solenoid Thermal Control

shown for blockage of the view to space. Smaller solenoids can be wound directly on a heat pipe as shown in Figure 32b and heat can be removed from the inside surface. This technique allows the use of a single radiator for heat produced by the klystron body and the solenoid. Where the temperature drop to the cooling surface is excessive, the ends of the solenoid can be cooled. This approach is made feasible first by the fact that inside and outside surface cooling is inadequate where the solenoid is thick and has a high power dissipation. Normally these conditions coincide with a relatively short length. Second, lightweight solenoids are made up of concentrically wound aluminum or copper foil with alternate layers of an electrical insulating film. Thus, thermal conductivity in the circumferential and axial directions can be two orders of magnitude higher than conductivity in the radial direction. An example of this configuration is shown in Figure 32c.

5.1.3.3 Cavities

Thermal control of the cavities of a klystron is concerned with maintaining the temperature of the tunnel tip (see Figure 33) below a maximum temperature limit. Since heat is removed from outside the cavity, it must be conducted along the drift tube, resulting in a temperature drop which must be minimized to provide an optimum radiator temperature. This optimization must be done at the time the klystron is designed, since the thickness of the tunnel affects the electrical characteristics.

Heat dissipated at the tunnel tips and along the drift tube is removed at the ends of the cavity and must be transported to a radiator where it can be rejected to space. If permanent magnets are used instead of a solenoid, a heat path can be placed where it will not interfere with the magnet. A solenoid, however, completely surrounds the body of the klystron, and heat must be brought through either by conduction through the solenoid itself or by means of a high conductance path penetrating the solenoid. Such penetrations will upset the magnetic field and therefore should be kept small. The exact size allowable must be verified experimentally. The best position for a penetration is at the output cavity, since there is normally a gap between the solenoid and the pole piece which can be used for a heat pipe flow passage in Figure 34a.

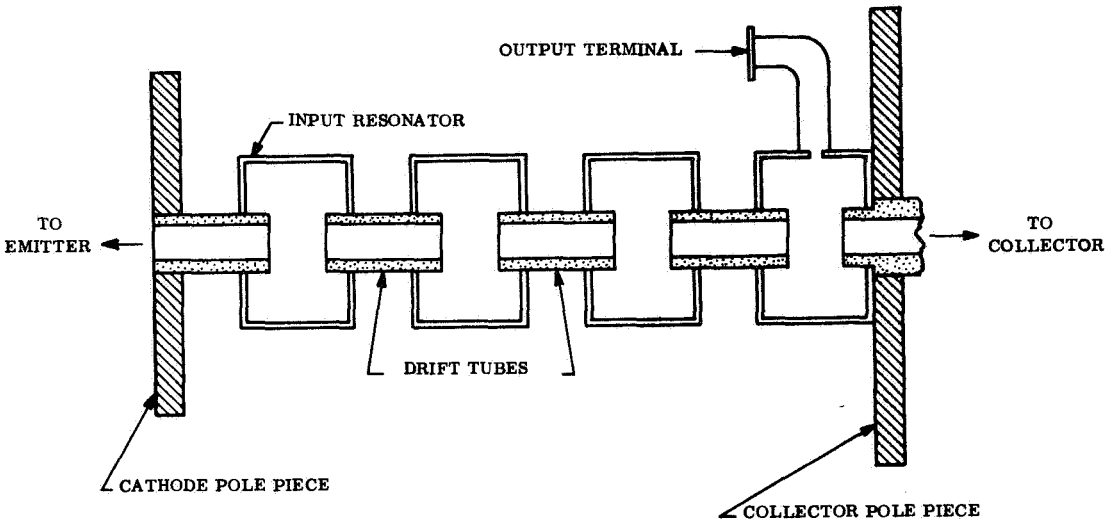

Figure 33. Klystron Cavities

Where the klystron is large enough that the solenoid surface can be penetrated at points along its entire length, heat flow paths either heat pipe or conduction, as shown in Figure 34b, can be used. Conduction is not normally adequate at the output cavity, however, since a considerably higher dissipation must be removed from this cavity.

5.1.3.4 Collector

Optimization of the thermal design of the collector is important, since most of the heat is dissipated in this element. Taking advantage of the fact that the collector can be designed to operate at a much higher temperature than the body, the total radiating area can be minimized by utilizing an independent radiator to reject heat dissipated in the collector.

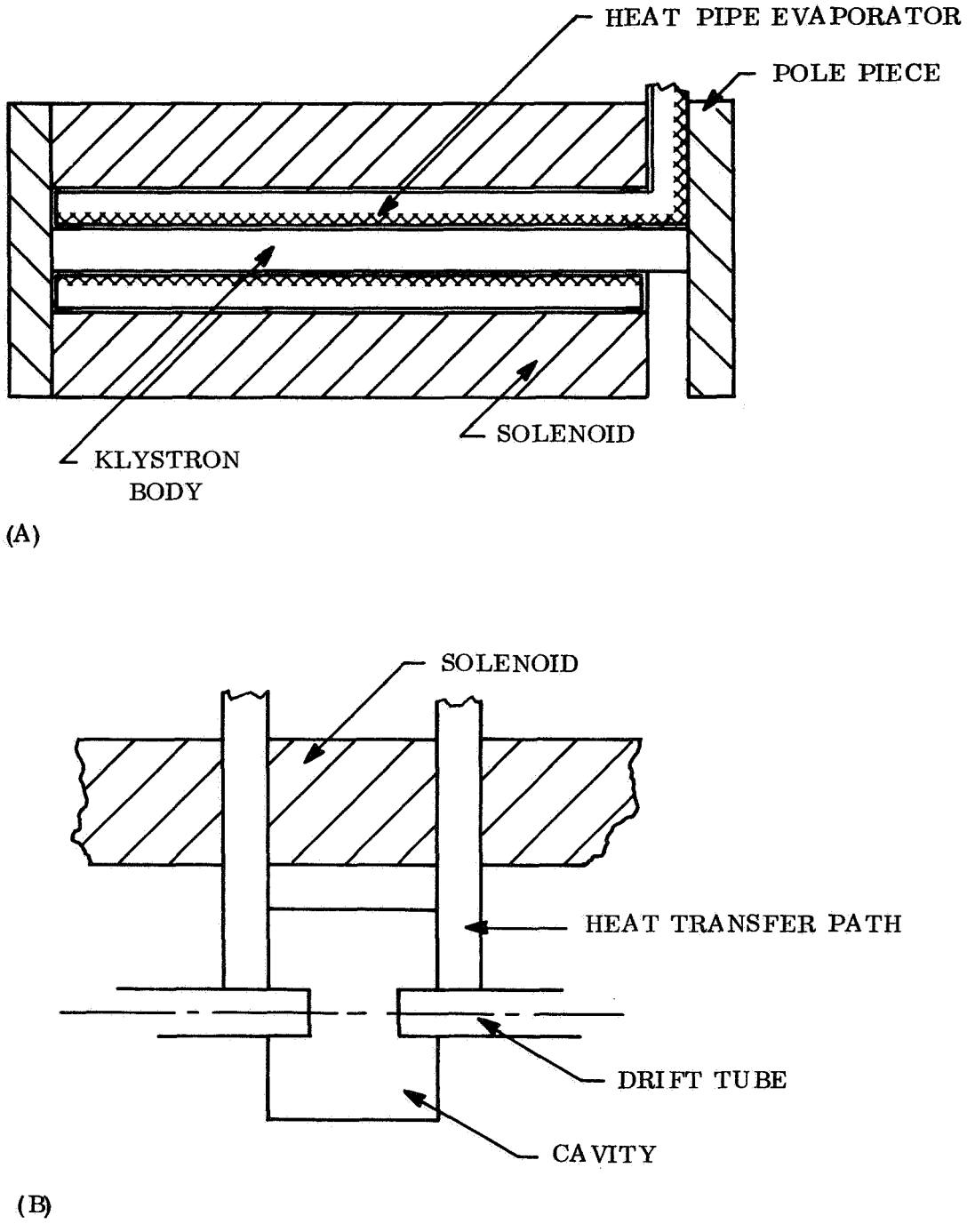

Figure 34. Solenoid Penetrations

The klystron collector operates at a high potential and therefore must be electrically insulated from the surrounding elements. Electrical isolation can be provided by the heat pipe itself by using dielectric wick material and working fluid. Ref. 4 describes the application of a heat pipe to a conventional depressed collector and outlines the methods used to overcome some severe problems encountered due to the dependence of breakdown potential on gas pressure. An alternate means of providing electrical insulation is to introduce a ceramic between the collector element and the heat pipe evaporator surface. Figure 35 shows such a configuration for a multi-element depressed collector. The operating temperature, dependent on the maximum temperature of the metal-ceramic seals, could be as high as 600 to 650^{o}C, which would allow the use of sodium as the working fluid. Sodium has the advantage of a high boiling burnout heat flux, which allows a relatively high power density at the evaporator surface. Furthermore, ground checkout is simplified by the ability of sodium to wick several inches against gravity.

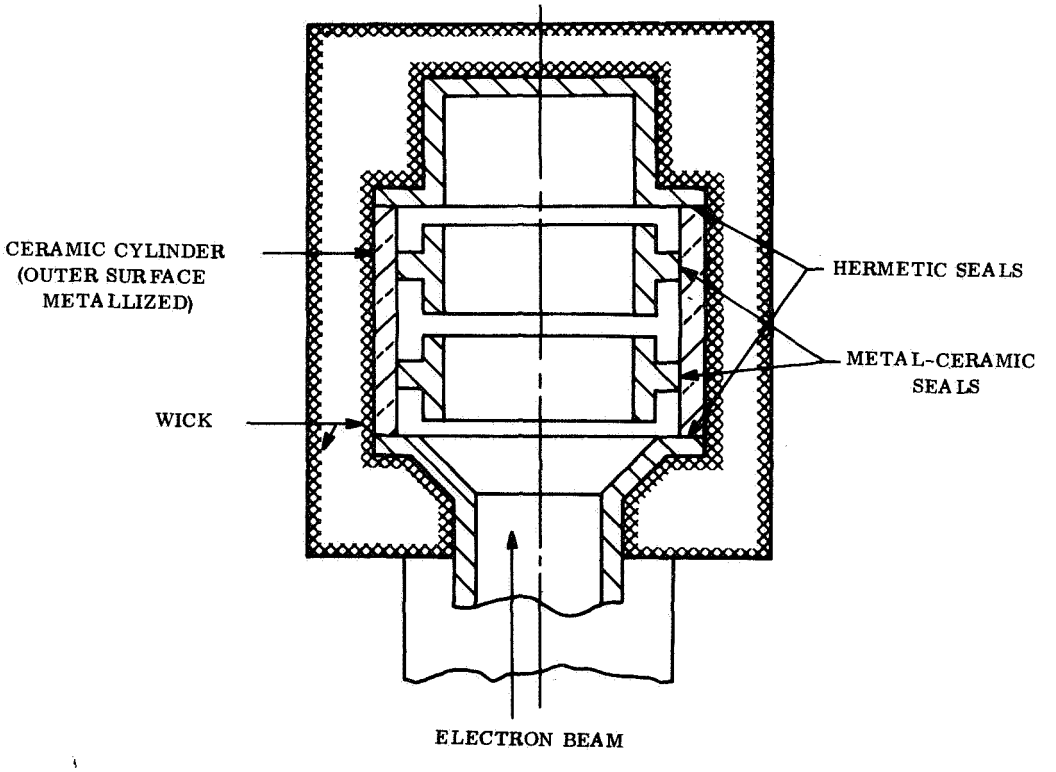

Figure 35. Multi-Element Klystron Depressed Collector

The integrated thermal control system for a klystron cannot be generally described because too many variables affect the configuration. Ref. 4 describes the thermal requirements for several particular spaceborne klystron designs in a frequency range from 850 to 11,000 megahertz.

5.1.4 TRAVELLING WAVE TUBE

The travelling wave tube (TWT) is very similar to the klystron described in the preceding section. The electron gun and collector can be identical to those of the klystron, but in place of the cavities, the TWT has a helix extending from the gun to the collector. Since the helix interacts with the beam along its entire length, the dissipation is distributed over the length, although not evenly. Cooling of the TWT helix can be accomplished in the same manner as for the body of the klystron except that, due to the relatively small surface area of the helix, care must be taken not to exceed the burnout heat flux of the evaporator surface. The following section of this report describes an actual TWT cooling system and outlines some of the problems encountered.

5.2 DEMONSTRATION OF COOLING OF A HIGH-POWER MICROWAVE TUBE

In order to demonstrate heat pipe cooling of a high-power microwave tube, a system was built and tested using an operating tube and a radiator of a configuration which would be suitable for use in a spacecraft. The tube used in this demonstration was a Watkins-Johnson travelling wave tube designated WJ-284-4. The specifications for the tube are contained in Appendix F. This TWT was selected primarily because (1) its thermal dissipation was in the range of interest (above 750 watts), (2) it could be conduction-cooled, (3) its operating temperature was high enough to allow rejection of the heat dissipated with a radiator of reasonable size, and (4) most of the equipment required to operate the tube was readily available. An outline of the WJ-284-4 shown in Figure 36 indicates the principal heat transfer surfaces for heat generated in the body of the tube (maximum temperature: $40^{\circ}C$) and in the collector (maximum temperature: $200^{\circ}C$).

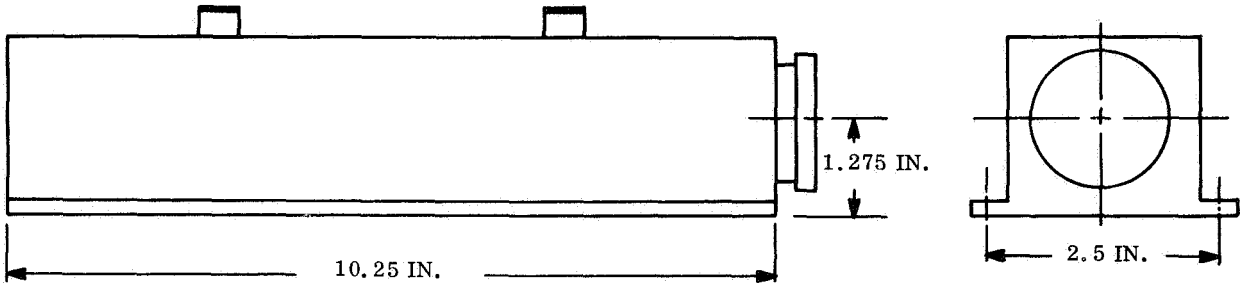

Figure 36. Travelling Wave Tube Configuration

The basic approach to the system design was intended to prove the feasibility of the heat pipe radiator and at the same time investigate installation techniques. Accordingly, rather than the equally spaced, parallel heat pipe arrangement described in Appendix B, a configuration with the heat pipes attached radially from the center of the radiator was investigated. In this configuration, the evaporators of all heat pipes are in close proximity and thus can easily be attached to a common heat source. The means of inter-

facing the heat pipes and the heat source is a threaded connection rather than one brazed or clamped, since this arrangement allows replacement of a defective heat pipe and provides adequate interface pressure to minimize interface temperature differentials.

Since the TWT for which the cooling system was designed was an existing model, the interface had to accommodate the TWT collector heat transfer surface. This surface is only 3.3 centimeters in diameter, however, and thus requires a relatively high pressure to reduce the interface temperature drop. The means of attachment chosen was a mechanical clamp designed to fit the TWT collector, provide the required interface pressure, and allow easy removal of the TWT.

To remove heat from the body of the TWT while not exceeding temperature limits requires a radiator separate from that used to cool the collector. Due to the length of the interface between this fin and the TWT mounting surface where the body heat is removed, a purely passive radiator is adequate.

Since two separate radiators are required, the mounting surface for the body is supported by the heat transfer block at the collector. In this way, alignment problems are minimized, since both points of attachment to the TWT are fastened to the same surface.

The final consideration, which affects the entire radiator analysis, is the test environment. Although the system was suitable for use in a space environment, as will be shown later, it was tested in air at room temperature. Data obtained from these tests provide a valid design verification without the added cost and complexity of space simulation.

5.2.1 TEST ASSEMBLY DESIGN

In the design of the test assembly, each temperature drop was evaluated starting with the collector and working out to the fin for a power dissipation in the collector of 750

watts. The heat transfer surface of the collector has an area of 8.58 square centimeters, which yields a power density of 87.5 w/cm^2 for 750-watt dissipation. Using a contact conductance from Ref. 5 of 2.56 w/cm^2 for a pressure of 4480 KN/M^2 (650 psi), the resulting temperature drop across the interface is 35^{o}C. Assuming the heat to flow half way through the thickness of the heat transfer block shown in Figure 37 and then radially to the midpoint of the heat pipe evaporator yields a conductance of 34 w/^{o}C or a temperature drop of 22^{o}C, thus resulting in a temperature at the threaded interface of the heat pipes of 143^{o}C for a collector temperature of 200^{o}C. To provide sufficient interface pressure on the threads to ensure good thermal contact, each heat pipe was fitted with a lock nut. After the heat pipe was screwed into the heat transfer block, the lock nut was tightened against the heat transfer block to put a minimum pressure of 4200 KN/M^2 (610 psi) on one side of the threads, resulting in a contact coefficient of 2.0 w/cm^2 ^{o}C. The interface was taken to be that shown on Figure 38. Note that contact is assumed on one surface of the threads only. The interface area is 6.6 square centimeters, resulting in an interface conductance of 13.2 w/^{o}C per heat pipe. Since there are four pipes, each carrying one fourth of the power, the resulting temperature drop across this interface, including losses due to the thermal resistance of the copper and stainless steel pipe, shown in Figure 38, increases this temperature drop to 28^{o}C, resulting in a temperature of 125^{o}C at the heat pipe evaporator. The analysis assumes that the heat must be conducted half way along the threads on each side. A value of 1.4 w/cm^2 ^{o}C (Ref. 6 for pool boiling) was used to account for the temperature drop at the evaporator surface. Thus, the calculated temperature of the vapor is 115^{o}C with a 750-watt power dissipation at the collector. The total thermal conductance from the TWT collector to the heat pipe vapor is 8.83 w/^{o}C.

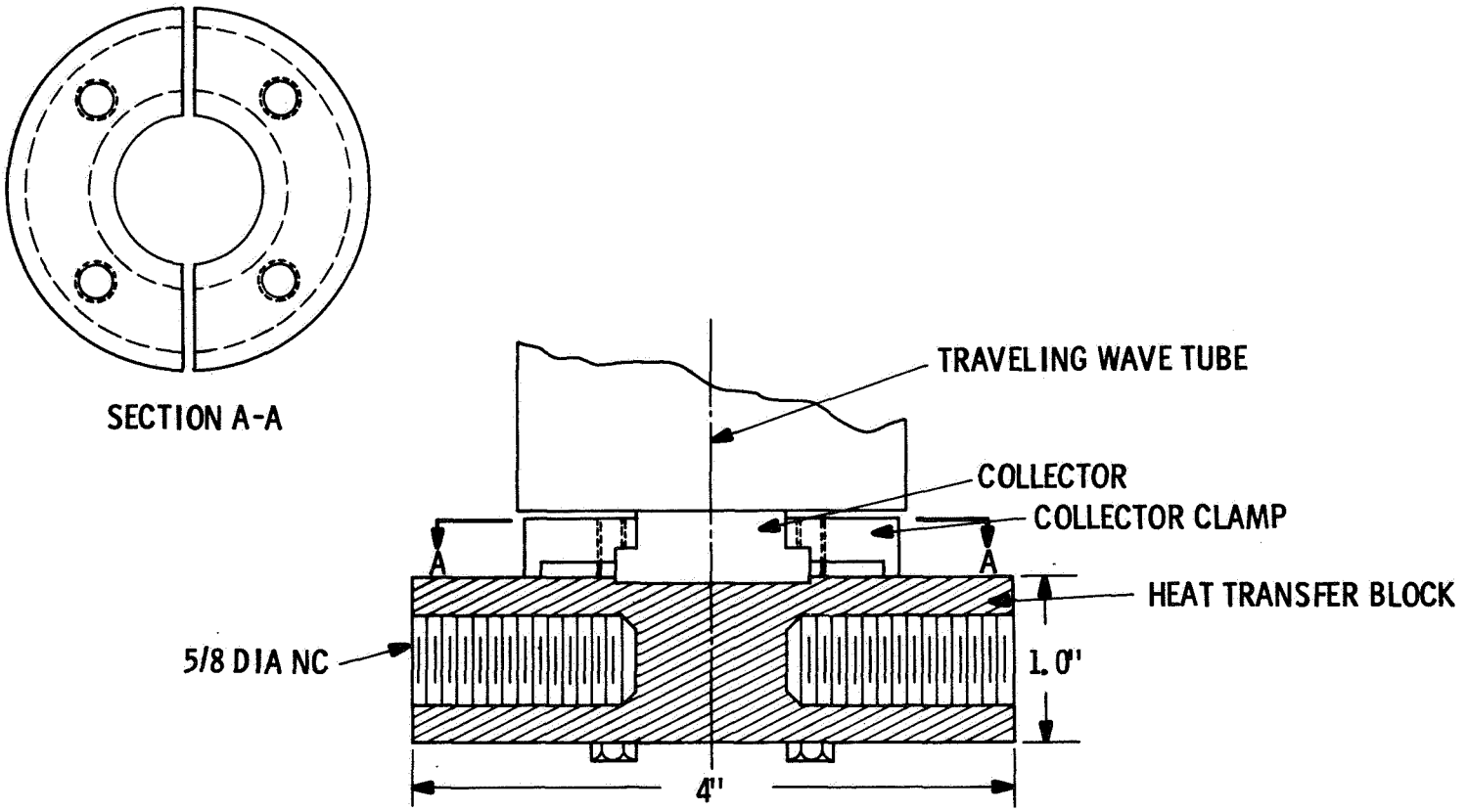

Figure 37. TWT Collector Thermal Interface

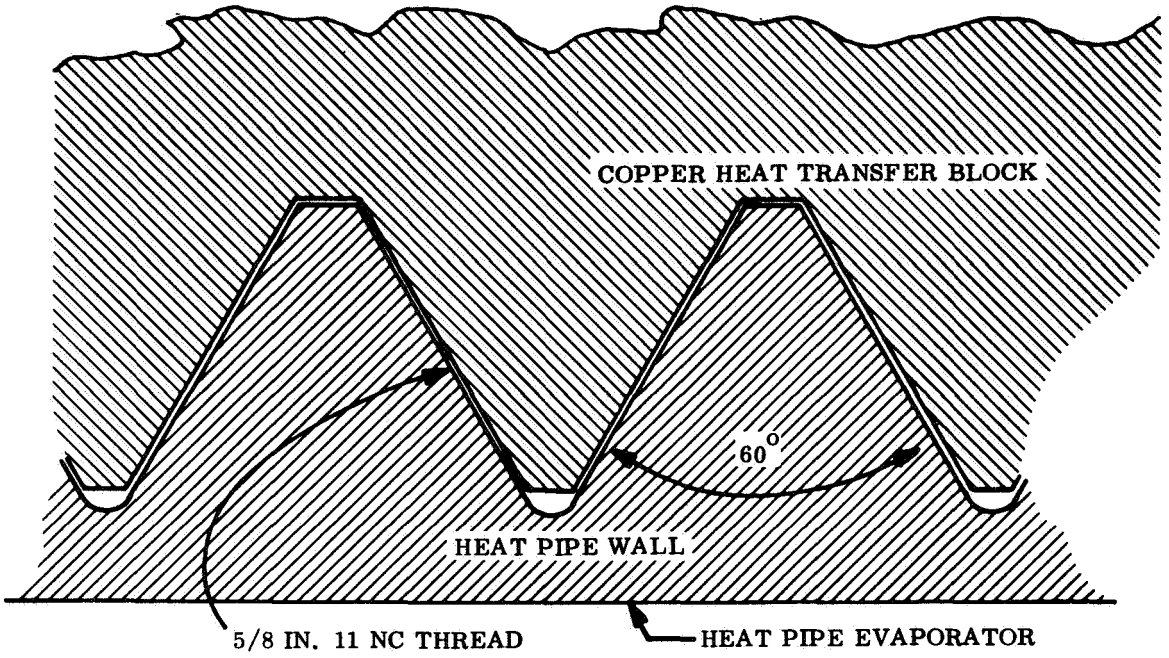

(A)

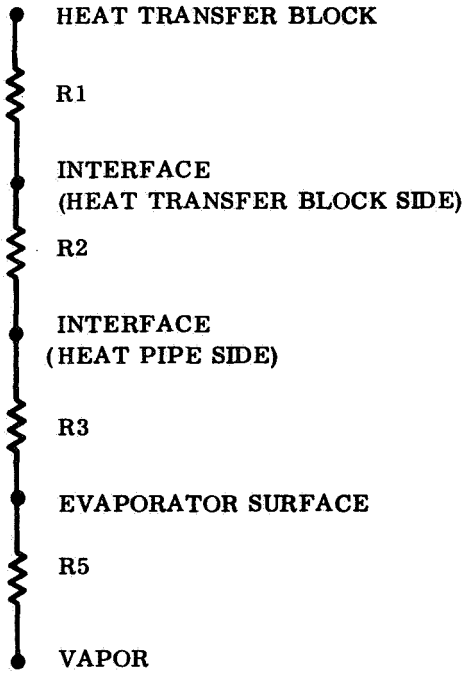

(B)

Figure 38. Threaded Interface

A rectangular plate with constant temperature diagonals is shown in Figure 39. The heat radiated from the plate is symmetrical about the diagonals and also horizontal and vertical lines passing through the center of the plate. The heat rejected, then, can be determined from 1/16 of the plate. From Figure 39 using the definition of fin effectiveness, η , from Ref. 7 the heat radiated from the differential element is:

$$dq = \epsilon \sigma (T^4 - T_s^4) \eta \, y \, dx \tag{5-8}$$

Integrating Equation 5-8 yields the total heat radiated from the plate, noting that $y = x$, yields:

$$q = 16 \epsilon \sigma \quad (T^4 - T_s^4) \int_0^{\frac{L\sqrt{2}}{4}} \eta \, x dx \tag{5-9}$$

Since there is no closed-form solution for fin efficiency, Equation 5-9 is evaluated numerically using values of η from Ref. 7. The analysis in the reference assumes one-dimensional heat transfer, since it is intended for fins of constant length. The application to the fin considered here is conservative, since two-dimensional flow will tend to make the fin more isothermal and thus more effective.

Area requirements for the radiator were determined iteratively from Equation 5-9 for the test conditions. To try to keep the size relatively easy to work with, the plate thickness was set at 0.090 inch and the material was aluminum. For a square configuration, an average fin effectiveness was determined for a radiating fin considering the change in fin length with position along the heat pipe. For purposes of computation of fin effectiveness, convection from the fin was converted to an effective emittance and combined with emissivity. (Results of this computation for a space environment are given later.) The result is an effectiveness for both radiation and convection on the basis of one-dimensional heat transfer in a direction normal to the axis of the heat pipe. While both the effective emittance and the one-dimensional analysis are only estimates for this

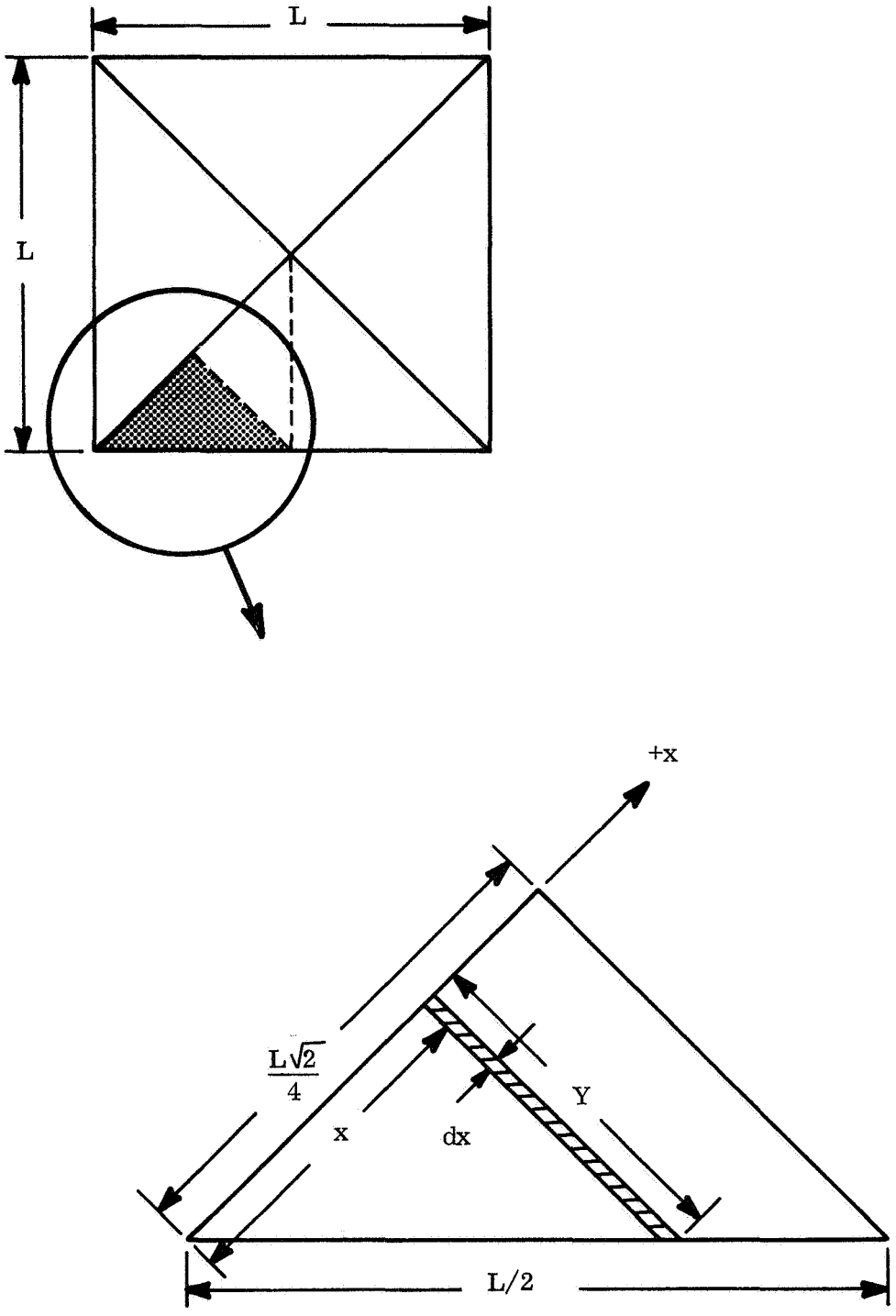

Figure 39. Radiator Analysis

configuration, both can be shown to be conservative. To reject 750 watts with a heat pipe temperature of 115°C, a 42-inch square radiator with an effectiveness of 0.51 was determined to have the required capacity. The radiator for the heat dissipated in the body was designed by using the standard convection fin approach, since radiation, for the lower operating temperature, accounts for much less heat transfer than convection.

5.2.2 TEST CONFIGURATION

The test assembly is shown in Figure 40. For convenience, the radiator plate is hinged at one edge to allow easy access to connections on the bottom. The TWT is attached as shown in Figure 41 to a mounting bracket extending downward from the heat transfer block. The body heat radiator is also attached to this bracket. Also visible in the photograph is the arrangement used to attach the heat pipes to the plate. (To avoid confusion, the reader should bear in mind that the TWT shown in Figure 41 has a rather clear reflection in the bottom of the plate of the TWT assembly.)

All tests were performed with the radiator in the horizontal position. This orientation should approach zero gravity conditions, since the heat pipes contain only enough water to saturate the wick and the average capillary rise is zero. Thermocouples were attached over the back surface of the radiator, on the heat pipes, and the TWT using Emerson and Cummins Eccoband 57C as shown in Figure 42. Locations of the thermocouples, shown on Figure 43, were intended to provide accurate temperature distributions.

Figure 44 shows the heat transfer block prior to installation of the TWT. The slight indentation at the center is for alignment purposes. Also visible in the figure are the lock nuts used to provide the interface pressure on the heat pipe interface which were referred to in the preceding section and the saddles used to provide the interface between the heat pipes and the radiator plate. The saddle, as shown in Figure 45, is a piece of aluminum of rectangular cross section which was milled along its length to provide intimate contact with the heat pipe. The saddles were slotted periodically, as

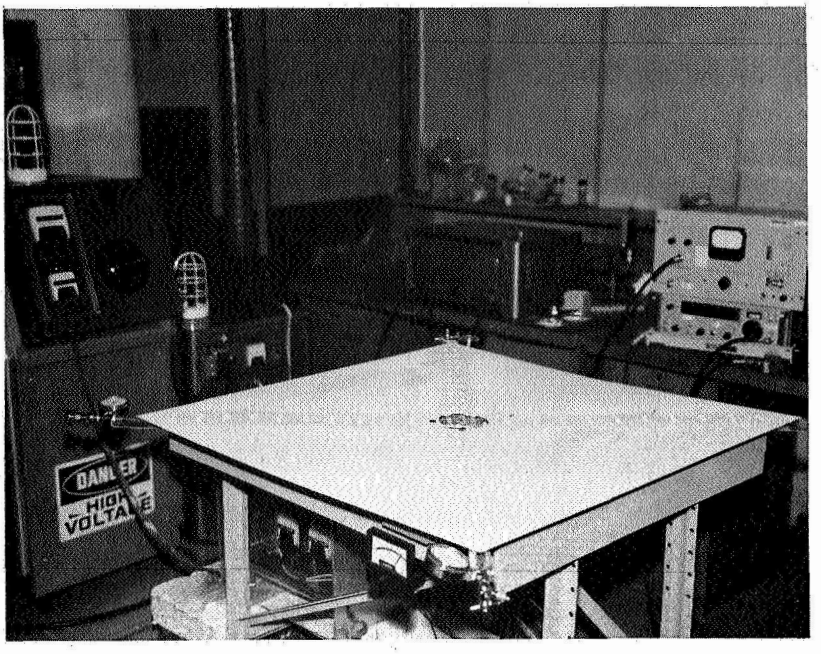

Figure 40. Test Assembly

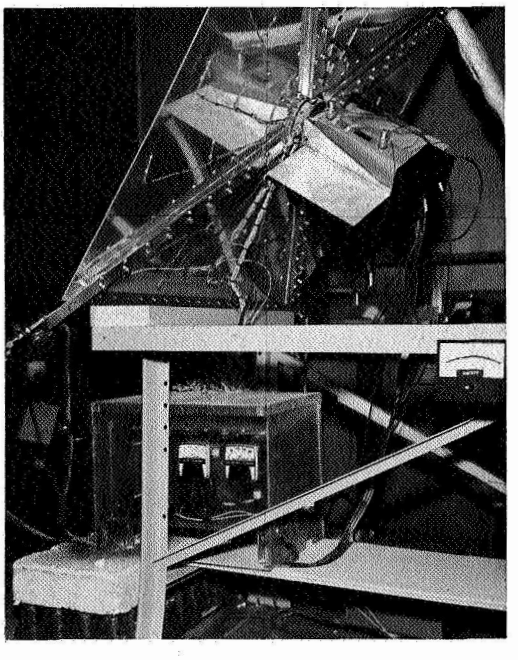

Figure 41. TWT Attachment

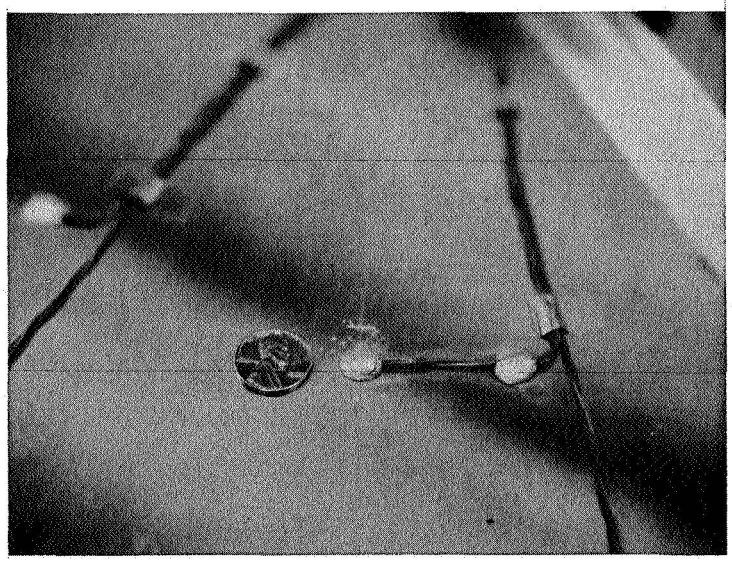

Figure 42. Thermocouple Attachment

Figure 45 shows, to provide clearance for thermocouples. All mechanical interfaces were coated with General Electric G640 Silicone Grease to minimize temperature gradients.

The TWT heat transfer block interface is shown in Figure 46. One half of the clamp used to attach the collector is also shown.

A block diagram of the operational 7.5 gigahertz amplifier system utilizing the WJ-284-5 TWT and the heat pipe fin is shown in Figure 47. Excitation was provided by a convectional reflex klystron and input power to the TWT controlled by means of a flap attenuator. A 20-decibel directional coupler provided a means of sampling the signal to determine power and frequency. The TWT was powered by an 8-kilovolt, milliampere supply provided with crowbar protection as well as overcurrent and thermal trip-outs.

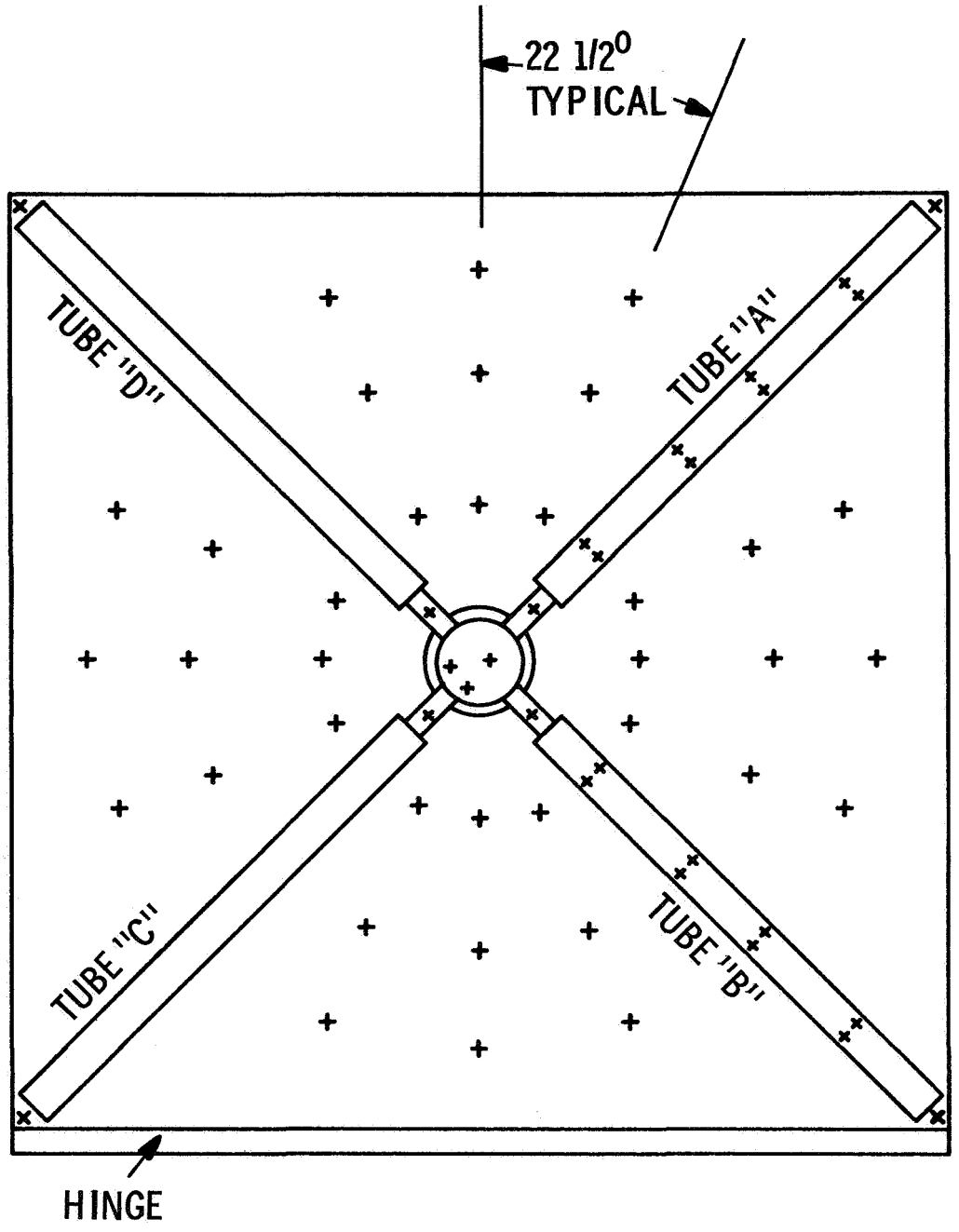

NOTE
+ THERMOCOUPLE LOCATIONS

Figure 43. TWT Instrumentation Map

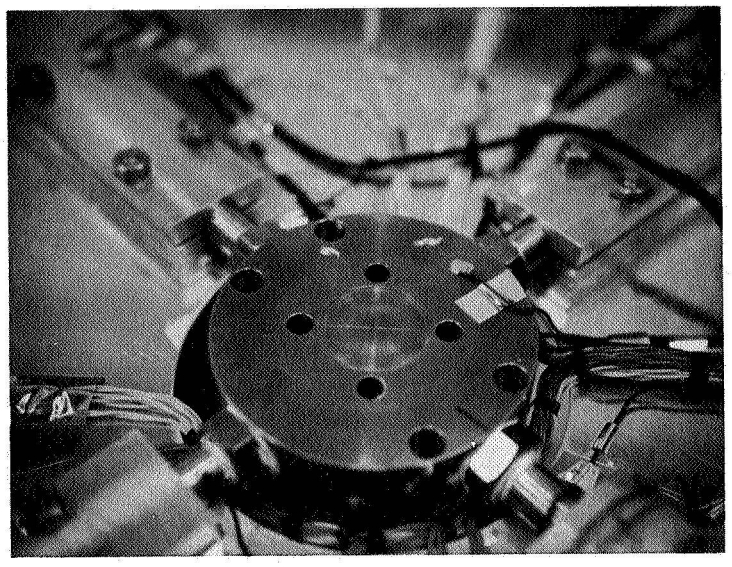

Figure 44. Heat Transfer Block

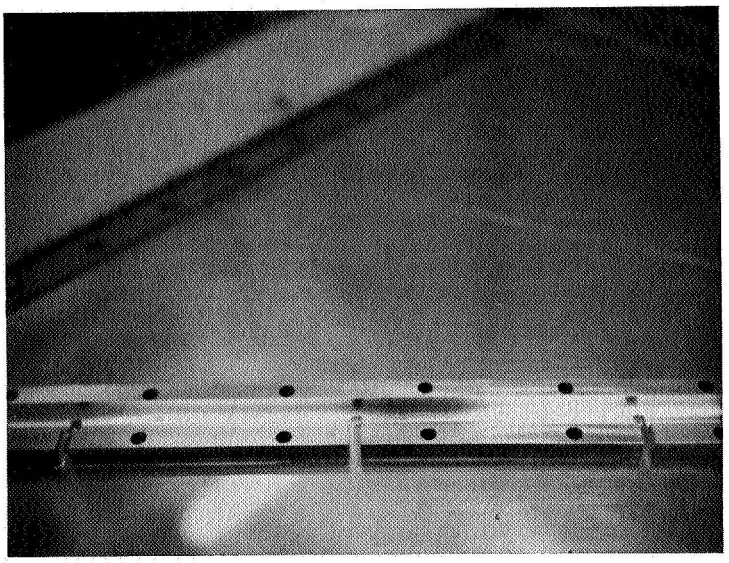

Figure 45. Heat Pipe Saddle

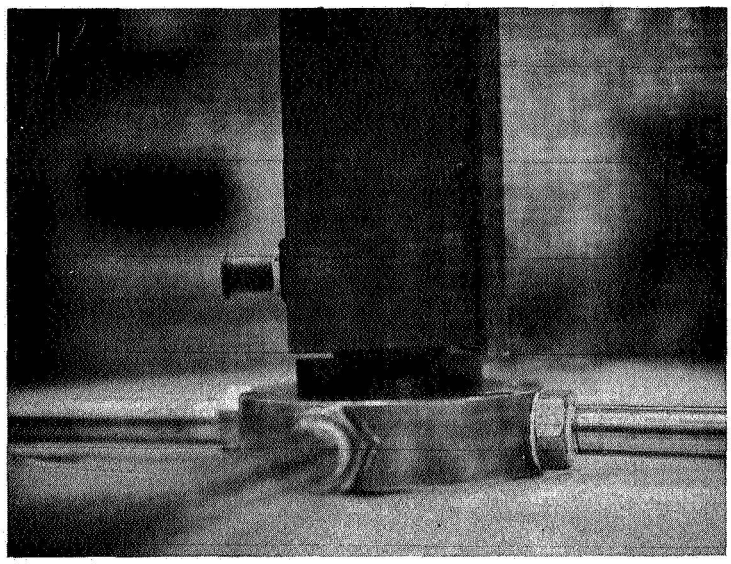

Figure 46. TWT Collector Interface

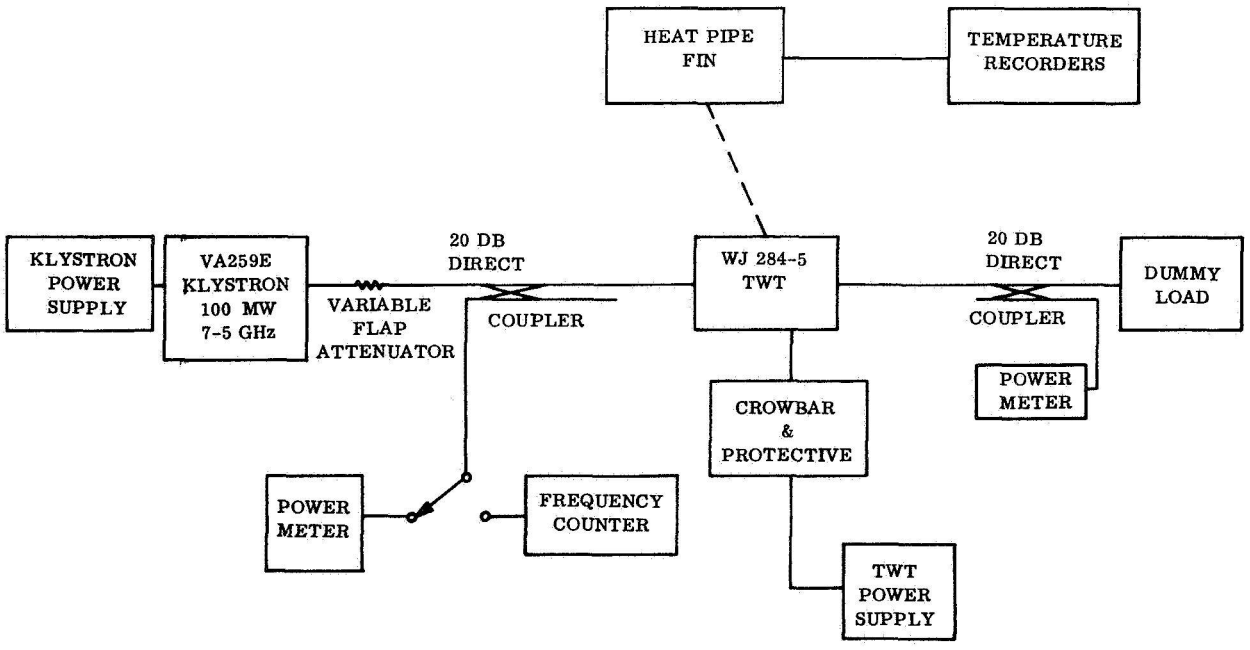

Figure 47. Block Diagram of Electrical Circuit

Output power from the tube was sampled through a 20-decibel directional coupler to determine power output, and a dummy load was used to absorb the full power.

System checkout was performed using a water heat sink clamped to the TWT collector. Table V shows the results of these tests and is indicative of operating conditions during runs with the heat pipe augmented fin.

Table V. System Checkout

		Run 1	Run 2
Test Condition			
	Filaments	7.0 vac @ 1.5A	7.0 vac @ 1.5A
	Collector Voltage	6375 vdc	5875 vdc
	Collector Current	175 ma	145 ma
	Helix Voltage	6375 ma	5875 ma
	Body Current	3.6 ma	2.9 ma
	Mod. Anode Voltage	6375 vdc	5875 vdc
	Cathode Current	171.5 ma	142.2 ma
RF Performance			
	Frequency	7.493 GHz	7.474 GHz
	Power IN	+20 dbm	+20
	Power OUT	52.83 dbm	51.38
	Sat Gain	32.83 db	31.38
	Efficiency	18%	16%
	Collector Temperature	65^{o}	50^{o}C

5.2.3 TEST RESULTS

In order to provide a basis for comparison of heat pipe performance, the initial testing was done with all four heat pipes unfilled. An electrically heated simulator was clamped to the heat transfer block in place of the TWT. Under these conditions, the only means of rejecting heat are (1) convection and radiation from the copper interface block and (2) conduction along the heat pipe walls to the fin. These heat-rejection paths are adequate for removing a limited quantity of heat as shown on Figure 48. Here it can be seen that the collector reaches the 200°C limit at somewhat over 100 watts and reaches 275°C at 200 watts, the same temperature where the system, with only a single heat pipe operating, can reject 600 watts of power.

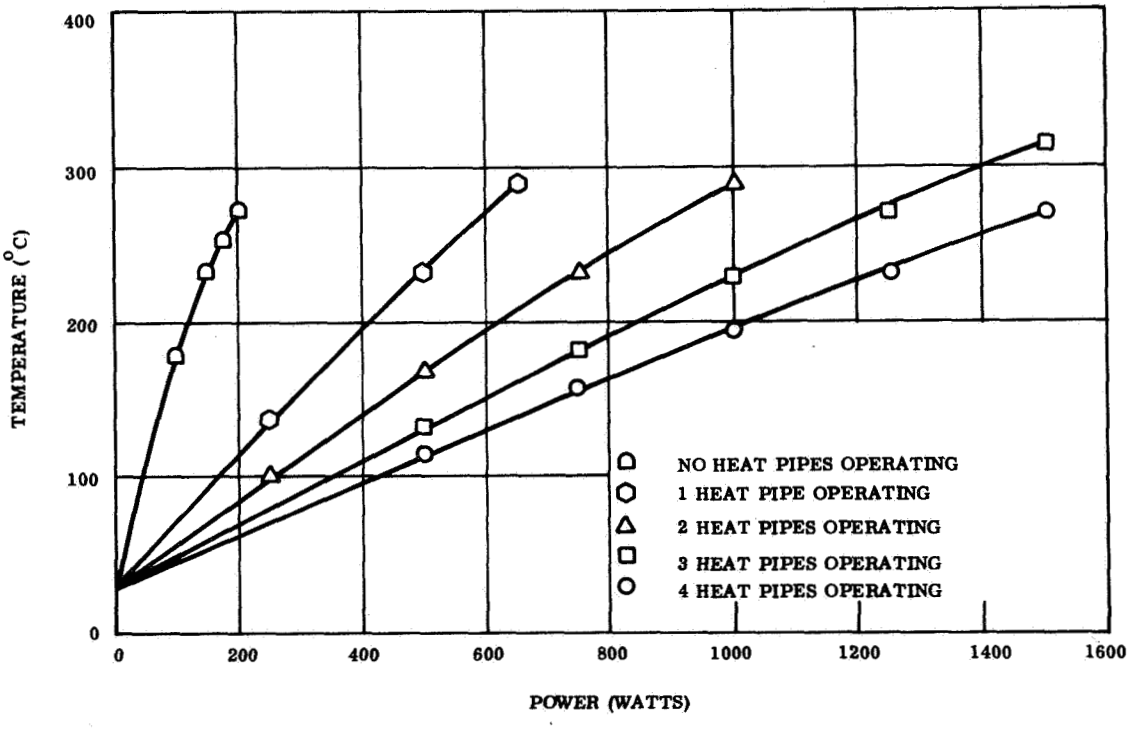

Figure 48. Collector Temperature Versus Power for Various Failure Modes

Upon completion of the tests with no heat pipes operating, tests were run to determine the performance of the system under various failure modes. After each was charged, a series of tests was run at various power levels. Thus, a series of test points was obtained for one, two, three, and all four heat pipes operating, in addition to those already discussed for no heat pipes operating. These points, also plotted on Figure 48, show collector temperature as a function of power input for various numbers of heat pipes operating or for various numbers of heat pipes failed. Viewed from this standpoint, the figure shows the operating characteristics of the system under various conditions of heat pipe failure. Results for all tests not included in this section are presented in Appendix D.

Temperature distributions over the fin are presented for a power level of 750 watts in Figures 49, 50, and 51 for four, three, and two heat pipes in operation. The symmetry and contours of the isotherms clearly demonstrate the operation of the heat pipes. At a power level of 1500 watts (with the electrical simulator), the isotherms do not change shape, but merely only level, as shown in Figures 52 and 53 for four and three heat pipes operating, thus showing the heat pipe capable of consistent operation at widely different power levels.

Other system charactersitics of interest are the interface temperature drops at the collector and at the heat pipes. These are shown in Figures 54 and 55, respectively. Both of these temperature drops are very significant in a thermal control system because they make up most of the total temperature difference between the collector and the radiator. Thus, they should be as small as possible to maximize the radiator temperature and thereby minimize area and weight.

The final tests performed on the thermal control system were to determine the effect of using the simulator in place of the TWT. Accordingly, the TWT was attached as shown in Figure 56 and operated at the design point, 750 watts, and also at 960 watts thermal dissipation at the collector. The results of the 750-watt run, shown in

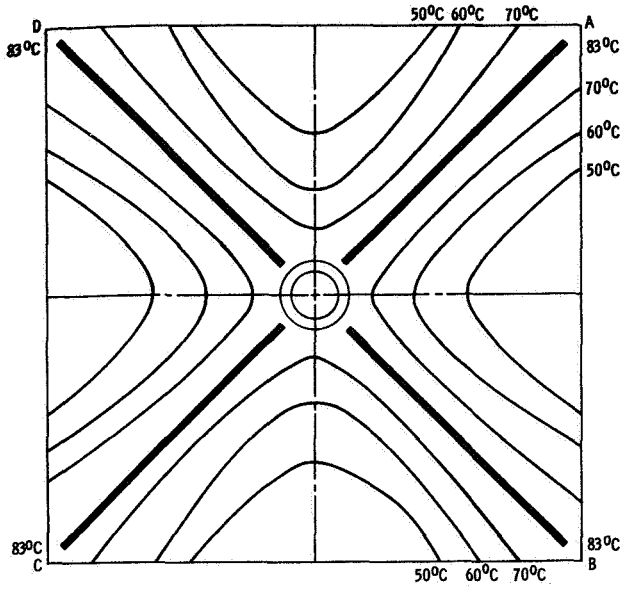

Figure 49. Temperature Distribution at 750 Watts with Four Heat Pipes (A, B, C, D) Operating

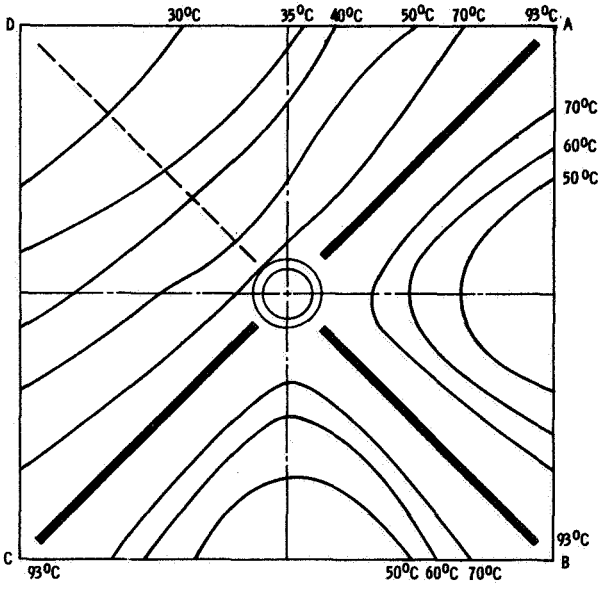

Figure 50. Temperature Distribution at 750 Watts with Three Heat Pipes (A, B, C) Operating

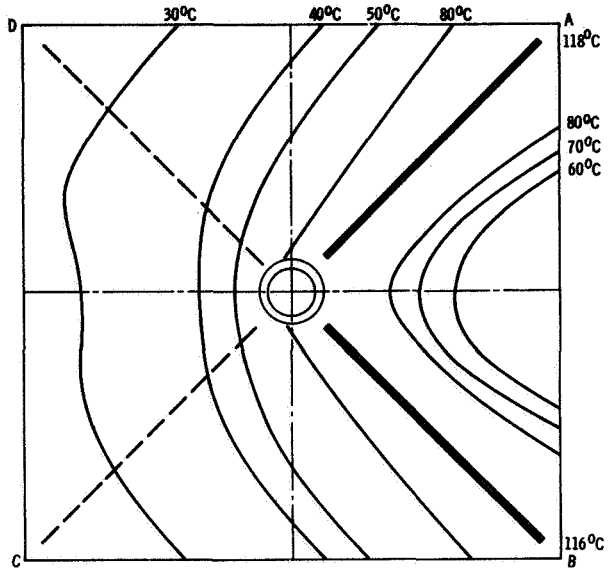

Figure 51. Temperature Distribution at 750 Watts with Two Heat Pipes (A, B) Operating

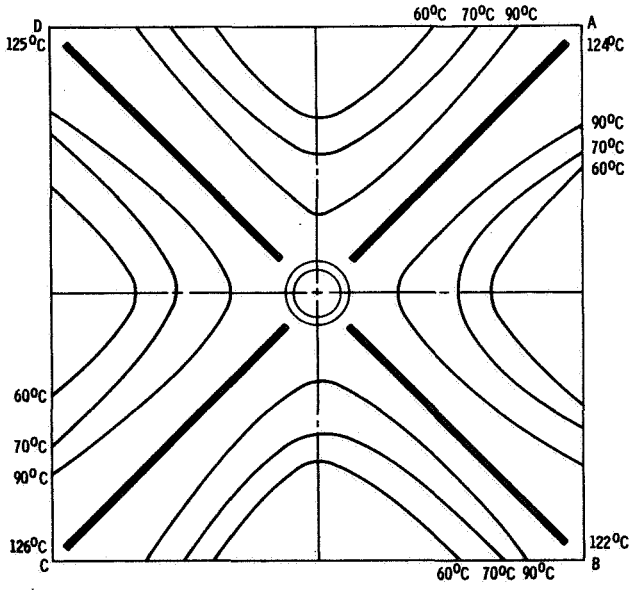

Figure 52. Temperature Distribution at 1500 Watts with Four Heat Pipes (A, B, C, D) Operating

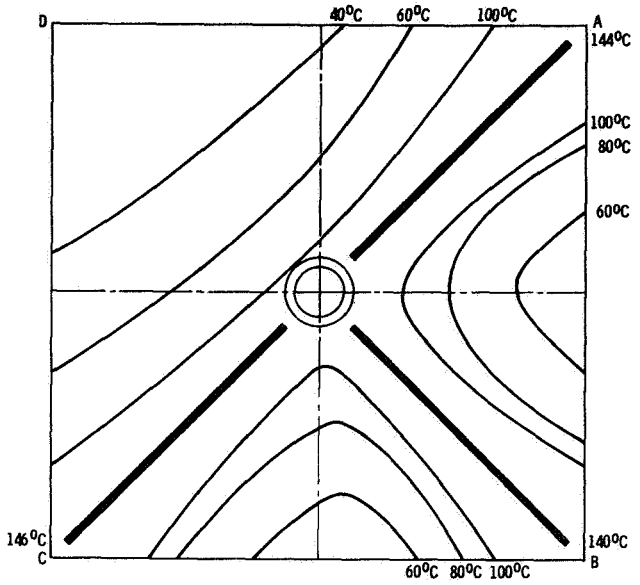

Figure 53. Temperature Distribution at 1500 Watts with Three Heat Pipes (A, B, C) Operating

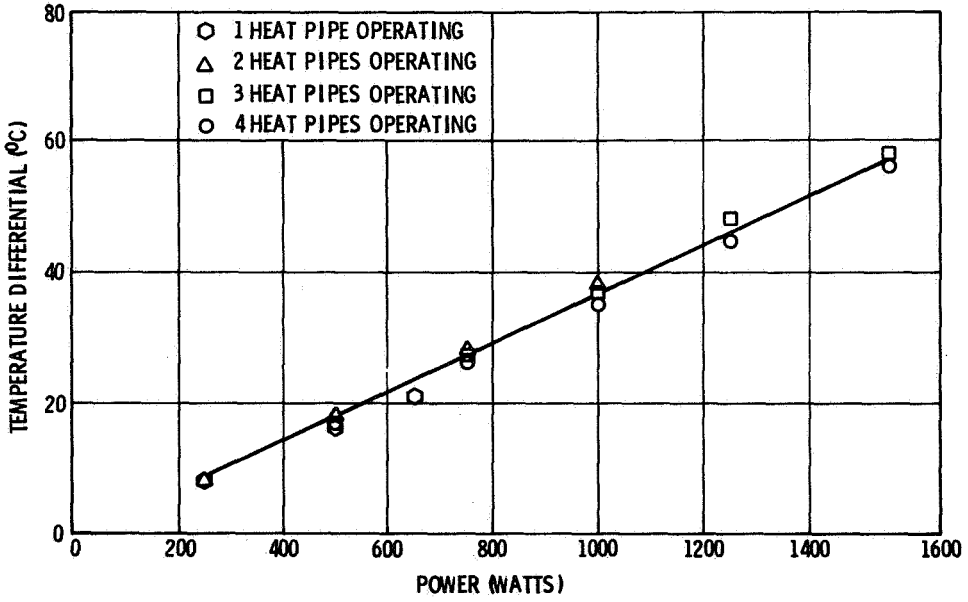

Figure 54. Collector Interface Temperature Differential

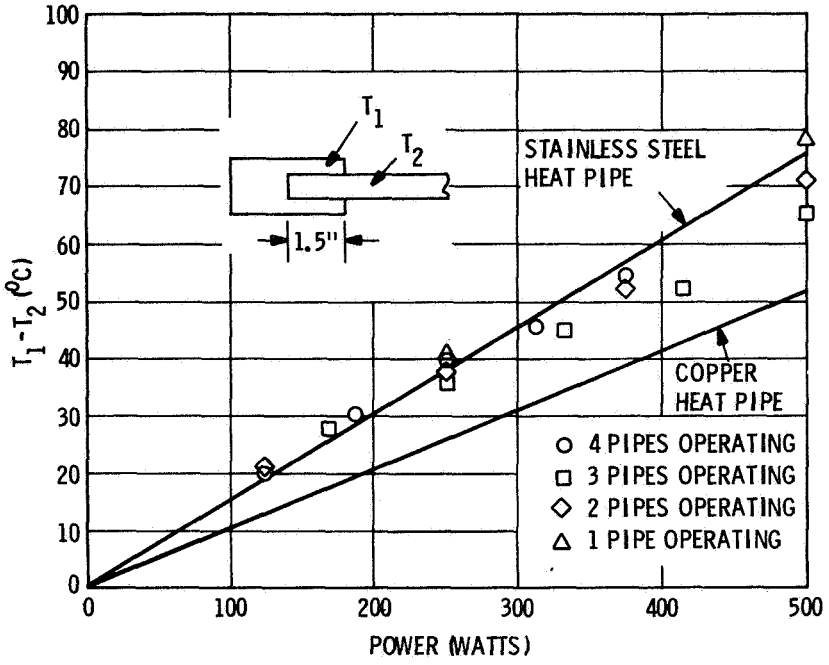

Figure 55. ΔT for Threaded Interface

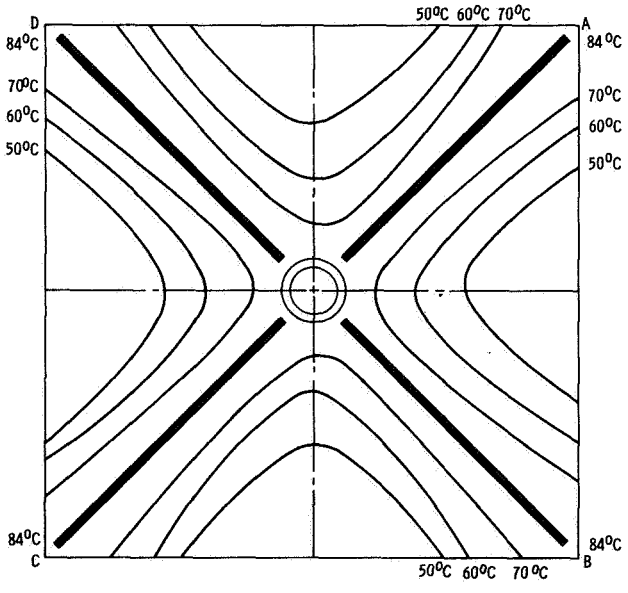

Figure 56. Temperature Distribution at 750 Watts with Four Heat Pipes Operating (Actual TWT Operating)

Figure 56, prove the characteristics obtained with the electrical simulator (Figure 49) to be valid.

For the tests using the TWT, additional temperatures were monitored on the tube itself. The temperature on the tube body heat transfer interface was maintained below $40^{o}C$, although forced air was required in the higher-power case. The temperature of the metal-ceramic seal near the collector was monitored by a thermocouple bonded to the metal side. The seal temperature was $140^{o}C$ at 750 watts and $155^{o}C$ at 930 watts collector dissipation. Both temperatures are lower than the temperature at the collector, indicating a heat flow from the collector toward the helix. This is to be expected since the radiator along the body of the tube operates more than $100^{o}C$ cooler than the collector.

5.3 CONCLUSIONS

The preceding analytical and empirical results have clearly demonstrated that cooling of a high-power microwave tube with a heat pipe radiator is a feasible concept. Furthermore, due to (1) the high reliability inherent in its design, (2) the ease with which redundancy can be designed into the radiator, and (3) the absence of an electrical power requirement, the heat pipe radiator will undoubtedly be used to provide temperature control for high-power output devices and other components where power densities are high or where physical location is too remote from a radiating surface to use purely passive thermal control.

The results of the test using all four heat pipes at a power of 750 watts show the calculations for the heat-rejection capacity of the radiator to have been overly conservative. As previously mentioned, this was expected due to the approach taken to the computation of fin effectiveness.

As a space radiator, the configuration tested is capable of rejecting 855 watts to space with the heat pipes operating at $115^{o}C$. This capacity can be increased to 1100 watts by attaching the heat pipes directly to an enlarged collector and using copper as

the heat pipe material. By these relatively small changes in design, the operating temperature of the heat pipes can be increased to 150°C, since the collector interface drop is eliminated. The high heat-rejection capacity, in addition to the increase in temperature over that of the radiator tested, is the result of the reduction of the sink from room temperature to absolute zero and the increase in effectiveness resulting from the absence of convection. Effectiveness is increased because the characteristic fin length, described in Appendix B, is reduced.

The data presented in Appendix B further illustrates the effect of the thermal design of the tube on the radiator. The radiator for a 5-kilowatt (thermal dissipation) tube which requires a 150°C sink has an area of 62-1/2 square feet and weighs 42-1/2 pounds. If improvements in the thermal design of the device itself can be made such that a 200°C radiator maintains the temperature-sensitive portions of the tube below their maximum limit, the radiator area can be reduced by 22 square feet and the weight by more than 11 pounds.

As these examples clearly show, significant reductions in radiator requirements can result from improved thermal design of transmitter devices, such as travelling wave tubes, klystrons, crossed-field amplifiers, and gridded tubes, intended for use in space. The goal of a completely optimized device can be reached only if thermal control considerations are included at all stages of tube design.

SECTION 6

REFERENCES

1. Beggs, J.E.: "Sealing Metal and Ceramic Parts by Forming Reactive Alloys," IRE Transactions of the Professional Group on Component Parts. Volume CP-4, Number 1, March 1957.

2. Dix, E.H.: Transactions of Institute of Metals Division. AIME, 137, 11, 1950.

3. Bates, J.F., and Loginow, A.W.: "Principles of Stress-Corrosion Cracking of Steels." Paper presented at Northest Regional Conference of the National Association of Corrosion Engineers (Niagra Falls, New York), October 22, 1963.

4. Branch, G.M., and Mirhan, T.G.: Analytical Designs of a Spaceborne Magnetically Focused Klystron Amplifier. NASA CR-72461, 1968.

5. Fried, E.: Study of Interface Thermal Contact Conductance. Summary Report of NASA Contract No. NAS 8-1127, 1965.

6. Kunz, H.R., Langston, L.S., Hilton, B.H. Wyde, S.S., and Nashick, G.H.: Vapor-Chamber Fin Studies - Transport Properties and Boiling Characteristics of Wicks. NASA CR-812, 1966.

7. Lieblein, S.: Analysis of Temperature Distribution and Radiant Heat Transfer Along a Rectangular Fin of Constant Thickness. NASA TN-D-196, 1959.

SECTION 7
BIBLIOGRAPHY

Beggs, J.E.: "Sealing Metal and Ceramic Parts by Forming Reactive Alloys," IRE Transactions of the Professional Group on Component Parts. Volume CP-4, Number 1, March 1957

Dix, E.H.: Transactions of Institue of Metals Division. AIME, 137, 11, 1950

Bates, J.F., and Loginow, A.W.: "Principles of Stress-Corrosion Cracking of Steels." Paper presented at Northeast Regional Conference of the National Association of Corrosion Engineers (Niagara Falls, New York), October 22, 1963.

Branch, G.M., and Mirhan, T.G.: Analytical Designs of a Spaceborne Magnetically Focused Klystron Amplifier. NASA CR-72461, 1968.

Fried, E.: Study of Interface Thermal Contact Conductance. Summary Report of NASA Contract No. NAS 8-1127, 1965.

Kunz, H.R., Langston, L.S., Hilton, B.H., Wyde, S.S., and Nashick, G.H.: Vapor-Chamber Fin Studies - Transport Properties and Boiling Characteristics of Wicks. NASA CR-812, 1966.

Lieblein, S.: Analysis of Temperature Distribution and Radiant Heat Transfer Along a Rectangular Fin of Constant Thickness. NASA TN-D-196, 1959.

Trefethen, L.: On the Surface-Tension Pumping of Liquids, or A Possible Role of the Candlewick in Space Exploration. General Electric Document 62SD114, February 1962.

Deverall, J.E., Salmi, E.W., and Knapp, R.J.: Orbital Heat Pipe Experiment. Report LA-3714, Los Alamos Scientific Laboratory, June 1967.

Anand, D.K.: "Heat Pipe Application to a Gravity-Gradient Satellite (Explorer XXXVI)." Proceedings of the ASME Aviation and Space Conference, pp. 634-638, June 1968.

Cotter, T.P.: Theory of Heat Pipes. Report LA-3246-MS, Los Alamos Scientific Laboratory, 1965.

Grover, G.M., Cotter, T.P., and Erickson, F.G.: "Structures of Very High Thermal Conductance," J. Appl. Phys. vol. 35, no. 6, June 1964.

Stenger, F.J.: Experimental Feasibility of Water Filled Capillary-Pumped Heat-Transfer Loops. NAS TM X-1310, 1966.

Proceedings of the ASME Aviation and Space Conference. pp. 634-676, June 1968.

Proceedings of Joint Atomic Energy Commission/Sandia Laboratories Heat Pipe Conference. Vol. I, SC-M-66-623, 1966.

Chambers, R.L., and Somers, E.V.: "Radiation Fin Efficiency for One Dimensional Heat Flow in a Circular Fin." (Preprint) 59-HT-8, ASME, August 1959.

Conway, E.C., and Wilmarth, R.W.: "Cooling of a High Power Electron Tube in a Space Vehicle." Proceedings of the 1968 IEEE Conference on Tube Techniques, 1968.

Basiulis, A., and Dixon, J.: "An Electrically Insulated Heat Pipe for Depressed Collectors." Proceedings of the 1968 IEEE Conference on Tube Techniques, 1968.

Millard, J.P.: "Results from the Thermal Control Coatings Experiment on OSO-III." (Preprint) 68-791, June 1968.

Linder, B.: "Series Emittance Thermal Control Coatings." Paper presented at the Thermal Control Working Group Meeting (Dayton, Ohio), August 1967.

Feldman, K.T., Jr., and Whiting, G.H.: "The Heat Pipe." Mech. Eng., pp. 30-33, February 1967.

Deverall, J.E., and Kemme, J.E.: High Thermal Conductance Devices Utilizing the Boiling of Lithium and Silver. Report LA-3211, Los Alamos Scientific Laboratory, October 1964.

Deverall, J.E., and Kemme, J.E.: Satellite Heat Pipe. Report LA-3278, Los Alamos Scientific Laboratroy, April 1965.

Haller, H.C., Lindow, E.G., and Auer, E.M.: Analysis of Low Temperature Direct Condensing Vapor-Chamber Fin and Conducting Fin Radiators. NASA TN D-3103, 1965.

Haller, H.C.: Comparison of Heat-Projection and Weight Characteristics of Several Radiator Fin-Tube Configurations. NASA TN D-2385, 1964.

Krels, R.P., Haller, H.C., and Auer, B.M.: Analysis and Design Procedures for a Flat, Direct Condensing, Central Finned-Tube Radiator. NASA TN D-2558, 1964.

Haller, H.C.: Analysis of a Double-Fin-Tube Flat Condenser-Radiator and Comparison with a Central Fin-Tube Radiator. NASA TN D-2558, 1964.

Haller, H.C., Liebline, S., and Lindow, B.G: Analysis and Evaluation of a Vapor-Chamber Fin-Tube Radiator for High Power Rankin Cycles. NASA TN D-2836, 1968.

APPENDIX A

HEAT PIPE PARAMETERS AND APPLICATIONS

The heat pipe is a closed system containing a two-phase fluid. Making use of the physical phenomena of phase equilibrium, phase change, and capillary action, the heat pipe can transport heat over relatively long distances through small cross sections with very little drop in temperature. Figure A-1 shows a heat pipe as a closed container lined with a wick saturated with a liquid; the remaining volume is filled with vapor of the same fluid. Heat input at the evaporator, as shown in the figure, causes liquid to vaporize, resulting in a local increase in pressure. This pressure gradient causes vapor to flow away from the "hot spot," which increases the pressure throughout the volume. This change in the equilibrium at the vapor-liquid interface at other surfaces of the container causes condensation. Thus, the latent heat of vaporization is transferred from the evaporator to the condenser. Condensate is returned by the wick, thus completing the cycle with no moving parts and no electrical power requirement.

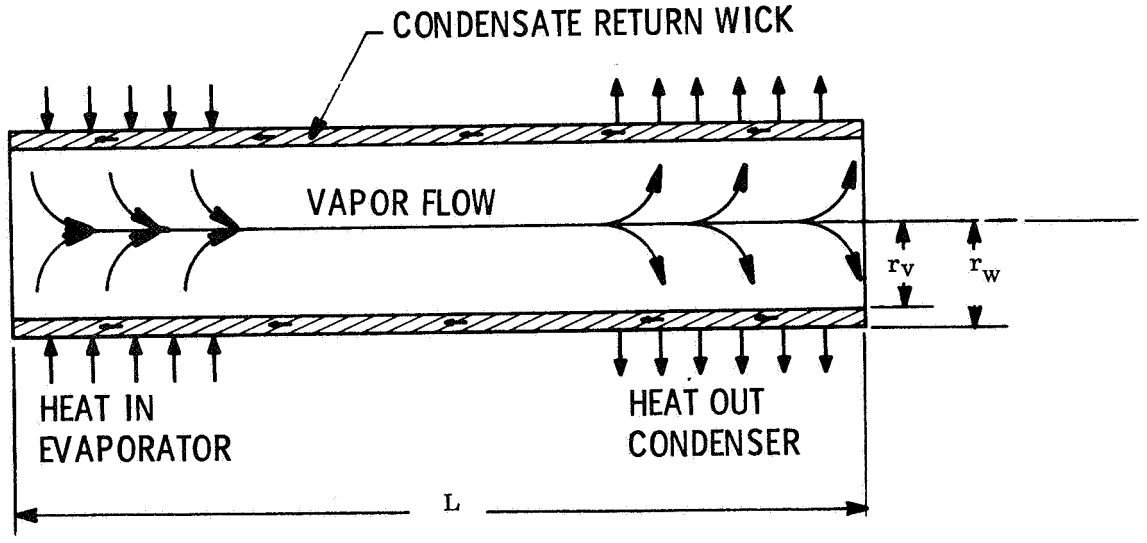

Figure A-1. The Heat Pipe

The use of the heat pipe for cooling spaceborne components was suggested at least as far back as early 1962 (Ref. A-1). Power dissipation levels at that time, however, were low enough that little interest was shown in the development of a working device.

Since that time, heat pipes have been developed for a broad range of applications over a temperature range from cryogenic to incandescent. At present, one heat pipe has been flown as a "piggyback" experiment (Ref. A-2) aboard the Agena used to orbit ATS/A, and two more have been operating successfully over an extended period aboard GEOS-B (Ref. A-3), thus firmly establishing the feasibility of zero gravity operation.

Nomenclature

ρ - density

γ - surface tension

λ - latent heat of vaporization

η - viscosity

ΔP - pressure drop

T - temperature

r - radius

L - total length

θ - wetting angle

e - wick void fraction

b - wick factor (see Ref. A-4)

Q - heat flow

$\dot{m}$ - mass flow rate

z - axial dimension

V - velocity

d - wick spacing

Subscripts

ℓ - liquid phase

v - vapor phase

c - capillary

w - outside surface of wick

A.1 DESIGN PARAMETERS

The four basic areas of design of a heat pipe are the vapor flow passage, the capillary structure, the evaporator area, and the condenser area. Since all depend to some extent on the properties of the working fluid, the fluid selection must be made before the heat pipe can be designed.

The selection of a working fluid for use in a heat pipe is extremely important when attempting to utilize the heat flow capability of this device to its fullest extent. The property requirements for a heat pipe working fluid are determined by the application, operating temperature, and heat flow capacity. The main characteristics of interest are as follows:

a. Melting Point. Since the material must flow through a capillary structure as it moves from the condensing section to the evaporator of the pipe, it must be in liquid form. Thus, the operating temperature must be above the melting point of the working fluid.

b. Vapor Pressure. The vapor pressure of the working fluid should be low enough at the operating temperature so that it can be easily contained. On the other hand, it must be high enough that the vapor will be sufficiently dense to carry the heat load without reaching choke velocity. Figure A-2 shows the vapor pressure of various heat pipe fluids as a function of temperature.

c. Latent Heat of Vaporization. A high latent heat of vaporization is important for a large heat flow capacity because it reduces the mass flow requirement. This reduces the required vapor flow cross section as well as the capillary cross section.

d. Liquid Viscosity. Since the liquid must flow through the capillary structure, the viscosity of the liquid phase of the working fluid should be as low as possible to minimize the pressure drop in the capillary.

e. Surface Tension. The return of the liquid phase of the working fluid from the condensing section to the evaporator of the heat pipe is accomplished entirely by capillary action. Since the force available for the movement of the fluid is proportional to the surface tension, it should be as high as possible.

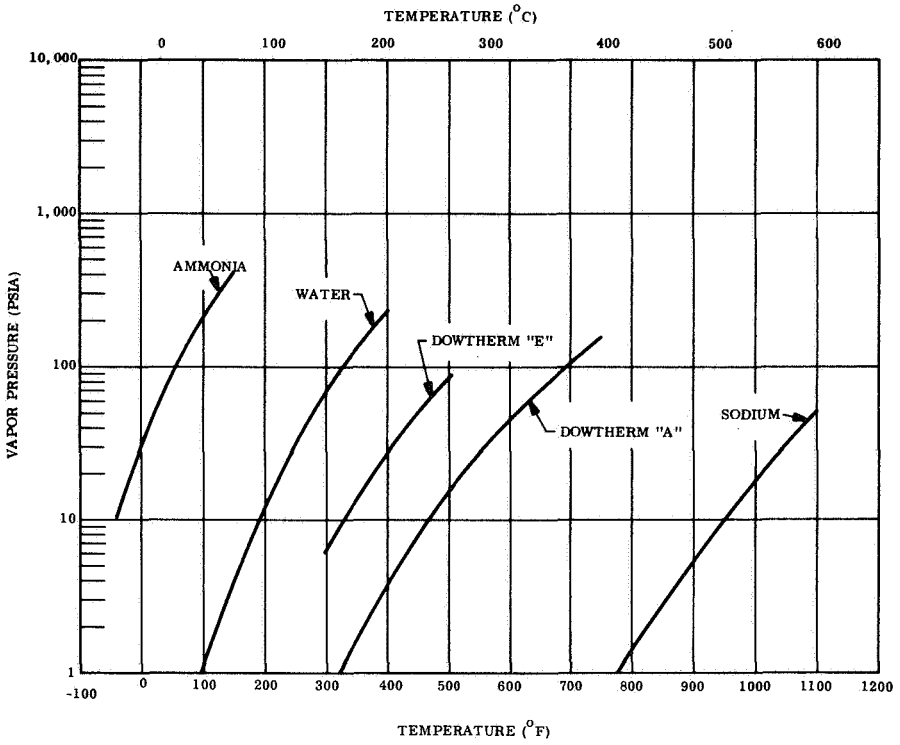

Figure A-2. Heat Pipe Fluids: Vapor Pressure Versus Operating Temperature

f. Wetting. The liquid phase of the working fluid must wet the surface of the capillary structure in order to pump the working fluid to the evaporator.

g. Corrosive Properties. No chemical interaction between any parts of the system can be tolerated. Not only would this endanger the mechanical integrity of the heat pipe, but solid contaminants could be deposited in the capillaries of the evaporator section and stop the flow of the working fluid. Noncondensible gases formed by corrosion reduce the efficiency of the heat pipe.

h. Density. The density of the liquid phase of the working fluid should be high to minimize the flow rate of the liquid through the capillary structure.

i. Stability. The fluid must be chemically stable at the operating temperature and pressure.

j. Thermal Conductivity. Where large quantities of heat are conducted radially through the fluid-filled wick at the condensing section of the heat pipe, large

temperature differentials can occur. Since this differential is almost a direct function of the thermal conductivity of the liquid, this property should be as high as possible.

k. Critical Heat Flux. The critical heat flux is the maximum heat flux which can be carried from a surface by a boiling fluid. While it depends in part on surface conditions, it is primarily a function of material and pressure. Its importance as a property of a heat pipe working fluid is that is determines the minimum area of the evaporator.

Some of the above properties are independent, while some must be considered relative to others. The simplest means of surveying the fluid properties is to consider them in relation to each of the four aspects of heat pipe design.

A.1.1 VAPOR FLOW PASSAGE AND CAPILLARY STRUCTURE

These two elements are considered together since they interact on each other. The maximum heat flow through a heat pipe occurs when the sum pressure drops due to vapor and liquid flow exactly equals the maximum pressure rise in the capillary:

$$\Delta P_v - \Delta P_\ell = \Delta P_c \qquad \text{(A-1)}$$

Cotter, in Ref. A-4, defines these three terms as:

$$\Delta P_v = \frac{4\eta_v LQ}{\pi \rho_v r_v^4 \lambda} \qquad \text{(A-2)}$$

for $|R_r| \ll 1$ and

$$\Delta P_v = \frac{(1 - 4/\pi^2)\, Q^2}{8\rho_v r_v^4 \lambda^2} \qquad \text{(A-3)}$$

for $|R_r| \gg 1$ where the radial Reynolds number is defined as

$$R_r = \frac{1}{2\pi\eta_v} \quad \frac{\dot{dm}_v}{dz} \tag{A-4}$$

The pressure drop in the liquid flowing through the capillary is given as

$$\Delta P_\ell = \frac{b\eta_\ell \, QL}{2\pi (r_w^2 - r_v^2) \, \rho_\ell \, e \, r_c^2 \, \lambda} \tag{A-5}$$

and the pressure rise due to capillary action is

$$\Delta P_c = \frac{2\gamma \cos\theta}{r_c} \tag{A-6}$$

Note that the pressure drop is defined for two flow regimes; thus, the pressure drop calculated for the vapor will differ, depending on the evaporation and condensation rates which are used in Equation A-4 to determine the radial Reynolds number.

For the purpose of determining the required heat pipe configuration for a given set of requirements, the use of the preceding equations is cumbersome and unnecessary. The geometry of the heat pipe is optimized when (Ref. A-4):

$$r_c = \frac{b\eta_\ell \, QL}{4\pi (r_w^2 - r_v^2) \, \rho_\ell \, e \, \lambda \, \gamma \cos\theta} \tag{A-7}$$

and

$$r_v/r_w = \sqrt{2/3} \tag{A-8}$$

Under these conditions the maximum heat flow is given as:

$$Q_{max} = \frac{\pi r_w^3 \, \lambda \gamma \cos\theta}{3L} \left[\frac{e\rho_v \rho_\ell}{3 b \eta_v \eta_\ell} \right]^{1/2} \tag{A-9}$$

For $|R_r| \ll 1$ and

$$Q_{max} = \frac{4\pi r_w^2 \lambda}{3} \left[\frac{2 \rho_v \rho_\ell e \gamma^2 \cos^2 \theta}{(\pi^2 - 4) bL \eta_\ell} \right]^{1/3} \quad \text{(A-10)}$$

for $|R_r| \gg 1$.

Results of Equation A-10 represent the most limiting case under most conditions, as shown in Figure A-3 for various fluids over a wide temperature range. The assumed configuration was a pipe 3.93 centimeters in internal diameter and 30.5 centimeters long. These results can be extended to other geometries by noting that the maximum heat transfer is directly proportional to the square of the internal diameter of the pipe and inversely proportional to the cube root of the length.

A.1.2 EVAPORATOR AREA

The evaporator area is important because it determines the heat flux in the evaporator. This, in turn, for a given power input, sets the operating point relative to two important points on the boiling curve, the onset of nucleate boiling and the critical heat flux. Figure A-4 shows the general relationships of the temperature difference between the evaporator surface and the vapor, ΔT, and the evaporator heat flux, Q/A. Over a range of ΔT from zero to point A on the figure, heat is removed by evaporation from the fluid surface. In the vicinity of point A, however, boiling begins, resulting in bubbles forming in the capillary. This disturbs the liquid flow, but is not accounted for in the theory represented by Equations A-1 through A-6. For high thermal conductivity fluids, such as liquid metals, the Q/A at which nucleate boiling begins is high enough that in most applications it can be overlooked. Where a working fluid having a very low thermal conductivity is used, however, nucleate boiling takes place at low values of Q/A.

As the ΔT increases from point A to point B on Figure A-4, boiling becomes more violent until at point B film boiling begins. Here, most of the evaporator is covered

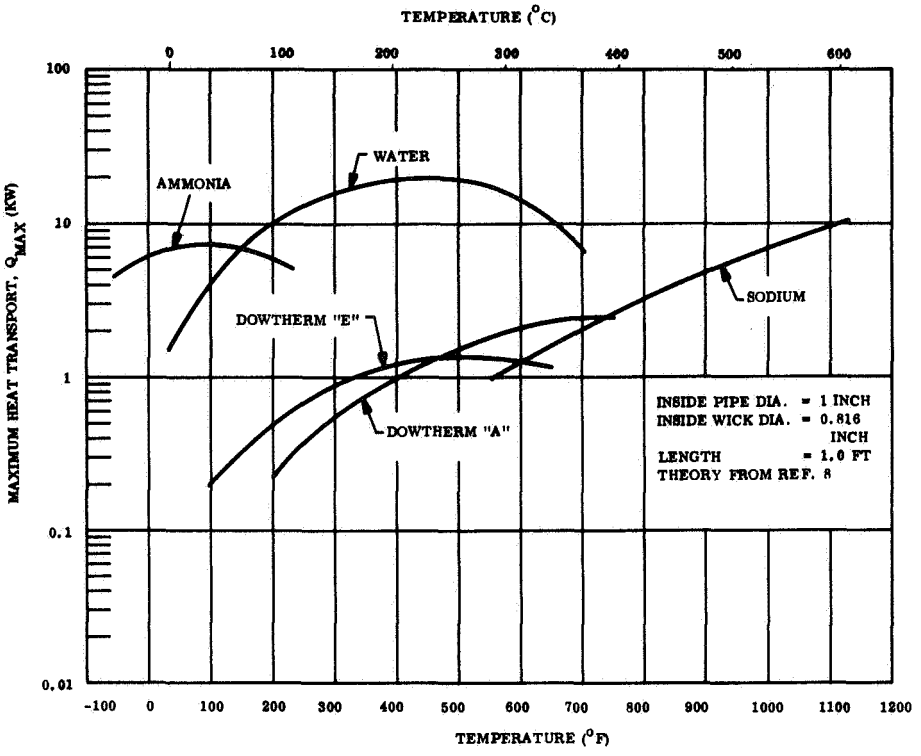

Figure A-3. Maximum Heat Pipe Capacity Versus Temperature

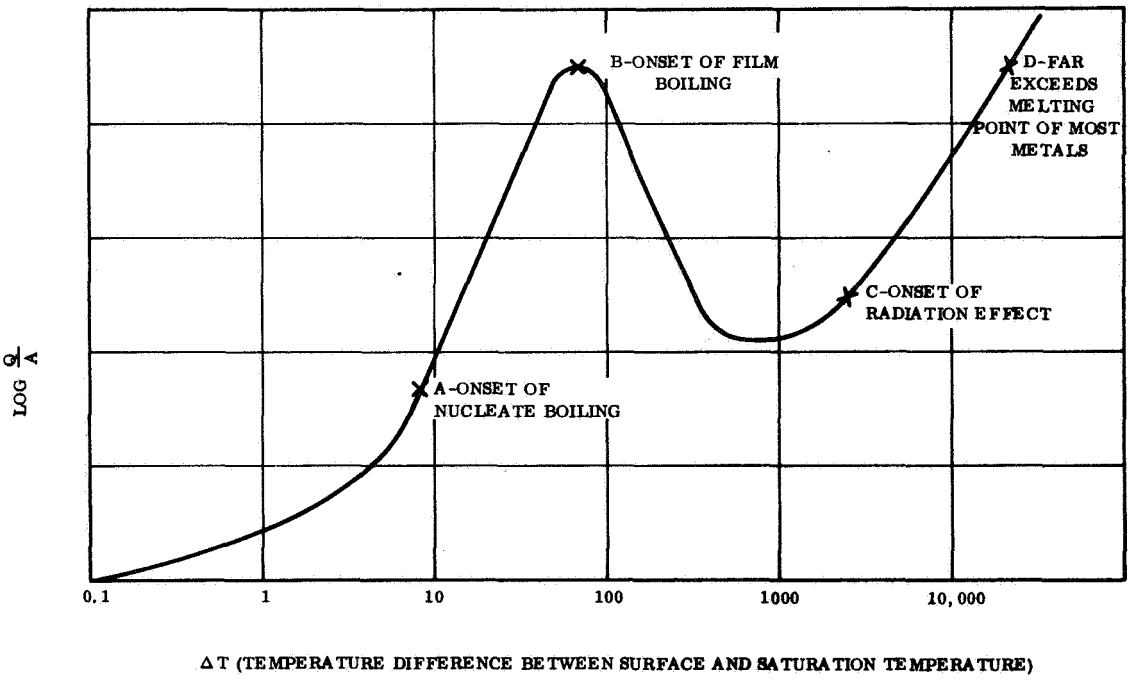

Figure A-4. Temperature Difference Between Evaporator Surface and Vapor (ΔT) and Evaporator Heat Flux (Q/A)

with a vapor film, limiting heat transfer and, if Q/A is not decreased, causing a drastic rise in the temperature of the evaporator surface. The heat pipe cannot operate beyond this point and thus, for a given heat load, the evaporator area must be sized to ensure operation below the critical heat flux. Ref. A-5 recommends that this limit be taken between 32 w/cm^2 and 64 w/cm^2. Ref. A-6 indicates for a water boiling from a wick, 46 w/cm^2 should not be exceeded. In general, it is best to stay as far below these limits as possible.

A.1.3 CONDENSER AREA

The surface area of the condenser affects both the maximum heat flow and the temperature drop in the heat pipe. The limit for condensation is recommended by Ref. A-5 to be the same as for evaporation. For a high power density in the evaporator, however, the temperature drop radially through the fluid filled wick can be excessive. Except for the liquid metals, a heat pipe fluid generally has low thermal conductivity. Heat removed in condensing the vapor on the inside of the wick must flow radially through the fluid-wick composite to the heta pipe wall, through the wall, and then to whatever heat sink is provided. For a layered screen wick, the thermal conductivity of the composite is little better than the conductivity of the fluid alone. For a condensation rate equivalent to 32 w/cm^2 the temperature drop through a water filled wick is 4600^{o}C/cm thickness at 100^{o}C. Thus, it is apparent that the thickness of the wick must be minimized if the heat pipe is to be useful. This can be done by using a wicking arrangement which is nonuniform circumferentially or by using an artery. Both concepts are shown in Figure A-5. Here, the vapor condenses on the thin portion of the wick, thus minimizing the distance which the heat must flow through the fluid. Practically, the wick can be kept to a thickness of 0.009 to 0.013 centimeter keeping the temperature drop below 60^{o}C even in the maximum power density case.

A.2 HEAT PIPE PERFORMANCE

In order to evaluate the theoretical equations for maximum heat pipe capacity, a heat pipe 51 centimeters long and 2.14 centimeters inside diameter was built and tested (see Figure A-6).

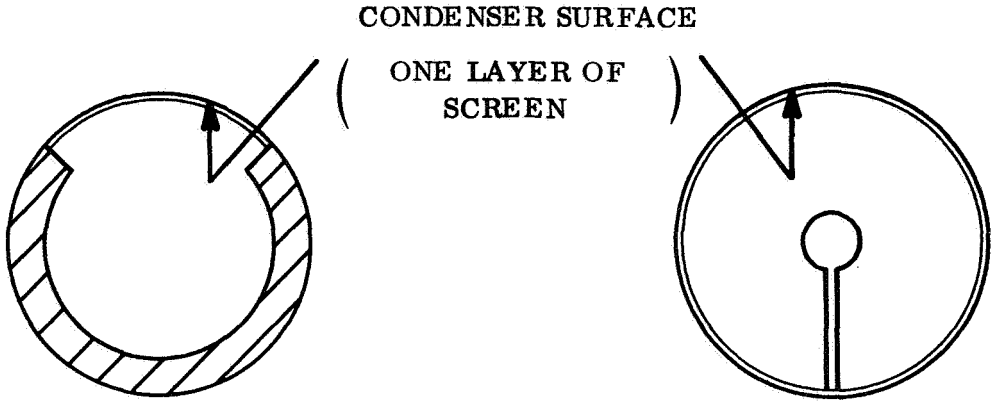

Figure A-5. Typical Nonuniform Wick Configurations

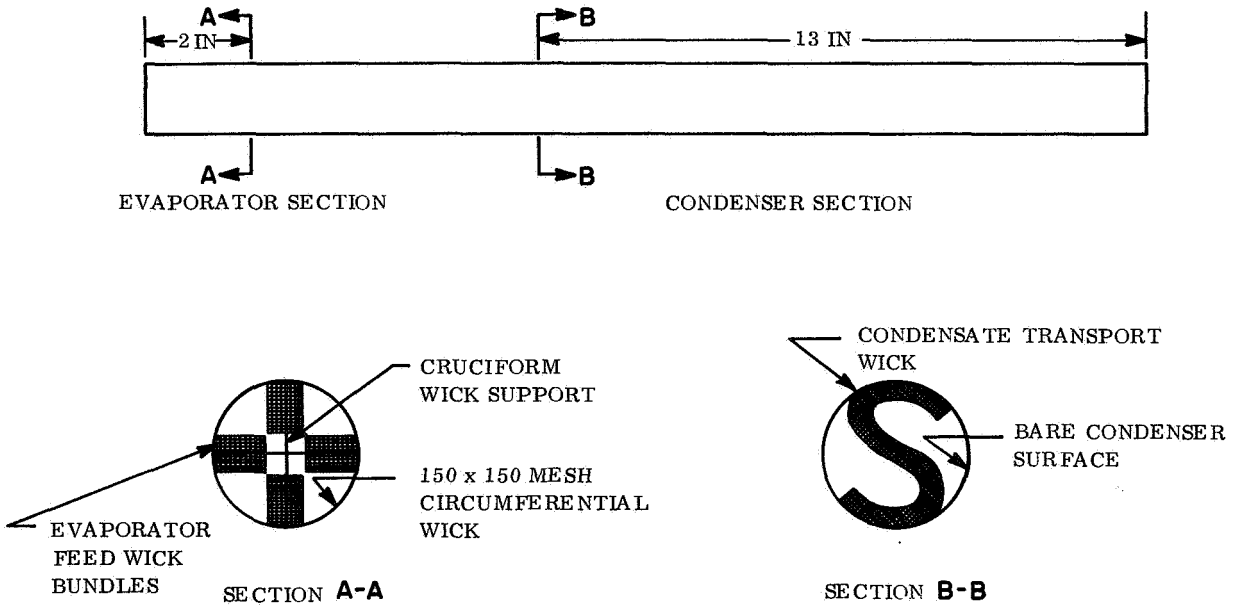

Figure A-6. Performance Evaluation Heat Pipe

The results of a series of tests run with this pipe showed a maximum capacity of slightly over 1.5 kilowatts at an operating pressure of 296 KN/m^2 (43.0 psia) and an internal temperature of 134°C (273°F) using 80 milliliters of water. According to Equation A-10 the pipe capacity should have been 10.6 kilowatts, a factor of over 7 higher. Evaporator power density was 43 w/cm^2 at the power, which is near the maximum value previously discussed. Tilting the pipe so that gravity aided condensate return increased capacity to over 2 kilowatts, indicating that either failure was not due to evaporator burnout or that the mechanism of evaporator failure is different when boiling from a wick than in pool boiling.

To visually inspect the action in the evaporator section of the heat pipe, two layers of 100 mesh screen were wound around a 1-inch diameter, electrically heated cylinder. The cylinder was placed in a shallow dish containing water to a depth of 0.1 inch. With sufficient heat applied to cause violent boiling over the portion of the cylinder covered with wick, the reason for at least part of the discrepancy between theoretical and test results was shown to be nucleate boiling in the wick, a phenomenon not accounted for in the theory. The pressure built up by water vaporizing beneath the screen increases until it is relieved by blowing water out through the mesh and away from the heated cylindrical surface. Since, in a heat pipe, heat transfer depends on vaporizing the fluid, this "spitting" reduces capacity. This situation can be relieved by reducing the heat flux in the evaporator (increase evaporator area) or by using a high conductivity fluid, such as one of the liquid metals, so that boiling takes place at the liquid surface instead of inside the wick.

A.3 HEAT PIPE FAILURE MODES

Heat pipe failure can occur in any of several ways in addition to exceeding the limits previously described.

A.3.1 LOSS OF FLUID

A loss of the heat pipe working fluid will obviously cause total failure. Where mech-

anical design is adequate and where welds are thoroughly checked for leakage at time of fabrication, loss can only be caused by penetration of the heat pipe wall. By choice of shield thickness, the probability of failure due to micrometeoroid penetration can be brought to almost any desired level, and therefore, fluid loss should not be a serious problem.

A.3.2 ENTRAINMENT

Where the vapor phase of the working fluid moves at high velocity, the force of the vapor on the returning liquid can force liquid from the wick, thus preventing it from reaching the evaporator. If the Weber number is well below 1, entrainment should be no problem. Where the Weber number (the ratio of the force on the returning liquid and the surface tension forces) is defined as:

$$We = \frac{\rho_v V_v^2 d}{\gamma} \qquad \text{(A-11)}$$

A.3.3 FREEZING OF THE WORKING FLUID

Where the working fluid freezes inside the heat pipe, problems may or may not exist, depending on the location of the frozen fluid. Where there is fluid, in solid form, in the evaporator, heat applied will melt and then vaporize the fluid. Condensation on the adjacent portion of the frozen fluid filled wick will melt more fluid, which in turn supplies the evaporator with the condensed and the melted fluid through the wick. If the latent heat of vaporization of the working fluid is greater than the latent heat of fusion, a given weight of condensing vapor will melt more than its own weight of frozen fluid, and thus the working fluid will progressively melt over the entire length of the heat pipe. If, however, there is no frozen fluid at the evaporator when heat is applied, obviously the heat pipe cannot operate. In such a case, heat must be either conducted along the pipe wall to where the frozen working fluid has collected or separate heaters must be used. Depletion of the evaporator can occur easily where the condenser is colder than the evaporator when the heat source is off. Vapor from the evaporator continually migrates to the

condenser and freezes until the evaporator is depleted. This can happen even when the fluid in the evaporator is frozen, due to sublimation. A small amount of inert gas introduced into the heat pipe can effectively block this migration, however, and hence the problem of freezing the working fluid can be eliminated.

A.4 REFERENCES

A-1. Trefethen, L.: On the Surface-Tension Pumping of Liquids, or A Possible Role of the Candlewick in Space Exploration. General Electric Document 62SD114, February 1962.

A-2. Deverall, J.E., Salmi, E.W., and Knapp, R.J.: Orbital Heat Pipe Experiment. Los Alamos Scientific Laboratory Report LA-3714, June 1967.

A-3. Anand, D.K.: "Heat Pipe Application to a Gravity-Gradient Satellite (Explorer XXXVI)," Proceedings of the ASME Aviation and Space Conference. June 1968, pp. 634-638.

A-4. Cotter, T.P.: Theory of Heat Pipes. Los Alamos Scientific Laboratory Report LA-3246-MS, 1965.

A-5. Parker, G.H., and Hamson, J.P.: "Heat Pipe Analysis." Proceedings of the ASME Intersociety Energy Conversion Engineering Conference, American Society of Mechanical Engineers, New York, New York, pp. 847-857, 1967.

A-6. Kunz, H.R., Langston, L.S., Hilton, B.H., Wyde, S.S., and Nashick, G.H.: Vapor-Chamber Fin Studies - Transport Properties and Boiling Characteristics of Wicks. NASA CR-812, 1966.

APPENDIX B

SPACE RADIATORS

B.1 INTRODUCTION

In a space environment, the only mode by which an electronic component can reject heat directly to space is by radiation. In the case of a component with a low thermal dissipation, it may be possible to reject the heat by radiation from the component baseplate while maintaining the component below some fixed upper temperature limit. The component baseplate acts as a radiator and the amount of heat rejected can be controlled, to a certain extent, through the use of coating materials. However, as component dissipations increase and/or the size of component baseplates decreases, a point is reached where it is no longer possible to reject a sufficient amount of heat from the baseplate to keep the component temperature from exceeding its specified upper limit. Hence, in order to maintain the component temperature below the upper limit, it is necessary to increase the heat rejection capability of the baseplate. One method of accomplishing this is to attach an extended surface or fin to the baseplate which increases the effective area for radiation. The fin can be of a completely passive nature or it can have heat pipes attached in order to bring it closer to the isothermal condition.

This appendix investigates weight-optimized passive fins and heat pipe fins over a wide range of power dissipations for various source temperatures.

The following nomenclature is used throughout Appendix B.

Q_o - heat radiated by an isothermal plate

ϵ - emissivity

A - area

F - radiation view factor

σ - Stefan Boltzmann constant

T_o - temperature

η - fin effectiveness

Q - heat radiated from a fin

ϕ_c - circular fin characteristic length

r - radius

r_o - heat source radius

K - thermal conductivity

t - fin thickness

ϕ_H - straight fin characteristic length

L - fin length

T_s - equivalent sink temperature

$\overline{S}$ - average incident solar energy

$\overline{A}$ - average incident reflected solar energy

$\overline{E}$ - average incident earth emitted energy

α_s - solar absorptivity

B.2 ASSUMPTIONS

In order to make a meaningful comparison between the two types of fins, the following simplifying assumptions were made:

a. The baseplate of the electronic device is isothermal.

b. Temperature drop between the baseplate and the fin is negligible.

c. All power is dissipated through the baseplate.

d. Fin material is aluminum:

1. Thermal conductivity = 80 Btu/hr-ft-^{o}F

2. Density = 0.1 lb/in^{3}

3. Specific heat = 0.2 Btu/lb-^{o}F

e. Fin surface emissivity = 0.85.

f. Fin radiates from one side to a 0^{o}F sink only.

g. View factor to space is 1.0.

These assumptions apply to both types of fins considered. The specific assumptions concerning the passive fin and the heat pipe fin will be delineated in their respective sections.

B.3 ANALYSIS

In general, the analysis consisted of finding the optimum (minimum weight) passive and heat pipe fins and comparing them on a weight and size basis over a wide range of power dissipations for various source temperatures. Before the detailed procedure is described for finding the optimum passive and heat pipe fins, a brief discussion of fin effectiveness is appropriate.

The heat rejected by a flat plate at a constant temperature radiating to an absolute zero sink is given by:

$$Q_o = \epsilon A F_A \sigma T_o^4 \qquad \text{(B-1)}$$

However, in the case of an extended surface, which is not uniformly heated, a temperature gradient exists along the surface in a direction moving away from the source. As a result, heat is dissipated at varying rates, depending on the distance from the source. To account for this varying heat dissipation, a quantity called fin effectiveness is introduced. This quantity is defined as the ratio of the heat actually dissipated by the fin to the heat which could be dissipated if the fin were isothermal at the root temperature. Hence:

$$\eta = \frac{Q}{Q_o} \tag{B-2}$$

Combining Equations B-1 and B-2, it can be seen that the heat rejected by an extended surface is:

$$Q = \eta \epsilon A F_A \sigma T_o^4 \tag{B-3}$$

Therefore, once the fin effectiveness is known, the heat rejection from the fin can easily be found. Fortunately, the governing differential equations have been solved previously, and the results presented in terms of fin effectiveness. Specifically, Ref. B-1 contains fin effectiveness values for a circular fin heated at the center and Ref. B-2 contains fin effectiveness values for a straight fin heated uniformly along one edge.

B.3.1 PASSIVE FINS

In the case of passive fins, it was assumed that the fin was circular in shape with a circular heat source rigidly attached at the center. The portion of the fin covering the baseplate was assumed to be isothermal at the source temperature. Hence, Ref. B-1 could be used to optimize the fin on a minimum weight basis. This reference presents values of fin effectiveness versus a dimensionless quantity with the ratio of outer radius to source radius as a parameter. The dimensionless quantity is defined as:

$$\phi_c = \sqrt{\frac{\epsilon \sigma T_o^3 (r - r_o)^2}{Kt}} \tag{B-4}$$

Since both the radius ratio and the radius difference was involved, it was necessary to pick a value of the source radius. Two cases were analyzed, one with $r_o = 1$ inch and one with $r_o = 5$ inch. These were selected because a 1-inch radius device size approximately corresponds to the size of gridded tubes, travelling wave tubes, Klystron collectors and solid-state devices. A 5-inch radius device size approximately corresponds to the size of a circular format crossed field amplifier.

Once the source radius was fixed, values for the outer radius and fin thickness were chosen and the fin effectiveness corresponding to the desired source temperature was obtained. The heat rejection rate was calculated using Equation B-3 and compared to the desired value. This procedure was repeated for various values of outer radius until the heat rejection was the same as the desired value. Then, the weight of the fin was calculated. Next, another thickness value was chosen and the entire procedure repeated to obtain another value of fin weight. This was repeated until the minimum weight fin was found.

Since this procedure involved many repetitive calculations, it lent itself to programming for a digital computer. The program was written, checked out, and used to calculate the optimum weight fin parameters for a range of heat rejection rates from 0 to 3 kilowatts over a range of source temperatures from 104°F (40°C) to 752°F (400°C).

B.3.2 HEAT PIPE FINS

A complete description of heat pipes is contained in Appendix A of this report. The heat pipe fin was assumed to be a heat pipe with a fin extending outward from it. This corresponds to a straight fin heated uniformly along one edge and hence Ref. B-2 could be used to optimize the fin on a minimum weight basis. This reference presents values of fin effectiveness versus a dimensionless quantity with the equivalent sink temperature ratio as a parameter. The equivalent sink temperature ratio is the ratio of the equivalent sink temperature to the source temperature. In this case, the ratio is zero since only an absolute zero sink is considered at present. The concept of equivalent sink temperature is considered later.

The dimensionless quantity is defined as:

$$\phi_H = \sqrt{\frac{\epsilon \sigma T_o^3 L^2}{Kt}} \qquad \text{(B-5)}$$

which is very similar to the one for circular fins except the radius difference is replaced by the fin length, 1. The remaining quantities are the same as those defined for circular fins.

The procedure for optimizing the straight fin is exactly the same as that for the circular fin with fin length being iterated upon for each value of fin thickness. However, all computations were carried out on a per foot of width basis. After the optimum weight fin was calculated for a certain value dissipation per foot and at a specified source temperature, the heat pipe weight was added to the fin weight and a weight/heat ratio was obtained by dividing the combined weight per foot by the heat dissipated per foot. This procedure was repeated for different values of heat dissipation until the minimum weight/heat ratio was obtained. This was taken to be the weight optimized heat pipe fin. For the purpose of this analysis, a heat pipe weight of 0.4 lb/ft was assumed. Experience has shown this to be a good average value over a wide temperature range. Considerably smaller heat pipe weights can be attained for specific designs.

Once again, this procedure was programmed for a digital computer. The program was utilized to compute optimum weight heat pipe fin parameters for a range of equivalent sink temperatures from 104^{o}F (40^{o}C) to 752^{o}F (400^{o}C) and a range of equivalent sink temperatures from -460^{o}F to $+30^{o}$F. Data for an equivalent sink temperature of -460^{o}F is presented in Section B.4 while the remaining data is utilized in Section B.5, which discusses effects of non-zero sinks.

B.4 DISCUSSION OF RESULTS

The results of this fin analysis are shown on Figures B-1 through B-6. Figures B-1 and B-3 compare passive fins with heat pipe fins on a heat rejection versus weight basis and on a heat rejection versus area basis, respectively, for a source radius of 5.0 inches.

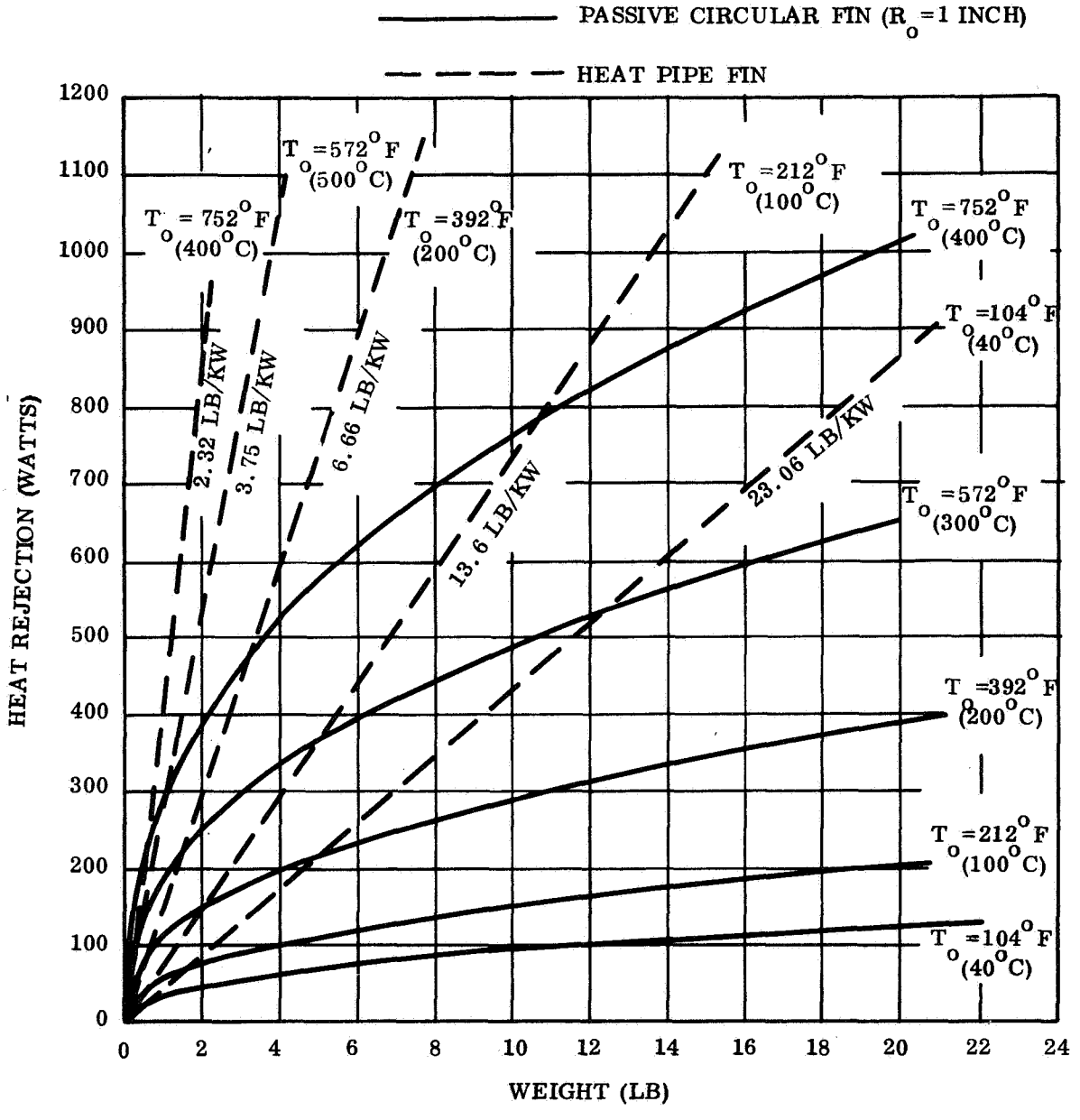

Figure B-1. Heat Rejection Versus Weight

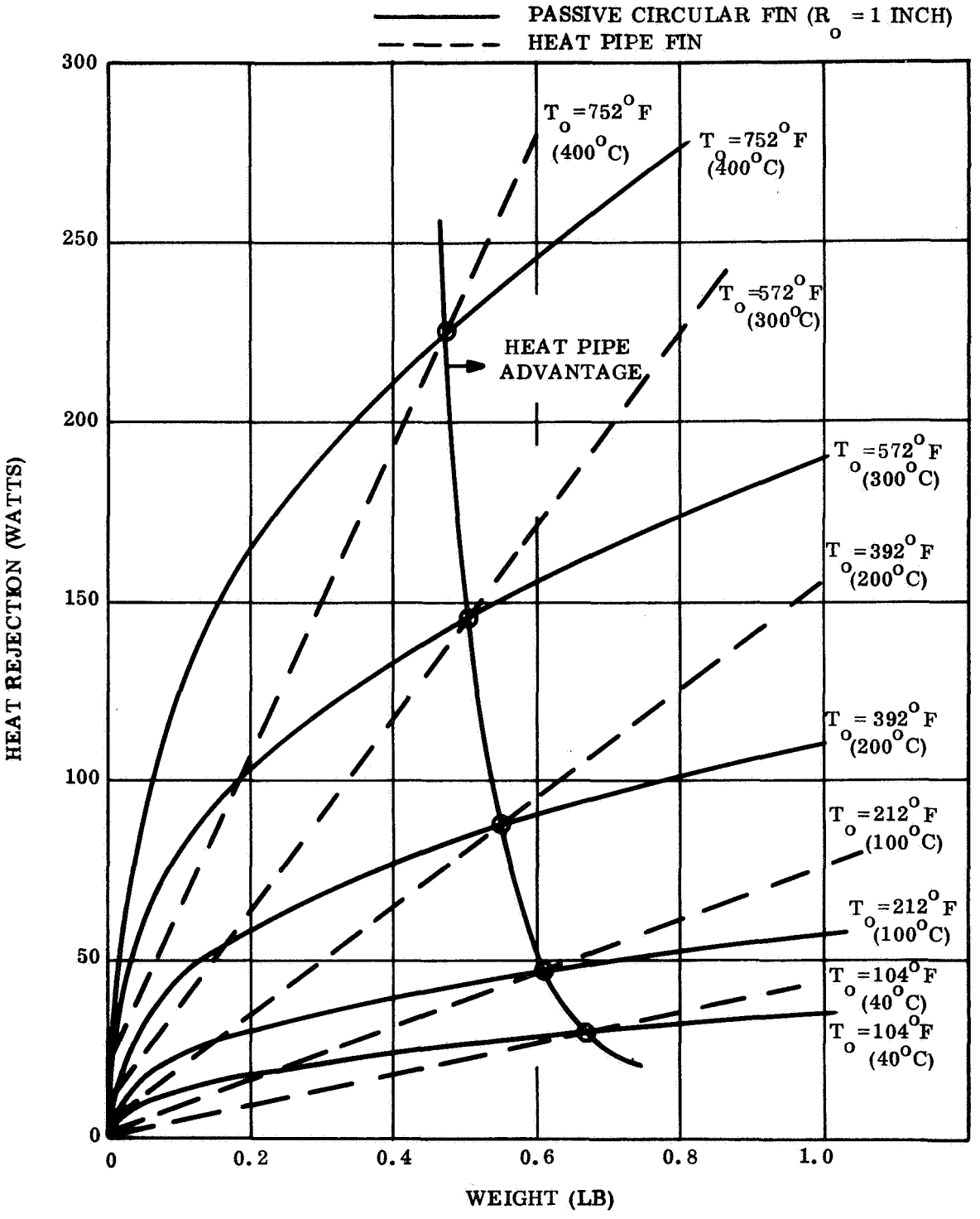

Figure B-2. Heat Rejection Versus Weight

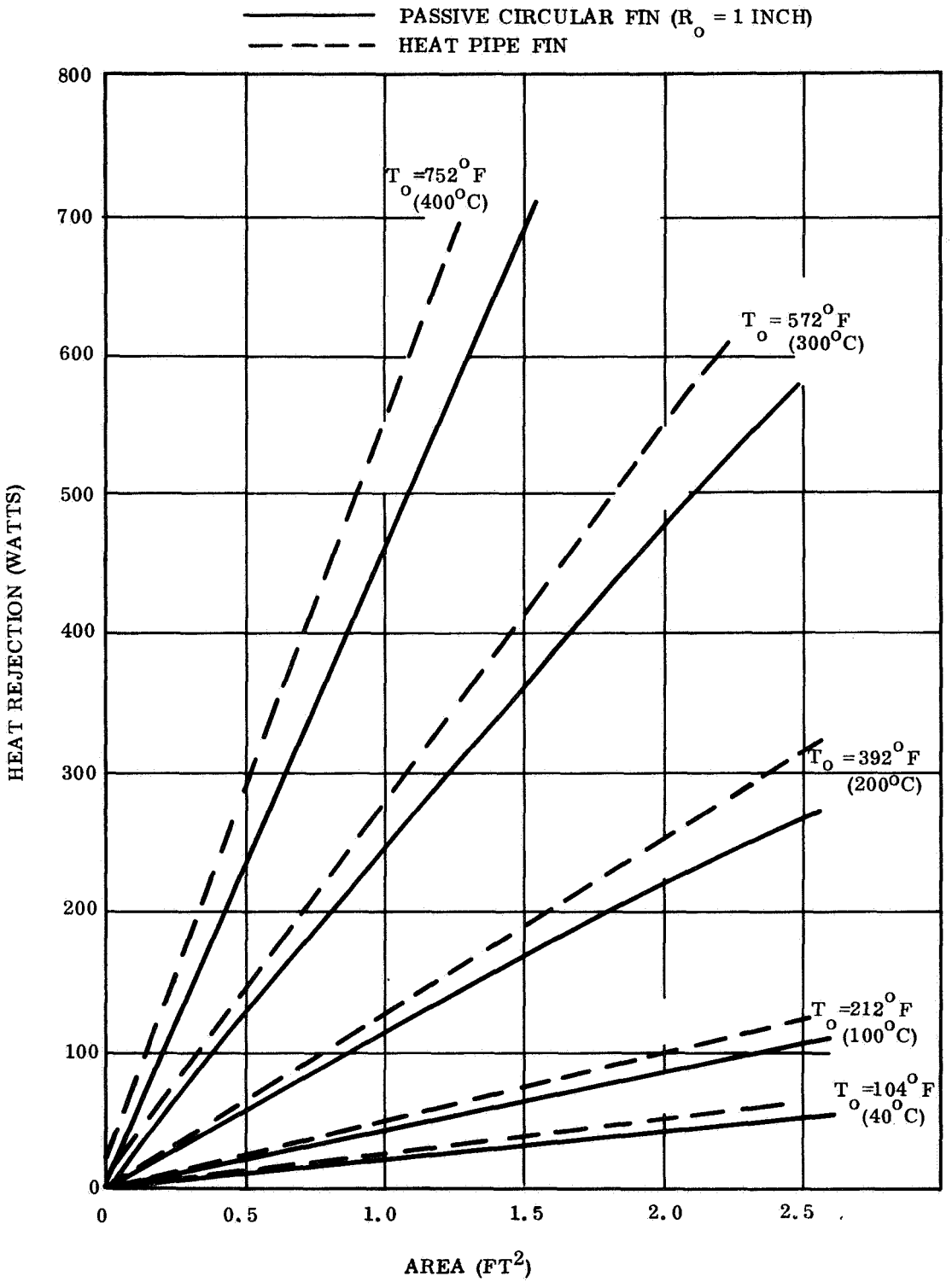

Figure B-3. Heat Rejection Versus Area

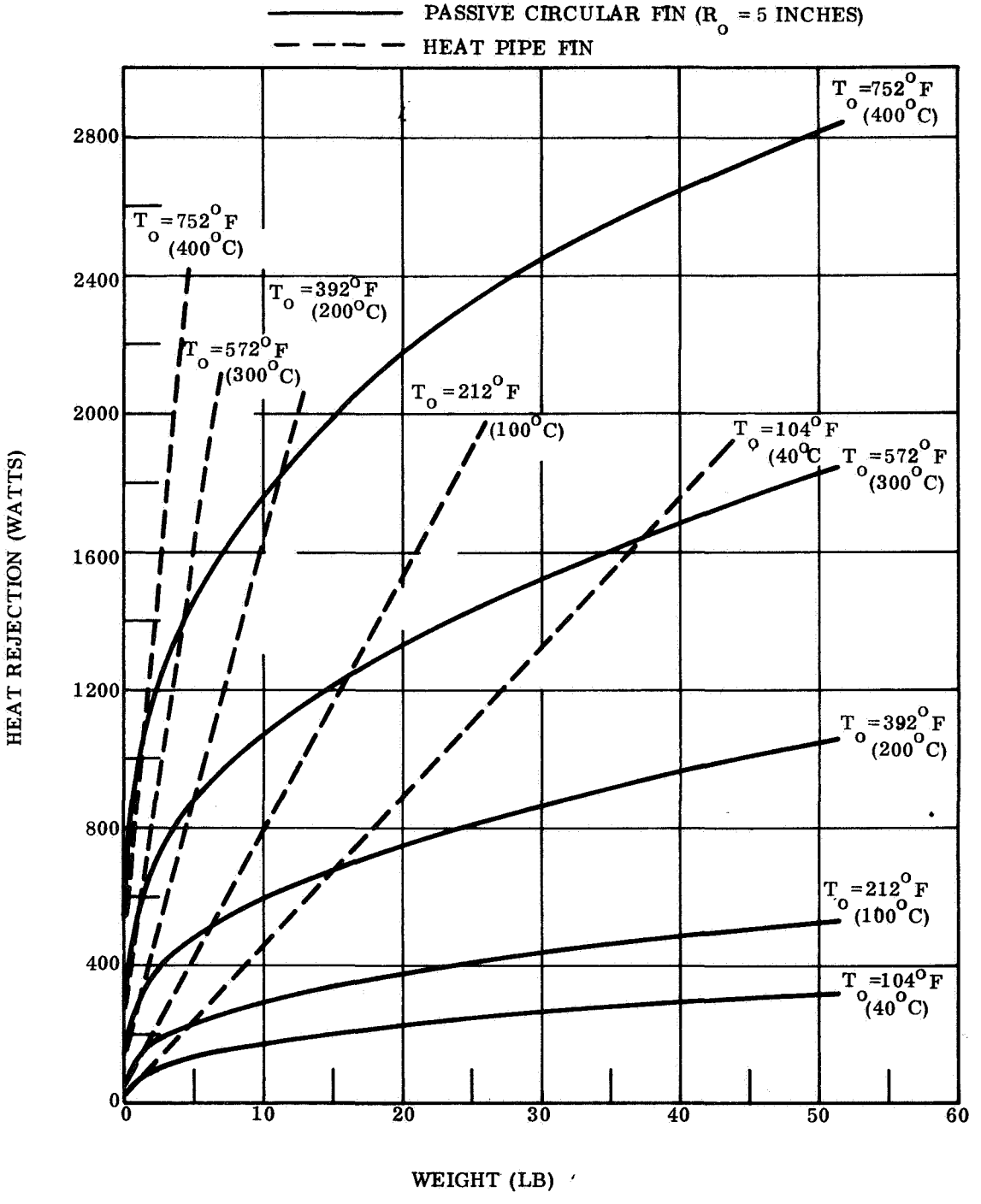

Figure B-4. Heat Rejection Versus Weight

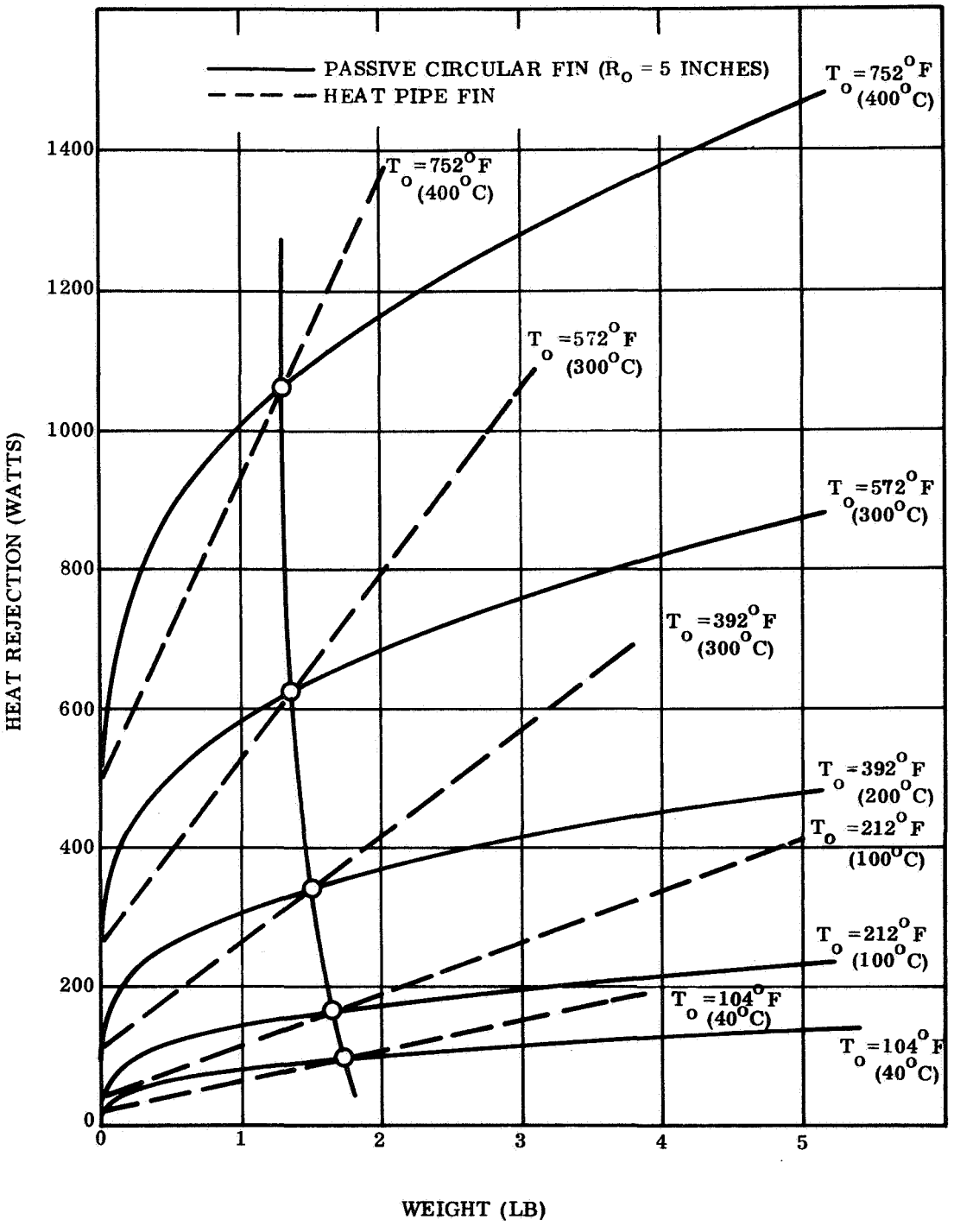

Figure B-5. Heat Rejection Versus Weight

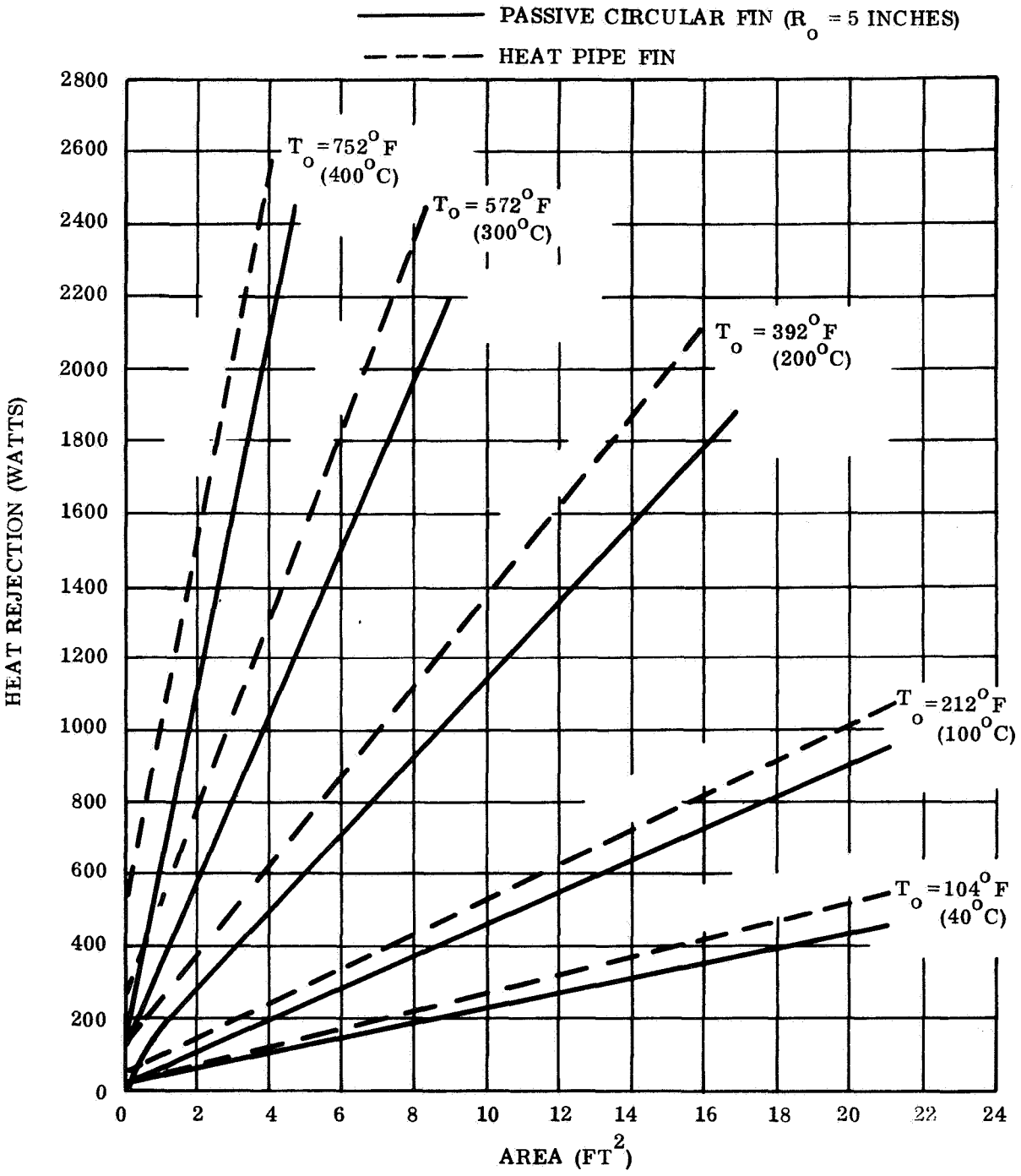

Figure B-6. Heat Rejection Versus Area

It can be seen from Figure B-1 that at any source temperature there is a definite advantage to heat pipe fins over passive fins except in the region near the origin. In order that this phenomenon could be studied more closely, the region near the origin was expanded and replotted as Figure B-2. This figure shows that there is a definite crossover of the heat rejection versus weight curves for heat pipe fins and passive fins at each value of source temperature. The locus of crossover points is also shown on Figure B-2. In the region to the left of this locus there is a weight advantage of passive fins over heat pipe fins. This is due to the fact that for small radiator sizes, the heat rejection capability of a fin is not appreciably increased with the addition of heat pipes whereas its weight is increased. However, in the region to the right of the locus of crossover points, the weight advantage of heat pipe fins over passive fins is immediately evident. In this region, the curves for the passive fins begin to flatten out requiring a large weight addition for a relatively small increase in heat rejection capability. The curves for the heat pipe fins remain linear.

Examining Figure B-3 discloses that heat pipe fins offer a definite area advantage over passive fins for all source temperatures at all heat rejection levels. It is known that a minimum area heat rejection surface is one that is at a uniform temperature (isothermal). This type of surface would have a fin effectiveness value of 1.0 and is an idealized case. However, since the addition of heat pipes makes a fin more isothermal, it is obvious that it will require less area to reject a given amount of heat at a specified source temperature.

The curves on Figures B-1, B-2, and B-3 do not start exactly at the origin because the baseplate itself has a certain heat rejection capability, depending on its temperature. The requirement for fins starts after this baseplate capability has been exceeded.

Looking at Figures B-4, B-5, and B-6, it can be seen that, in general, the results for a source radius of 5.0 inches show the same trends as do the results for a source radius of 1.0 inch. As a result, the preceding discussion is applicable to the results for both source sizes.

It should be mentioned that, although there is a definite crossover point between passive fins and heat pipe fins on a heat rejection versus weight basis, in some instances it may be desirable to pay a slight weight penalty in favor of the simplicity of a completely passive fin. In other instances, it may be necessary to use a heat pipe fin strictly on the basis of area limitation.

B.5 EXTERNAL FLUXES ON RADIATORS

B.5.1 THERMAL CONTROL COATINGS

The net heat radiated from the surface of a radiator which is receiving external inputs (solar, albedo and earth radiation fluxes) can be expressed by

$$Q = \eta \epsilon A (\sigma T_o^4 - \sigma T_s^4) \tag{B-6}$$

where T_s is an equivalent sink temperature for the particular environment. The equivalent sink temperature is given by

$$\sigma T_s^4 = \frac{\alpha_s}{\epsilon} (\bar{S} + \bar{A}) + \bar{E}$$

For the case of a fin coated with a material having properties and receiving a normal solar input, the equivalent sink temperature is

$$\sigma T_s^4 = \frac{\alpha_s}{\epsilon} S \tag{B-7}$$

where S is the solar constant.

The above equations indicate that a radiator at a given source temperature (T_o) will reject a maximum amount of heat when ϵ is a maximum and α_s is a minimum. From a design viewpoint, in order to reject a specified quantity of heat at a given source

temperature, the application of a coating with such properties will reduce the area and weight requirements of the radiator.

In addition to initially having the desired properties, the coating properties must remain reasonably stable for the duration of the mission. Solar wind protons and solar ultraviolet radiation produce radiative property degradation in thermal control coatings. There are, however, coatings which do not degrade to a great extent and are probably applicable for use in missions of extended duration. The best of these coatings are of two types:

a. Second surface mirrors

b. White thermal control coatings

Table B-1 is a compilation of the properties of those coatings which would lend themselves best to high efficiency space radiators.

Table B-1. Thermal Control Coatings

Coating Identification	α_s (Near Normal)	ϵ (At 300°K)	$\frac{\alpha_s}{\epsilon}$	Source
Z-93	0.17	0.90	0.19	IITRI*
S-13	0.19	0.81	0.23	IITRI
S-13G	0.23	0.88	0.26	IITRI
Series Emittance Coatings	0.05-0.10	0.80-0.85	0.06-0.13	General Electric
SI-100 (OSR)	0.05	0.76	0.07	OCLI**

*Illinois Institute of Technology Research Institute
** Optical Coatings Laboratroy, Inc.
Note: α_s and ϵ are laboratory measured values. (Prior to exposure to solar radiation)

B.5.1.1 Second Surface Mirrors

The state-of-the-art coatings which exhibit the least degradation with exposure to solar radiation are the so-called second surfacr mirrors. These coatings employ a dielectric film, which is transparent to the solar spectrum, over a highly reflecting metallic substrate.

The SI-100 (OSR) coating consits of approximately 1000 A of silver deposited on the back of 8 mils of fused silica. The coating has shown extreme stability in both laboratroy tests and spacecraft experiments; no change was exhibited in 1580 ESH in the OSO-III thermal control experiment. Another coating, MSI-100 has been developed by OCLI and is reputedly more stable to ultraviolet radiation than SI-100. Exposure of this material to the equivalent of five suns for 700 hours has indicated no measurable change in α_s. The major drawbacks of these materials are their very high cost and possible difficulties in application to unusually shaped surfaces. They are also approximately twice as heavy as the white thermal control coatings.

The series emittance coatings utilize the same principles as the SI-100 coatings with the exception of a flexible substrate replacing the fused silica. The properties shown in Table B-1 can be achieved by depositing silver on 5 mils of Teflon. This coating has been utilized in tape form by applying a pressure-sensitive adhesive to the metal surface and then bonding the coating onto the structure. It is also possible to apply the film by spray coating the dielectric directly onto the metallic structure. This, however, would necessitate a high temperature curing process and fairly close control over the thickness of the sprayed coating. The advantages of these coatings (in tape form) are low cost, relative ease of application to unusual surfaces and ease of replacing damaged areas. Their flexible substrate makes them less fragile than the SI-100 coatings.

B.5.1.2 White Thermal Control Coatings

The most stable of the white paints are Z-93 (zinc oxide in potassium silicate) and S-13 (zinc oxide in silicone) both developed by the Illinois Institute of Technology Research Institute.

The white paints are particularly susceptible to α_s degradation from "particulate" environments such as the solar wind and from exposure to ultraviolet. Although the paints discussed in this section are quite good in low inclination orbits, their degradation may increase significantly in a polar orbit due to increased particle bombardment. The "second-surface mirror" coatings appear to be the best coatings available at this time and are recommended in preference to the white paints.

Figures B-7 and B-8 present area and weight requirements, per kilowatt of vehicle power dissipation, as a function of source (device) temperature for minimum weight heat pipe radiators; curves for equivalent sink temperatures ranging from -460°F to $+30^{\circ}$F are included. The optimization of the fins was accomplished as discussed in Section B.4 of this appendix. Inspection of the curves shows the radiator requirements are less dependent upon sink temperature as the source temperature increases. As an example of this, the weight and area requirements for a 100°F source temperature radiator are increased by 32.4 and 31 percent, respectively, as the sink temperature changes from -50°F to 0°F. The corresponding increases for a 300°F radiator are only 6.8 and 3.8 percent. For a 10-kilowatt vehicle, this represents weight and area increases of 110 pounds and 170 square feet for a 100°F radiator. This is opposed to seven pounds and five square feet for a 300°F radiator.

It is also extremely important to notice that at a given sink temperature the radiator requirements are reduced drastically as the source temperature increases. For a -50°F equivalent sink temperature, the area requirements for 100°F and 400°F heat pipe radiators are 55 ft^2/kw and 7.8 ft^2/kw respectively, a decrease in area of approximately 86 percent. The corresponding weight requirements are 34 lb/kw and 6.9 lb/kw, a decrease of approximately 80 percent. This is representative of the type of tradeoff which could be achieved by utilizing a thermally integrated cross-field amplifier as the transmitting device as opposed to solid-state devices.

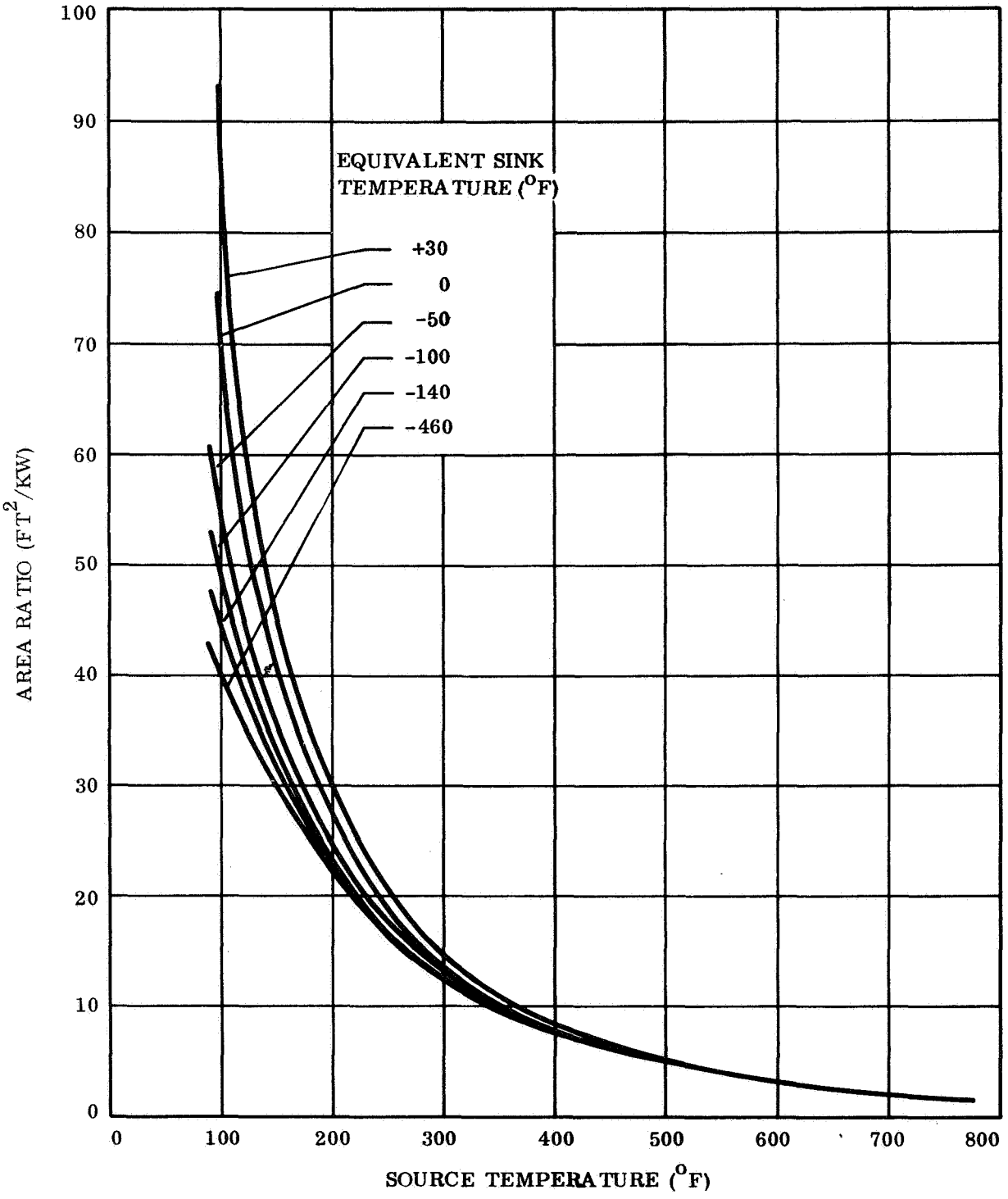

Figure B-7. Weight Optimized Heat Pipe Fin: Area to Power Ratio Versus Source Temperature

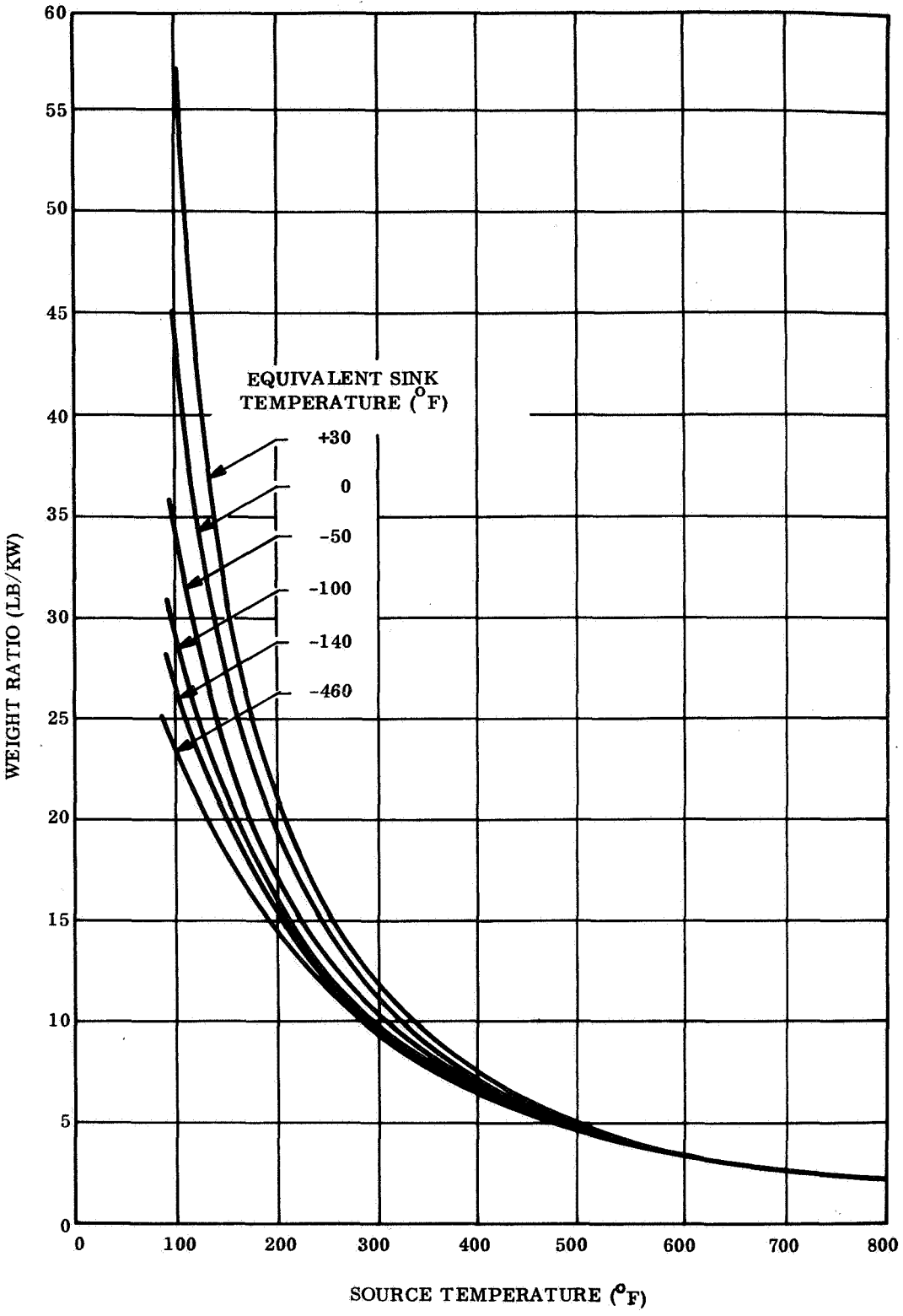

Figure B-8. Weight Optimized Heat Pipe Fin: Weight to Power Ratio Versus Source Temperature

Figures B-9 and B-10 are the area and weight requirements for minimum area radiators. These curves assume a radiator effectiveness of 100 percent (see Section B.3) which can be approached physically by utilizing a radiator which is completely made up of heat pipes. The weight of a continuous heat pipe surface was assumed to be six pounds per square foot; this is considered to be a reasonable value for a radiator of this type which is fabricated of stainless steel. This value will vary as a function of source temperature radiator material but, except in very specific cases, (Reference B-3) can probably not be reduced by more than 50 percent. It is important to note that the minimum area (isothermal) radiators are no more than 40 to 50 percent smaller than the minimum weight radiators. The weight increases are on the order of 200 to 500 percent.

The physically realizable radiators are thus bounded by requirements as represented by Figures B-7 and B-8 (minimum weight) and Figures B-9 and B-10 (minimum area). Figure B-11 combines information from these curves to illustrate the limits involved in trading off weight and area; the curves are for equivalent sink temperatures of 0^{o}F and -100^{o}F. The 0^{o}F sink represents a vehicle in a 100 nautical mile twilight orbit (hot case) utilizing radiators with a somewhat degraded white paint $\left(\frac{\alpha_s}{\epsilon} = 0.35\right)$ as a coating. The -100^{o}F sink corresponds to a vehicle in a 800 nautical mile high-noon orbit utilizing radiators with a degraded (cold case) SI-100 or series emittance coating $\left(\frac{\alpha_s}{\epsilon} = 0.18\right)$.

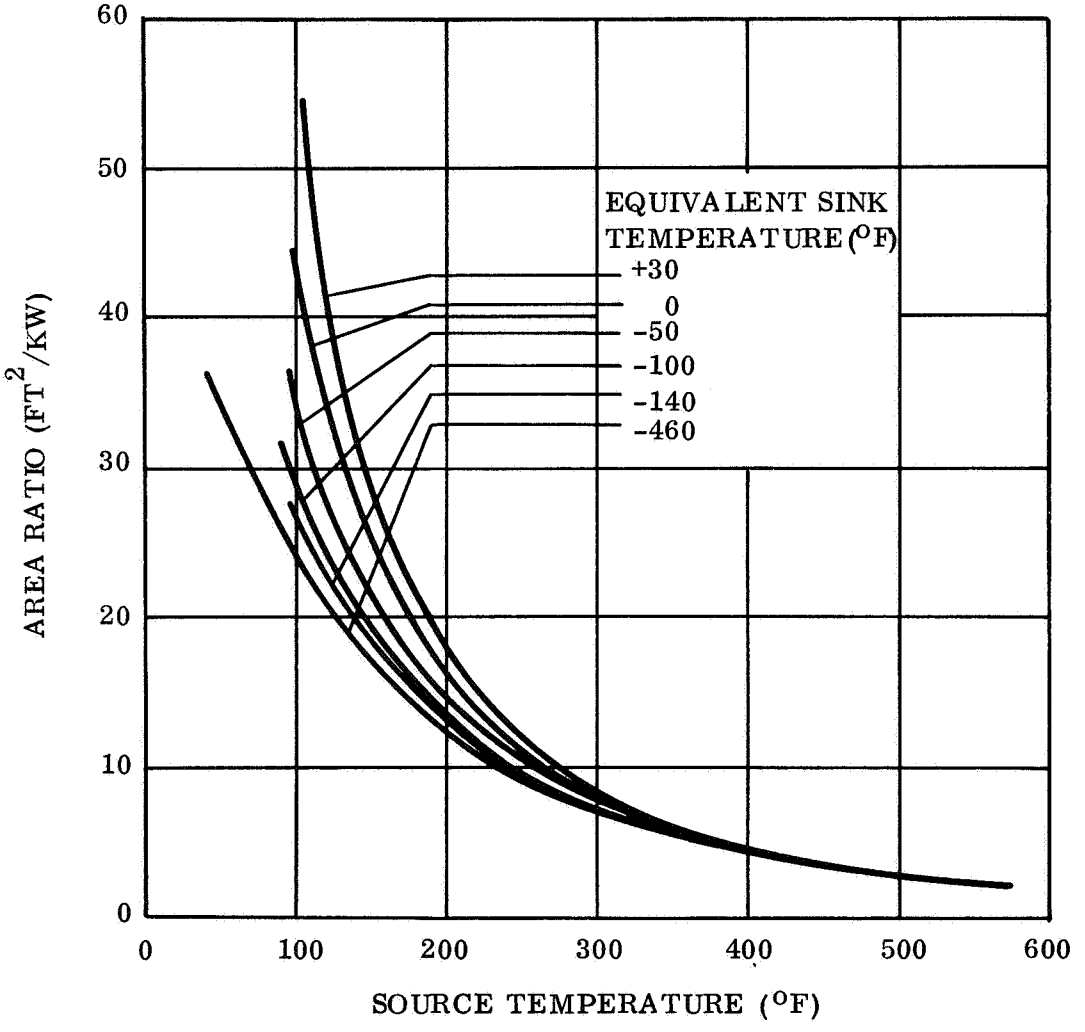

Figure B-9. Minimum Area Fins: Isothermal Radiator Area to Power Ratio Versus Source Temperature

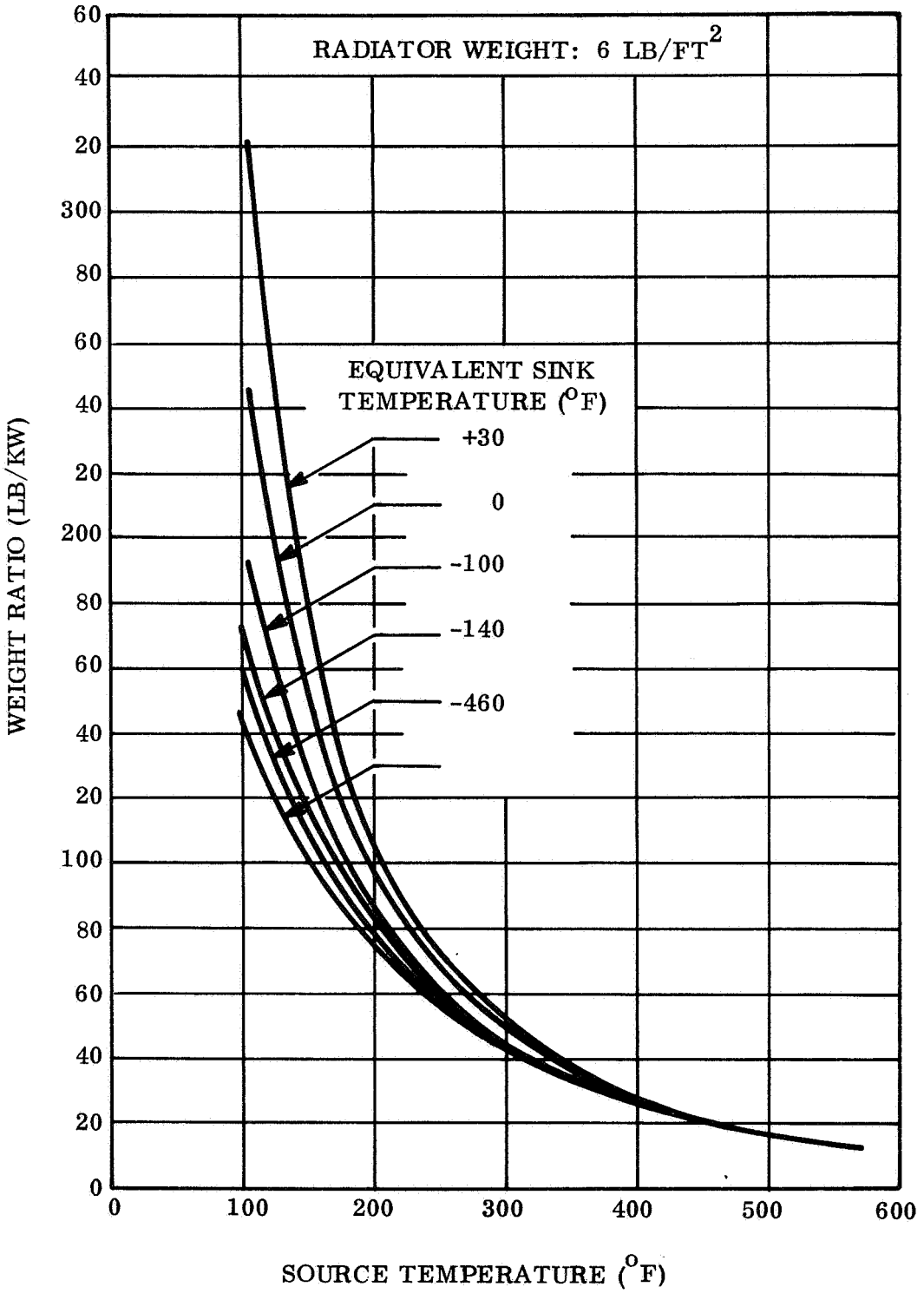

Figure B-10. Minimum Area Fins: Isothermal Weight to Power Ratio Versus Source Temperature

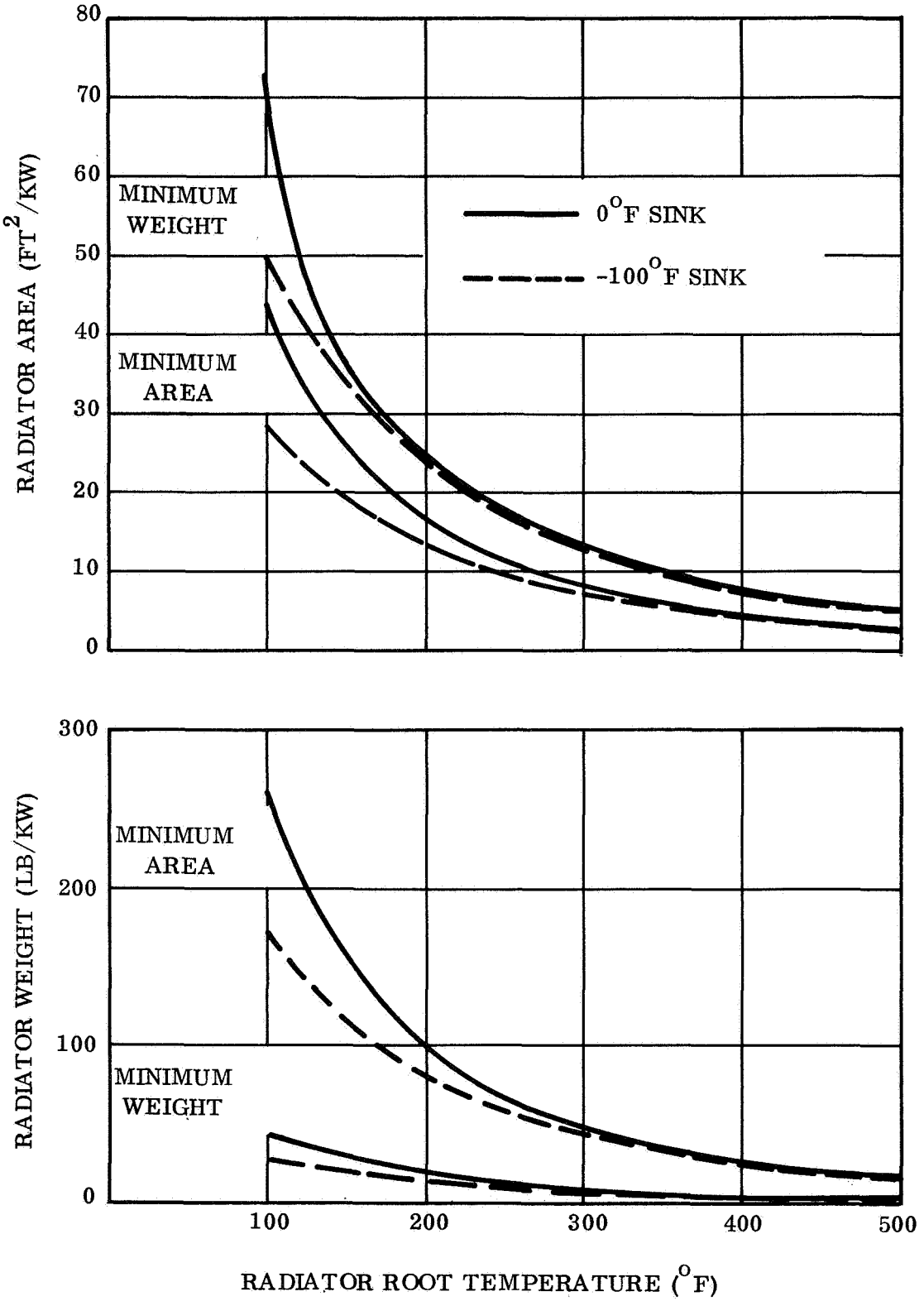

Figure B-11. Radiator Requirements: Minimum Weight and Minimum Area Heat Pipe Radiators

B.6 REFERENCES

1. Chambers, R. L., and Somers, E. V.: Radiation Fin Efficiency for One Dimensional Heat Flow in a Circular Fin. (Preprint) 59-HT-8, ASME, August 1959.

2. Lieblein, S.: Analysis of Temperature Distribution and Radiant Heat Transfer Along a Rectangular Fin of Constant Thickness. NASA-TN-D-196, 1959.

3. Turner, R. C., and Harbough, W. E.: Design of a 50,000 Watt Heat-Pipe Space Radiator, Proceedings of the ASME Aviation and Space Conference. June 1968, pp. 639-643.

APPENDIX C

TEMPERATURE CONTROL

Temperature control in a spacecraft is accomplished by regulation of conduction, radiation, or forced convection paths between source and sink. This appendix describes several techniques and devices for thermal control of dissipating components and their application to thermal control of cathode heaters and high-power tube cooling.

Nomenclature

L_c - total condenser length

L_g - length of condenser filled with noncondensable gas

T - temperature

P - pressure

V - volume

V_t - volume of gas reservoir

Q - heat dissipation

ϵ - emissivity

A - area

σ - Stefan-Boltzman constant

T_o - source or device temperature

η - fin effectiveness

α_s - solar absorptivity

T_s - equivalent sink temperature

W - weight

H_f - latent heat of fusion

ρ - density of phase change material

τ - orbital period

ψ - duty cycle—ratio of component "on" time to total orbit time

C.1 TEMPERATURE CONTROL TECHNIQUES

The regulation of a heat transfer path can be accomplished in any of several ways, depending upon environment, duty cycle, and requirements. Passive coatings, described in Appendix B, apply where the heat loads are relatively constant and the temperature control range wide enough to allow for whatever variations exist. When passive means are inadequate, however, one or more of the following devices must be used. In all of these devices, the passive radiator is the ultimate heat rejection surface: the control device merely varies the view between the surface and the heat sink, the temperature of the surface or the conductance between the heat source and the radiator.

C.2 CONTROLLABLE HEAT PIPE

The controllable heat pipe is one which uses a noncondensable in conjunction with the working fluid to achieve thermal control. Since the flow of the working fluid vapor is in one direction, toward the condenser, the vapor noncondensable gas mixture moves toward the condenser. There the working fluid condenses leaving only the gas. Since the movement of vapor toward the condenser is continuous, the gas is pushed to the farthest end. In practice, the vapor phase of the working fluid and the noncondensable gas separate into two distinct zones with an interface as shown in Figure C-1. The condenser simply radiates from its surface or is attached to a heat sink, such as a fin which is capable of extracting a given quantity of heat per unit length at a given temperature. Due to the low thermal conductance of the heat pipe wall and the noncondensable gas in the axial direction, however, only the portion of the condenser filled with working fluid vapor yields heat to the sink. Thus, if L_c is the total condenser length and L_g is the length of the condenser filled with the noncondensable, then since the heat extracted must equal the heat added

$$Q_{in} = Q_{out} = q \cdot (L_c - L_g) \tag{C-1}$$

where q is the heat extracted per unit length of condenser at temperature T. L_g depends on the gas volume and pressure, but the pressure is dependent upon temperature, since the heat pipe fluid operates along the saturation curve (pressure versus temperature)

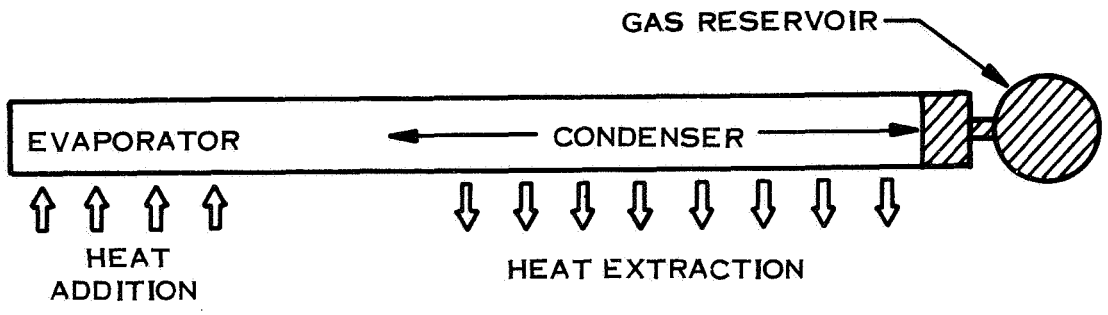

Figure C-1. Controllable Heat Pipe

for the fluid. Since static equilibrium exists at the interface, the pressure of the vapor and the pressure of the gas are equal. Assuming the perfect gas laws hold for the noncondensable gas, the following relationship can be used to evaluate the unknowns in Equation C-1:

$$\frac{PV}{T} = \text{constant} \qquad \text{(C-2)}$$

In a normal design, however, evaluation of Equations C-1 and C-2 is not required since the temperature, T, and q are known. The goal is to make use of these relationships to design the controllable heat pipe to maintain a component at the evaporator within a given temperature range T_1 to T_2 for a range of power input to the evaporator from Q_1 to Q_2. Writing Equation C-2 for two sets of conditions yields

$$\frac{V_1}{V_2} = \frac{T_1 \; P_2}{T_2 \; P_1} \qquad \text{(C-3)}$$

As indicated previously, temperature and pressure are interdependent and thus, for a given temperature range, the ratio of the volume of the noncondensable gas at the extremes of the temperature range is uniquely determined by Equation C-3. The actual volumes depend on the value of q. Assuming to be constant from T_1 to T_2, the system is sized so that the vapor-gas interface is at the end of the condenser nearest the gas reservoir at Q_2. Thus, at T_2,

$$V_t = V_2 \text{ and } L_g = 0 \tag{C-4}$$

Then, at Q_1, for the temperature to be at T_1, the interface moves nearer the evaporator by an amount which is determined by writing Equation C-2 for the two conditions and subtracting one from the other, yielding, after rearranging terms:

$$L_g = \frac{Q_2 - Q_1}{q} \tag{C-5}$$

For a condenser of constant internal cross sectional area, A_c, the new volume of gas is:

$$V_1 = V_t + A_c L_g \tag{C-6}$$

Combining Equations C-3, C-4, C-5, and C-6 yields the relationship required to determine the gas reservoir volume for a given set of conditions

$$V_t = \frac{A_c (Q_2 - Q_1)}{q \left[\frac{T_1 P_2}{T_2 P_1} - 1 \right]} \tag{C-7}$$

The preceding analysis assumes that the gas reservoir is at constant temperature and that there is no axial conduction along the heat pipe except by heat pipe action. The reservoir must be placed in the spacecraft in a location where the temperature is constant or a known function of power dissipation so that it can be accounted for in the analysis. The effects of axial conduction can be determined only for a specific configuration.

Temperature control of the heat pipe to less than 1 degree has been demonstrated by test for power variations of 10 to 1. This close tolerance, however, is held in the heat

pipe, not at the heat source itself. The temperature at the source varies more widely since temperature drop from the source to the heat pipe vapor is dependent on power density.

Applied to maintaining a radioisotope heated cathode at temperature despite decay of the heat source, the system would dispose of the excess heat at initial conditions and yield a minimum heat leak at end of life. A surface at $800^{o}C$ radiates 12.1 watts/in^2 with an emissivity of 0.25. Thus, the heat pipe should have a small diameter and radiate directly from its surface. A heat pipe having an outside diameter of 0.125 inch will reject an excess of 15 watts at the initial conditions from a length of 3.14 inches.

For a 5-mil thick heat pipe wall, the results of Equation C-7 show that 0.25 in^3 of gas is required to hold the temperature change over the design life of the system to $5^{o}C$ ($9^{o}F$) where sodium is the working fluid. No other temperature control system described in this appendix is suitable for controlling a radioisotope heated capsule due to their size and introduction of an excessive heat leak at end of life.

Applied to spacecraft thermal control, the controlled heat pipe shows a great deal of promise. If the heat pipes in the radiators described in Appendix B were made controlled pipes, the radiator would be sized for the maximum area condition. Added weight of the gas reservoir would vary widely, depending on gas pressure and container shape and material and the desired temperature range. For most spacecraft applications, a 10 percent increase in the weight estimates given in Appendix B should be adequate. Tradeoff curves are not presented for this system since the weight is dependent on the temperature range. The controllable heat pipe radiator, however, will show an advantage over any system using shutters both in area and weight for a given dissipation. This advantage is even greater when solar energy is incident on the radiator since there are no blades to cause an increase in solar absorptance.

C.3 PHASE CHANGE SYSTEMS

A material that undergoes a solid-liquid phase change may be employed as a temperature control device for a component whose thermal dissipation varies within an orbital period. The material is placed between the component and a passive space radiator such that it absorbs heat while the component is on and rejects this same heat when the component is off. The melting temperature of the phase change material (PCM) must be approximately equal to the desired operating temperature of the system. Where the duty cycle of the component is regular, temperature may be maintained between narrow limits.

In order to be considered for use as a PCM, a material should have certain physical and chemical properties. A list of these is presented in Ref. C-1 and will be repeated here:

a. High heat of fusion

b. Reversible solid-liquid transition

c. Low coefficient of volumetric expansion in both liquid and solid phases

d. High density

e. Low change in density during phase transition

f. Nontoxicity and noncorrosiveness

g. High thermal conductivity in both liquid and solid phases

h. Low vapor pressure near the melting point

i. High specific heat in both liquid and solid phases

j. Good environmental compatibility.

Lists of candidate materials found in Ref. C-1 all possess the above properties to some extent. It should be noted that materials developed specifically for use as

temperature control devices could have more desirable characteristics than those currently available.

Basically, the PCM stores heat during the component's "on" period and conducts it to the radiator during the "off" period. In this way, radiator temperature is kept constant over the entire orbit. Radiator area is sized to reject the orbital average generated heat at this constant temperature. The amount of PCM necessary is determined as that which will absorb the difference in heat generated and heat radiated during the "on" portion of the orbit with no change in temperature. The following equations give area and PCM weight requirements as functions of component and orbital parameters.

$$A = \frac{\psi Q}{\eta \epsilon \sigma \left(T_o^4 - T_s^4 \right)} \tag{C-8}$$

$$W_{pcm} = \frac{\psi \tau \left[Q - \eta \epsilon A \sigma \left(T_o^4 - T_s^4 \right) \right]}{H_f} = \frac{\psi \tau (1 - \psi) Q}{H_f} \tag{C-9}$$

Integrated average sink temperatures are used in these equations.

The major difficulty with using the phase change technique is maintaining good heat transfer characteristics throughout both liquid and solid phases and at the boundary between these phases. In practice, it has been found necessary to supplement internal conduction of the material with a highly conductive core. To date, the most promising core design is an expanded copper foam which has a copper total volume ratio of about 0.15. The phase change material is packed into the voids in this core and the heat transfer problem is reduced greatly. The core, however, adds weight to the system which is given by the expression:

$$W_{core} = \left(\frac{0.15}{0.85}\right)\left(\frac{\rho_{core}}{\rho_{pcm}}\right) \quad (W_{pcm}). \tag{C-10}$$

An analysis was undertaken to estimate area and weight requirements for phase change systems. A typical orbit was chosen and four operating temperatures in the range from approximately 38 to 315°C (100 to 600°F) were investigated. The effect of duty cycle on these requirements was determined. All data is presented on per kilowatt of heat rejection basis.

The assumptions made in this analysis are listed here:

a. Orbit = 15 nmi high noon ($\tau = 1.46$).

b. Baseplate = the weight optimized heat pipe fin as obtained from Appendix B of this report.

c. Baseplate $a_s/\epsilon = 0.3/0.85$.

d. Core = the expanded copper foam described above.

e. PCM = materials and properties for the four temperature levels considered (shown in Table C-1).

Area requirement was calculated from Equation C-8. Weight requirement is the sum of the weights of the PCM, the core, and the radiator baseplate. Graphs of these parameters are labeled "PCS" in Figures C-2 through C-5.

C.4 THERMAL SHUTTER SYSTEMS

The most common thermal control system presently used on spacecraft which have noncontinuously operating components is the thermal shutter or louver system. These systems employ temperature sensing elements which control the opening and closing of lightweight blades placed on the space-facing side of a passive baseplate radiator. The

Table C-1. Phase Change Materials and Properties*

System Temperature, Deg. F	100	212	380	600
ORBIT				
Period, Hrs	1.46	1.46	1.46	1.46
Passive Sink, deg. F	-40	-40	-40	-40
Louver Sink, deg. F	-28	-28	-28	-28
BASEPLATE				
Effectiveness (ϵ = 0.85)	0.61	0.59	0.57	0.55
Effectiveness (ϵ = 0.15)	0.87	0.85	0.83	0.81
Weight, lb/ft^2	0.61	0.72	0.83	0.94
PHASE CHANGE MATERIAL *	Dibasic Sodium Phosphate	Dihydrodeca-borane	Aluminum Chloride	Sodium Hydroxide
Chemical Formula	$Na_2HPO_4 \cdot 12H_2O$	$B_{10}H_{14}$	$AlCl_3$	NaOH
Heat of Fusion, BTU/lb	122.4	113.4	192.5	90.0
Density, lb./ft^3	94.8	93.0	152.0	133.0
EMISSIVITIES				
Passive Radiator	0.85	0.85	0.85	0.85
Open Louver Radiator	0.70	0.70	0.70	0.70
Closed Louver Radiator	0.15	0.15	0.15	0.15

*Properties obtained from Reference C-2

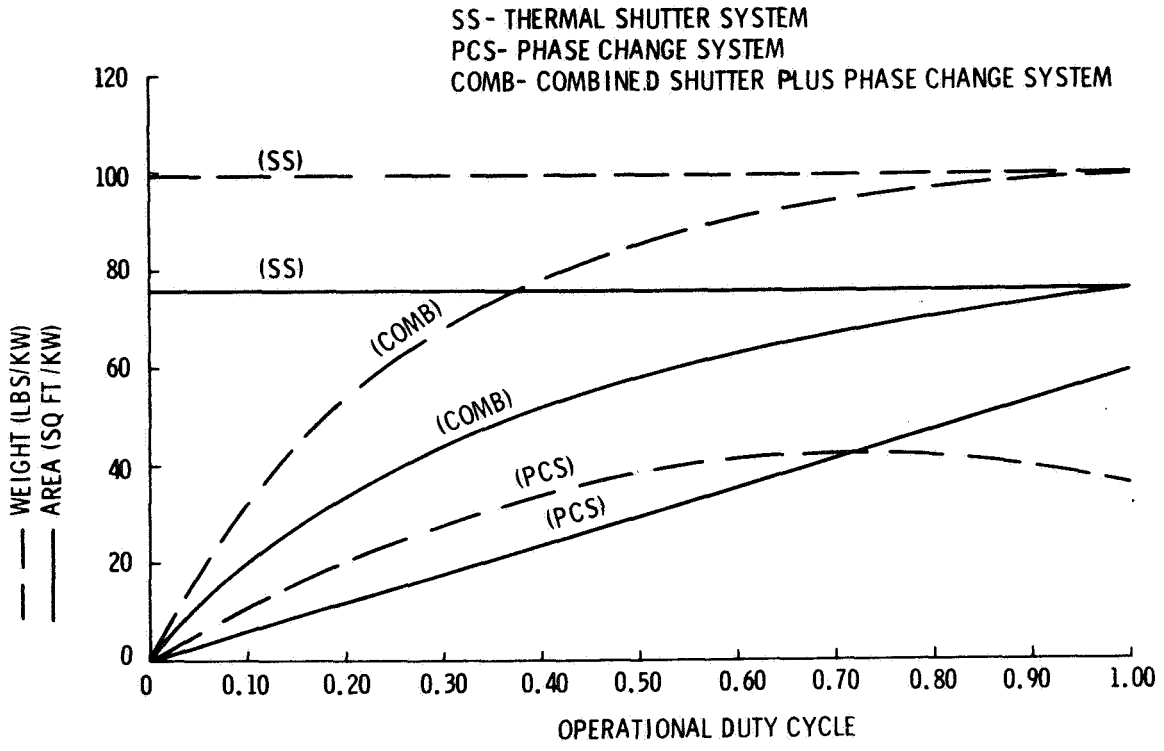

Figure C-2. Weight and Area Requirements for 100°F Thermal Shutter, Phase Change, and Combined Systems

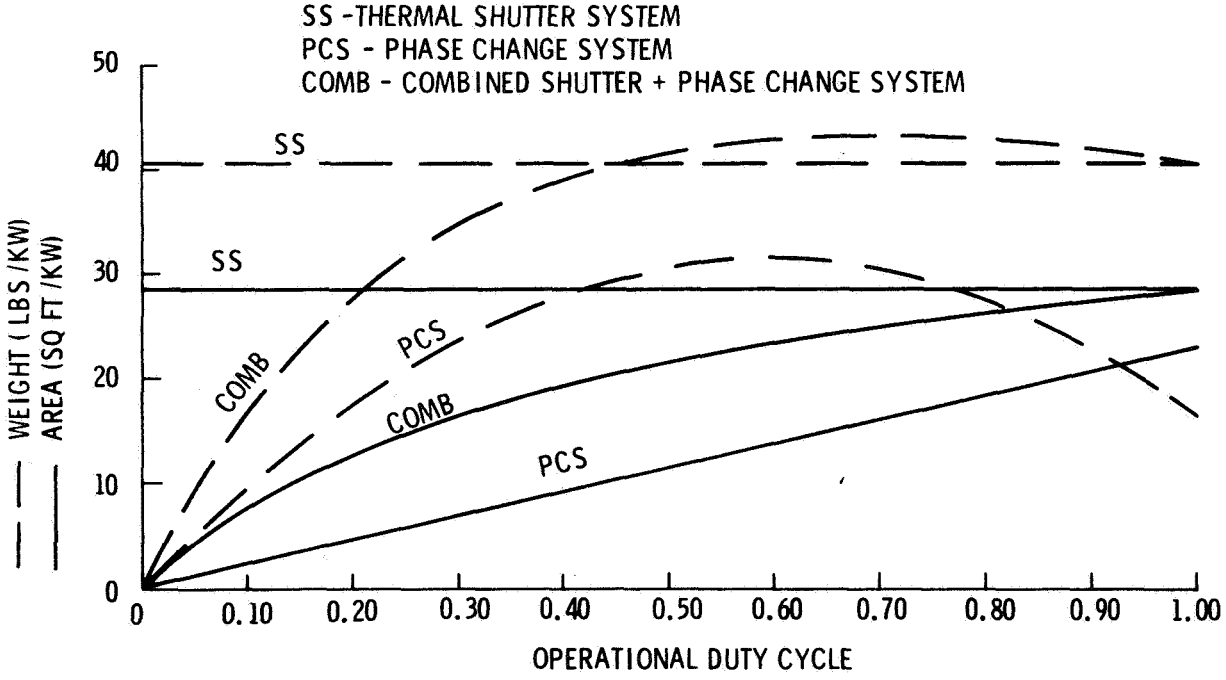

Figure C-3. Weight and Area Requirements for 212°F Thermal Shutter Phase Change, and Combined Systems

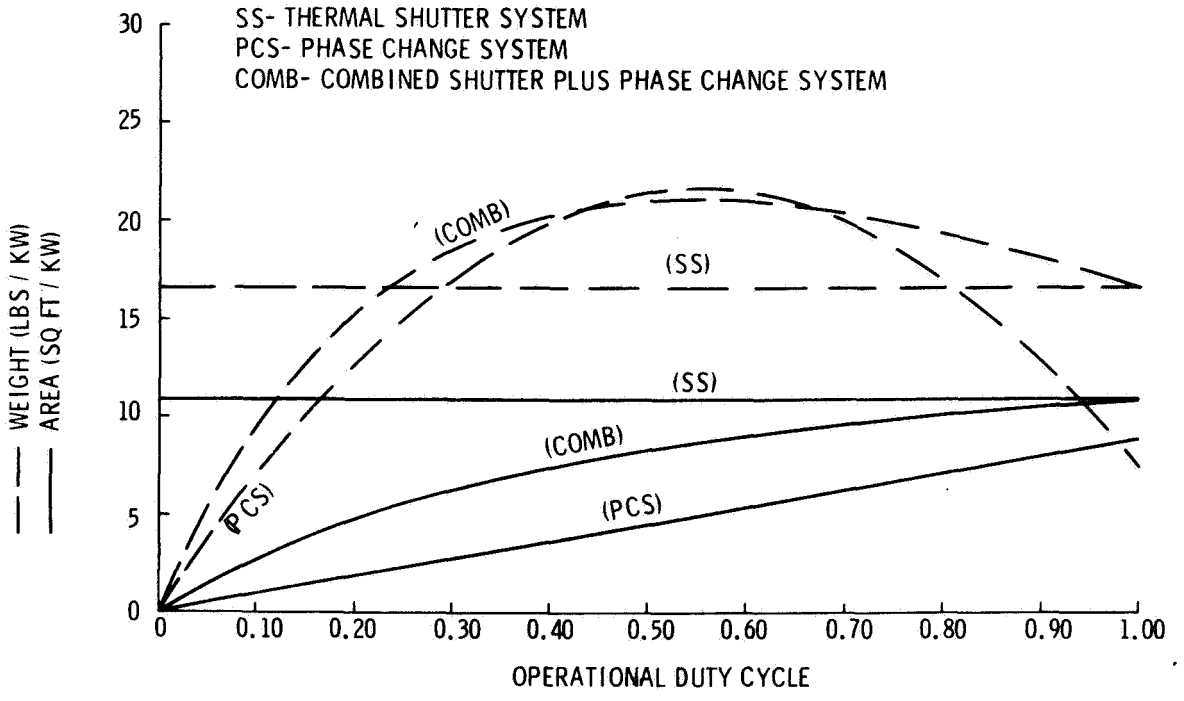

Figure C-4. Weight and Area Requirements for 380°F Thermal Shutter, Phase Change, and Combined Systems

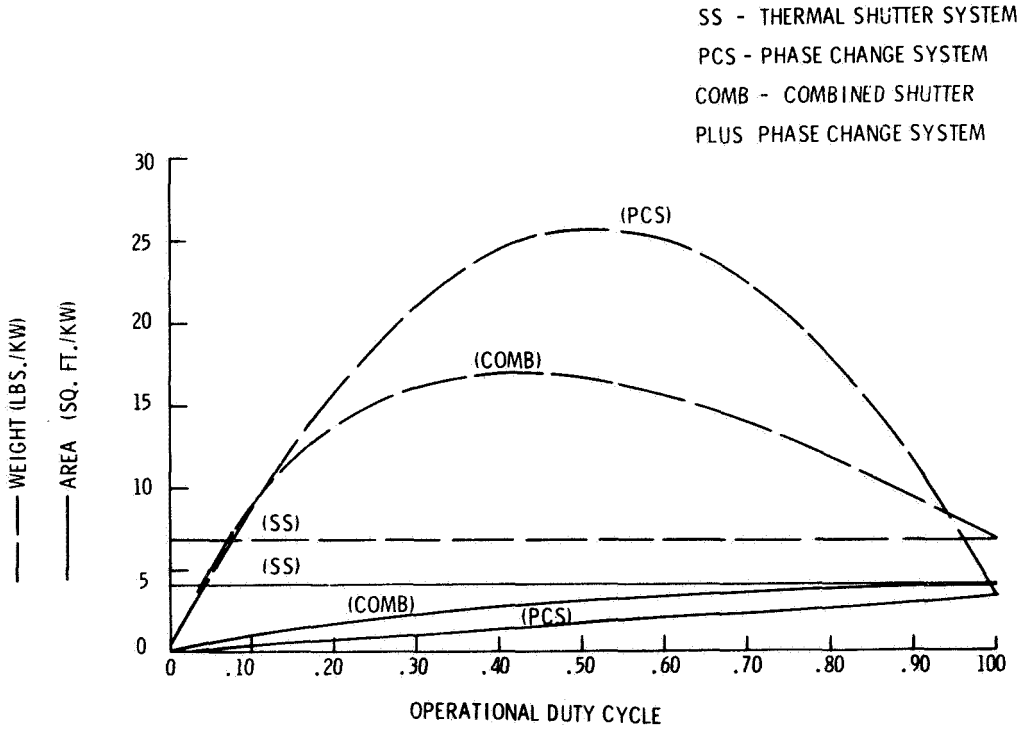

Figure C-5. Weight and Area Requirements for 600°F Thermal Shutter, Phase Change, and Combined Systems

effective radiation properties of the baseplate are changed and the louvers are thus heat valves which inhibit heat flow to space as vehicle temperature decreases.

By proper selection of sensors, actuators, and linkage, it is possible to set the louver operating temperature at any value and to control the rate of opening and closing with temperature changes. Currently sensors are either bimetallic or fluid actuated to obtain proportional control. For high dissipation devices which are either on at full power or off at zero power, it may be desirable to provide on-off control of the shutter blades (corresponding to fully open-fully closed positions). To do so, however, would probably necessitate the use of electrical power.

All shutter systems exhibit some heat leak in the closed position. This leak takes place mainly around the edges of the blades, rather than through them and is analyzed by assuming the baseplate radiates to space with low effective emissivity. Test results have shown this emissivity to fall in a range from 0.1 to 0.15. Because the leak is significant, it may be necessary to provide "compensation" heaters that are activated when a component is off. These heaters dissipate a minimal amount of heat to overcome the leakage and maintain component temperature at some specified lower limit.

The addition of a louver system to a passive radiator increases the area required to reject a given quantity of heat. This is because, even in the fully open position, the effective emissivity and adsorptivity of the integrated system cannot equal the properties of the baseplate coating. The effective emissivity is decreased by thermal interactions between the baseplate and the blades, and the absorptivity is increased due to the effect of the created "cavities" on incident solar flux (see Ref. C-3). Consequently, area and weight penalties are incurred whenever shutter systems are used.

Louver systems must always be designed to dissipate the maximum component heat. Area and weight are independent of duty cycle since it is assumed that the louvers will close and limit heat rejection whenever the component is off. The weight of a louver

system (not including baseplate) is a function of the area covered. The use of 0.7 lb/ft^2 is used in this study. The area and weight requirements of a louver system are:

$$A = \frac{Q}{\eta \epsilon_{\text{louvers, max}} \sigma \left(T_o^4 - T_s^4 \right)}, \qquad \text{(C-11)}$$

and

$$W = 0.7\ (A) \qquad \text{(C-12)}$$

NOTE: Effective sink temperature must be obtained using the effective a_s/ϵ ratio of the louver system. Typical analytical values are given in Figures C-6 and C-7.

For the analysis, the orbital and component operating parameters were the same as those chosen for the phase change system. The assumptions are listed here:

a. Orbit: 150 nmi high noon ($\tau = 1.46$)

b. Baseplate: the weight optimized heat pipe fin as obtained from Appendix B.

c. Baseplate $a_s/\epsilon = 0.3/0.85$

d. Louver system: The effective radiation properties are listed in Table C-1 Weight = 0.7 lb/ft^2, $a_s/\epsilon = 0.33/0.7$.

Area requirement is obtained from Equation C-11. Weight is the sum of that of the louver system (Equation C-12) and that of the baseplate. Curves are shown in Figures C-2 through C-5 and are labeled "S S."

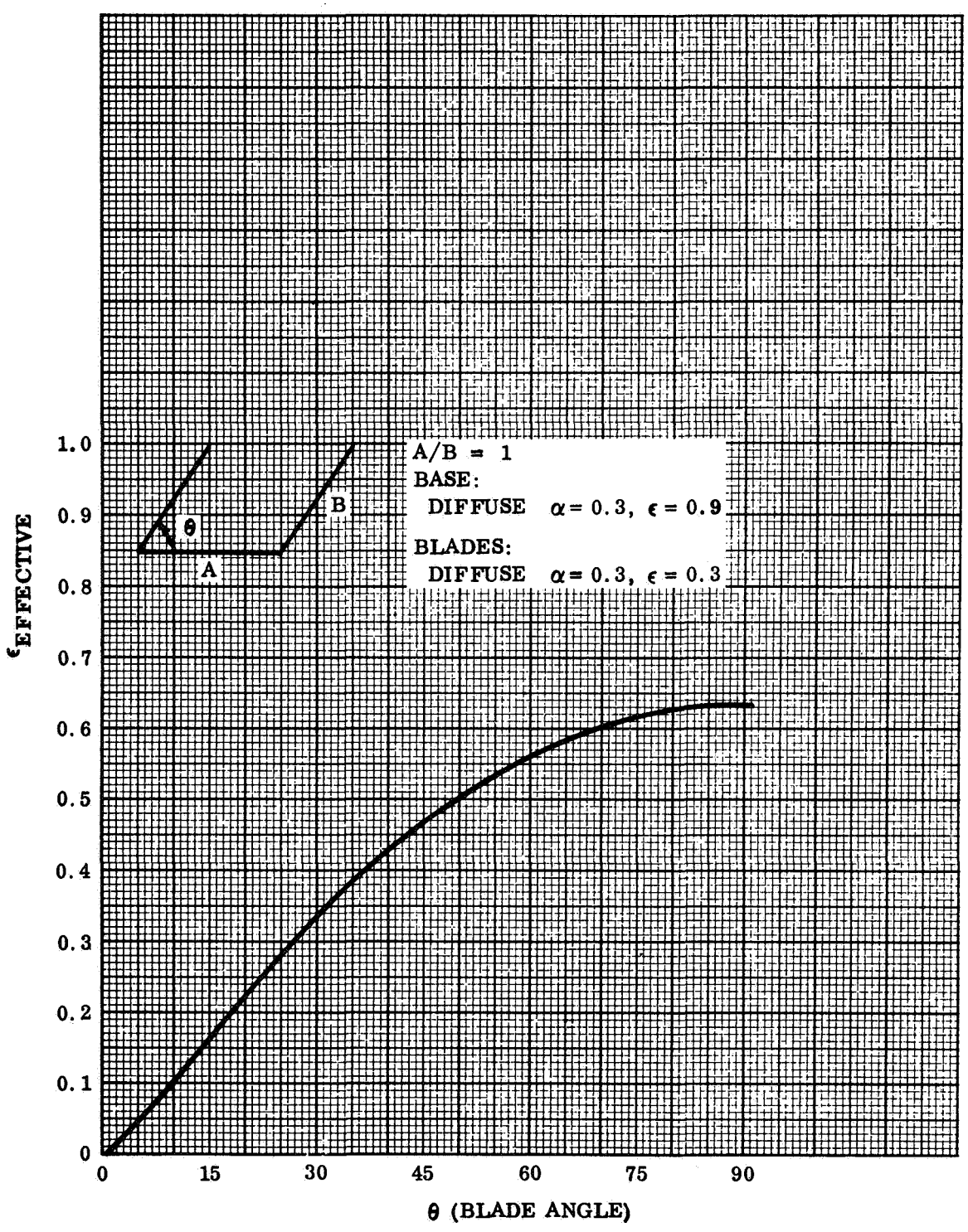

Figure C-6. Effective Emissivity Versus Blade Angle

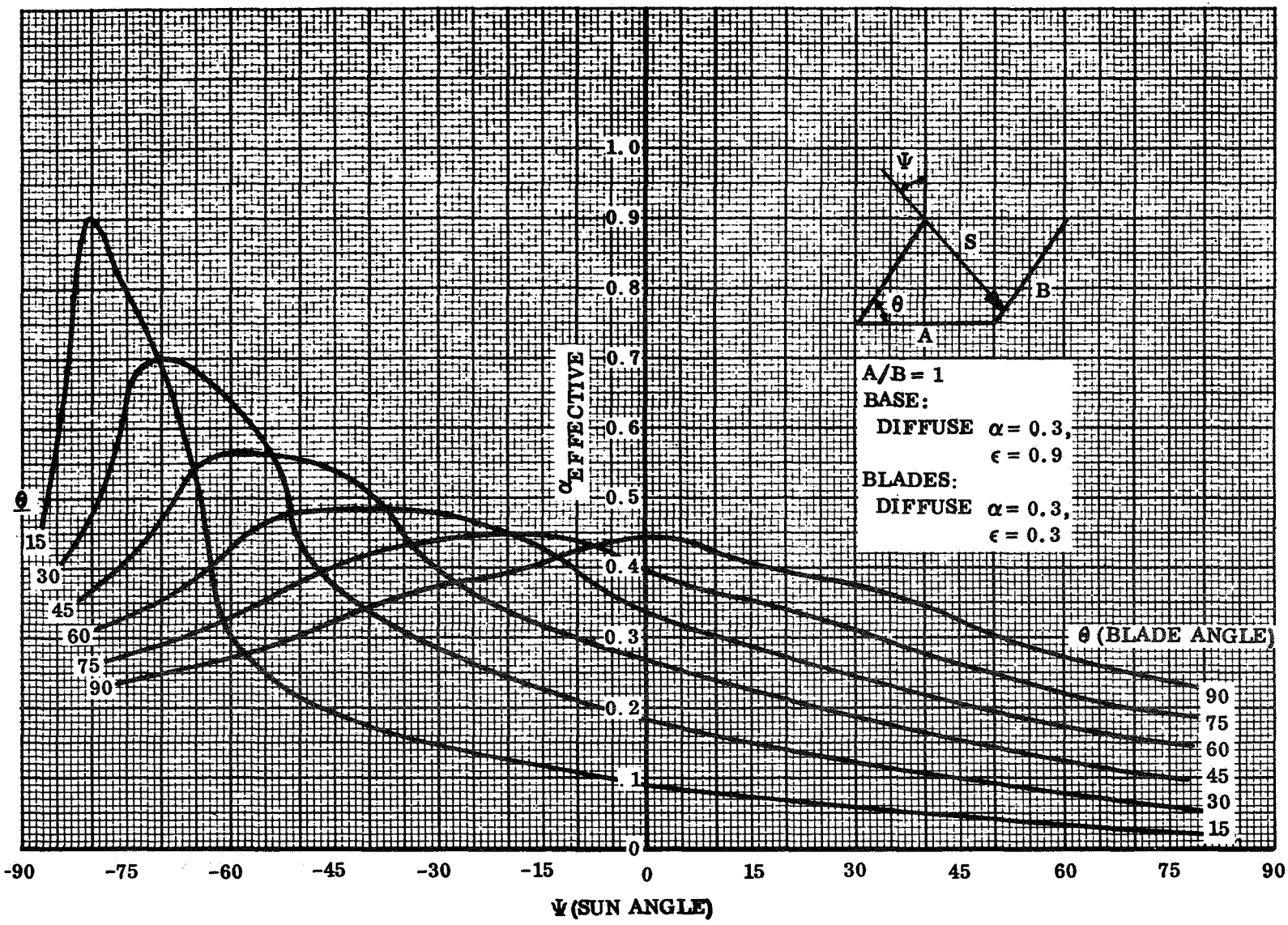

Figure C-7. Effective Absorptivity Versus Sun Angle and Blade Angle

C. 5 COMBINED SYSTEMS

It is possible to combine louver and phase change systems, as described in the previous sections, to obtain the advantages of both. Radiating area for a pure louver system can be reduced by providing phase change material to "smooth out" component heat pulses. Conversely, PCM weight can, in some cases, be decreased by incorporation of a shutter system on the baseplate of a pure phase change system.

A combined system offers the best temperature control of components whose thermal dissipations vary cyclically or irregularly. The system includes phase change material, thermal shutters, and compensation heaters. PCM weight must be sized for the expected duty cycle, operating temperature, and orbit. Radiator area should be provided to dissipate the orbital average generated heat through the louver system. Compensation heaters are activated during excessively long component "off" periods. In this way, temperature control within $\pm$ 10^{o}C should be possible over a very wide range of operating conditions.

Equations for determining area and weight (excluding baseplate) requirements are given below:

$$A = \frac{\psi Q}{\left[\psi (\eta \epsilon)_{\text{louvers open}} + (1-\psi)(\eta \epsilon)_{\text{louvers closed}}\right] \sigma \left(T_o^4 - T_S^4\right)} \qquad \text{(C-13)}$$

$$W = \frac{\psi \tau \left[Q - (\eta \epsilon)_{\text{louvers open}} A \sigma \left(T_o^4 - T_s^4 \right) \right]}{H_f} \qquad \text{(C-14)}$$

Component and orbital parameters chosen for the analysis of combined systems are consistent with those previously assumed so that tradeoffs are possible. The assumptions are repeated here:

a. Orbit: 150 nmi high noon (τ = 1.46)

b. Baseplate: the weight optimized heat pipe fin as obtained from Appendix B

c. Baseplate a_s/ϵ = 0.3/0.85

d. PCM core: the expanded copper foam described in Section C.3

e. PCM and louver system: Properties of these items are shown in Table C-1. Weight of louver system = 0.7 lb/ft^2, a_s/ϵ = 0.33/0.7

Area requirement is calculated from Equation C-13. Weight includes PCM, core, louvers, and the optimum passive radiator plate. Results are plotted in Figures C-2 through C-5.

C.6 COOLING SYSTEM COMPARISON

Because all analyses were made for identical conditions, the three systems (phase change, shutters, and combined) as represented on Figures C-2 through C-5 can be compared with respect to area and weight requirements. The curves represent total system requirements including radiator plates and all elements of the control devices. Controllable heat pipe radiators are not included as discussed in Section C.2.

It is implicitly assumed in the analysis that all three systems can maintain temperature with the same accuracy over the duty cycle range. This is not strictly true. Phase change systems lose their effectiveness at duty cycles other than that for which they are designed. Shutter systems are usually supplemented with compensation heaters for long component "off" periods. Combined systems actually offer more flexible and better control than either of its component systems taken alone.

For an area critical vehicle, a PCM or combined system can always reduce area requirement. The weight penalty is a function of orbital period, duty cycle, and operating temperature. This can be determined from the curves for the latter two variables

and, from the equation it can be seen that system weight is approximately a direct function of orbital period.

Weight can be saved by proper system selection. For the 100 nmi orbit and component temperatures below about 200°C, minimum weight is offered by phase change systems. For an 800 nmi orbit, phase change systems are the choice only for temperatures below about 100°C.

Phase change and combined systems offer no advantage at or close to duty cycles of 1.0. Below this value the benefits are shown by the curves.

C.7 REFERENCES

C-1. Fixler, S.: "Passive Thermal Control by Phase-Change Materials." Space/Aeronautics, February, 1966.

C-2. Perry, J., ed: Chemical Engineer's Handbook. Third ed., McGraw-Hill, 1950.

C-3. Conway, E.C., and Berman, R.W.: Analytical Determination of Effective Radiative Properties of a Shutter Type Temperature Control System. General Electric Company, TIS 65SD329, Philadelphia, Pennsylvania, September, 1965.

APPENDIX D

TEST RESULTS

The figures contained in this appendix represent the temperature data taken during the collector colling tests. The numbers shown are the temperatures of the indicated points.

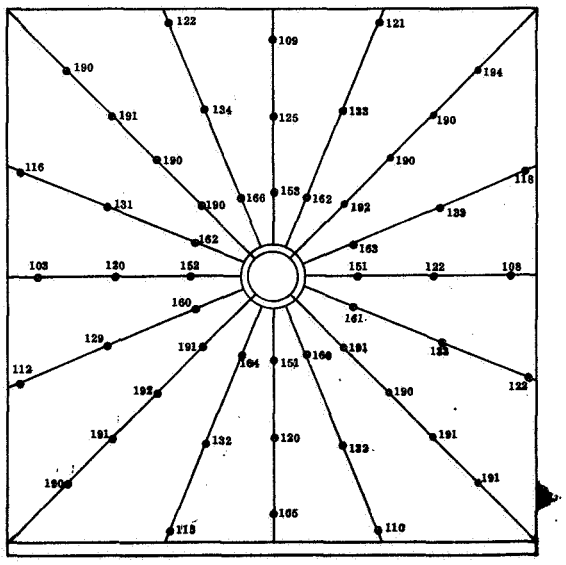

Figure D-1. 930 Watts: Four Heat Pipes Operating, Actual TWT Operating (Temperature in ^{o}F)

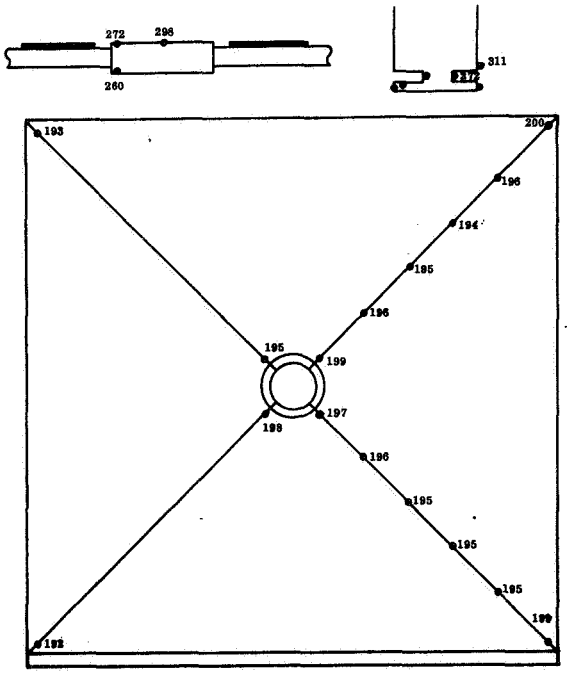

Figure D-2. 930 Watts: Four Heat Pipes Operating, Actual TWT Operating

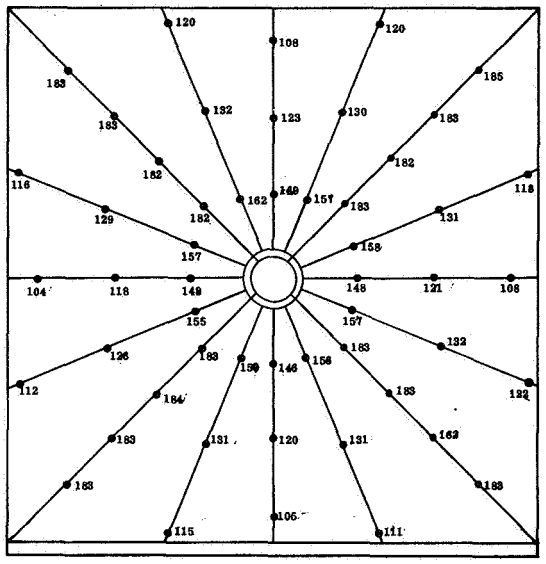

Figure D-3. 750 Watts: Four Heat Pipes Operating, Actual TWT Operating (Temperature in ^{o}F)

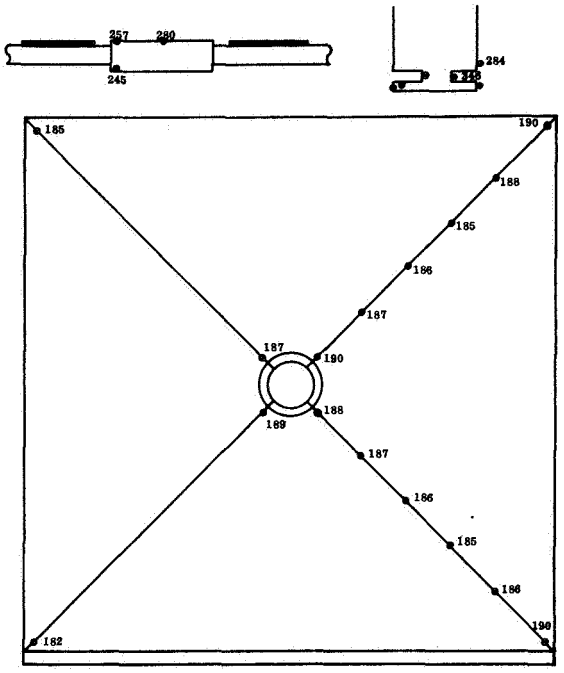

Figure D-4. 750 Watts: Four Heat Pipes Operating, Actual TWT Operating

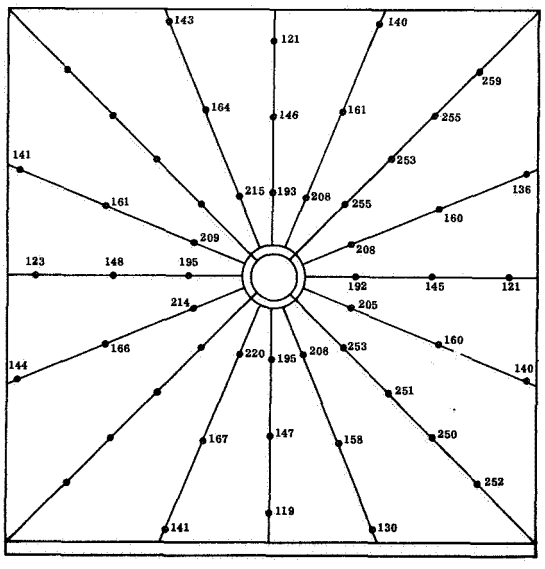

Figure D-5. 1500 Watts: Four Heat Pipes Operating (All Temperatures on Radiator)

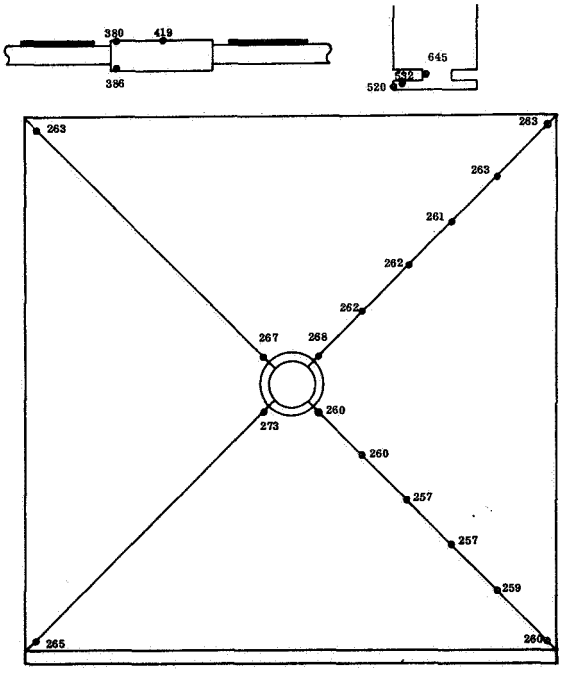

Figure D-6. 1500 Watts: Four Heat Pipes Operating (Temperatures on Heat Pipes) Heat Transfer Block, and Collector)

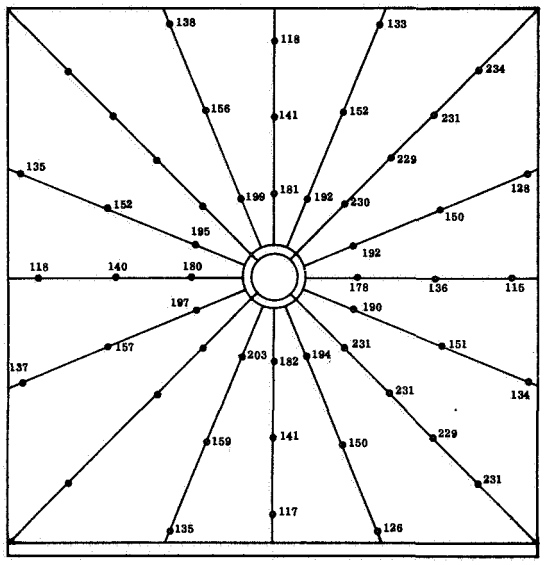

Figure D-7. 1250 Watts: Four Heat Pipes Operating

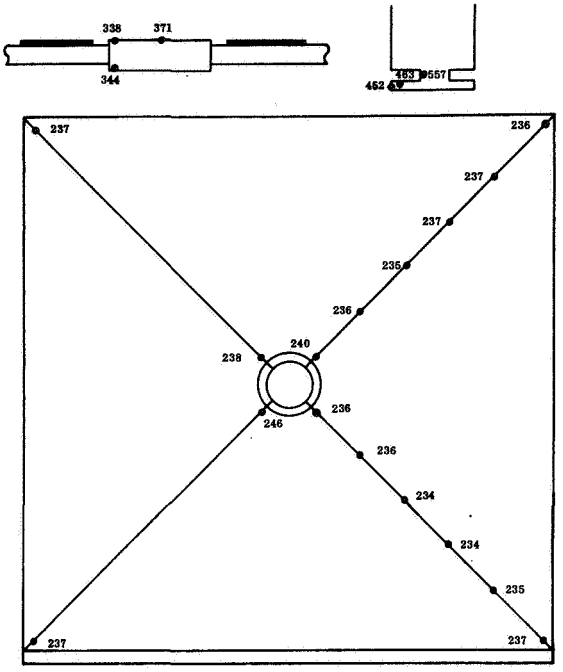

Figure D-8. 1250 Watts: Four Heat Pipes Operating

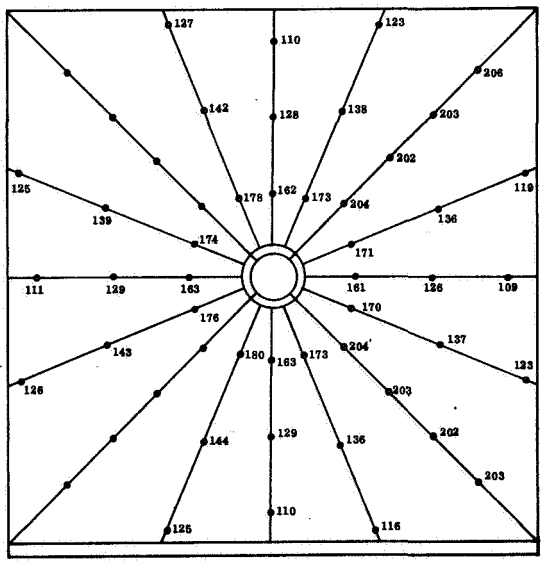

Figure D-9. 1000 Watts: Four Heat Pipes Operating

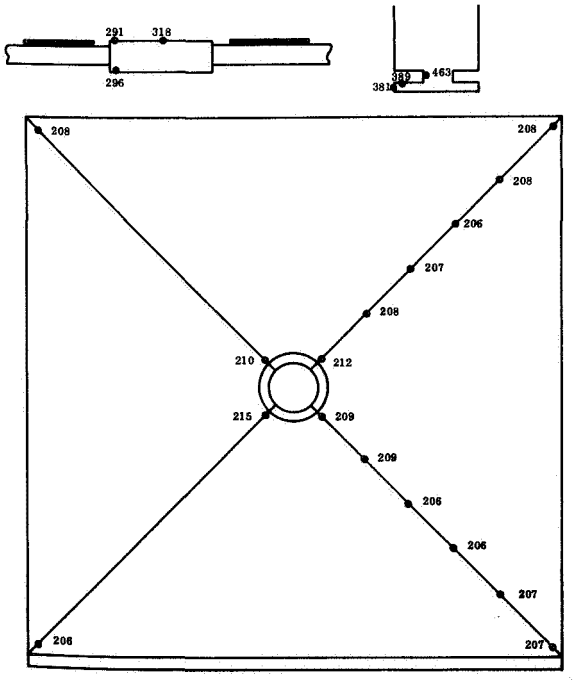

Figure D-10. 1000 Watts: Four Heat Pipes Operating

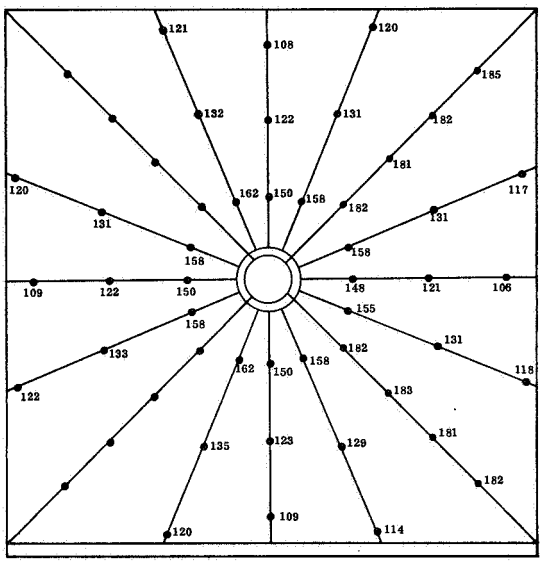

Figure D-11. 750 Watts: Four Heat Pipes Operating

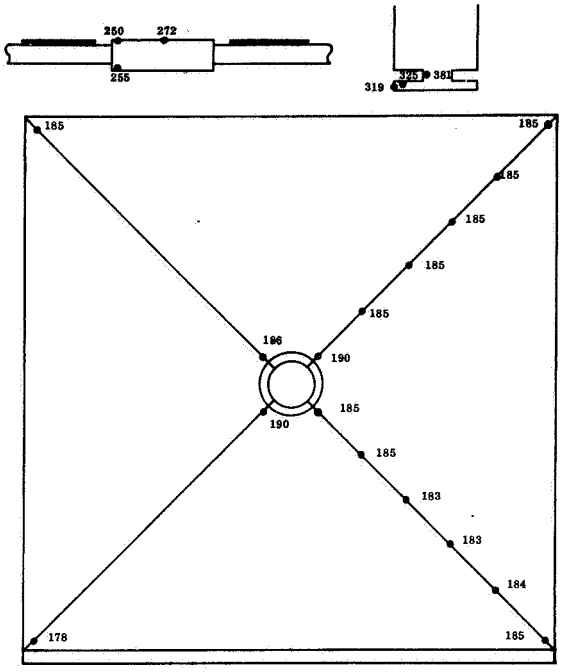

Figure D-12. 750 Watts: Four Heat Pipes Operating

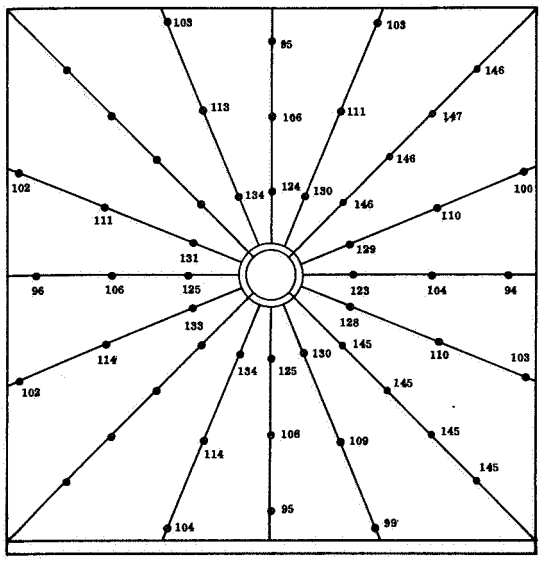

Figure D-13. 500 Watts: Four Heat Pipes Operating

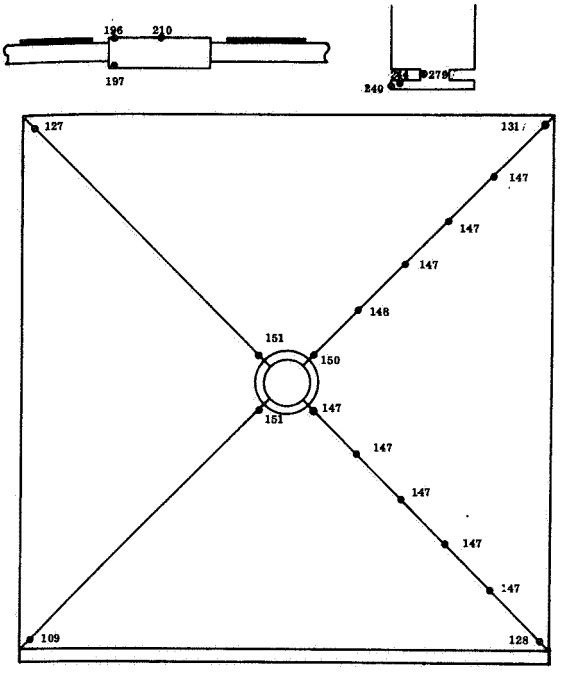

Figure D-14. 500 Watts: Four Heat Pipes Operating

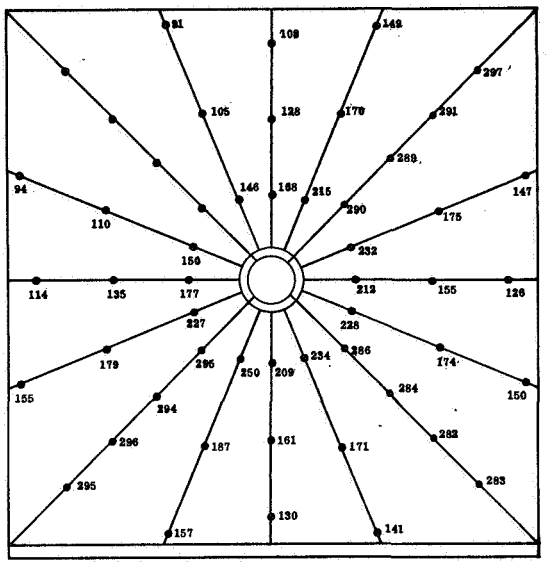

Figure D-15. 1500 Watts: Three Heat Pipes Operating (A, B, and C)

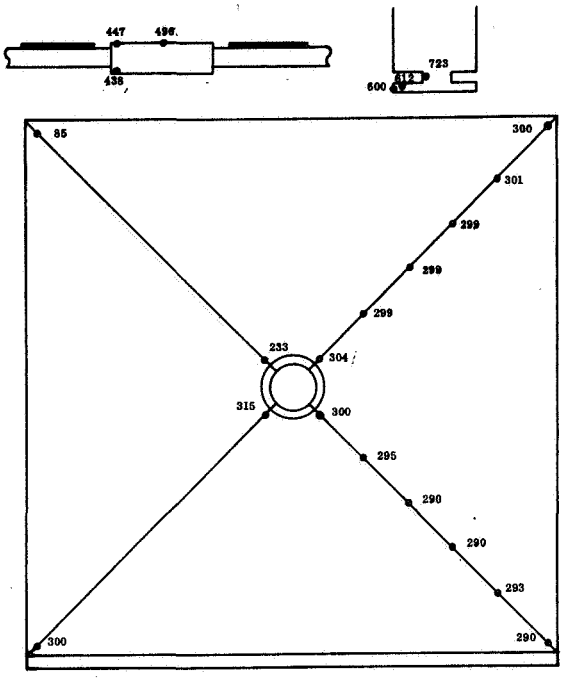

Figure D-16. 1500 Watts: Three Heat Pipes Operating (A, B, and C)

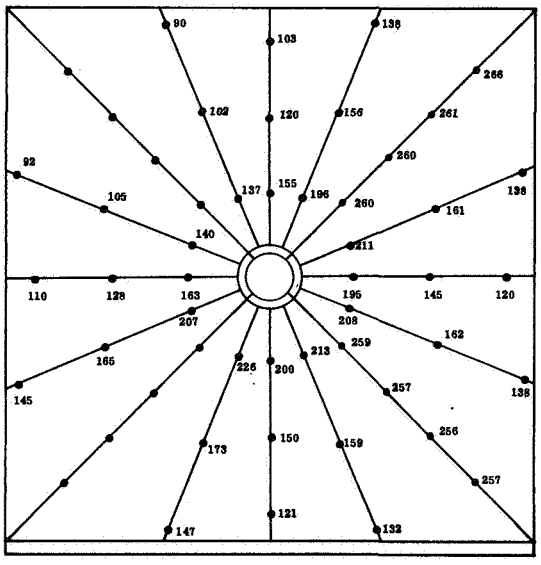

Figure D-17. 1250 Watts: Three Heat Pipes Operating (A, B, and C)

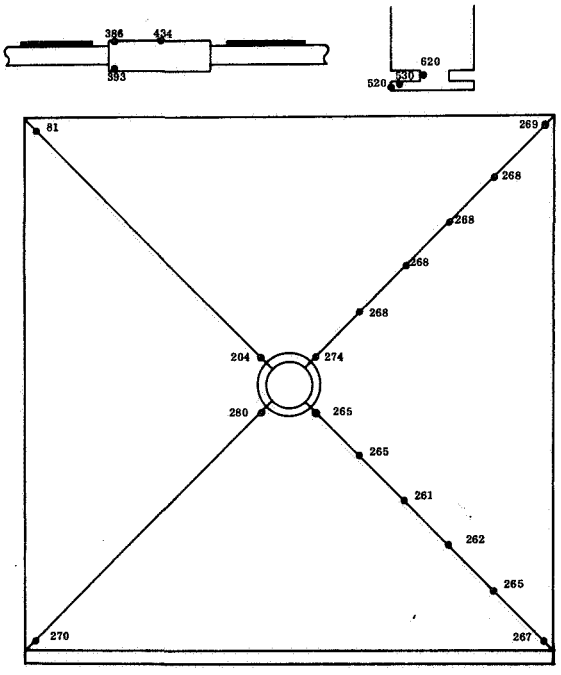

Figure D-18. 1250 Watts: Three Heat Pipes Operating (A, B, and C)

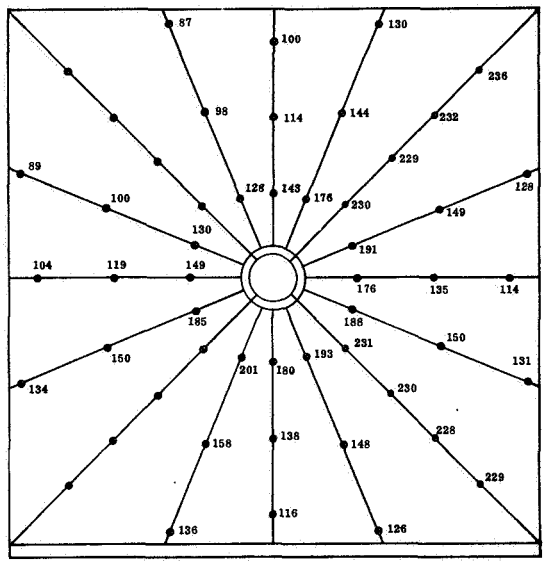

Figure D-19. 1000 Watts: Three Heat Pipes Operating (A, B, and C)

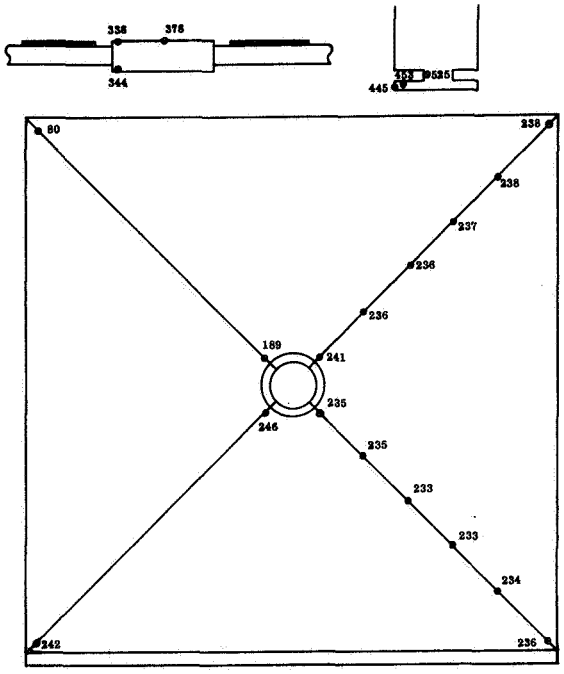

Figure D-20. 1000 Watts: Three Heat Pipes Operating (A, B, and C)

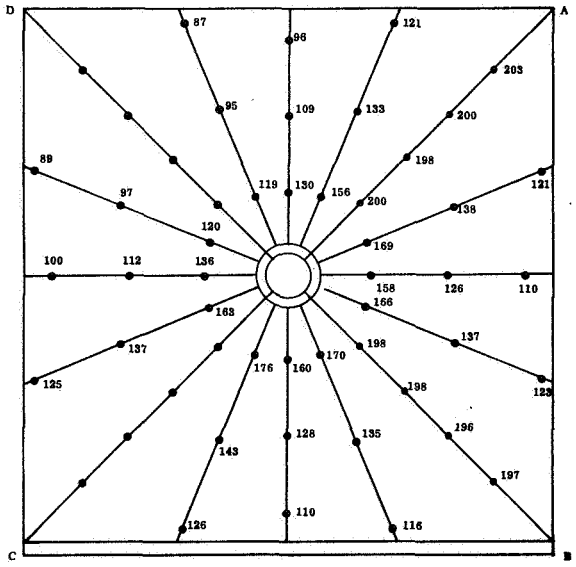

Figure D-21. 750 Watts: Three Heat Pipes Operating (A, B, and C)

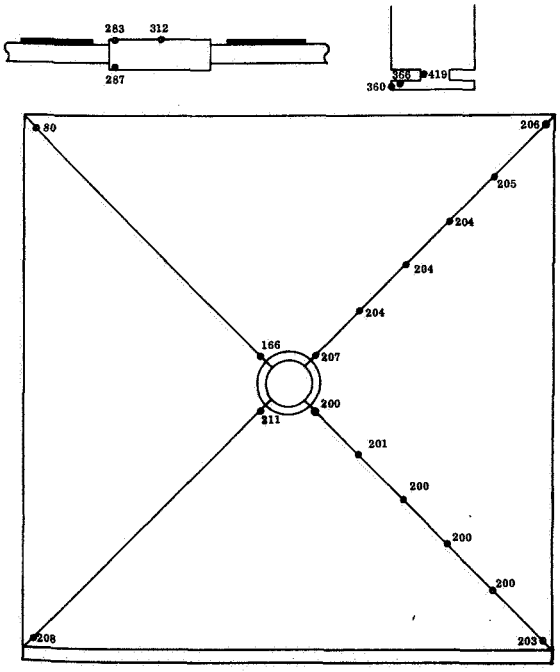

Figure D-22. 750 Watts: Three Heat Pipes Operating (A, B, and C)

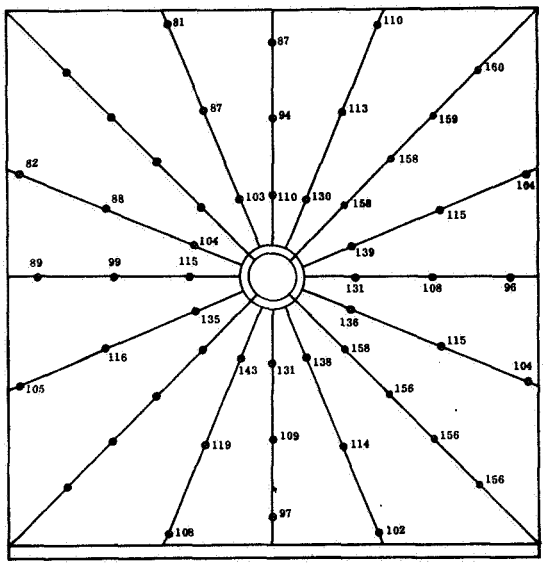

Figure D-23. 500 Watts: Three Heat Pipes Operating (A, B, and C)

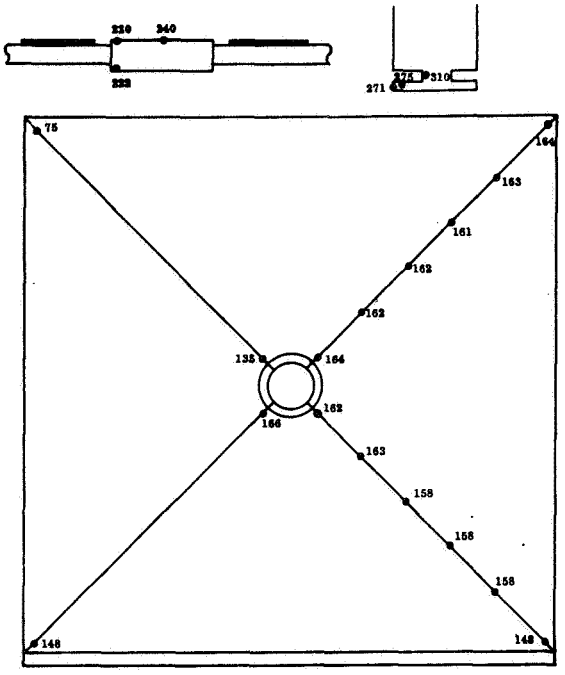

Figure D-24. 500 Watts: Three Heat Pipes Operating (A, B, and C)

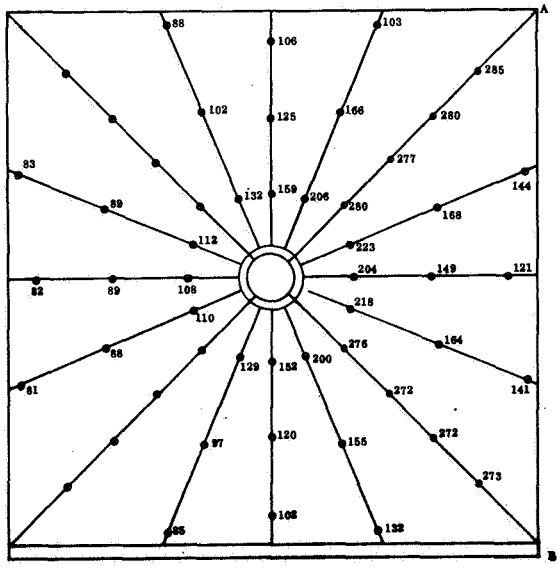

Figure D-25. 1000 Watts: Two Heat Pipes Operating (A and B)

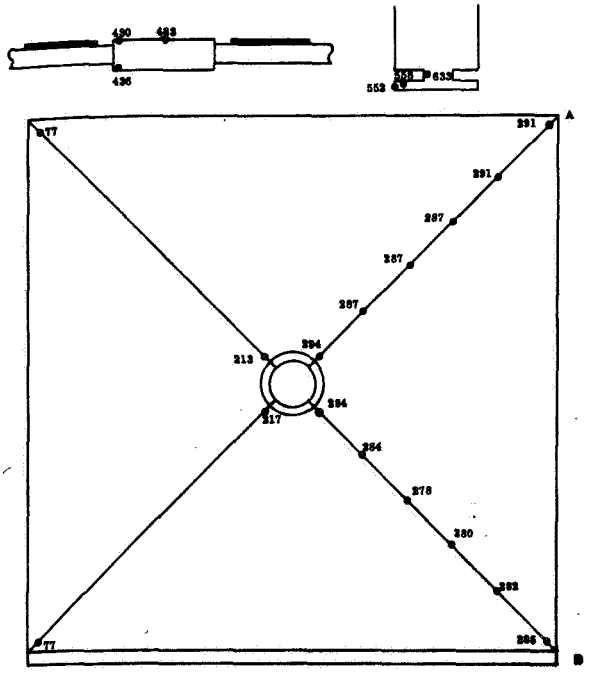

Figure D-26. 1000 Watts: Two Heat Pipes Operating (A and B)

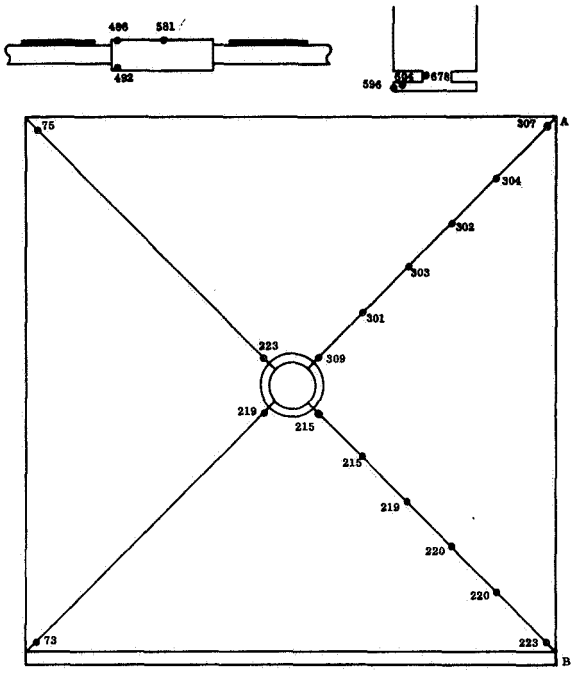

Figure D-27. 1000 Watts: Two Pipes Operating (A and B)

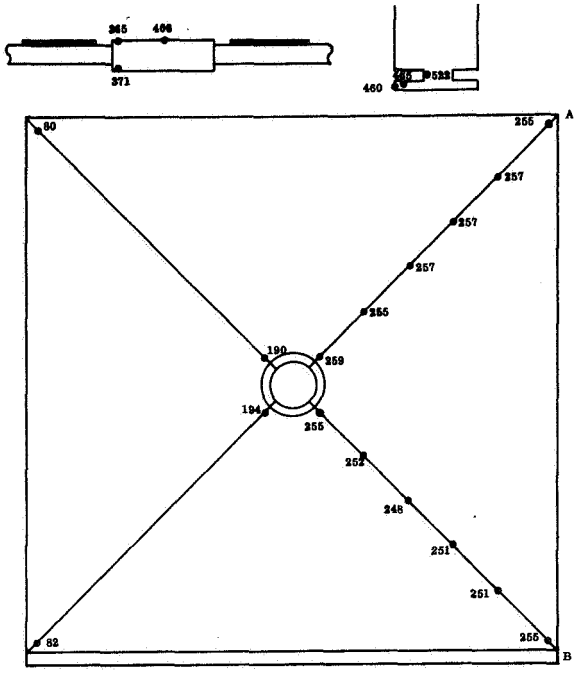

Figure D-28. 775 Watts: Two Heat Pipes Operating (A and B)

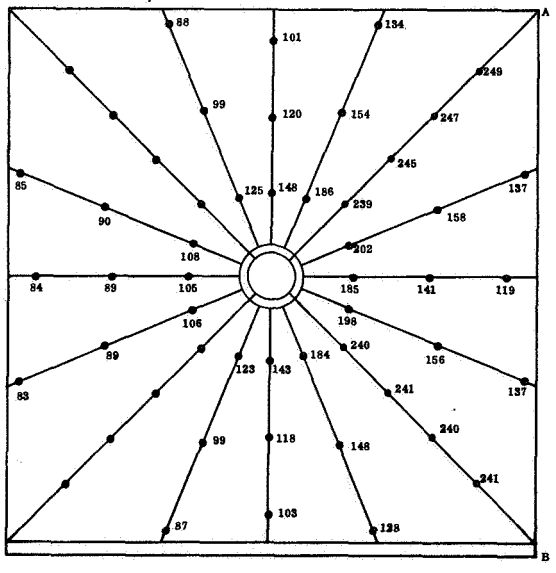

Figure D-29. 750 Watts: Two Heat Pipes Operating (A and B)

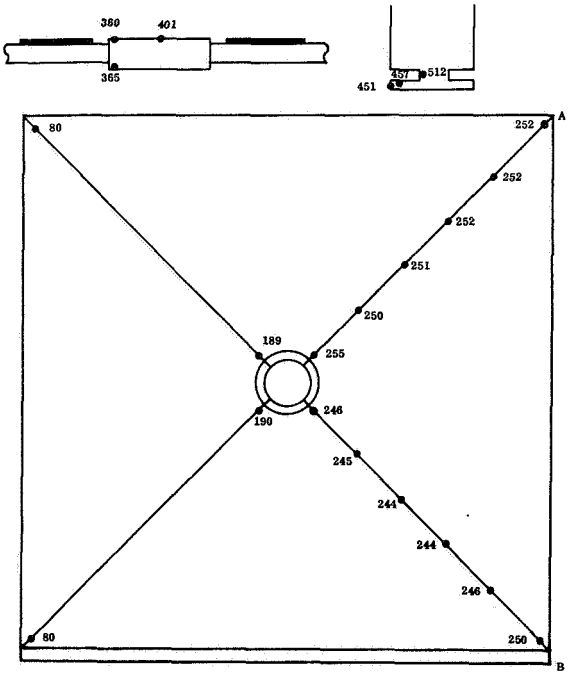

Figure D-30. 750 Watts: Two Heat Pipes Operating (A and B)

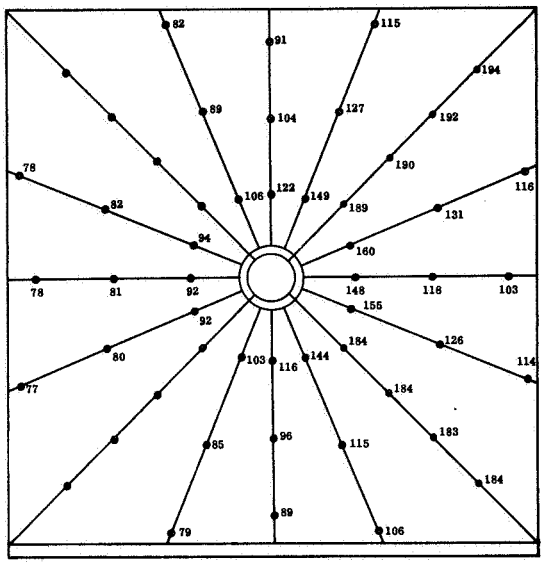

Figure D-31. 500 Watts: Two Heat Pipes Operating (A and B)

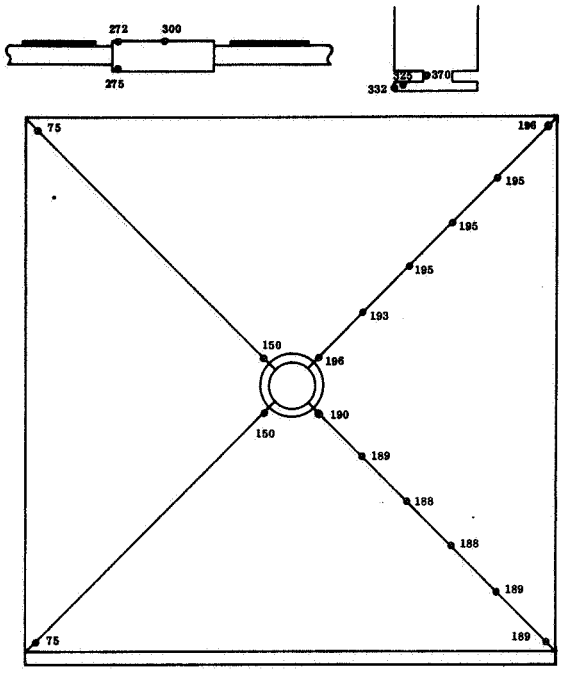

Figure D-32. 500 Watts: Two Heat Pipes Operating (A and B)

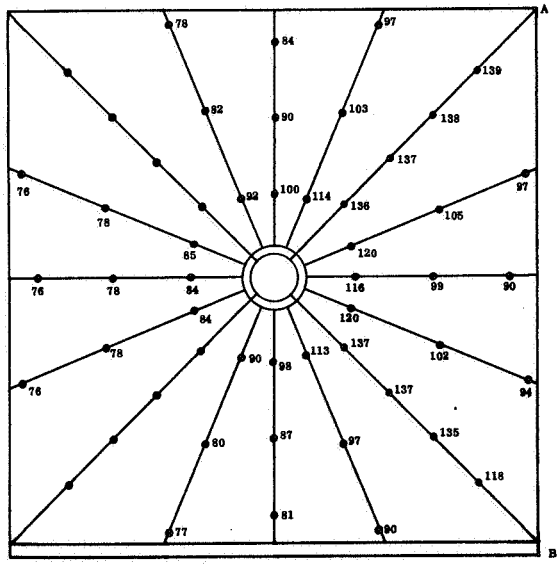

Figure D-33. 250 Watts: Two Heat Pipes Operating (A and B)

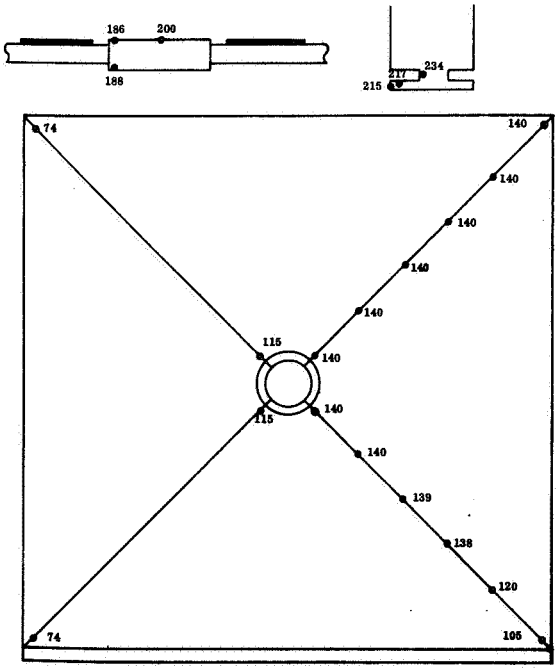

Figure D-34. 250 Watts: Two Heat Pipes Operating (A and B)

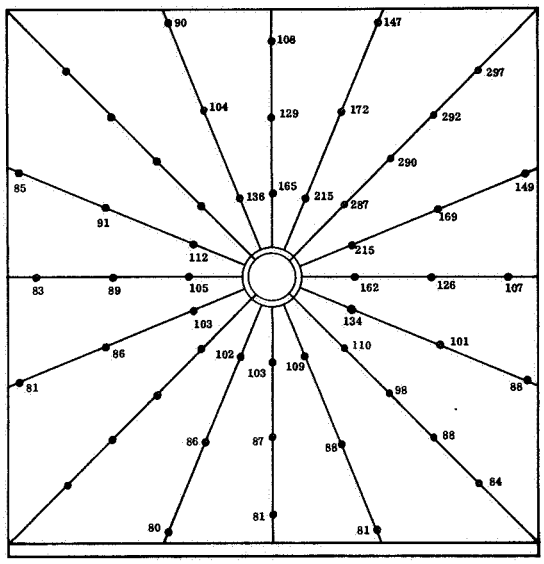

Figure D-35. 650 Watts: One Heat Pipe Operating (A)

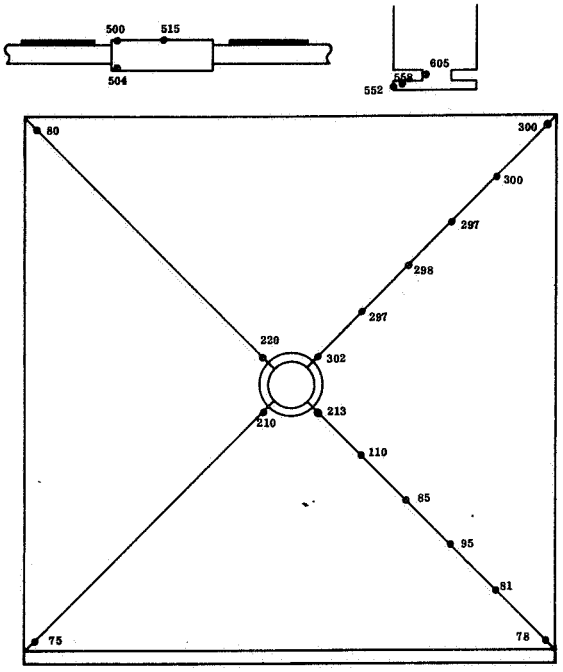

Figure D-36. 650 Watts: One Heat Pipe Operating (A)

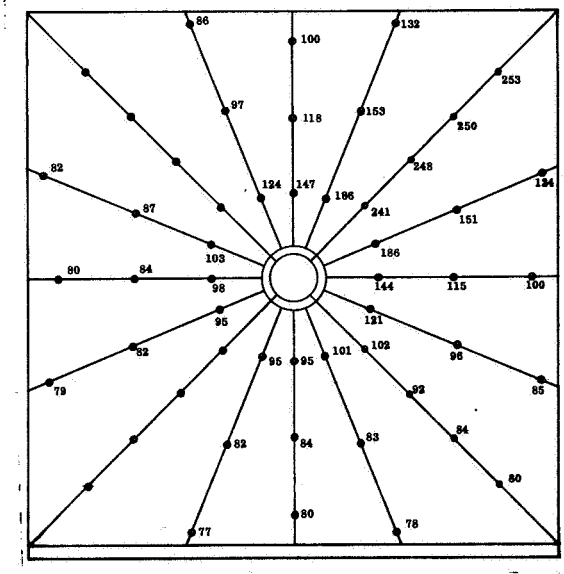

Figure D-37. 500 Watts: One Heat Pipe Operating (A)

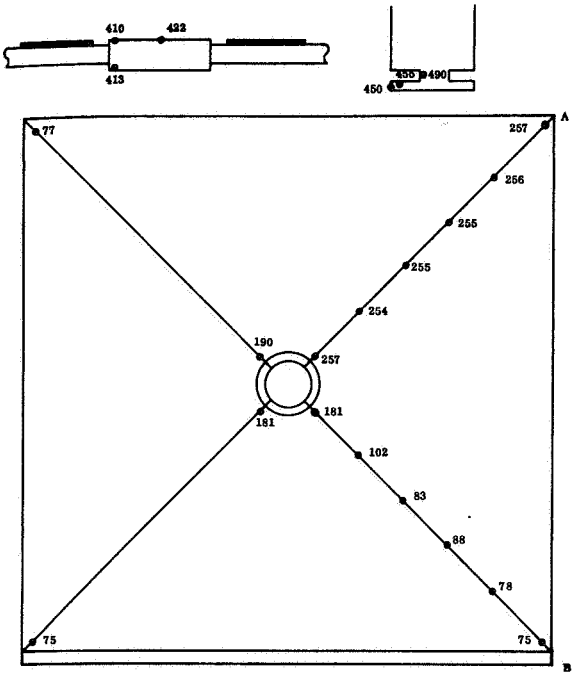

Figure D-38. 500 Watts: One Heat Pipe Operating (A)

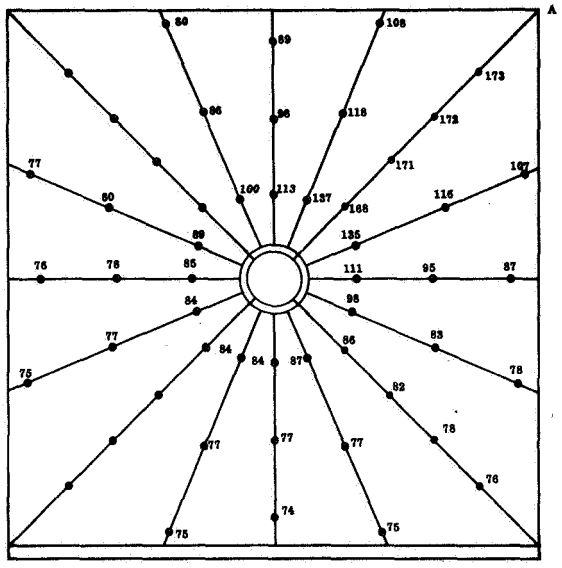

Figure D-39. 250 Watts: One Heat Pipe Operating (A)

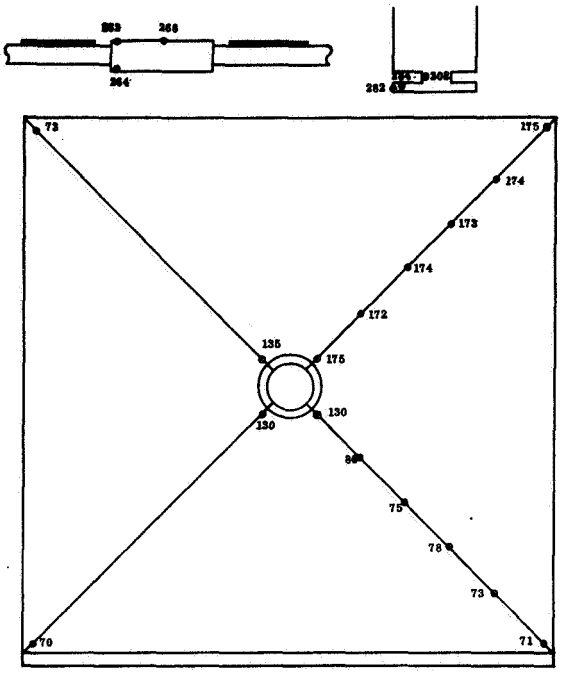

Figure D-40. 250 Watts: One Heat Pipe Operating (A)

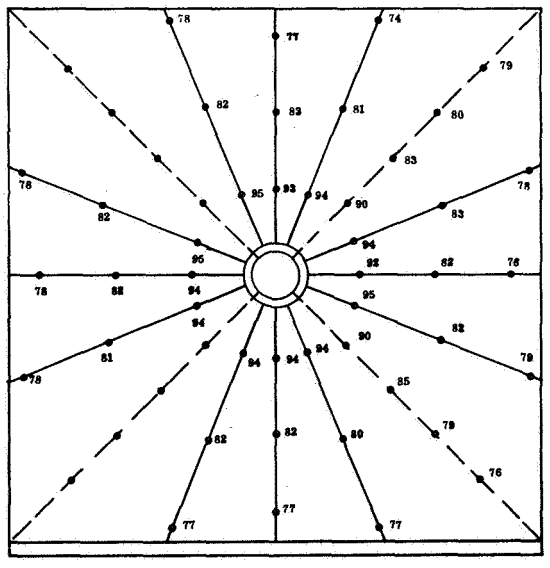

Figure D-41. 200 Watts: No Heat Pipes Operating

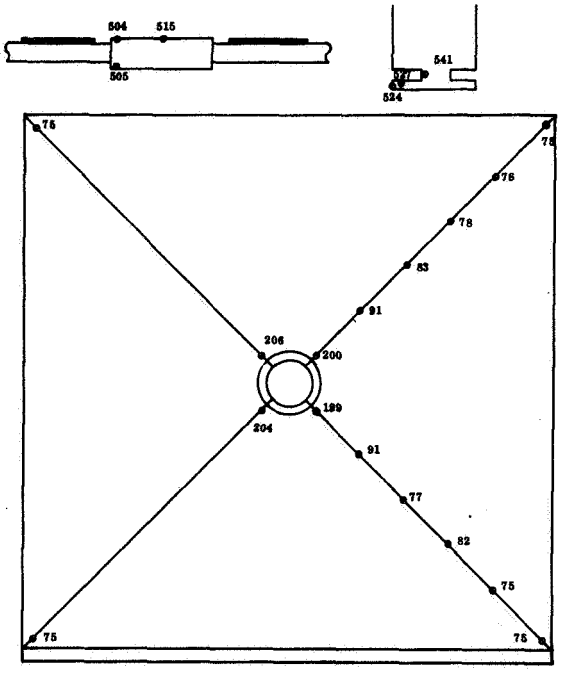

Figure D-42. 200 Watts: No Heat Pipes Operating

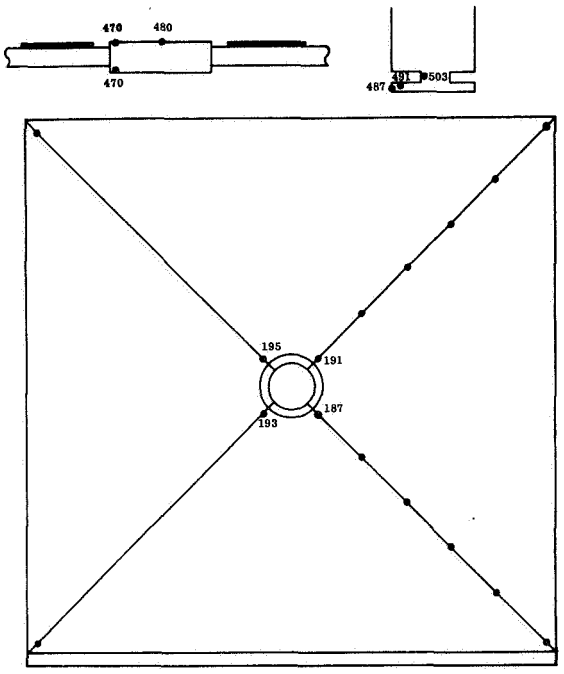

Figure D-43. 175 Watts: No Heat Pipes Operating

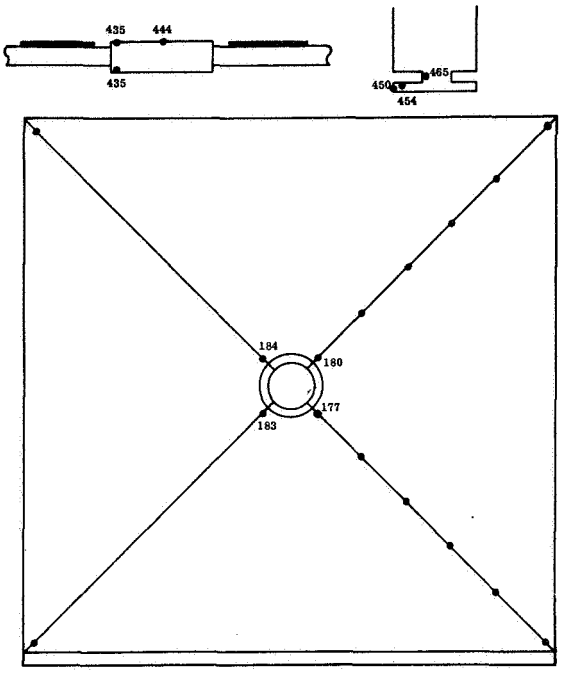

Figure D-44. 150 Watts: No Heat Pipes Operating

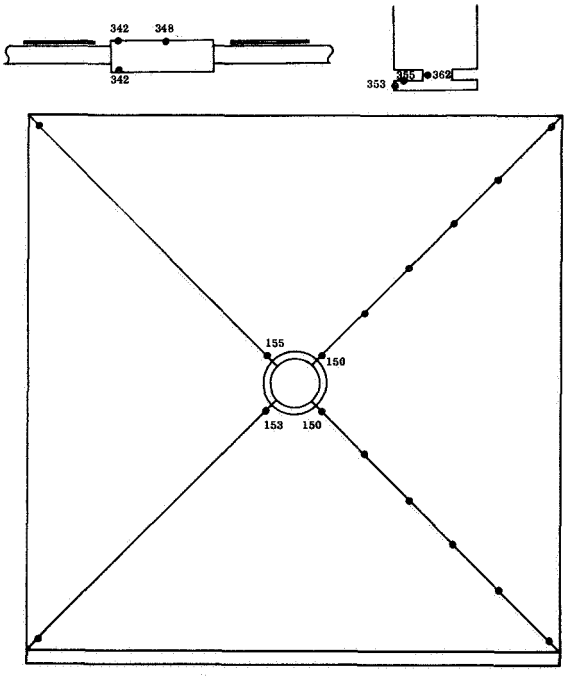

Figure D-45. 100 Watts: No Heat Pipes Operating

APPENDIX E

ISOTOPE LICENSE APPLICATION

This appendix contains the application for the license required to obtain and use the Promethium -147 fuel capsule in the cathode heating demonstration. The enclosure is a copy of the document submitted to the AEC in June 1968.

LICENSE APPLICATION FOR

PROMETHIUM-147 FUEL CAPSULE

FOR CATHODE HEATING PROGRAM

Prepared by: Frank J. Witt

June 10, 1968

TABLE OF CONTENTS

FIGURE

TABLE OF CONTENTS (Continued)

I. INTRODUCTION

A program is being performed by GE/MSD Spacecraft Department to investigate improvements to microwave vacuum tubes for space applications. One specific requirement of the Contract (NAS 12-565) is to demonstrate non-electric heating of a vacuum tube cathode. The heat source selected for the demonstration is a radioisotope fuel capsule which is to be Government Furnished Property. Arrangements have been made through the AEC to obtain, on loan, an existing radioisotope heat source fuel capsule. On the basis of applicability and availability the AEC has allocated the promethium-147 fueled capsule which has been utilized on the Advanced Manned Strategic Aircraft (AMSA) thermal preconditioner unit for Wright Paterson Air Force Base, Dayton, Ohio.

II. TEST DESCRIPTION

The purpose of the test is to demonstrate a method of non-electric heating of a vacuum tube cathode. It is intended to use the energy from the radioactive decay of the promethium-147 to heat the cathode of an L-65C triode to its emission temperature. For this purpose, the L-65C has been modified to remove its electrical heater and incorporate an isothermal heat transfer device, a heat pipe, into the cathode structure (See Figure I).

With the heat pipe, heat can be transferred from a threaded section external to the heat pipe to the tube cathode without a significant drop in temperature. The heat pipe will be inserted into a threaded hole in a high thermal conductivity copper block. The copper block will be used to transfer heat from the promethium-147 fuel capsule to the heat pipe. The fuel capsule will be clamped to the block to provide adequate heat transfer area. (Clamping pressure will be below that which could damage the fuel capsule) The complete test setup is shown in Figure II. The entire assembly will be thermally insulated so that the L-65C cathode will be heated to emission temperatures (600 to 700^{o}C).

III. HEAT SOURCE DESCRIPTION

The heat source capsule as shown in Figure III may consist of either the electrically simulated or the promethium-147 fueled capsule. Both configurations are identical along the outer clad envelope, but differ within the actual heat source. The information used in this section has been extracted from Reference 1 unless otherwise indicated.

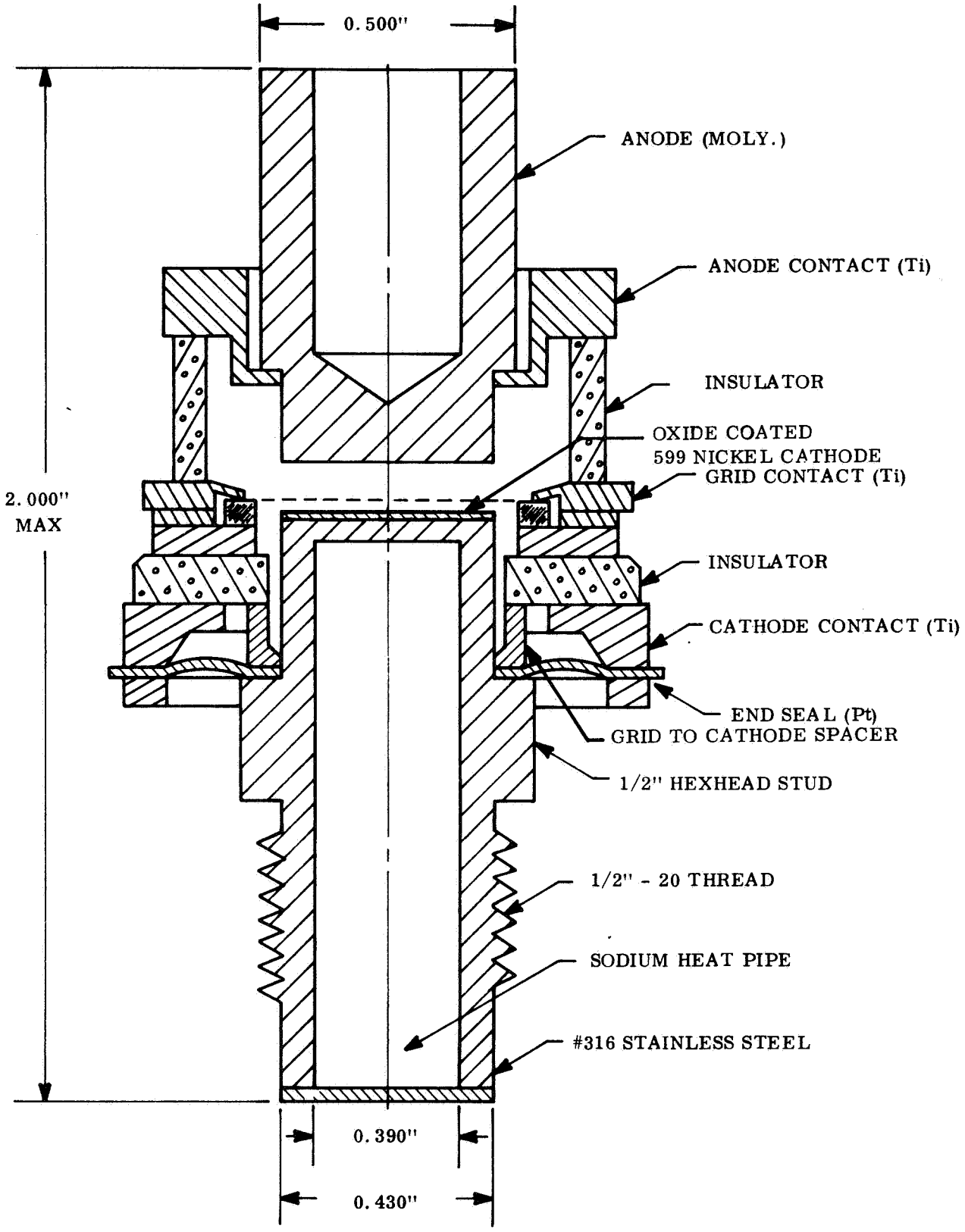

Figure I. Cathode Structure and Heat Pipe

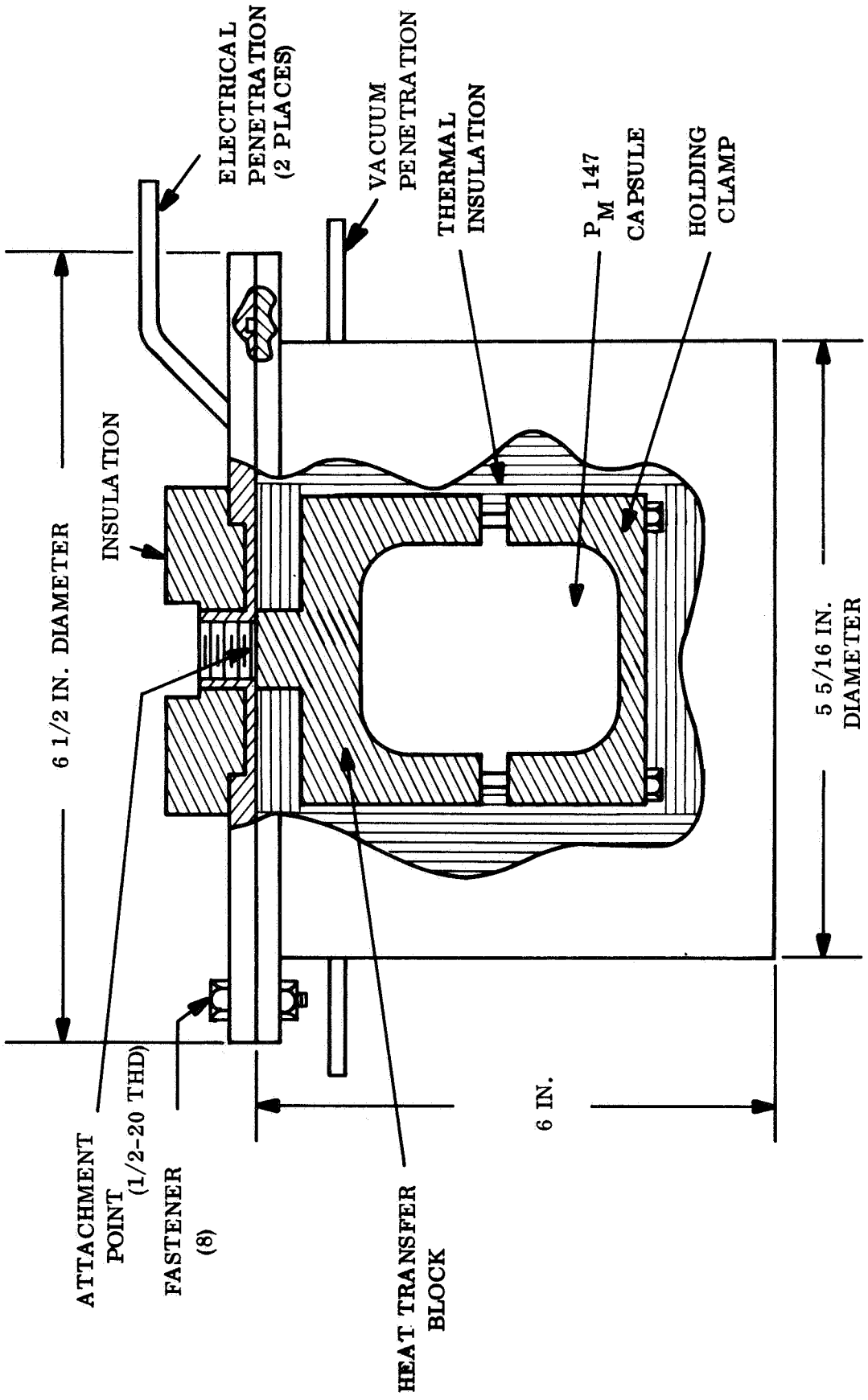

Figure II. Triode Heater Assembly Utilizing AMSA Fuel Capsule

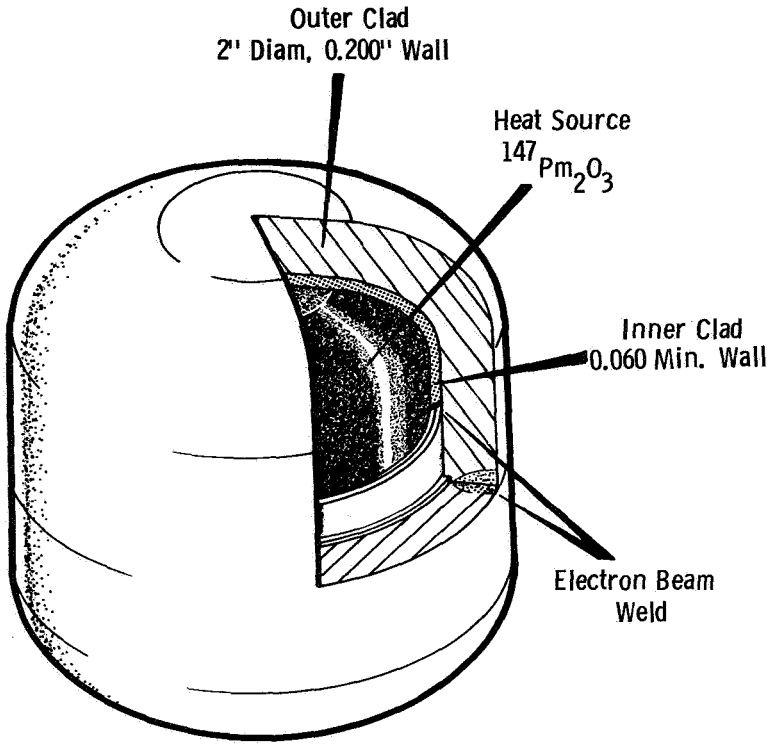

AMSA THERMAL POWER CAPSULE

Figure III. AMSA Thermal Power Capsule

A. AMSA Promethium-147 Fuel Capsule

The rounded corner cylindrical AMSA fuel capsule shown in Figure IV consists of a core of sintered $^{147}Pm_2O_3$ clad with 0.060 inch tantalum. A secondary cladding of 0.200 inch Unitemp L-605 alloy provides the outer containment. The constraints on the design of the fuel capsule imposed by the AMSA Thermal Preconditioner Unit application included:

Fuel Form - $^{147}Pm_2O_3$ with demonstrated cladding compatibility.

Fuel Loading - nominal 60 watts, thermal

Radiation - minimum consistant with the design

Fuel Containment - no fuel release for a period of 1 year following terminal velocity impact at the critical angle against a rigid medium

Dimensions - 2.00 inch diameter and 2.00 inch length with a 0.645 inch radius connecting the cylindrical and end surfaces

The inner clad is fabricated of tantalum material with a 99.9% minimum purity. The outer clad is fabricated of Unitemp L-605 alloy (Universal Cyclops Steel Corporation) from the same heat as stock used for corrosion and physical tests. Compatability studies at Battelle Northwest have shown that Pm_2O_3 can be adequately contained in tantalum up to 1200°F for several months or longer (Reference 2). Long term testing also demonstrated the importance of adequate purification of the oxide. Trace impurities such as carbon, CO_2, CO or H_2O greatly accelerated the reactions of the oxide with certain metals and alloys. Little or no reaction occurs between the purified oxide used in the AMSA capsule and the tantalum inner clad when tested up to 1200°F.

1. Heat Source Fabrication

The AMSA radioisotope encapsulation process depicted in Figure V includes:

a) Promethium-147 purification

b) Conversion to oxide (Pm_2O_3)

c) Sintering Pm_2O_3 pellets for fuel core densification

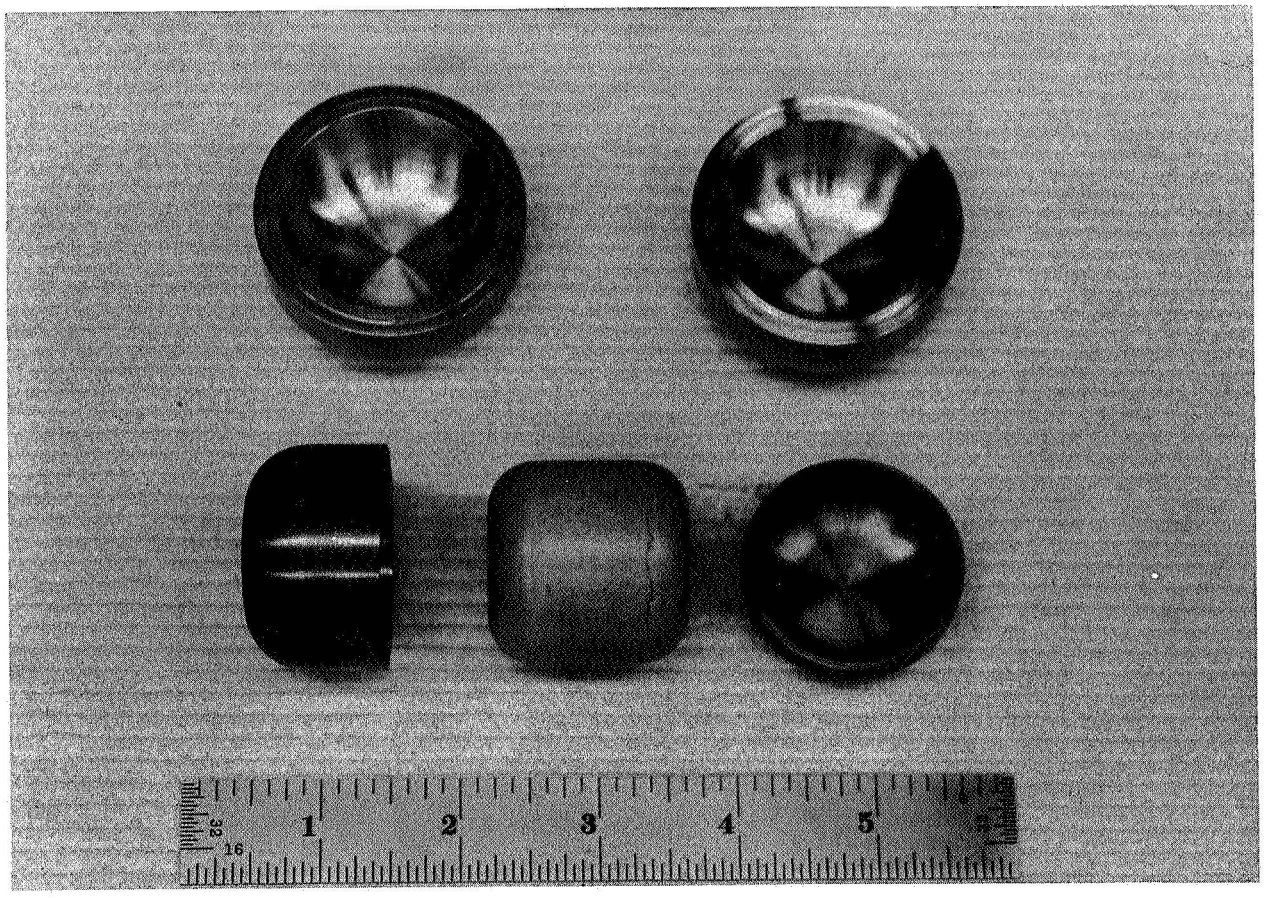

PNL 0671707-2

Figure IV. AMSA Capsule Components

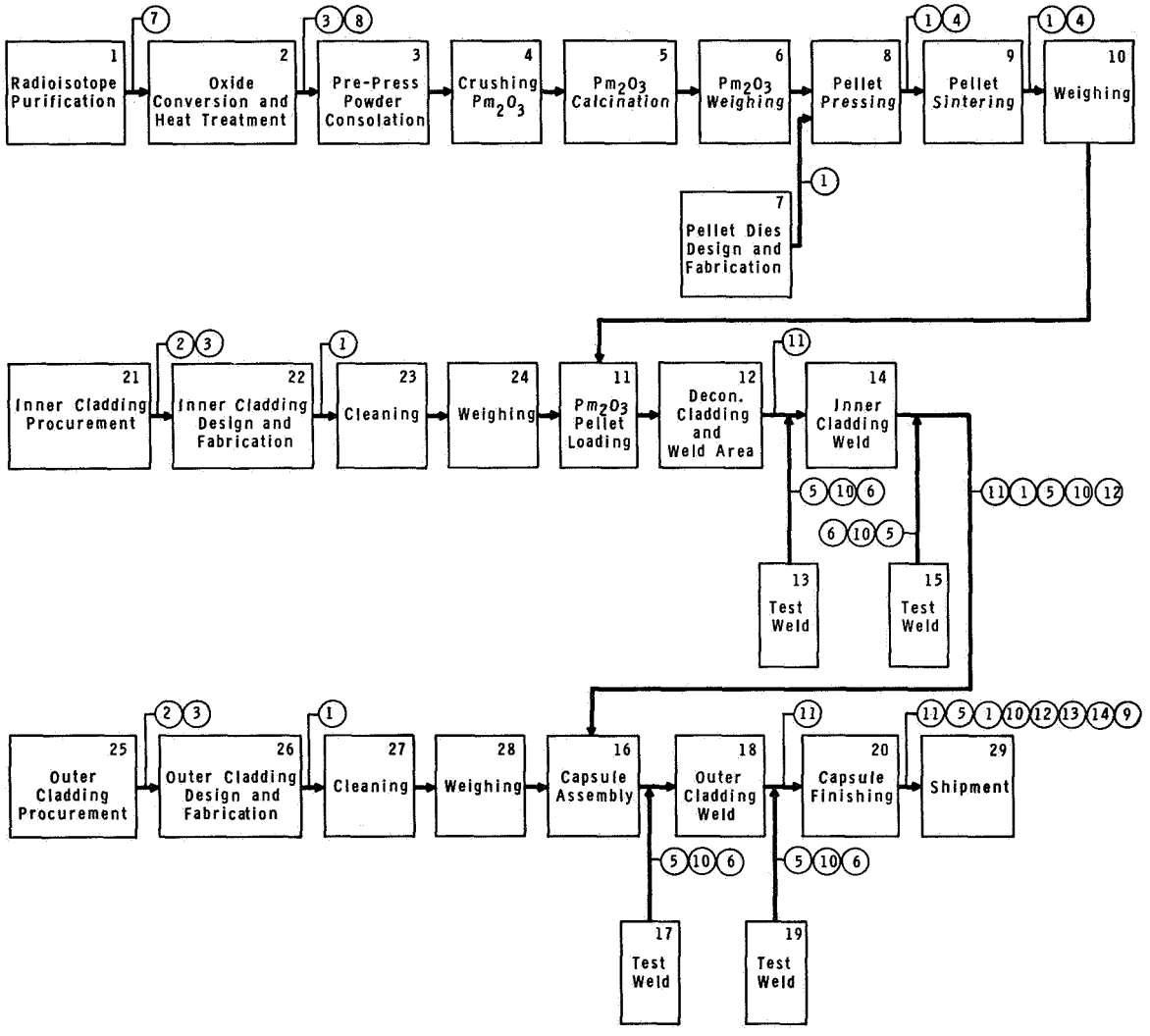

1. Dimension Measurements
2. Dye Penetrant
3. Impurity Analysis
4. Density Determination
5. He Leak Check
6. Metallography
7. Isotopic Analysis
8. X-Ray Diffraction
9. Radiography
10. Ultrasonic Testing
11. Decon. Smear Check
12. Radiation Mapping
13. Gamma Spectrometry
14. Calorimetry

Figure V. AMSA Radioisotope Encapsulation Process

d) Inner cladding (tantalum) encapsulation by electron beam welding

e) Outer cladding (Unitemp L-605 alloy) encapsulation by electron beam welding

f) Capsule finishing, i.e., decontamination, helium leak check, dimensions, ultrasonic weld test, radiation mapping, gamma spectrometry, and calorimetry.

The promethium processing is described in Section III B.

The inner and outer clad welds were accomplished by electron beam welding. Prior to welding, the tantalum inner cladding was evaluated for:

a) impurity analysis of tantalum per Quality Assurance Procedure F*

b) Dimensions and capsule integrity per Quality Assurance Procedure G

c) Smearable activity at weld area per Quality Assurance Procedure H

An inner clad test weld (No. 1) was fabricated prior to encapsulating the $^{147}Pm_2O_3$ and was inspected to verify welding parameters, weld penetration and capsule integrity per Quality Assurance Procedure I. A photomicrograph of a typical inner clad weld is shown in Figure VI. The actual tantalum inner cladding weld was evaluated per Quality Assurance Procedure J for smearable contamination, weld penetration, dimensions, leakage and radiation levels. A post test inner clad weld (No. 2) was fabricated and inspected to verify welding parameters, weld penetration and capsule integrity per Quality Assurance Procedure K.

Prior to welding, the Unitemp L-605 alloy outer cladding was evaluated for:

a) Chemical impurity analysis per Quality Assurance Procedure L

b) Dimensions and capsule integrity per Quality Assurance Procedure M

* Quality Assurance procedures appear in Appendix

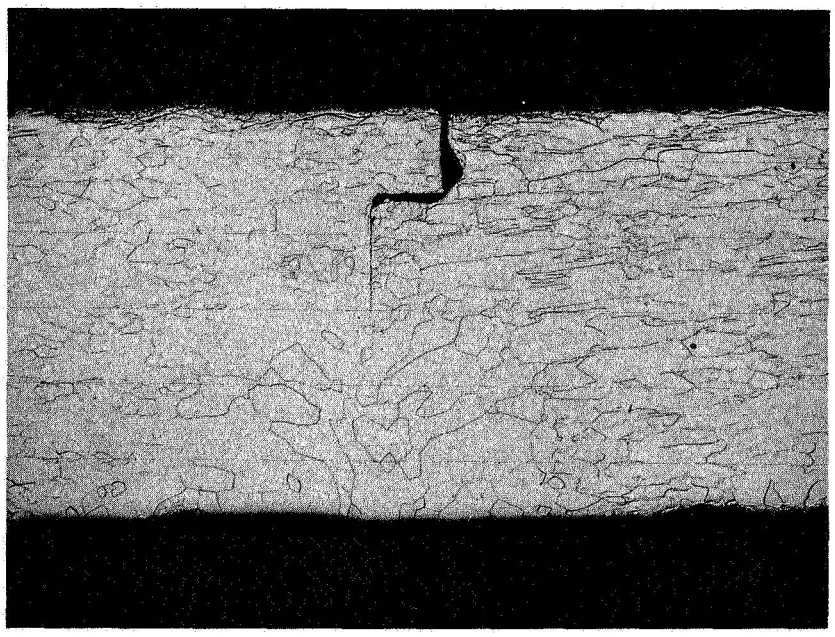

467-1711 36X

Figure VI. AMSA Capsule - Typical Inner Clad Weld

An outer clad test weld (No. 1) was fabricated prior to encapsulating the tantalum inner capsule and was evaluated to verify welding parameters, weld penetration and capsule integrity per Quality Assurance Procedure N. A photomicrograph of a typical outer clad weld is shown in Figure VII. The actual Unitemp L-605 alloy outer cladding weld was evaluated for smearable contamination per Quality Assurance Procedure O and for weld penetration, dimensions, leakage, radiation levels, gamma spectra, and heat output per Quality Assurance Procedure Q. The finished AMSA capsule is shown in Figure VIII. A post test outer clad weld (No. 2) was fabricated and evaluated to verify weld penetration, weld parameters and capsule integrity per Quality Assurance Procedure P. The results of the final dimensional inspection are reported in Quality Assurance Procedure R.

2. Heat Source Impact Tests

Since the promethium-147 fuel capsule was flown in an Air Force aircraft for the AMSA thermal preconditioner application, Sandia Corporation conducted a three phase test program to evaluate the impact resistance of the fuel capsule (Reference 3). In Phase I, analogue capsules were impacted into granite targets to obtain a preliminary evaluation of the critical capsule impact attitude (the attitude resulting in rupture of the cladding at the minimum impact velocity). Test results indicated that the 22½ to 45 degree range was critical.

In Phase II, capsules of two designs, fabricated at Battelle Northwest, were tested to compare the impact resistance of the two designs and to obtain preliminary data about the critical impact angle and velocity. The capsule design requiring the more complex fabrication process had no significant advantage over the other design. The critical impact angle was found to be 45 degrees. Welding process problems and a requirement for improved nondestructive testing techniques were indicated.

In Phase III, flight quality capsules fabricated by Battelle Northwest were impacted to obtain additional data about the critical impact attitude and velocity, and to compare the capsule damage from impact into soil, concrete and granite targets. Impacts of the bare capsule into soil and concrete targets at 185 to 200 percent of the experimentally determined sea level equilibrium velocity of approximately 340 ft/sec did not appear to significantly impair the capsule fuel containment capability. Capsule impacts into granite targets at impact attitudes of 35 to 55 degrees at approximately 85 percent of the experimentally determined sea level equilibrium velocity ruptured the capsule.

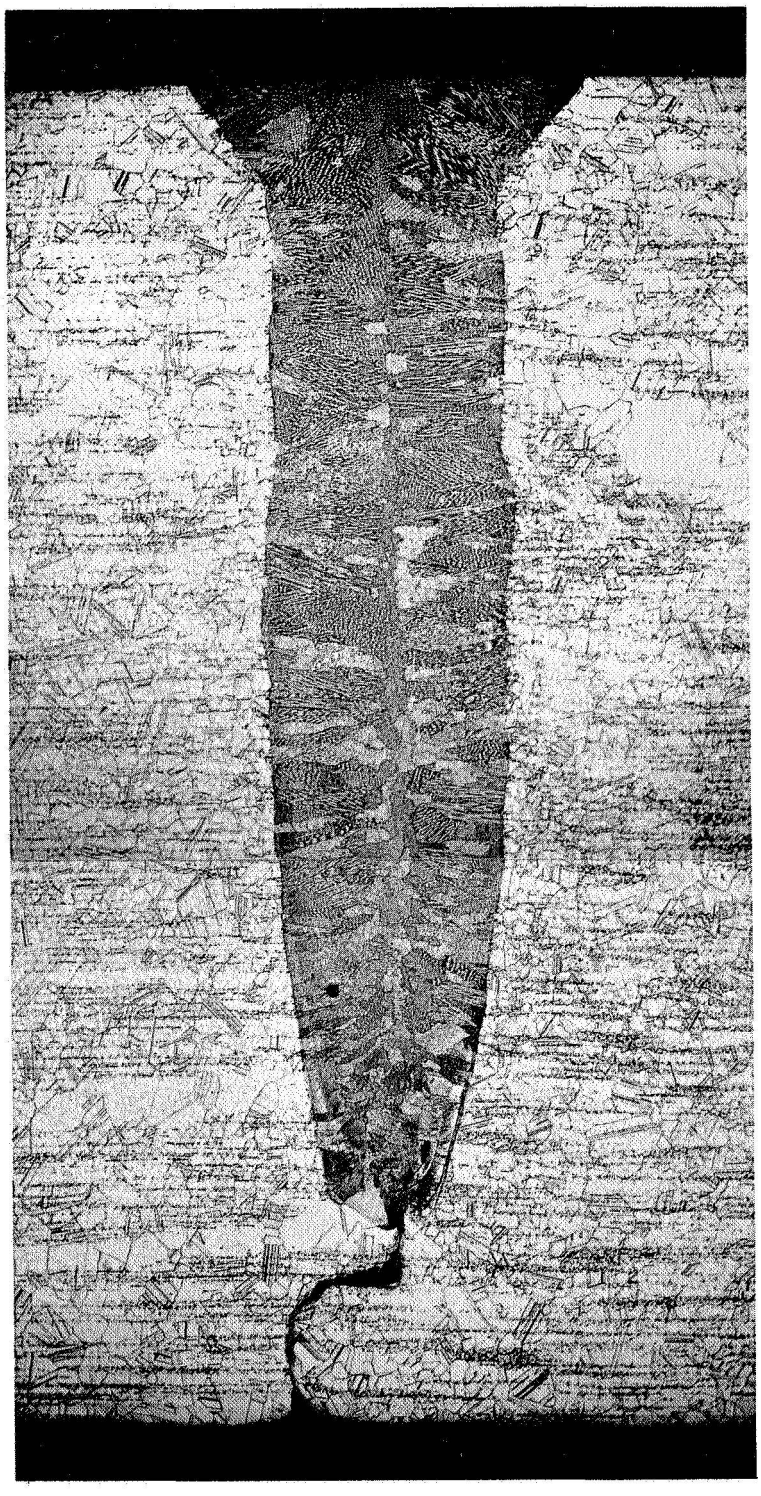

567-10708A - B

Figure VII. AMSA Capsule - Typical Outer Clad Weld

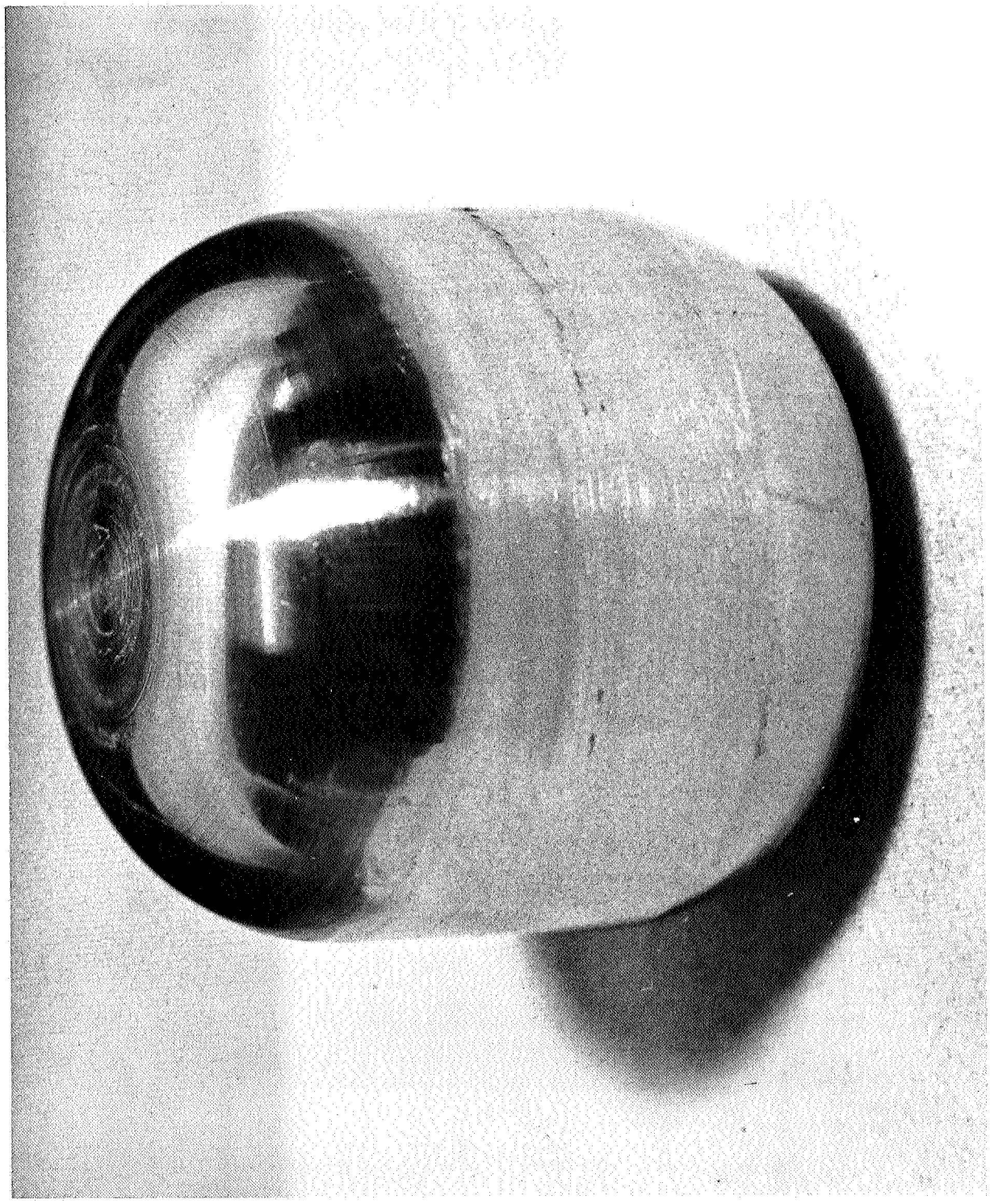

Figure VIII. AMSA Heat Source Capsule

The results of the impact test program indicate that the capsule may reasonably be expected to provide fuel containment for all except the most advesse impact conditions. The impact resistance of the AMSA fuel capsule has been presented to describe its rugged design. The actual test environments for the cathode heating program application is so much less severe than that experienced in the impact program. As an additional safeguard, Battelle Northwest is planning to perform non-destructive testing of the AMSA capsule prior to delivery to GE/VFSTC. This quality assurance program which includes a helium leak check, smear check ultrasonic weld inspection and radiography will insure that the capsule integrity has not changed as a result of the Air Force test program.

B. Promethium-147 Fuel

1. Promethium-147 Fuel Purification

Promethium-147 (half-life 2.62 years) is one of the rare earth uranium-235 fission products which may be obtained by chemical separation of spent reactor fuel utilizing a series of successive precipitation processes (References 4 and 5). Two major contaminants of Pm-147 are found: Pm-146 (half-life 5.5 years, Reference 6), and Pm-148 (which has two isomers with half-lives of 5.4 days and 42 days). After lag storage to allow for decay of the gamma emitting Pm-148, the rare earth crude is further refined to isolate the Pm-147 from its adjacent rare earth neighbors and all other impurities.

Isolation of promethium from its adjacent rare earth neighbors and all other impurities is accomplished by a displacement cation exchange process (Reference 7) utilizing an ammonia buffered solution of the complexing agent DTPA (Diethylenetriaminepentaacetic acid) as the separating agent. The separation is conducted in a 7-column ion-exchange facility, installed, together with associated tanks, valves and instrumentation, in a heavily shielded manipulator cell. The flowsheet and column arrangement is shown schematically in Figure IX.

With the very high Ce-144 and Eu-154 decontamination factors achieved in the ion-exchange process, pure promethium does not require extensive shielding for the final conversion to treated oxide. The promethium product solution is therefore collected as it flows from the final purification column and transferred to the lightly shielded glove box facilities for oxide conversion. The radiochemical purity of the Pm-147 is verified per Quality Assurance Procedure A.

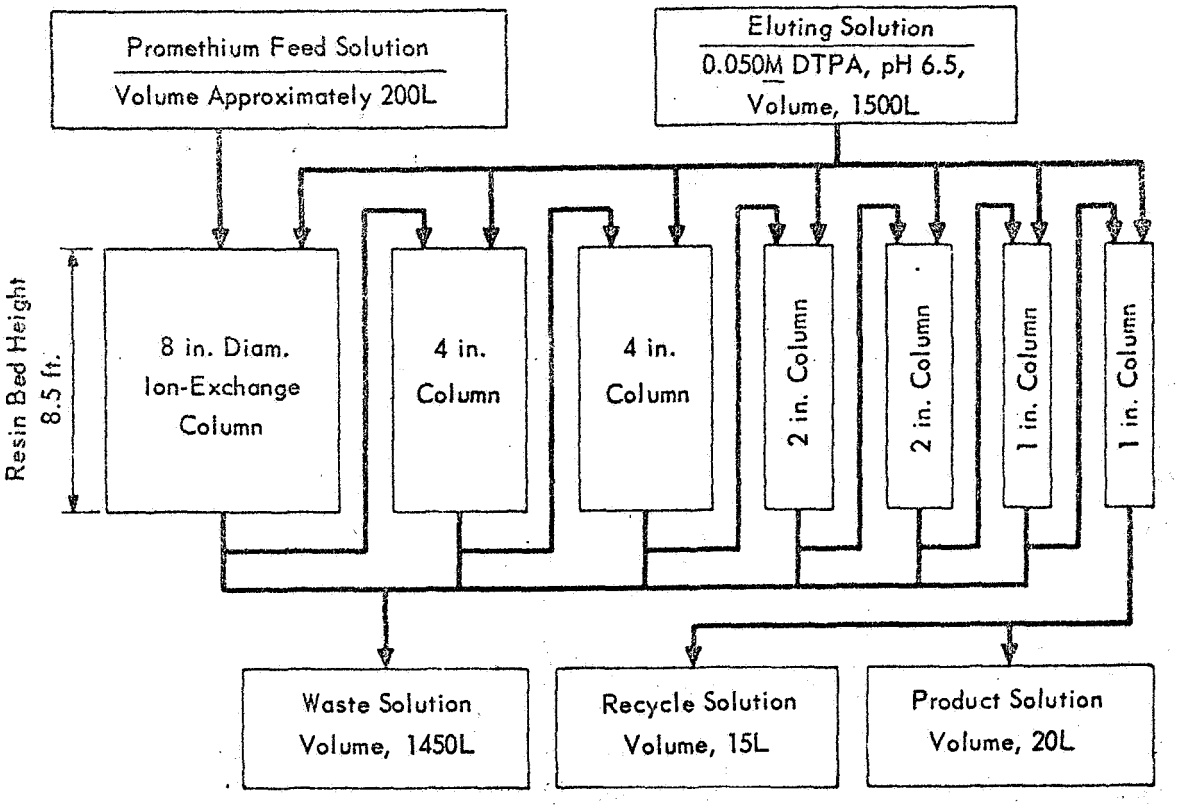

Run Conditions:

Elution Temperature	65 C
Elution Flow Rate	4 ml/min-cm^2
Rate of Band Advance	16-18 cm/hr

Run Cycle Time

Absorption Cycle	4 hr
Elution Cycle	160 hr
Turn Around Time	72 hr

Figure IX. Promethium Purification Flowsheet

The oxide conversion chemistry process consists of the following operations:

a. Vacuum transfer of up to 9 liters of promethium produce solution (~45 gms Pm) from the purification facility to a glass precipitator in the glove box,

b. Heating of the promethium solution to 80°C via a steam coil in the precipitator and simultaneous sparging,

c. Vacuum addition of sufficient oxalic acid (as a slurry) to ensure complete precipitation of the promethium as oxalate,

d. A 30 minute digestion period followed by cooling to 25°C (cooling water through the coil) to promote growth of large crystals and lower solubility,

e. A double wash by the decantation of the precipitate to remove traces of stainless steel corrosion products acquired during storage in the steel product storage tanss,

f. Slurry transfer of the precipitate to a quartz filter tube containing a quartz frit at the bottom,

g. Insertion of the loaded filter tube into a vertically mounted tube furnace followed by an 8-hour heating cycle at 1100°C to convert the oxalate precipitate to Pm_2O_3.

h. A special oxide treatment step consisting of 4 hours at 1100°C with oxygen flowing up through the filter tube and contents at a slow rate, followed by a similar treatment with 6% hydrogen-94% argon to ensure removal of final traces of bound CO_2 and yield a Pm_2O_3 product slightly deficient in oxygen.

Radiochemical analysis, corrected to October 1, 1967 indicated that the Pm_2O_3 capsule contained:

Pm-147 168,100 Ci

Pm-146 0.0756 Ci max.

$$\frac{\text{Pm-146}}{\text{Pm-147}} = 0.25 \pm 0.2 \times 10^{-6} \text{ Ci/Ci}$$

Pm-148m 0.00302 Ci max.

$$\frac{\text{Pm-148}}{\text{Pm-146}} \leq 0.04 \text{ Ci/Ci}$$

Eu-154 504 μ Ci

$$\frac{\text{Eu-154}}{\text{Pm-147}} = 3.0 \times 10^{-9} \text{ Ci/Ci}$$

Ce-144 168 μ Ci max.

$$\frac{\text{Ce-144}}{\text{Pm-147}} < 10^{-9} \text{ Ci/Ci}$$

Figures X, XI and XII indicate the radioactive decay of the above isotopes.

The samarium-147 daughter constituted the principal impurity. Spectrographic analysis, per Quality Assurance Procedure B indicated impurities to be less than 1% other than samarium X-ray diffraction analysis per Quality Assurance Procedure C, confirmed the crystal structure of the Pm_2O_3 to be 100% monoclinic.

2. Preparation of Pm_2O_3 Pellets

At the time the AMSA capsule was fabricated, the technology was not sufficiently advanced to permit the fabrication of the large $^{147}Pm_2O_3$ pellet in one piece. Therefore, this capsule contains three pieces; the semi-dome ends are separate pieces from the central cylindrical section. This in no way affects the heat generation or integrity of the capsule.

After pressing to 75 to 80% of theoretical density but prior to sintering, the fuel pellets were inspected per Quality Assurance Procedure D for dimensions and density. After sintering the pellets were again inspected for dimensions and density per Quality Assurance Procedure E.

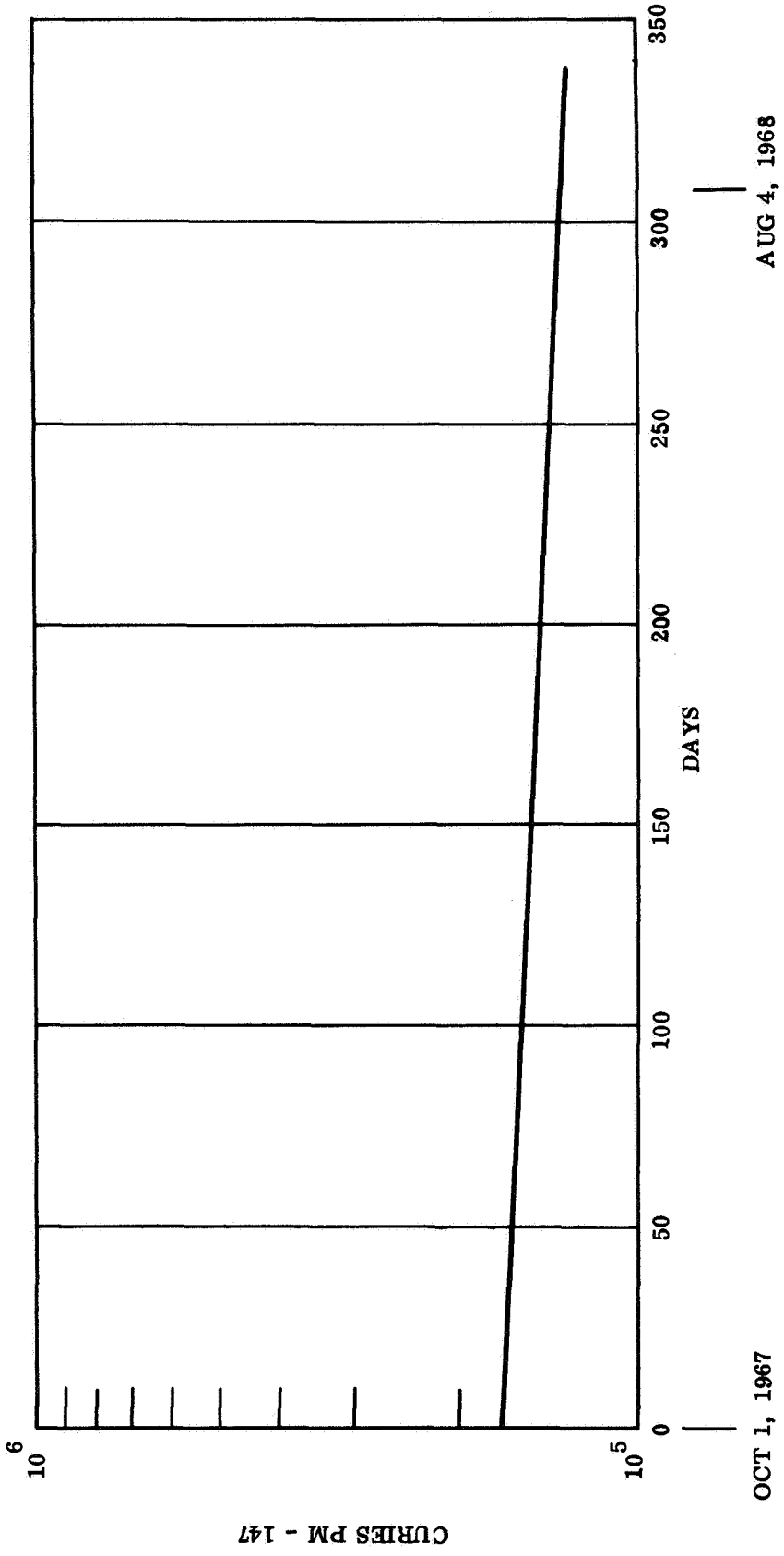

Figure X. Pm-147 Activity Versus Time

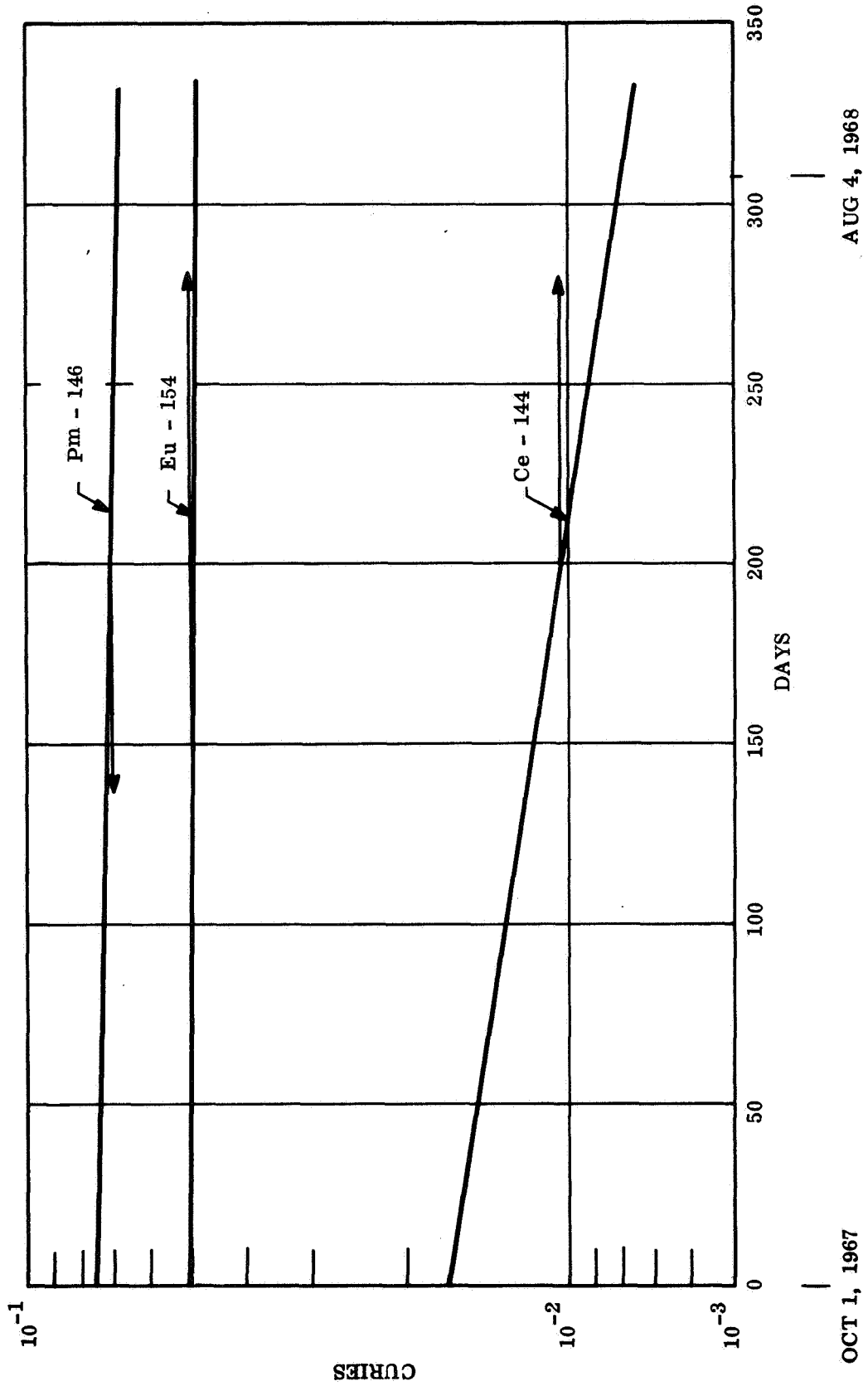

Figure XI. Pm-146, Eu-154, and Ce-144 Activity Versus Time

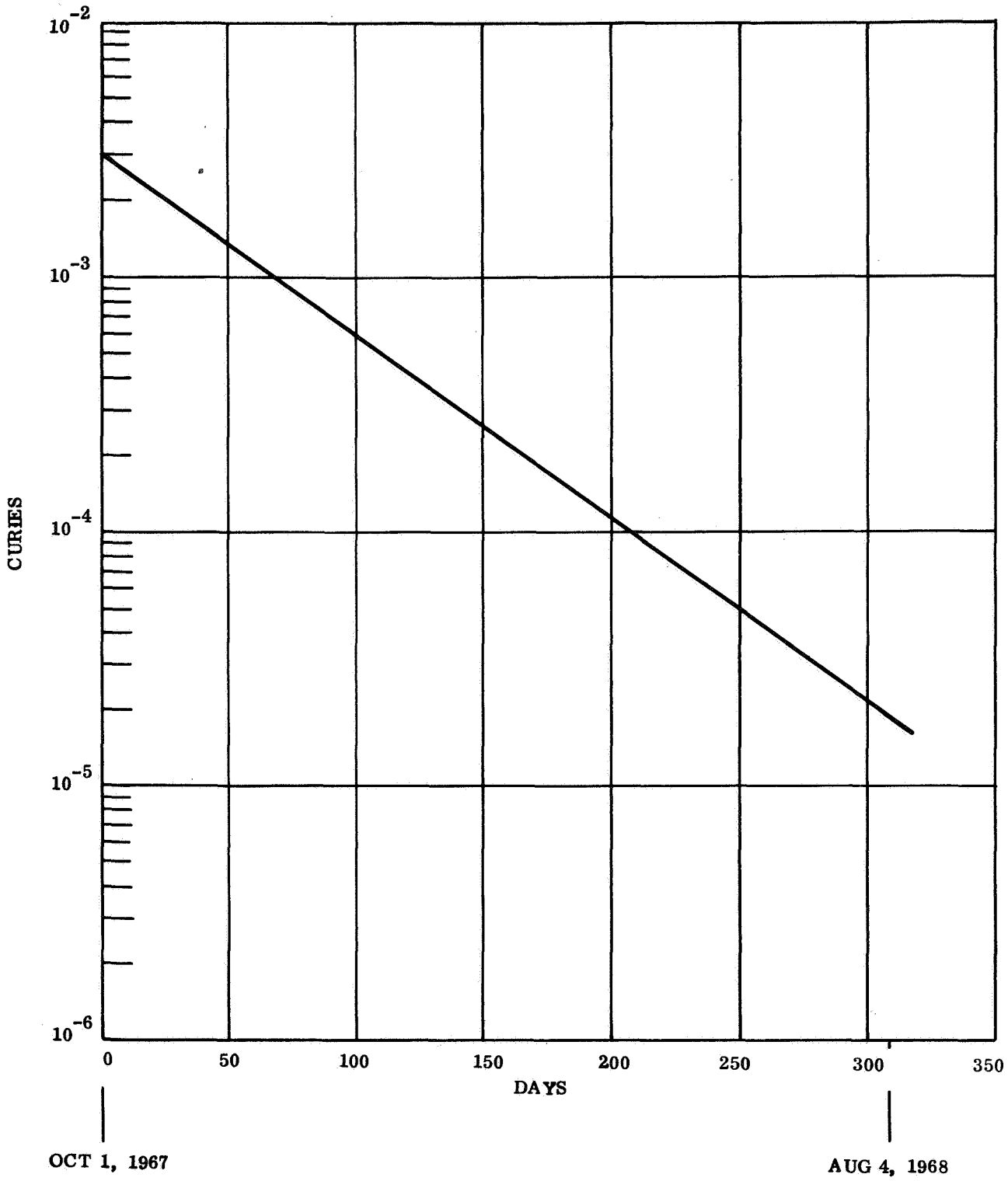

Figure XII. Pm-148m Activity

3. Calorimetry

The thermal output of the doubly clad $^{147}Pm_2O_3$ capsule was determined by calorimetric measurements. The thermal power was measured at 60.3 watts on October 1, 1967.

Figure XIII illustrates the thermal decay of the AMSA Pm-147 capsule. The decay curve represents the decay of Pm-147, whereas, the thermal power of the capsule includes the activities of Pm-146, Pm-148m, Ce-144 and Eu-154, each with their own decay characteristics. However, the small amounts of these contaminants (Section III-B-1, Promethium-147 Fuel Purification) will not affect the curve of Figure XIII to any noticeable degree. For example, the thermal activity of all the contaminants combined will not amount to the 0.2 watts of calorimeter thermal power tolerance.

4. Properties of Pm-147 Fuel

The properties shown in Table I of promethium-147 fuel were obtained from reference 9 unless otherwise indicated.

Table I. Properties of Pm-147 Oxide fuel

Nuclear Properties		
Half-Life	Pm-147	2.620 ± 0.005 yr.
	Pm-146	5.5 yr (6)
	Pm-148m	42 days
	Pm-148	5.4 days
Specific Activity	928.4 ± 1.7 Ci/g of Pm-147	
Heat Generation	0.3330 ± 0.0005 w/g of Pm-147	
	0.3587 ± 0.0010 w/k Ci of Pm-147	
	2788 ± 8 Ci of Pm-147/w	
Radiation Properties	Pm-147	0.225 MeV beta (100%)
		0.12 MeV gamma (0.003%)
		0 to 0.225 MeV bremsstrahlung
	Pm-146	0.78 MeV beta (35%)
		0.45 MeV gamma (65%)
		0.75 MeV gamma (65%)
Maximum Permissible Concentration in Air	For continuous exposure, 2×10^{-8} μCi/ml or tenfold lower by federal regulation.	

Table I (Continued)

Physical Properties Pm-147 Oxide

Density g/cm^3	7.3
Promethium Content wt.%	86
Power Density, W/cm^3	2.09
Specific Power, W/g	0.286
Melting Point, ^oC	2270
Heat of Formation, K cal/mole	-432
Heat Capacity, cal/mole-^oC	$(28.99 + 0.00576\ T - 415{,}900/T^2)$
Thermal Conductivity, cal/sec-cm^oC	$\left[0.0045 + 1.414 \times 10^{-8}\ (1020 - T)^2\right]$
Thermal Expansion Coefficient	9×10^{-6}
Vapor Pressure	$(\log_{10} P = 15.62 - 39{,}800/T)$

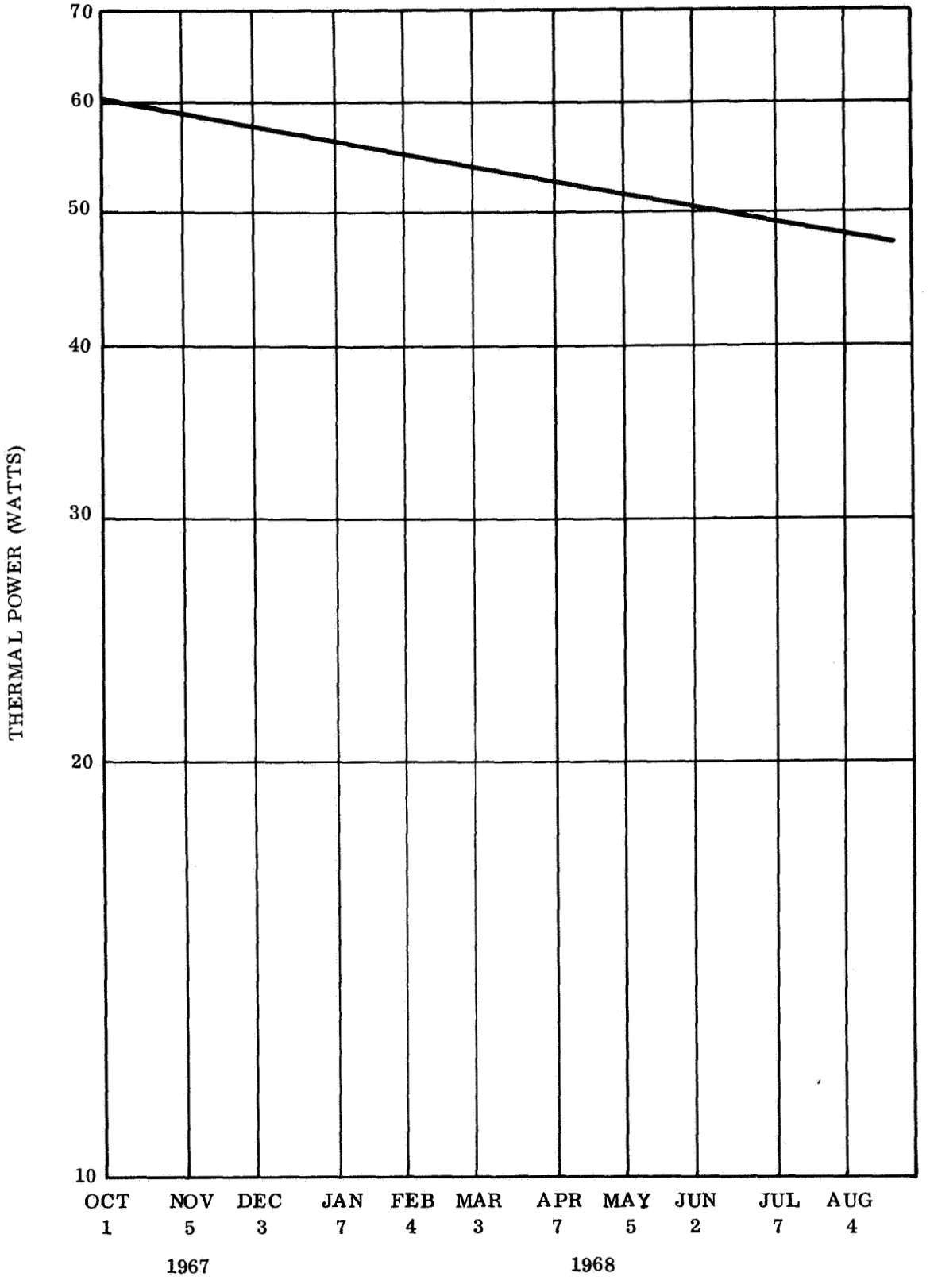

Figure XIII. Thermal Decay of AMSA Pm-147 Capsule

IV. AMSA CAPSULE SHIPMENT

The AMSA capsule will be shipped from Battelle Northwest to GE/VFSTC and back by the AEC/Richland Operations Office in a Department of Transportation (DOT) approved shipping container. The DOT permit no. is SP 4951. The shipping drum is shown in Figure XIV with the cover removed. The internal bird cage structure supports a sealed 2R container which holds the fuel capsule (See Figure XV). Temperatures measured at various locations throughout the shipping container, after the capsule was held in it for 64 hours are shown in Figures XVI and XVII. These temperatures will be lower when received at GE/VFSTC because of the radioactive decay of Pm-147 to about 80% of that measured in October 1967.

V. TEST FACILITY

The receipt, storage and testing of the promethium-147 fuel capsule will be performed within the RTG Storage Building at GE/ Valley Forge Space Technology Center. An artist sketch of the facility is shown in Figure XVIII.

The building is constructed of one-foot thick solid concrete block walls with two inch thick masonite doors to provide shielding. The facility is surrounded by an eight-foot cyclone fence 21 feet from the building for security and for enclosing the radiation area.

An alarm system for alpha airborne radiation, security and ventilation of RTG heat generation is provided. The ventilation blower exhausts the room air through an absolute filter. The room is maintained at a slight negative pressure at all times to contain radioactive contamination in the event of an accidental release. All internal surfaces of the facility are covered with a non-porous, strippable coating to facilitate decontamination, if necessary. The building drains are piped to a 500 gallon retention tank in the event that decontamination be required.

In addition to the 11 by 24 foot storage area, a shielded work area of the same size is available. A two ton hoist and monorail is used to transfer shipping casks containing fuel capsules from a truck to the storage area.

The building has been in use since February 1968 for storage and acceptance testing of SNAP-19 and SNAP-27 fuel capsules. The building plans and specifications have been reviewed and approved by the Operational Safety Division of the AEC Albuquerque Operations Office.

Figure XIV. AMSA Capsule Shipping Drum Interior

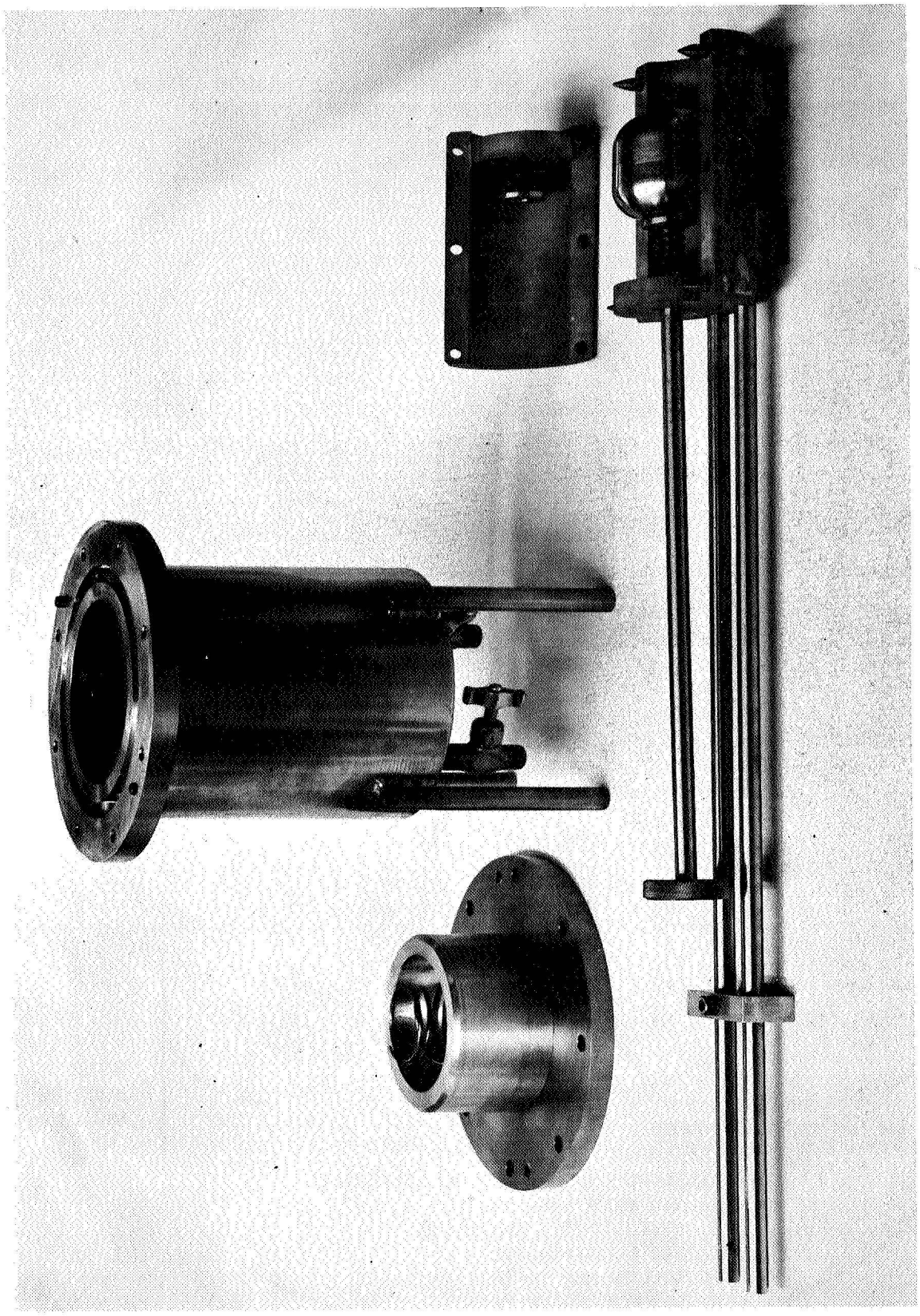

Figure XV. 2R Container and Inner Holding Fixture Assembly

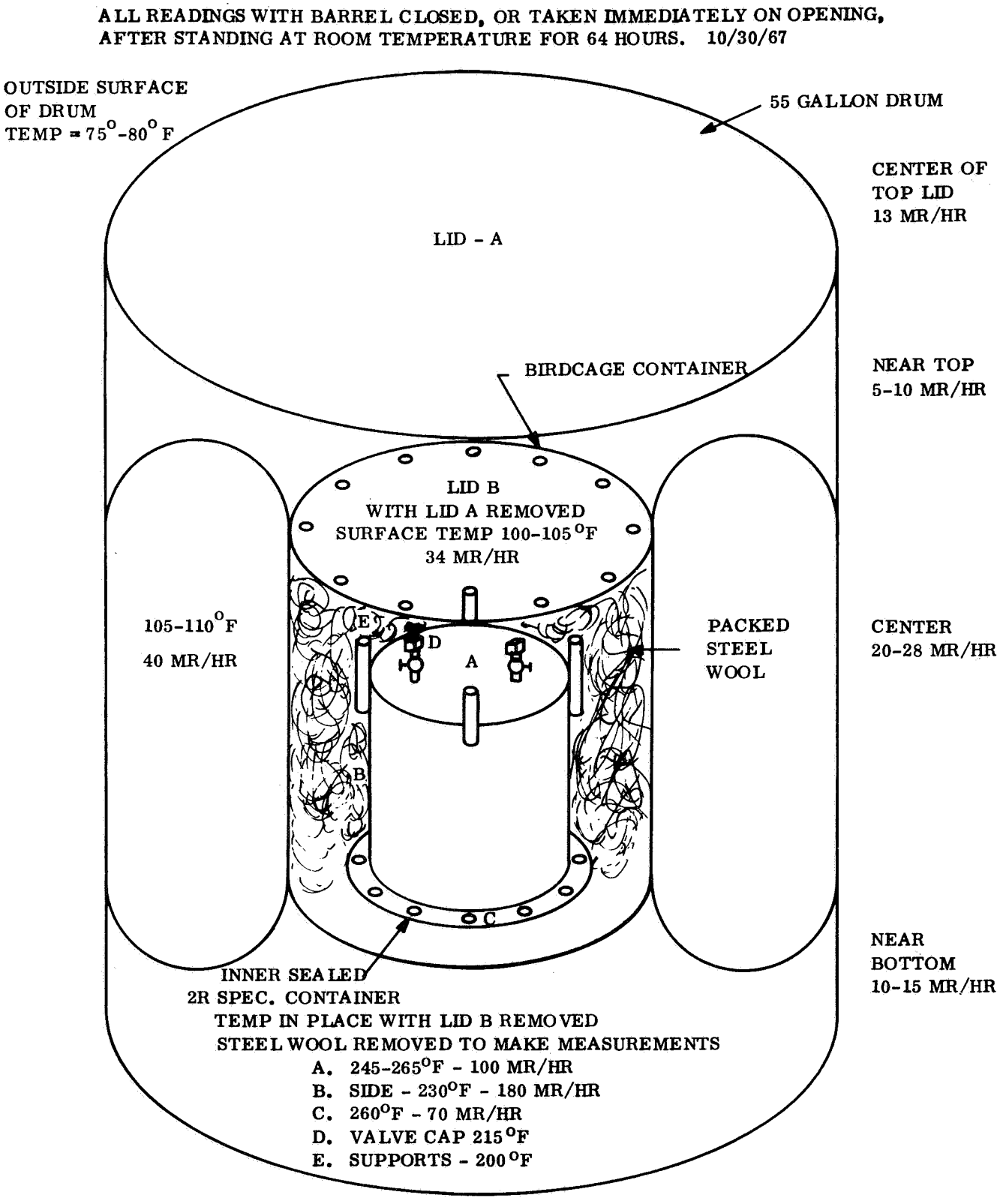

Figure XVI. Temperature and Radiation Measurements of AMSA Capsule Shipping Drum

2R INNER CONTAINER (SEALED) REMOVED FROM SHIPPING DRUM AFTER 64 HOURS. STAND 30 MIN. IN AIR - ROOM TEMP - SETTING ON TABLE TOP (NON-METALLIC) 10/30/67

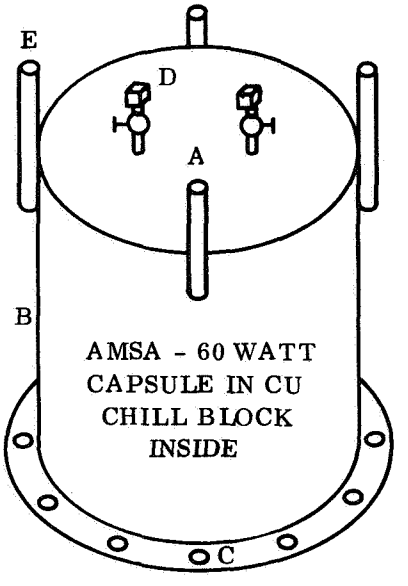

A - SURFACE - 230°F 100 MR/HR
B - SURFACE - 200°F 180 MR/HR
C - SURFACE - 225°F 70 MR/HR
D - VALVE CAPS - 140°F
E - SUPPORTS - 135°F

AFTER 2R SPEC. CONTAINER OPENED, IMMEDIATELY AFTER ABOVE MEASUREMENTS WERE MADE.

NOTES:

1. TEMP TOP OF COPPER BLOCK 245°F
   SIDE OF COPPER BLOCK 245°F.

2. RADIATION FIELD TO HANDS IN SCREWING EYE BOLT INTO TOP OF COPPER BLOCK = 220 MR/HR.

3. TEMP OF AMSA CAPSULE IMMEDIATELY AFTER REMOVING COPPER CHILL BLOCK - 330°F.

4. TEMP OF AMSA CAPSULE AFTER SETTING ON CERAMIC SURFACE FOR TWO HOURS IN STILL ROOM TEMPERATURE AIR 480°F - A RING GAGE 2.005 IN. DIA. PASSED OVED CAPSULE AT THIS POINT WITH MIN. INTERFERENCE - LENGTH = 1.999 IN. - WT. = 745.2 GRAMS.

5. RADIATION = 1100 MR/HR WITH CP BETA SHIELD IN ACTUAL CONTACT WITH CAPSULE (UNCORRECTED FOR GEOMETRY OF CP CHAMBER)

Figure XVII. Temperature and Radiation Measurements of AMSA Capsule 2R Container

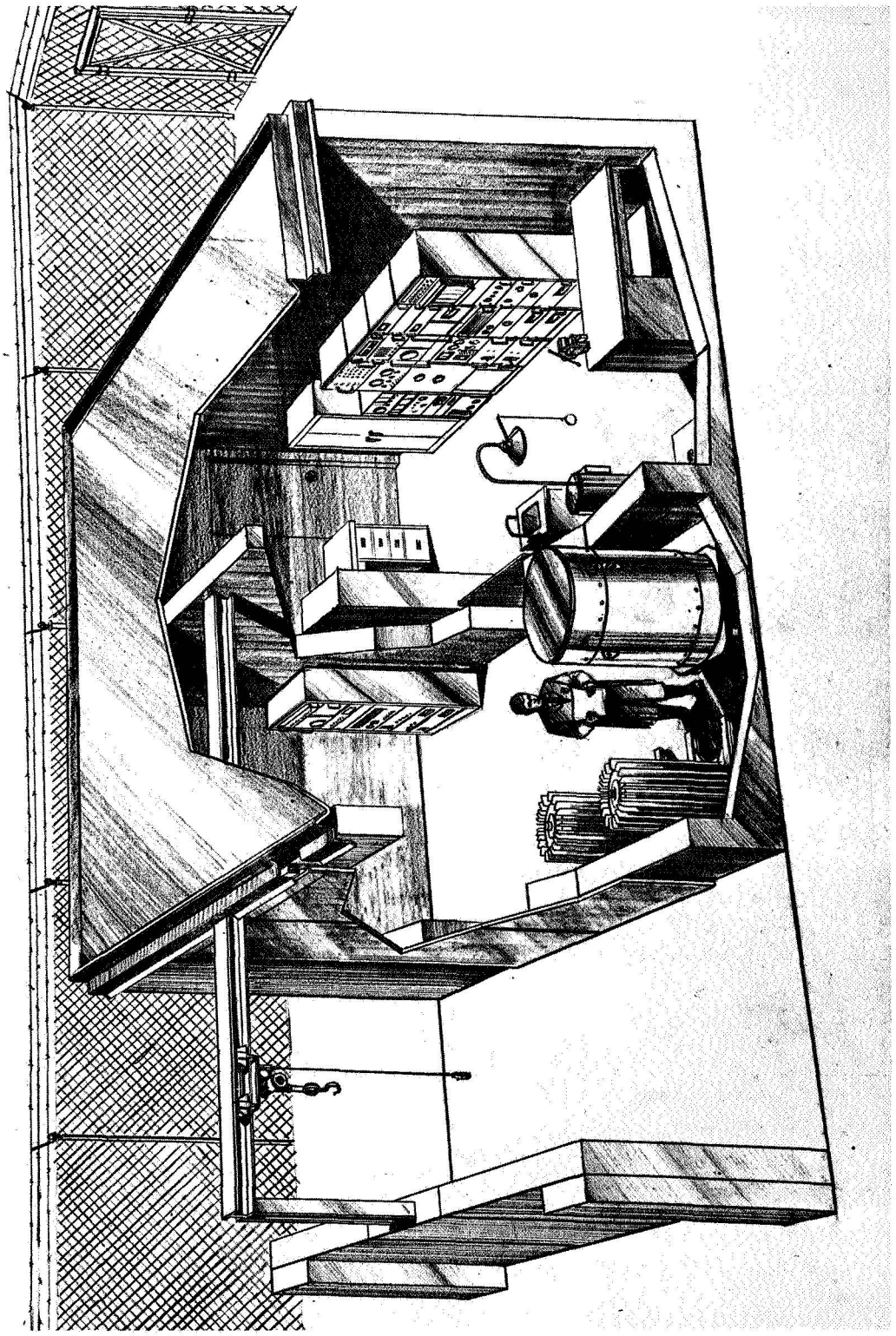

Figure XVIII. RTG Storage Building

VI. RADIOLOGICAL SAFETY PROGRAM

A. Radiation Dose Rates

The dose rates of the AMSA $^{147}Pm_2O_3$ capsule were measured at twelve and eighteen inches from the surface contour on October 9, 1967 and are shown on Figure XIX. Radiation measurements at different locations on the shipping drum and on the 2R inner container are shown in Figures XVI and XVII respectively. These values should be reduced by a factor of about 0.8 to account for the Pm-147 decay from October 1967 to July 1968 when the capsule will be tested at GE/VFSTC. The radiation level should not exceed 6 mr/hr at 1 meter from the center of the capsule when it is used at GE/VFSTC.

B. Radiological Controls and Procedures

The radiological protection plan for the radioisotope heating of vacuum tube cathode program shall be in accordance with the two policies that govern;

General Electric Company, Missile and Space Division
Policy on Safety No. 10.101
U. S. Atomic Energy Commission Code of Federal
Regulations, 10CFR-20.

The MSD Health Physicist shall be designated the Radiation Protection Officer. His responsibilities are as follows:

1. He shall conduct his operations in accordance with the applicable Division policies and provisions of the AEC code of Federal Regulations 10CFR-20.

2. He shall conduct such surveys as may be necessary for him to ascertain that the policies of this program are being followed.

3. He shall inform the program manager of the exposure status of each man who is occupationally exposed. This shall be done at a frequency that is sufficient to allow the program manager to establish timely preventive controls.

4. He shall maintain all records relating to environmental and personnel exposure to radiation, contamination levels and airborne concentrations of radioactive material.

5. He shall inform management of any actual or potential condition which he believes may result in needless or excessive exposure to radiation.

6. He shall be responsible for the maintenance and calibration of all radiation detection and measurement equipment and the interpretation or evaluation of data derived therefrom.

7. He shall issue and collect personnel dosimeters used by program personnel and visitors.

8. All liaison and correspondence with regulatory agencies concerning radiological protection shall be coordinated by the Health Physicist.

9. He shall coordinate with Industrial Security in establishing security emergency plans.

10. He shall supervise all movements of the fuel capsule.

11. He shall instruct all persons who are occupationally exposed to radiation in the safety problems associated with exposure to radiation and radioactive materials.

12. He shall review and approve all detailed test procedures relating to the fuel capsule.

The nuclear safety engineer shall directly supervise operations involving the radioisotope fuel capsule. His responsibilities are as follows:

1. He shall be present during operations which involve removal and insertion of the fuel capsule from the shipping container and testing of the fuel capsule in the test fixture.

2. He shall review and evaluate nuclear safety aspects of the test program and shall recommend any changes required to insure safe operations.

3. He shall integrate test plans with the Health Physicist safety procedures, such that the engineering test data obtained during test operations, as well as the radiological protection of test personnel and of the test area, are not compromised.

4. He shall prepare the material required for application for byproduct material license from the AEC and for approval of IRAG (GE Ionizing Radiation Advisory Group).

5. He shall prepare fuel capsule operating and handling procedures.

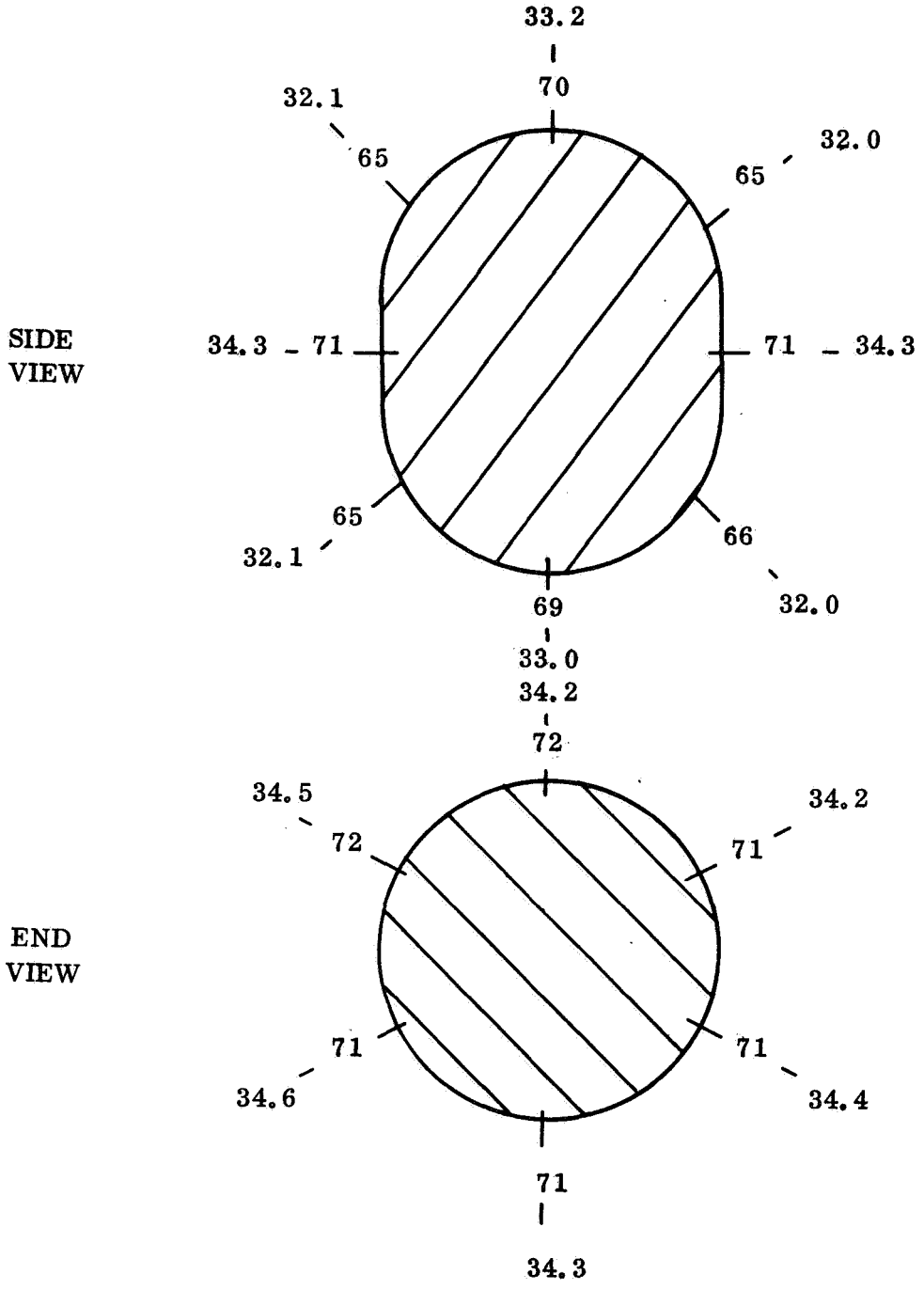

INNER NUMBERS ARE 12 IN. FROM CENTER OF CAPSULE, IN MR/HR
OUTER NUMBERS ARE 18 IN. FROM CENTER OF CAPSULE.

Figure XIX. Radiation Map of AMSA $^{147}Pm_zO_3$ Heat Source Capsule (Date of Measurement: October 9, 1967)

6. He shall prepare with the Health Physicist, detailed procedures to be followed in the event of a radiological emergency.

The operations with the promethium-147 fuel capsule at GE/Valley Forge Space Technology Center will all be conducted in the RTG Storage Building (Building 800). These operations involve receipt, storage, testing and shipment. The radiological safety procedures for each operation is covered in the following sections. Film badges will be required for all personnel who enter Building 800.

The $^{147}Pm_2O_3$ AMSA capsule design, impact test results, and fabrication quality assurance program have demonstrated that isotope containment within the capsule can be assumed. However, whenever a radioisotope source is unpackaged or handled, regardless of the known integrity of the capsule, it is common practice to perform smear and airborne activity tests to guard against the remote possibility that leakage from the capsule has occurred.

1. Receipt

The Health Physicist and Nuclear Safety Engineer shall be present at the time of receipt. The Health Physicist shall obtain wipe samples from the surface of the shipping container and shall count the samples for beta activity (PC-3T proportional counter or equivalent).

2. Storage

The promethium-147 fuel capsule shall be stored for approximately a one-month period (Mid July to mid August 1968) in its shipping container and in the RTG Storage Building (Building 800). This storage building is a secure area since all doors are locked and alarmed and the gate is locked. Access to the building is controlled by security. During storage in Building 800, the following conditions shall apply:

a. The shipping container the promethium-147 fuel capsule shall be posted with a durable, clearly visible label bearing the radiation caution symbol and the words CAUTION RADIOACTIVE MATERIAL, PROMETHIUM-147, 168, 100 CURIES ON OCTOBER 1, 1967.

b. The Health Physicist shall perform a periodic check (three to five times a week) on the stored shipping container. This shall include wipe samples from the surface of the shipping container which will be assayed for beta activity. (PC-3T proportional counter or equivalent).

c. The Health Physicist shall designate, that floor enveloped, inside of which personnel shall monitor and record time of operation. Time within this radiation area shall be identified with a person's full name, pay and social security numbers in the log book.

3. Testing

The actual test of utilizing the promethium-147 fuel capsule to heat the cathode of the vacuum tube triode shall be conducted in Building 800. It is presently planned that the demonstration test shall be completed within an eight hour period. During the time that the promethium-147 fuel capsule is outside its shipping container, the Health Physicist and Nuclear Safety Engineer shall be in attendance. The radiological procedures for the testing shall be as follows:

a. While the promethium-147 fuel capsule is being removed from the shipping container and is being installed in the test fixture, access to the test area shall be limited to only the Health Physicist and test personnel directly involved with the test.

b. The test personnel shall be supplied film badges, dosimeters and wrist film badges as required by the Health Physicist.

c. Before describing fuel capsule removal operations, details of the shipping container are in order. (See Figures XVI and XVII) The shipping container is constructed of two concentric cylinders, both airtight. The outer cylinder is the gamma shielding member plus a secondary physical barrier to possible escaped radioisotope. The inner cylinder (of stainless steel) is the primary radioisotope capsule's physical barrier and is constructed to facilitate removal of the promethium-147 capsule in a safe manner.

d. Perform a radioactive wipe survey of the outside of the drum containing the AMSA capsule.

e. Remove the cover of the drum and take a smear sample from the drum interior. Obtain dose rate readings at various distances.

f. Remove the cover of the bird cage container inside the drum, using the 3/8" T-handle Allen wrench, and take smear samples from the contents.

g. Prior to removal of valve caps on 2R container, ascertain that valves are closed. Remove the valve caps using Channelok adjustable pliers. Obtain wipe samples from internal surface of valve caps.

h. Attach air monitor to one valve and an absolute filter to the other. Open both valves and obtain a five minute air sample and analyze for beta activity. If the wipe checks and air activity are within background levels, the 2R container shall be lifted from the birdcage and moved to the test fixture assembly area.

i. Prior to handling the promethium-147 fuel capsule, all test personnel shall be specially trained and drilled in performing the test operations. Dry runs utilizing the electrical simulator shall be conducted prior to promethium-147 fuel capsule testing. This shall insure that test personnel shall handle the fuel capsule in a safe manner and shall minimize radiation exposure to these personnel.

j. Remove the cover of the 2R container and take wipe tests of its contents.

k. Attach handle and pusher rod to the inner holding fixture and remove same from the 2R container.

l. Remove spring tension from capsule by withdrawing pusher rod and rotating it 90 degrees.

m. Screw eye bolt into top half of inner holding fixture.

n. Remove the two screws holding top half of inner fixture in place, using 3/16" Allen wrench.

o. Remove top half of inner fixture, using conventional tongs, exposing capsule to view.

p. Take wipe samples of capsule surface.

q. Remove the fuel capsule from the inner shipping container and insert it into the copper heat block using the handling tongs shown in Figure XX.

r. The test fixture assembly shall be completed in such a manner that radiation exposure shall be minimized. Dry runs using the electrical simulator shall be used to estimate expected personnel radiation exposure and shall be evaluated to determine whether test operations may be modified to minimize radiation exposure.

s. The promethium-147 fuel capsule shall be sealed in the test fixture and operated under a vacuum. The vacuum system exhaust shall be discharged through an absolute filter. The fuel capsule temperature shall be carefully monitored during the test and shall not be allowed to exceed 1800°F which is well above expected test conditions of 1400°F maximum.

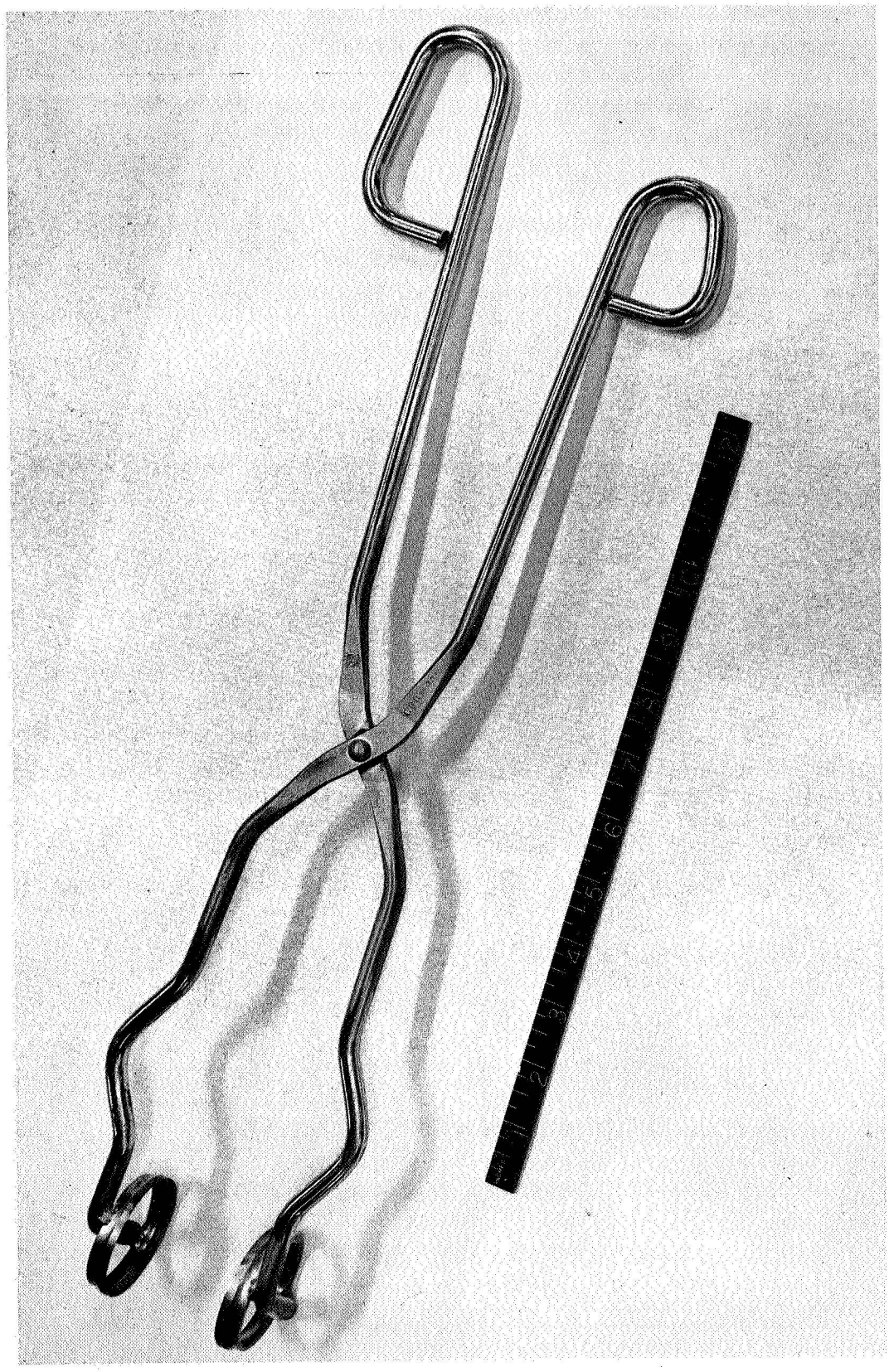

Figure XX. Special Tongs for Grasping AMSA Capsule

t. After the fuel capsule is sealed in the test fixture and the system is under a vacuum, visitors shall be permitted to witness the test behind a roped off area.

u. During the test, the Health Physicist shall monitor the airborne beta activity levels and obtain wipe samplesoof the test fixture.

v. At the completion of the test, the test fixture shall be sampled for airborne beta contamination prior to opening the system. The test fixture housing shall have two sampling valves. One valve shall be connected to the air sampling equipment while the other valve shall be connected to an absolute filter.

w. If the test fixture sample does not indicate the presence of contamination, the disassembly operation can proceed. At this point, only the Health Physicist, Nuclear Safety Engineer and test personnel shall have access to the test area.

x. The test fixture shall be cooled down by purging an inert gas through the system and discharging the gas through an absolute filter. After the fuel capsule is cooled down to a temperature that will permit safe handling, the gas purge shall be secured and the absolute filter checked for beta contamination.

y. The test fixture shall be disassembled and the fuel capsule inserted and sealed in the shipping container. The internal surfaces of the test fixture shall be wiped for beta contamination analysis.

z. The sealed shipping container surface shall be surveyed by wipe samples for beta contamination. The Health Physicist shall measure and record the gamma exposure rates at the surface and 1 meter from the center of the shipping container. The radiation levels shall not exceed 10 CFR-71 AEC regulations (Reference 10) of

surface 200 mr/hr

1 meter from center 10 mr/hr

aa. On the basis of the results of all radiation measurements, the Health Physicist shall inform the test conductor that the shipping container is released for shipment.

C. Emergency Plan

An emergency is defined as a release of potentially hazardous amounts of promethium-147 from the fuel capsule.

The emergency will be divided into two parts, Phase I and Phase II. Phase I will consist of the emergency, the response of the personnel in the immediate area, notification of the guard, notification of the Phase I emergency team, their evaluation of the extent of the emergency and notification of the Phase II emergency team. Phase II will consist of all further actions taken to control the emergency and minimize its effects.

1. Phase I

a. Personnel in Immediate Area

1) Evacuate

The primary response to any emergency is for an individual to hold his breath and evacuate the area as rapidly as possible. Proceed far enough away to be out of any plume (i.e., at least 50 yards upwind).

2) Contain

All doors in Building 800 will be closed. The ventilation system containing an absolute filter will be in operation and will provide a slightly reduced pressure in the building to minimize the outflow of contamination. No attempt at time consuming jobs should be taken at this time.

3) Notify

Dial AFIRE and notify guard

a) who is calling

b) nature of emergency

c) location of emergency

4) Contamination Control

Avoid the spread of contamination by remaining in one area until a Health Physicis check can be made. Those who have to move should check for personnel contamination on a hand and foot monitor.

5) Phase II Instructions

Personnel in the area should take no further action until instructed by Phase II Emergency Team.

b. Patrolman

1) Notify

Upon receipt of emergency, either by phone or by alarm from Building 800, the guard will call all personnel on the Phase I Emergency Team. He will inform them of all information.

2) Further Responsibilities

The guard may be instructed by Phase I personnel to:

a) Go to Building 800 to assure all doors are closed.

b) Keep all unauthorized personnel from hazard area.

c) Assist personnel in area.

3) Phase II Instructions

Upon notification by the Phase I emergency team, the guard will call all personnel listed for the Phase II emergency team. He will inform them as instructed by the Phase I team.

The patrol should then be available for further duties as instructed by the Phase II emergency team.

c. Phase I Emergency Team

1) Immediate Response

Upon notification, instruct the guard what additional precautions are necessary. Proceed to VFSTC as quickly as possible.

2) Evaluate the extent of the emergency.

The following steps should be taken to evaluate the extent of the emergency.

a) Survey all personnel who were in the immediate area. Question them as to the events of the emergency and subsequent actions. Instruct them in personnel decontamination procedures if necessary.

b) Survey the area outside of the containment and set up contamination zones, if necessary.

c) Enter hazard area using proper contamination procedures (protective clothing, supplied air, buddy system, etc.). Survey the area and make visual observations.

d) Recommend subsequent actions that may be needed immediately (i.e., possible double containment area evacuation, etc.)

e) Notify guard to call in Phase II personnel.

3) Phase II Instructions

Await the arrival of Phase II emergency team before attempting large scale actions. Advise Phase II personnel upon their arrival of the situation and survey results.

d. Phase II Emergency Team

1) Responsibilities

The Phase II Emergency Team will have the following general responsibilities:

a) Care of exposed personnel. This will include personnel decontamination, medical attention, and urinalysis.

b) Minimize hazard. Actions may have to be taken to provide better containment of the contamination.

c) Decontamination. Actions will have to be taken to decontaminate all contaminated equipment and areas.

d) Evaluate the extent of the emergency. This will include soil and water samples, vegetation samples, and air samples both off site and on site. It might also entail extensive personnel monitoring.

e) Notification and public relations. This will include notifying GE management, State Department of Health, and AEC. It will also include press releases and briefing of all affected personnel.

f) Disposal of Source. This will include coordination with AEC, containing the source for shipment and actual shipment.

D. Training

The test personnel shall obtain on-the-job training to insure safe handling of the promethium-147 fuel capsule and to minimize radiation exposure. Dry runs shall be conducted with the electrical simulator to train the test personnel on safe handling procedures. During these dry runs, the Health Physicist shall instruct the personnel concerning the reasons for the precautions that must be adhered to and the response to an emergency situation. The dry runs shall be used to evaluate the test procedures to ascertain that all operations are performed in such a manner to minimize personnel radiation exposure.

VII. REFERENCES

1. BNWL-CC-1430, Handling Procedures for the AMSA $^{147}Pm_2O_3$ Heat Source Capsule, November 22, 1967.

2. BNWL-327, Promethium Heat Source Compatibility Studies, Part I: Studies at 1100°C, November 1966.

3. SC-DR-67-718, AMSA Fuel Capsule Impact Tests, August, 1967.

4. L. A. Bray and H. H. Van Tuyl, Laboratory Development of a Carrier-Precipitation Process for the Recovery of Strontium from Purex Wastes, HW-69534, General Electric Company,

5. W. V. DeMier, G. L. Richardson, A. M. Platt, and W. H. Swift, Development of Radioactive Waste Fractionization and Packaging Technology, HW-SA-2786, General Electric Company, Richland, January 1963.

6. L. R. Bunney and E. M. Scadden, Decay Characteristics of Pm-146, USNRDL-TR-1109, November 1966.

7. E. J. Wheelwright, et. al., Ion-Exchange Separation of Kilocurie Quantities of High Purity Promethium, BNWL-318, Battelle Memorial Inst., Richland, Washington, December 1966.

8. F. Weigel and V. Scherer, Radiochemica Acta, 4 197-203 (A65).

9. H. H. Van Tuyl, Promethium Isotopic Power Data Sheets, BNWC-45, Battelle Memorial Inst. Richland, Washington, March 15, 1965.

10. AEC Regulation 10 CFR-71, Packaging of Radioactive Materials for Transport.

APPENDIX

QUALITY ASSURANCE PROCEDURES

Quality Assurance Procedure A

Pm_2O_3 AMSA Capsule

Procedure

Radiochemical Purity Analysis

Step Nos. on Figure V

1-7

Location of Step in Process Flow

After Promethium-147 purification

Type of Test

Radiochemical

Reason for Test or Inspection

To verify Promethium-147 is within specification limits

Design Specifications or Limits

Less than 0.25 ppm ^{146}Pm; curie ratio of 148 Pm/146 Pm less than 0.1; ^{154}Eu, ^{144}Ce none detectable.*

* This limit for ^{154}Eu and ^{144}Ce was erroneously placed in process design specifications. Limit should have been a curie ratio of 10^{-7} curie/curie of ^{147}Pm for both ^{154}Eu and ^{144}Ce, corresponding to the maximum quantities permissable without causing shielding requirements more restrictive than that caused by the ^{146}Pm present.

Quality Assurance Procedure B

Pm_2O_3 AMSA Capsule

Procedure

Spectrographic Analysis

Step Nos. on Figure V

2-7

Location of Step in Process Flow

Oxide conversion and heat treatment

Type of Test

Emission spectrography

Reason for Test or Inspection

To verify oxide is within specification limits

Design Specifications or Limits

Less than 1% other than Sm.

Quality Assurance Procedure C

Pm_2O_3 AMSA Capsule

Procedure

Analysis of $^{147}Pm_2O_3$

Step Nos. on Figure V

5-8

Location of Step in Process Flow

After oxide conversion and calcination

Type of Test

X-ray diffraction analysis

Reason for Test or Inspection

To confirm $^{147}Pm_2O_3$ used is in the monoclinic crystallographic form

Design Specifications or Limits

Monoclinic form

Quality Assurance Procedure D

Pm_2O_3 AMSA Capsule

Procedure

$^{147}Pm_2O_3$ pellet inspection

Step Nos. on Figure V

8-1
8-4

Location of Step in Process Flow

After cold pressing

Type of Test

Dimension check

Reason for Test or Inspection

To determine that pellets are proper size to obtain length to diameter ratio needed after sintering

Design Specifications or Limits

As pressed - 75-80% of theoretical density

Quality Assurance Procedure E

Pm_2O_3 AMSA Capsule

Procedure

$^{147}Pm_2O_3$ pellet inspection

Step Nos. on Figure V

9-1
9-4

Location of Step in Process Flow

After sintering

Type of Test

Density calculation

Reason for Test or Inspection

After sintering to verify final density to assemble in cladding and meet wattage requirements

Design Specifications or Limits

As sintered OD 1.450 max.; length 1.450" max.
dome radii 0.36" R.

Quality Assurance Procedure F

Pm_2O_3 AMSA Capsule

Procedure

Tantalum Inner Cladding Evaluation

Step Nos. on Figure V

21-3

Location of Step in Process Flow

Raw material

Type of Test

Impurity analysis

Reason for Test or Inspection

To verify purity of inner cladding

Design Specifications or Limits

99.9% minimum purity

Quality Assurance Procedure G

Pm_2O_3 AMSA Capsule

Procedure

Tantalum Inner Cladding Evaluation

Step Nos. on Figure V

22-1
21-2

Location of Step in Process Flow

After capsule fabrication

Type of Test

Dimensional checks and dye penetrant test

Reason for Test or Inspection

To verify dimensions and capsule integrity

Design Specifications or Limits

All irregularities will be reported, dimensions in accordance with drawing H-3-27668. Bleed back from penetrant will require further investigation.

Quality Assurance Procedure H

Pm_2O_3 AMSA Capsule

Procedure

Tantalum Inner Cladding Evaluation

Step Nos. on Figure V

11-11

Location of Step in Process Flow

After pellet loading.

Type of Test

Decontamination smear test.

Reason for Test or Inspection

To verify that outer surface of cladding is free of smearable $^{147}Pm_2O_3$, prevent weld contamination.

Design Specifications or Limits

Non-smearable.

Quality Assurance Procedure I

Pm_2O_3 AMSA Capsule

Procedure

Tantalum Inner Cladding Test Weld No. 1

Step Nos. on Figure V

13-5
13-10
13-6

Location of Step in Process Flow

After test weld.

Type of Test

Helium leak test, ultrasonic weld evaluation and metallography.

Reason for Test or Inspection

To verify welding parameter and weld penetration, capsule integrity.

Design Specifications or Limits

Leak rate less than 10^{-6} std atm cc/sec; 50% minimum weld penetration as determined by ultrasonic test and confirmed by metallography.

Quality Assurance Procedure J

Pm_2O_3 AMSA Capsule

Procedure

Tantalum Inner Cladding Evaluation

Step Nos. on Figure V

14-11
14-12
14-1
14-5
14-10

Location of Step in Process Flow

After inner capsule welding.

Type of Test

Decontamination, dimensions, helium leak test, ultrasonic test and radiation mapping.

Reason for Test or Inspection

$^{147}Pm_2O_3$ free; to make outer capsule assembly; insure weld closure; determine weld penetration; determine radiation field.

Design Specifications or Limits

Non-smearable; to meet drawing H-3-27668; leak rate less than 10^{-6} std atm cc/sec; 50% minimum weld penetration; less than 30 mr/hr at one meter.

Quality Assurance Procedure K

Pm_2O_3 AMSA Capsule

Procedure

Tantalum Inner Cladding Test Weld No. 2

Step Nos. on Figure V

15-5
15-10
15-6

Location of Step in Process Flow

After test weld.

Type of Test

Helium leak test, ultrasonic weld evaluation and metallography.

Reason for Test or Inspection

To verify welding parameter and weld penetration, capsule integrity.

Design Specifications or Limits

Leak Rate less than 10^{-6} std atm cc/sec; 50% minimum weld penetration as determined by ultrasonic test and confirmed by metallography.

Quality Assurance Procedure L

Pm_2O_3 AMSA Capsule

Procedure

L-605 Alloy Outer Cladding Evaluation

Step Nos. on Figure V

25-3

Location of Step in Process Flow

Raw material.

Type of Test

Chemical impurity analysis.

Reason for Test or Inspection

To confirm chemical content of alloy.

Design Specifications or Limits

To be from same heat as stock used for corrosion and physical test.

Quality Assurance Procedure M

Pm_2O_3 AMSA Capsule

Procedure

L-605 Alloy Outer Cladding Evaluation

Step Nos. on Figure V

26-1
25-2

Location of Step in Process Flow

After outer cladding fabrication.

Type of Test

Dimension check and dye penetrant.

Reason for Test or Inspection

To verify dimensions and capsule integrity.

Design Specifications or Limits

Dimensions in accordance with drawing H-3-27669; any bleed back indications will require additional investigation or rejection.

Quality Assurance Procedure N

Pm_2O_3 AMSA Capsule

Procedure

L-605 Alloy Outer Cladding Evaluation Test Weld No. 1

Step Nos. on Figure V

17-5
17-10
17-6

Location of Step in Process Flow

After test weld.

Type of Test

Helium leak test, ultrasonic weld evaluation and metallography.

Reason for Test or Inspection

To verify welding conditions.

Design Specifications or Limits

Leak rate less than 10^{-6} std atm cc/sec; 85% minimum weld penetration, weld voids 0.015" maximum magnitude limited to one per quadrant, confirmed by metallography.

Quality Assurance Procedure O

Pm_2O_3 AMSA Capsule

Procedure

L-605 Alloy Outer Cladding Evaluation

Step Nos. on Figure V

18-11

Location of Step in Process Flow

After assembly and final welding.

Type of Test

Decontamination smear test.

Reason for Test or Inspection

To verify outer capsule as welded, free of smearable $^{147}Pm_2O_3$.

Design Specifications or Limits

Non-smearable.

Quality Assurance Procedure P

Pm_2O_3 AMSA Capsule

Procedure

L-605 Alloy Outer Cladding Evaluation Test Weld No. 2

Step Nos. on Figure V

19-5
19-10
19-6

Location of Step In Process Flow

After test weld.

Type of Test

Helium leak test, ultrasonic weld evaluation, metallography.

Reason for Test or Inspection

To verify welding conditions.

Design Specifications or Limits

Leak rate less than 10^{-6} std atm cc/sec; 85% minimum weld penetration, weld voids 0.015" maximum magnitude limited to one per quadrant, confirmed by metallography.

Quality Assurance Procedure Q

Pm_2O_3 AMSA Capsule

Procedure

Final Inspection

Step Nos. on Figure V

20-11
20-5
20-1
20-10
20-12
20-13
20-14

Location of Step in Process Flow

After final finishing.

Type of Test

Decontamination, helium leak test, dimensions, ultrasonic weld test, radiation mapping, gamma spectrometry, calorimetry.

Reason for Test or Inspection

$^{147}Pm_2O_3$ free, confirm weld integrity, to fit preconditioner; radiation integrity; radiation spectrum; to establish actual heat output.

Design Specifications or Limits

Non-smearable; leak rate less than 10^{-6} std atm cc/sec.; 85% minimum weld penetration, detect weld voids, one per quadrant of 0.015" diameter permitted; less than 30 mr/hr at one meter; 65 watts on July 1, 1967.

Quality Assurance Procedure R

Pm_2O_3 AMSA Capsule

Type of Test

Final Dimensional Inspection 20-5

Identification of Part Tested

Final outer assembly capsule no. 44, welded, with excess weld bead removed.

Time and Place of Test

10/9/67, 325 Building, 300 Area

Equipment Identification

Dial type calipers.

Brief Description of Test Method

Not applicable.

Calibration Standards Used

Calipers checked before and after use with known standards. Tolerances are $\pm$ 0.001" unless otherwise noted.

Test Results

$\frac{2.004"}{2.005"}$ Diameter X $\frac{1.999"}{2.000"}$ Length

This dimensional test was made after capsule was placed on ceramic brick for a period of 2 hours and temperature was recorded at 480°F. Ring gage, (GO gage) 2.005" I.D., furnished by AC Electronics per sketch SK-51222 passed over the capsule when fitted cold to the "hot" capsule.

Checked by N. C. Davis - D. W. Brite

0.645 inch radius at each end.

APPENDIX F

CROWBAR CIRCUIT

Travelling wave tubes in general require extremely fast acting circuitry for the protection of the delicate helix structure. These circuits must usually provide voltage decay within 100 microseconds or less after removal of helix or collector voltages. Also necessary is an overload circuit which removes all voltages within 100 microseconds when the helix current exceeds its maximum value. Faults or arcs occurring from the cathode and proceeding to the modulating anode and helix in succession must be extinguished almost instantaneously to avoid permanent damage to the tube. The electronic "crowbar" is ideally suited for this application. It consists of a suitable discharge or dump tube (or SCR) which acts as a virtual short across the load when triggered and diverts the current from the load while the operating voltages are removed.

A schematic diagram of the crowbar employed for protecting the TWT is shown in Figure F-1. The crowbar was tested by applying high voltage (6 to 8 kilovolts) and then dropping a small piece of solder across the high voltage terminals. The results were that no visible damage to the solder could be detected, indicating practically instantaneous firing of the hydrogen thyratron crowbar tube and adequate TWT protection.

A description of the tube characteristics is given in Table F-1 and Figure F-2.

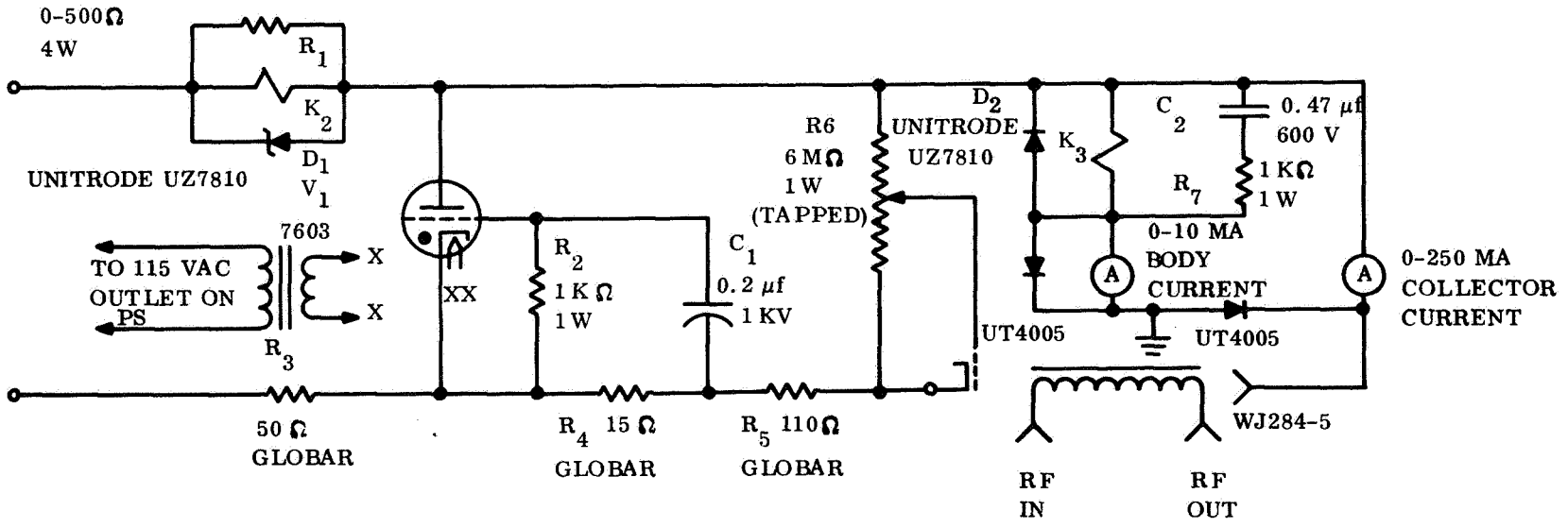

K_2 G.E. CR120G10A01

K_3 KORMAN 5DICA40D

Figure F-1. Crowbar Circuit with TWT Installed

Table F-1. Tentative Specification WJ-284-5
6.0 to 8.0 GHz, 200 Watt PPM-Focused Travelling-Wave Tube

Performance[1]	Typical	Guaranteed
Frequency	5.0 - 9.0 GHz	6.0 to 8.0 GHz
Power Output, Saturated	210 w	200 w, min
Gain, Large Signal	32 db	30 db, min
Efficiency	25%	23%
Electrical Requirements	**Typical**	**Range**
Heater Voltage	7.0 v	7.0 to 8.0 v
Heater Current	1.5 amp	1.4 to 1.6 amp
Cathode Voltage[2]	-6750 v	-6700 to -6800 v
Cathode Current	200 ma	190 to 210 ma
Anode Voltage	+150 v	0 to 200 v
Anode Current	0.2 ma	0.1 to 0.8 ma
Helix Voltage[2]	Ground potential	Ground potential
Helix Current	4.0 ma	3.0 to 10.0 ma
Collector Voltage[2]	-2550 v	-2500 to -2700 v
Collector Current	196 ma	185 to 205 ma
Environmental Characteristics		
Heat Sink Temperature		$-45^{\circ}C$ to $+75^{\circ}C$
Vibration		5 to 2000 c/s 10 g, rms
Shock		100 g, 11 ms
Altitude		0 to 70,000 feet
Acceleration		50 g at 20 sec
Mechanical Characteristics		
Tube Length		12.5 inches, max
Tube Cross-Section (excluding connectors)		2.75 x 3.0 inches, max
RF Connector		TNC (female)
DC Connectors		Flying leads
Weight		10 lbs, max
Cooling		Conduction from bottom surface

1 Efficiency is defined as the minimum RF output power across the band, divided by the total dc power input, including heater power.

2 The helix is connected to the tube capsule which is at ground potential. All voltages except heater voltage are measured with respect to ground. Cathode and one heater terminal are common.

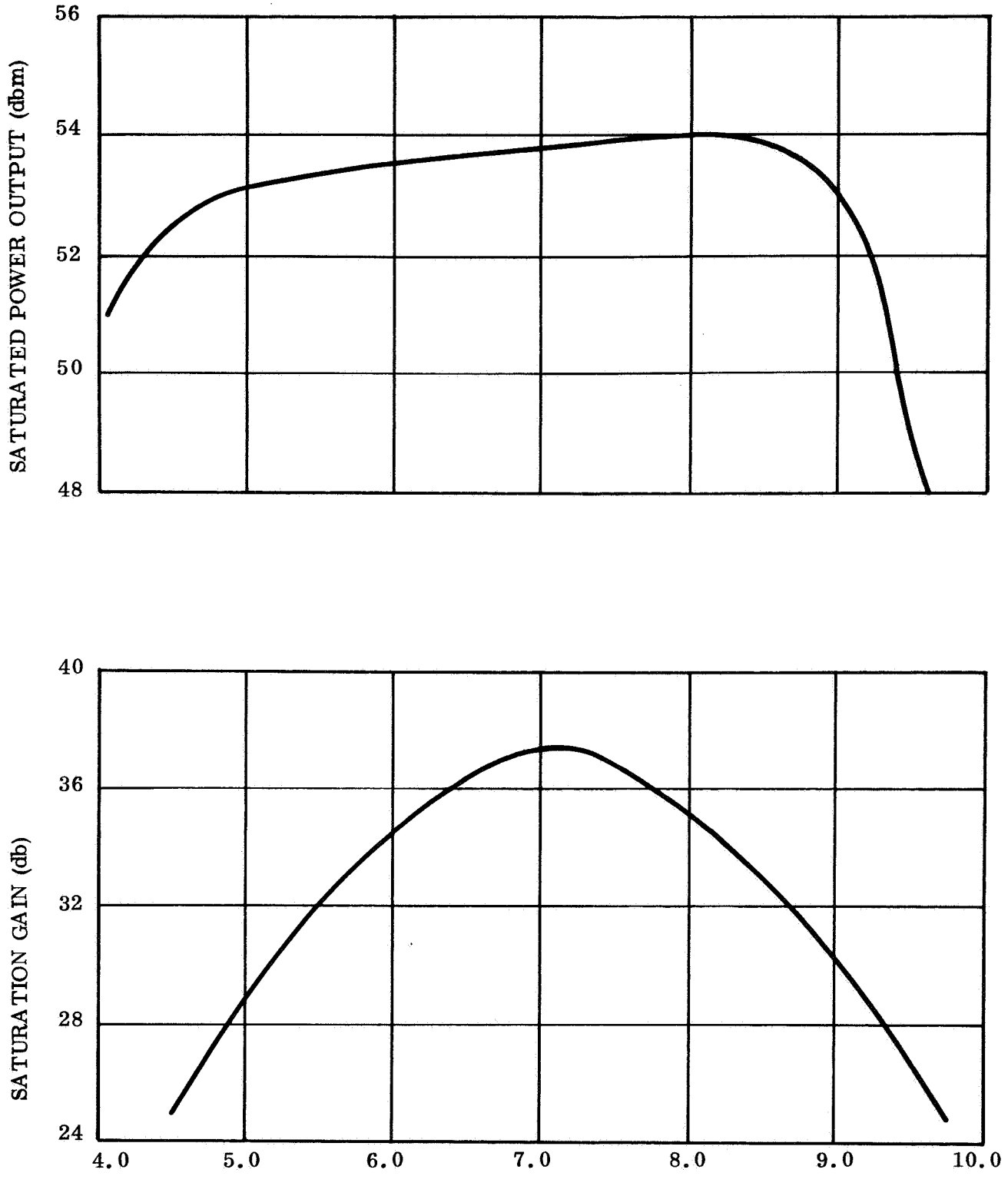

Figure F-2. Saturated Power Output and Saturated Gain Versus Frequency for the WJ-284-5

Report Distribution List For

Contract No. NAS 12-565

NASA Electronics Research Center
575 Technology Square
Cambridge, MA 02139

AMT/Technical Information Branch
(20 + 1 reproducible)
T/Technology Utilization (3)
AT/Technical Programs Office (1)
DL/Patent Counsel (1)
RRD/W. Rindner (1)
ROI/C. Veronda (1)
Technical Monitor (5)

NASA Scientific and Technical Information Facility (3)
P.O. Box 33
College Park, MD 20740

National Aeronautics and Space Administration
Washington, DC 20546

SAC/A. Andrus (1)
RET/H. Anderton (1)
MLO/S. Fordyce (1)
SAL/J. Lehmann (1)
RV-1/C. Mook (1)
RET/O. Stanton (1)

NASA/Goddard Space Flight Center
Greenbelt, MD 20771

562/A. Block (1)
712/D. Hepler (1)
523/W. Hughes (1)
731/L. Kleinberg (1)

NASA/Langley Research Center
Hampton, VA 23365

W. Cuddihy, M.S. 473 (1)
S. Katzoff, M.S. 116 (1)
B. Kendall, M.A. 473 (1)

NASA/Lewis Research Center
Cleveland, OH 44135

R. Alexovich, M.S. 54-3 (1)
H. Kosmahl, M.S. 54-3 (1)
P. Kuhns, M.S. 54-3 (1)
P. Ramins, M.S. 54-3 (1)

NASA/Manned Spacecraft Center
Houston, TX 77058

EE3/J. Fowler (1)
EE/G. Gibson (1)
EE3/M. Hamilton (1)
EE/R. Kosinski (1)
EB3/J. McCaulley (1)
EE/R. Sawyer (1)

NASA/Marshall Space Flight Center
Huntsville, AL 35812

A. Byrd, R-SSL-NR (1)
C. Fritz, R-P&VE-PEC (1)
E. Hamilton, R-ASTR-A (1)
W. Kaspareck, R-ASTR-M (1)
R. Mixson, R-ASTRA-I (1)
G. Saunder, R-ASTRA-IR (1)

Martin Moon (3)
Division of Public Information
Atomic Energy Commission
Washington, DC 20545

R. Shivers (5)
Division of Isotopes Development
Atomic Energy Commission
Washington, DC 20545

C. Vogel (1)
Battelle Memorial Institute
Richland, WA 99352

Jet Propulsion Laboratory
4800 Oak Grove Drive
Pasadena, CA 91003

L. Derr (1)
A. Galbraith (1)
W. Hagemeyer (1)
R. Mathison (1)
J. Schwartz (1)

CBS Laboratories
High Ridge Road
Stamford, CT 06905
Attn: Mr. R.L. Stow (1)

Eimac
Division of Varian
R&D Advanced Products Operation
301 Industrial Way
San Carlos, CA 94070
Attn: Mr. Anderson (1)

Eimac
Division of Varian
301 Industrial Way
San Carlos, CA 94070
Attn: Mr. L. Reed (1)

Hughes Aircraft Company
Electron Dynamics Division
11105 S. La Cien Ega Boulevard
Los Angeles, CA 90009

H. Griffin (1)
J. Mendel (1)

Hughes Research Laboratories
Malibu, CA 90265
Attn: J. Heney (1)

Litton Industries
Electron Tube Division
960 Industiral Road
San Carlos, CA 94070
Attn: W. Day (1)

Microwave Associates
Burlington, MA 01803
Attn: S. Paik (1)

Raytheon Company
Microwave & Power Tube Division
Waltham, MA 02154

L. Clampitt (1)
G. Friedman (1)

Varian Associates
Palo Alto, CA 94302
Attn: A. Whitol (1)

Hughes Aircraft Company
594 Marrett Road
Lexington, MA 02173
Attn: H. Boling (1)

Westinghouse Electric Corporation
Atomic, Defense & Space Group
Hobbs Brook Park
275 Wyman Street
Waltham, MA 02154
Attn: D.M. Bennett (1)

Westinghouse Electric Corporation
Defense and Space Center
Aerospace Division
Friendship International Airport
Box 746
Baltimore, MD 21203
Attn: D.H. Siegfried (1)

Westinghouse Electric Corporation
Elvira, NY 14903
Attn: Library (1)

TRW, Incorporated
One Space Park
Redondo Beach, CA 90278
Attn: Dr. R.F. Mettler (1)

TRW, Incorporated
TRW Systems
Northwest Industrial Park
33 Third Avenue
Burlington, MA 01803
Attn: R. Kerber (1)

Stanford Research Institute
333 Ravenswood Avenue
Menlo Park, CA 94025
Attn: D. Geppert (1)

Watkins-Johnson Company
3333 Hillview Avenue
Stanford Industrial Park
Palo Alto, CA 94304

B.P. Israelsen (1)
J.P. McNaul (1)

Lancer Associates
16 Adams Street
Burlington, MA 01803
Attn: L.L. Bibbins (1)

SFD Labs Incorporated
800 Pahway Avenue
Union, NJ 07083
Attn: Dr. G. Farney (1)

Microwave Electronics
3165 Porter Drive
Palo Alto, CA 94304
Attn: Dr. S. Koisel (1)

Sperry Electron Tube Division
Gainesville, FL 32601
Attn: Library (1)

ITT Electron Tube Division
Easton, PA 18042
Attn: A.W. McEwan (1)

Isotopes-Nuclear Systems Division
P.O. Box 4937
Middle River, MD 21220

Attn: A. Streb, Manager of Advanced Programs (1)

Radio Corporation of America
Electronic Companents and Devices
New Holland Avenue
Lancaster, PA 17604
Attn: J. Polkosky (1)